Investigating the inhibition of anti-apoptotic BCL-2 family proteins in pediatric cancer cells

Dissertation

zur Erlangung des Doktorgrades

der Naturwissenschaften

vorgelegt am Fachbereich

Biochemie, Chemie und Pharmazie

der Johann Wolfgang Goethe-Universität

Frankfurt am Main

von

Sarah Kehr

aus Speyer

Frankfurt am Main, 2020

(D30)

Vom Fachbereich Biochemie, Chemie und Pharmazie (FB14) der Johann Wolfgang Goethe-Universität Frankfurt am Main als Dissertation angenommen.

Dekan: Prof. Dr. Clemens Glaubitz

1. Gutachter: Prof. Dr. Robert Fürst

2. Gutachter: Prof. Dr. Simone Fulda

Datum der Disputation: 03.12.2020

Table of Contents

List of Abbreviations

°C	Degree Celsius
2D	Two-dimensional
3D	Three-dimensional
µg	Microgram
µl	Microliter
µm	Micrometer
AIF	Apoptosis-inducing factor
AML	Acute myeloid leukemia
APAF-1	Apoptotic protease-activating factor-1
APS	Ammonium persulfate
ARMS	Alveolar rhabdomyosarcoma
ATCC	American Type Culture Collection
BAD	BCL-2-associated agonist of cell death
BAK	BCL-2 antagonist killer
BAX	BCL-2-associated X protein
BCA	Bicinchoninic acid
BCL-2	B-cell lymphoma-2
BCL-2A1	BCL-2-related protein A1
BCL-B	BCL-2-like protein 10
BCL-w	BCL-2 like 2
BCL-X_L	B-cell lymphoma extra-large
BET	Bromodomain and extraterminal
BH3	BCL-2 homology 3
BID	BH3-interacting domain death agonist
BIK	BCL-2 interacting killer
BIM	BCL-2-interacting mediator of cell death
BMF	BCL-2-modifying factor
BOK	BCL-2 related ovarian killer
BSA	Bovine serum albumin
CARD	Caspase activation and recruitment domains
Caspase	Cysteinyl-aspartate specific protease
CDKN2	Cyclin-dependent kinase inhibitor 2A
CHAPS	Cholamidopropyldimethyl ammonio propane sulfonate
chr	Chromosome
cIAP	Cellular inhibitor of apoptosis
CLL	Chronic lymphocytic leukemia
cm	Centimeter

List of Abbreviations

CML	Chronic myelogenous leukemia
CNS	Central nervous system
CNV	Copy number variations
CO_2	Carbon dioxide
CTG	CellTiter-Glo®
Ctrl	Control
d	Day
DAB	Diaminobenzidine
DAPI	4′,6-Diamidin-2-phenylindol
DD	Death domain
dd	Distilled deionized
DEVD	1-letter amino acid abbreviation for “Asp-Glu-Val-Asp”
DISC	Death-inducing signaling complex
DLBCL	Diffuse large B-cell lymphoma
DMEM	Dulbecco’s Modified Eagle’s Medium
DMSO	Dimethyl sulfoxide
DNA	Deoxyribonucleic acid
DSMZ	Deutsche Sammlung von Mikroorganismen und Zellkulturen
DTT	Dihydro threitol
ECL	Enhanced chemiluminescence
ECM	Extracellular matrix
EDTA	Ethylenediaminetetraacetic acid
EMA	European Medicines Agency
ER	Endoplasmatic reticulum
ERG	ETS-related gene
ERK	Extracellular signal-regulated kinase
ERMS	Embryonal rhabdomyosarcoma
et al.	Et alii (Latin); and other
ETS	E-twenty six
EV	Empty vector
EWSR1	Ewing sarcoma breakpoint region 1
FACS	Fluorescence-activated cell sorter
FADD	Fas-associated death domain
FBW7	F-box/WD repeat-containing protein 7
FCS	Fetal calf serum
FDA	Food and Drug Administration
FGFR4	Fibroblast Growth Factor Receptor 4
FITC	Fluorescein isothiocyanate
FLI1	Friend leukemia 1 transcription factor

FOXO3A	Forkhead box transcription factor-3A
FSC	Forward scatter
fwd	Forward
GAPDH	Glyceraldehyde-3-phosphate dehydrogenase
GLI	Glioma-associated oncogene
h	Hour
hh	Hedgehog
HDAC	Histone acetylase
HRK	Harakiri
HRP	Horse radish peroxidase
HDAC	Histone deacetylase
HRP	Horseradish peroxidase
huMCL-1	Humanized MCL-1
ICAD	Inhibitor caspase-activated DNAse
i.e.	Id est (Latin); that is
IGF	Insulin-like growth factor
i.v.	Intravenous
IgG	Immunoglobulin
IP	Immunoprecipitation
IR	Infrared
JAK	Janus kinase
JNK	Jun N-terminal kinase
KD	Knockdown
KO	Knockout
kDa	Kilodalton
M	Molar
mA	Milliampere
MAP	Methotrexate, adriamycin and cisplatin
MCL	Mantle cell lymphoma
MCL-1	Myeloid cell leukemia-1
MDR1	Multidrug-resistance protein 1
mg	Milligram
min	Minute
ml	Milliliter
MM	Multiple myeloma
mm	Millimeter
mM	Millimolar
MMP	Mitochondrial membrane potential
MOMP	Mitochondrial outer membrane permeabilization

List of Abbreviations

mRNA	Messenger ribonucleic acid
mtDNA	Mitochondrial DNA
MYC	Myelocytomatosis (protein name)
NB	Neuroblastoma
NF-κB	Nuclear factor-κB
ng	Nanogram
NHL	Non-Hodgkin lymphoma
NHT	Non-human target
nM	Nanomolar
NOXA	Phorbol-12-myristate-13-acetate-induced protein 1
ns	Not significant
(N)SCLC	(Non-)small cell lung cancer
NOM	Nuclear outer membrane
PARP	Poly(ADP-ribose)-polymerase
PBS	Phosphate-buffered saline
PBS-T	Phosphate-buffered saline with 0.1% Tween 20
PCD	Programmed cell death
PCR	Polymerase chain reaction
PDB	Protein data bank
pH	Power of hydrogen
PI	Propidium iodide
PIC	Protease inhibitor cocktail
PROTAC	Proteolysis-targeting chimera
PS	Phosphatidylserine
PTM	Posttranslational modification
PUMA	P53-upregulated modulator of apoptosis
qRT-PCR	Quantitative real time PCR
RAS	Rat Sarcoma (protein name)
RB1	Retinoblastoma protein
rev	Reverse
RMS	Rhabdomyosarcoma
RNA	Ribonucleic acid
RNAi	RNA interference
rpm	Revolutions per minute
RPMI	Roswell Park Memorial Institute
RR	Relapsed and refractory
RT	Room temperature
SCCHN	Squamous cell carcinoma of the head and neck
SD	Standard deviation

List of Abbreviations

SDS	Sodium dodecyl sulfate
SDS-PAGE	SDS-polyacrylamide gel electrophoresis
sec	Seconds
siRNA	Small interfering RNA
SMAC	Second mitochondria-derived activator of caspases
SSC	Side scatter
STAT	Signal transducer and activator of transcription
SUFU	Suppressor of fused homolog
TEMED	Tetramethylethylene diamine
TM	Transmembrane domain
TMRM	Tetramethylrhodamine methyl ester
TNFα	Tumor necrosis factor
TP53	Tumor protein P53
TRADD	TNF-receptor associated death domain
TRAIL	TNF-related apoptosis-inducing ligand
TRITC	Tetramethylrhodamine
U	Units
UT	Untransfected
V	Voltage
VAC	Vincristine, actinomycin-D and cyclophosphamide
VDAC2	Voltage-dependent anion-selective channel protein 2
VIDE	Vincristine, irinotecan, doxorubicin and etoposide
vs.	Versus
XIAP	X-linked inhibitor of apoptosis
zVAD.fmk	N-benzyloxy-carbonyl-Val-Ala-Asp-fluoromethylketone

List of Figures

List of Tables

1 Abstract

Cancer is amongst the leading causes of death in childhood. Rhabdomyosarcoma (RMS) is the most frequently occurring soft tissue sarcoma in children and adolescents. It presumably arises from mesenchymal progenitors of skeletal muscle cells and presents with different subtypes that differ both histologically and genetically. Osteosarcoma (OS) and Ewing sarcoma (ES) are the most frequently diagnosed pediatric bone tumors. Even though the prognosis of these cancer entities improved significantly during recent decades, the survival rates are currently stagnating. Especially, dismal prognosis of relapsed and metastasizing cases of these malignancies urgently call for novel treatment options. BCL-2 proteins are vital guardians that control intrinsic apoptosis. Furthermore, it was shown that BCL-2 proteins critically regulate apoptosis in pediatric solid tumors. BH3 mimetics are small molecules that bind and inhibit anti-apoptotic BCL-2 proteins. They have already been investigated as cancer therapeutics for several years and show first encouraging clinical results. Therefore, we hypothesized that targeting BCL-2, MCL-1 and BCL-X_L might be a promising approach to treat RMS, OS and ES.

In this study, we aimed to comprehensively evaluate the potential of anti-apoptotic BCL-2 family proteins as therapeutic targets for pediatric solid tumors such as RMS, OS and ES.

Notably, RMS, OS and ES cells largely expressed the most relevant BCL-2 family protein members. However, cells were widely insensitive to single pharmacological inhibition of either BCL-X_L, BCL-2 or MCL-1 by A-1331852, ABT-199 and S63845, respectively. This finding was independent of their BCL-2 family protein expression levels. Significantly, co-administration of A-1331852 and S63845 induced cell death in RMS, OS and ES cell lines in a highly synergistic manner. Transient silencing of MCL-1 and/or BCL-X_L verified the co-dependency of RMS cells on these proteins for survival. Importantly, A-1331852/S63845 co-treatment was more efficient in causing cell death in RMS, OS and ES cells than either inhibitor combined with ABT-199. Efficacy of A-1331852/S63845 co-treatment could be additionally demonstrated in a primary sample of pediatric malignant epithelioid mesothelioma.

Mechanistically, concomitant A-1331852/S63845 treatment mediated rapid intrinsic apoptosis involving swift loss of the mitochondrial outer membrane potential as well as activation of caspases-3, -8 and -9. An observed caspase-dependent loss of MCL-1 might further amplify the A-1331852/S63845-triggered pro-death signaling. Furthermore, we identified BAX and BAK as key mediators of apoptosis caused by dual inhibition of MCL-1 and BCL-X_L. A-1331852/S63845-induced cell death was relying on BAX and/or BAK in a cell line dependent manner. Interestingly, treatment with A-1331852 and S63845 liberated BAK from its interaction with MCL-1 and BCL-X_L. Moreover, BAX and BAK were activated and interacted with each other to form a pore in the outer mitochondrial membrane. Further, in RD cells BIM and NOXA partially contributed to A-1331852/S63845-mediated cell death. Consistently, in this cell line BIM and NOXA

were disrupted from their binding to BCL-X_L and MCL-1 by A-1331852 and S63845, respectively. However, BH3-only proteins were not involved in A-1331852/S63845-induced cell death in Kym-1 cells. Therefore, we concluded that BH3-only proteins played only a marginal and cell line dependent role in mediating cell death caused by MCL-1 and BCL-X_L co-repression.

Notably, A-1331852/S63845 co-treatment spared non-malignant fibroblasts, myoblasts and peripheral blood mononuclear cells, which suggests a therapeutic window for its application *in vivo*. Besides, we could demonstrate that sequential BH3 mimetic treatment still significantly induced cell death, albeit to minor extents compared to its dual administration. Importantly, we successfully evaluated concomitant treatment with A-1331852 and S63845 in multicellular RMS spheroids and in an *in vivo* embryonic chicken model of RMS. These findings stress the high transcriptional relevance of A-1331852/S63845 as an emerging novel cancer regimen.

Collectively, the thesis at hand explored the great potential of co-treatment with A-1331852 and S63845 in pediatric solid tumors and unveiled the underlying molecular mechanisms of cell death in RMS. Together, the current investigations support further preclinical and clinical studies to evaluate the effect of dual MCL-1 and BCL-X_L targeting in pediatric solid tumors.

2 Introduction

2.1 Pediatric cancer

Even though less than 1% of all cancer malignancies represent pediatric cases, cancer is a leading cause of death in childhood (1,2). Approximately 300,000 children and adolescents (< 20 years) worldwide are diagnosed with cancer each year and the cases appear to rise further (2). Incidence rates are highest in infants (< 5 years) and adolescents (15 - 19 years) (1). Importantly, pediatric cancer arises predominantly in developing cells that underlie massive proliferation during childhood. The most common entities are the hematological malignancies leukemia (~25%) and lymphoma (~16%) as well as tumors that arise in the central nervous system (CNS) (~17%). The remaining ~42% of pediatric cancers are solid tumors of the bone, organs or tissue (Figure 2.1) (1-3).

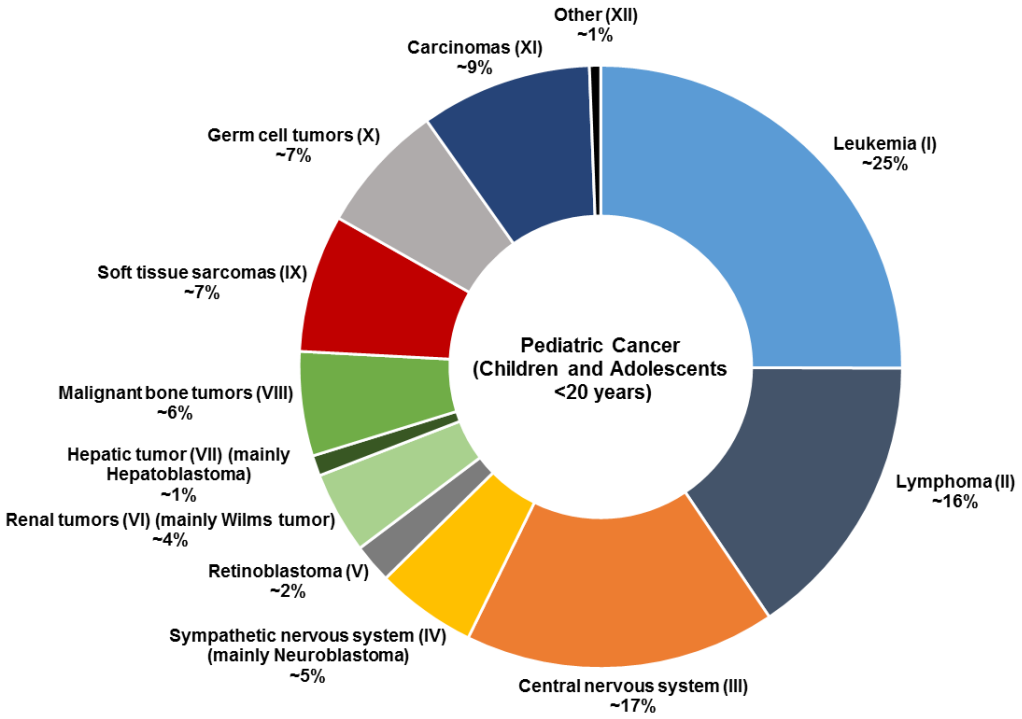

Figure 2.1: Percent distribution of childhood cancers.

Cancer entities are categorized according to International Classification of Childhood Cancer (ICCC) categories for children and adolescents younger than 20 years (all races, both sexes). Numbers adapted from (1-3).

Cancer cases of the individual entities varies considerably between the age groups. Whereas the incidence of cancers such as leukemia, neuroblastoma (NB) and retinoblastoma significantly decreases with increasing age, lymphomas, malignant bone tumors and carcinomas are more likely to develop in older children and adolescents. In contrast, cancer entities such as soft tissue sarcomas display largely stable case counts throughout different age groups. The incidence of

tumors in the CNS, on the other hand, peaks in children between 5 and 9 years. Additionally, case numbers are reported to be dependent on sex and race (2).

The 5-year survival of children suffering from cancer increased during recent years, from 63% in 1975 - 1979 to 84% in 2008 - 2014 (1). Unfortunately, the cure rate is highly dependent on the country in which the diagnosed children reside. While ~80% of childhood cancers can be cured in high-income countries, the chances of a child to recover from cancer in low-and middle-income countries is only ~20%. Lack of diagnosis or late diagnosis as well as difficulties to access medical treatment are major causes for these numbers (4,5). Moreover, approximately two-thirds of patients surviving cancer in childhood will establish at least one secondary malignancy within 30 years upon recovery with one-third of these malignancies being severe or life-threatening (6,7). The chances of a childhood cancer survivor to present with a second neoplasm is 10- to 20-fold higher compared to the healthy population (7). Thus, constant improvement of treatment and surveillance is inevitable to further augment the quality of life for these patients.

2.1.1 Rhabdomyosarcoma

Rhabdomyosarcoma (RMS) accounts for ~3.5% of all cancer cases in children aged under 14 years and ~2 - 3% of all cancer cases in adolescents (3). Although being a rare disease, 50% of all soft tissue sarcomas (ICCC category IX) in children between 0 - 14 years are classified as RMS (3). While RMS is the most frequent pediatric soft tissue sarcoma, the incidence in adults is low (8). Overall, RMS affects slightly more males than females and more Black than Caucasian people (3). This tumor entity arises presumably from mesenchymal progenitor cells of skeletal muscle that fail to differentiate (9). Even though the cell of origin is still debated, RMS histologically resembles fetal striated muscle cells (10). Generally, RMS can form at and metastasize to any anatomical site (11), but it is mostly found in the head and neck region (~40%), genitourinary tract (~25%) and in the extremities (~20%) (3). The Li-Fraumeni syndrome and neurofibromatosis type 1 might be genetic risk factors, thus contributing to disease development (12,13).

Over 70 years after the first closer examination of skeletal muscle tumors by Stoudt *et al*. (14), the characterization and classification of RMS into different subtypes has evolved. Today, most RMS cases are identified as embryonal RMS (ERMS) (~60 - 70% of all cases) and alveolar RMS (ARMS) (~20% of all cases) (3). Moreover, two rarer subtypes are recognized, namely pleomorphic RMS, which typically appears in adults, and spindle cell/sclerosing RMS (15). While ERMS occurs more frequently in younger children (1 - 4 years), the number of ARMS cases is relatively equal throughout the distinct age groups (3). Differences between these two subtypes can also be observed concerning their localization. Head/neck region (~30% of all ERMS cases) and genitourinary area (~30% of all ERMS cases) are prominent sites for ERMS development, whereas ARMS frequently presents at the extremities (~40% of all ARMS cases) (3). Histological features such as growing of the cells around open central spaces for ARMS and the resemblance to

undifferentiated muscle cells in ERMS cases are characteristics supporting the diagnosis (16,17). Moreover, ARMS and ERMS exhibit distinct genetic alterations. Prominently, ERMS frequently harbors copy number variations due to gains and losses of chromosomes with the loss of heterozygosity at chromosome 11 (locus 11p15.5) being present in more than two-thirds of all ERMS cases (18). This results in an increase of insulin-like growth factor II (IGFII) which inhibits myogenic differentiation and mediates tumor progression (19). Further frequent genetic aberrations in ERMS are mutations in the genes coding for rat sarcoma (RAS), tumor protein P53 (TP53), fibroblast growth factor receptor 4 (FGFR4) and amplifications of myelocytomatosis (MYC), all being crucial players of tumor development (20-22). In contrast to ERMS, ~60% of the ARMS subtypes exhibit chromosomal translocations between chromosomes 2 and 13 producing a gene product of the transcriptional activation domain of forkhead box (FOXO) transcription factor FKHR and the DNA binding domain of Paired Box 3 (PAX3) (t(2;13)(q35;q14) (23-25). Beside the PAX3/FOXO1 fusion protein, also PAX7/FOXO1 fusion proteins occur (t(1;13)(q36;q14), albeit in a low number of ARMS cases (~20%) and being associated with younger patients whose tumors are localized in their extremities (26). However, not all alveolar patients present the fusion protein. A low amount of ARMS cases (~20%) is described to be fusion-negative but displays mutations typical for embryonal tumors (27-29). Moreover, some ERMS cases were discovered to be fusion-positive as well, although this is very rare (~5% of all RMS cases) (27,30). The question whether ARMS and ERMS share common molecular disease-driving events cannot conclusively be answered yet, although it was shown that genes typically mutated in ERMS overlap with the ones that are influenced by the PAX7/FOXO1 or PAX3/FOXO1 fusion protein (21,31).

Treatment of RMS patients is multimodal and classically comprises surgery, radiotherapy and chemotherapy. Naturally, the procedure and kind of treatment is dependent on critical features such as tumor localization, stage and severity of the disease as well as the patient´s age. Even after years of research, the gold standard therapy for the RMS intermediate risk group still consists of repetitive cycles of vincristine, actinomycin-D and cyclophosphamide (VAC). Extensive trials of the Intergroup Rhabdomyosarcoma Study Group and the Children´s Oncology Group including other chemotherapeutics, i.e. doxorubicin, ifosfamide or irinotecan did not reveal any beneficial effect of these agents (11,32). Concerning RMS, younger patients generally exhibit a more favorable prognosis than adolescents or adults (11). Overall, the 5-year survival rate of RMS has increased to ~60% over the last decades (33). This seems promising at the first view, however, mostly ERMS cases, having a 5-year survival rate of ~70%, attribute to these numbers (33). The chances of patients suffering from the more aggressive ARMS to survive 5 years upon disease onset amounts to only ~50% (33). Treatment of metastasizing RMS is highly challenging, though ~12% of all RMS and ~24% of all ARMS patients already exhibit metastases upon diagnosis (34). Alarmingly, the 3-year overall survival of patients presenting with metastasizing RMS drops to ~25% (34). In addition, ~30% of all RMS patients experience a relapse, which decreases the 5-year survival rate

to only ~17% (35). Consequently, this calls for novel treatment regimens with potent antitumor effects.

2.1.2 Osteosarcoma

Osteosarcoma (OS) accounts for ~3 - 4% of all cancer cases in children and adolescents (1,3). Representing ~56% of all malignant bone tumors in patients under 20 years of age it is the most abundant cancer entity in this ICCC category (VIII) (3). Adolescents from 12 to 19 years of age display the highest OS incidence rates (3). Notably, Black children and adolescents have higher incidence rates than Whites (3). Likewise, boys with tall body stature have a slightly increased risk to develop OS in comparison to females (3,36). OS originates from mesenchymal cells destined to mature to bone cells (37) and can mainly be found at the metaphysis of quickly growing bones such as the long bones of the lower limbs (~80%), the central axis (trunk) (~5%) and the long bones of the upper limbs (~10%) (3).

The molecular background of OS is characterized by an overall complex heterogenic genomic instability including structural variations and copy number variations (CNV) (38). For instance, a study by Stephens *et al*. demonstrated that 3 out of 9 primary OS samples exhibited signs of a process they dubbed “chromothripsis” in which a single event might be able to cause a plethora of chromosomal rearrangements (39). Moreover, localized hypermutations termed “kataegis” are evident in half of OS tumors (38). Common somatic mutations in OS often affect the tumor suppressors TP53 and retinoblastoma protein (RB1) (38).

OS is treated by a combination of surgical removal and repetitive cycles of chemotherapy. Standard therapy comprises the chemotherapeutics methotrexate, doxorubicin (adriamycin) and cisplatin (MAP) which are still the agents of choice, even after years of research (40). The 5-year survival rate for children and adolescents suffering from OS is ~68% (1). Nevertheless, this rate drops to ~30% for patients harboring metastases (41). Given that 15 - 20% of patients have already developed metastases at the time of diagnosis, mostly in the lungs, these numbers are alarming and call for further research in order to investigate novel treatment regimens (42). Additionally, patients with OS might develop micrometastases that are challenging to detect in common screenings (42). The survival rates for patients with recurrent disease is even poorer with only ~17% of patients surviving 10 years upon relapse (43).

2.1.3 Ewing sarcoma

Ewing sarcoma (ES) was first described by James Ewing almost 100 years ago and represents ~2 - 3% of all cancer cases in children and adolescents (1,3,44). After OS, it is the second most frequently occurring malignant bone tumor (ICCC category VIII) in patients younger than 20 years, accounting for ~34% of all cases (3). Similar to OS, the incidence rate of ES peaks in the second decade of life between 10 and 19 years (3). Males are slightly more likely to develop ES than

females and strikingly White children have a 6-fold increased incidence rate than Black children (3). In contrast, Asians and African-Americans are rarely affected by this tumor entity (45). ES consists of small, round poorly differentiated cells and the cell of origin is still highly debated (46). Potential candidates are bone marrow-derived mesenchymal stem cells as well as neural-crest derived stem cells (46). ES often presents at bones of the central axis (trunk) (~45%) such as the pelvis, ribs, clavicle and sternum. Additionally, it can also develop at the long bones of the lower limbs (~30%) and upper limbs (~15%) (3). Besides the bones, ES rarely grows in soft tissue including the buttock or the chest wall (45,47).

Chromosomal translocations are the prevalent molecular characteristic of ES, while other genomic events, which mostly involve cyclin-dependent kinase inhibitor 2A (CDKN2) and TP53, are scarce (46). Fusion genes frequently emerge between Ewing sarcoma breakpoint region 1 (EWSR1) on chromosome 22 and one of the members of the E-twenty six (ETS) transcription factors. In ~ 85% of the cases, EWSR1 fuses with the ETS family member friend leukemia 1 transcription factor (FLI1) on chromosome 11 resulting in the t(11;22)(q24;12) fusion gene (46,48). Depending on the breakpoint of FLI1 on exon 6 or exon 5 these fusions are called type 1 or type 2, respectively (49). Translocations with the ETS members ETS-related gene (ERG) creating a t(21;22)(q22;12) fusion are rare (~10%), as are fusions with other ETS members (46,50). Importantly, chimeric fusions are described to deregulate the involved transcription factor thus causing malignant transformation by i.e. a block in differentiation, escape from cell death and increased proliferation (46,51). Furthermore, ~95% of ES cells express CD99 on their surface, a cell surface glycoprotein that is not exclusive for ES, but can be a helpful marker regarding its diagnosis (52).

As many other cancers, ES is treated in a multimodal way by surgery, radiotherapy and irradiation. In most cases, chemotherapy consists of combinations of DNA damaging agents, such as doxorubicin, etoposide, ifosphamide, cyclophosphamide and irinotecan and microtubule-interfering agents such as vincristine that are administered in cyclic treatment schedules. VIDE (vincristine, irinotecan, doxorubicin and etoposide) is the treatment most frequently applied, albeit choice of chemotherapeutic agents varies depending on disease stage and metastatic state of the cancer (46,53). The prognosis to recover from ES is relatively promising as the overall 5-year survival rate in children and adolescents is ~70% (1). However, the survival rates for relapsed and metastatic ES remain low with ~4 - 23% (depending on the time of the relapse) and ~20 - 30%, respectively (54-56). ES shows a relatively high rate of relapse (~25% for those with localized disease) (57) and an early spread resulting in ~25% of the patients presenting with metastases already at the time of diagnosis (56). Metastases are mainly detected in the lung, bone and bone marrow (45,58,59). Similar to OS, ES was suggested to develop micrometastases (60-62), a circumstance that exacerbates a comprehensive detection of all metastatic events. The still dismal prognosis for patients suffering from relapsed and metastasizing ES as well as the ability of ES to quickly evolve therapy resistance (62) demonstrate an urgent need for further treatment options.

2.2 Apoptosis

Programmed cell death (PCD) is a basic cellular process that was first introduced in 1964 to describe a form of cell death during development which follows a sequence of defined events culminating into a controlled disassembly of the cell (63). There exist several distinct types of PCD, such as necroptosis, ferroptosis, autophagic cell death and apoptosis (64-66). Carl Vogt was the first to observe cells undergoing apoptosis in 1842 during his studies on tadpoles (67), however, it was not until 1972 when Kerr *et al*. dubbed this form of cell death "apoptosis" being derived from the Greek meaning "falling leaf" (68). Today, apoptosis is the mode of PCD that is most thoroughly investigated. Since its discovery, research has made remarkable progress to understand this extremely structured and indeed highly conserved process as homologues of the central proteins of apoptosis, the BCL-2 family proteins, could be determined already in *C.elegans* (69). Apoptosis plays vital roles both in development and (patho)physiology. The most popular example is the removal of interdigital webs during embryogenesis, but also lymphocyte selection and the shaping of organs, e.g. the chambers of the heart, are dependent on this form of PCD (70-72). Apoptosis generally ensures cellular homeostasis by removing irreparably damaged cells (73). Nevertheless its aberrant regulation can lead to diseases, such as Alzheimer's disease, cardiovascular disease, cancer and many other (74). Importantly, the ability to evade apoptosis due to accumulation of mutations and/or DNA damage is a hallmark of cancer (75). Apoptotic cells display a row of biochemical characteristics, namely caspase activation, DNA and protein fragmentation as well as mitochondrial outer membrane permeabilization (MOMP) (73,76). The externalization of phosphatidylserine (PS) is another characteristic of apoptosis, even though its presence has also been reported in necroptotic cells (77,78). These features lead to numerous morphological alterations, which are cell shrinkage, pyknosis (due to chromatin condensation), plasma membrane blebbing/budding and the fragmentation of cellular components into so-called "apoptotic bodies" (73,76). These are eventually engulfed by macrophages or other immune cells, thus resulting in an ordered demolition and recycling process which hinders an immune response (79).

2.2.1 The extrinsic apoptotic pathway

There are two major apoptotic pathways: extrinsic and intrinsic apoptosis (Figure 2.2) (65). They have been exploited in cancer therapy for many years as various chemotherapeutics mediate their effects via these pathways (80). Extrinsic apoptosis is triggered by ligands of the tumor necrosis factor (TNF) family such as CD95 ligand (FAS ligand), TNF-related apoptosis-inducing ligand (TRAIL) and tumor necrosis factor α (TNFα) that bind their respective receptors (CD95 (FAS), TRAIL receptor 1/2 and TNFα receptor 1/2) (81,82). Upon receptor activation and oligomerization, the FAS-associated death domain (FADD) or TNF-receptor associated death domain (TRADD) is recruited to the receptors via their intracellular death domain (DD). Specifically, FADD interacts with CD95 and TRAIL whereas TRADD is required to bind to the TNF receptors (81). The respective receptors together with FADD/TRADD and pro-caspase-8 build a complex called death-inducing

signaling complex (DISC) (83). DISC formation activates caspase-8 by autoproteolytic cleavage, which in turn can directly activate the executioner caspases-3 and -7 (73). Furthermore, caspase-8 can cleave the BH3-only protein BH3-interacting-domain death agonist (BID) to produce tBID thereby providing a crosstalk to the intrinsic apoptotic pathway (65).

2.2.2 The intrinsic apoptotic pathway

Growth factor deprivation, intracellular stress such as mutations and DNA damage as well as other stressors are able to initiate the pathway of intrinsic apoptosis (73). It is frequently engaged by activation, mobilization or upregulation of BCL-2 homology 3 (BH3)-only proteins, which are pro-apoptotic members of the B-cell lymphoma 2 (BCL-2) protein family. BCL-2 proteins interact with and inhibit each other in a complex way that is explained in detail in section 2.2.3. In brief, the fine balance between these proteins is tipped towards a pro-death fate if the pro-apoptotic BCL-2 proteins overcome the inhibition by the anti-apoptotic BCL-2 members (84,85). Finally, this results in the activation of the pro-apoptotic BCL-2 proteins BCL-2-associated X protein (BAX) and BCL-2 antagonist killer (BAK) that form pores in the outer mitochondrial membrane (described in detail in section 2.2.3) (86). Pore assembly permeates the outer mitochondrial membrane and leads to breakdown of the mitochondrial membrane potential (MOMP) (87). Importantly, complete MOMP is a prerequisite to execute intrinsic apoptosis, however also two partial forms of MOMP have been described. One is incomplete MOMP, which occurs when the majority, but not all mitochondria of a cell undergo MOMP and inhibited caspase activation prevents apoptosis (87,88). The second one is minority MOMP (i.e. when only a minor amount of mitochondria undergo MOMP in response to sublethal stress) that causes slight caspase activation which does not induce apoptosis, but can potentially result in malignant transformation (87,89). Permeabilization of the mitochondrial membrane liberates effector molecules such as Cytochrome c (Cyt c) and second mitochondrial activator of caspases (SMAC) from the mitochondrial intermembrane space into the cytosol (87). SMAC contributes to caspase activation by binding inhibitor of apoptosis (IAPs) proteins, which usually sequester caspases and thereby block their activation (90,91). Another way to facilitate activation of caspases is performed by Cyt c and the apoptosome assembly. The apoptosome complex consists of Cyt c, pro-forms of the initiator caspase-9 and heptamers of apoptotic protease activating factor-1 (APAF1) molecules that bind each other via their caspase activation and recruitment domains (CARD) (92). Caspase-9 is activated by autoproteolytic cleavage, in turn cleaves, and hence activates executioner caspases (e.g. caspase-3 and -7) (93). Initiation of this caspase cascade, which might further be enhanced by caspase-8, culminates into a structured dismantling of the cell (see also 2.2.4) (73). A publication by McArthur *et al.* in 2018 suggested that during MOMP additionally also the inner mitochondrial membrane (including mitochondrial DNA (mtDNA)) herniates into the cytosol. This can then activate an innate immune response via interferon signaling, an indicator that apoptosis might not be as immunologically silent as first thought (94).

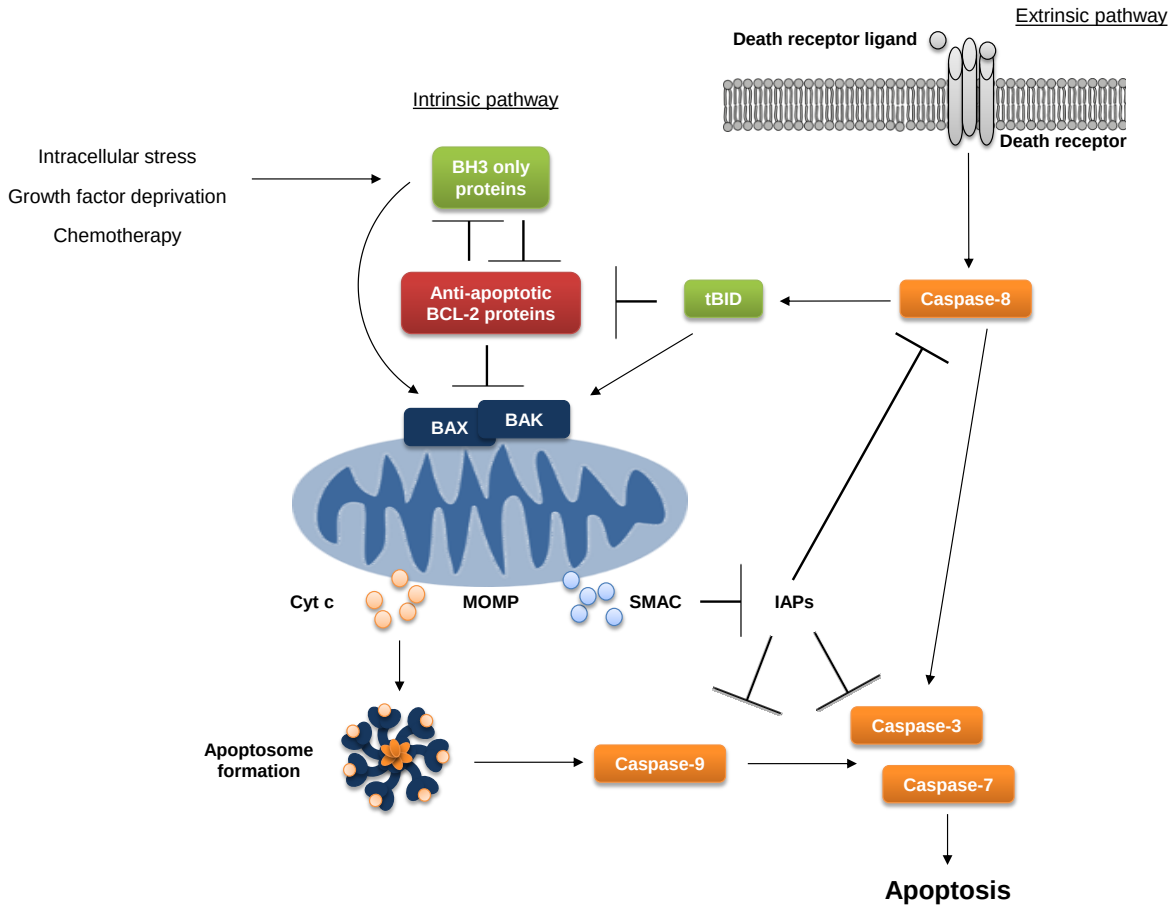

Figure 2.2: Apoptosis signaling pathways.

Apoptosis can be engaged by the intrinsic and the extrinsic apoptotic pathway. The extrinsic pathway is initiated when death receptors are bound by their respective ligands, which culminates in activation of caspase-8. Further, caspase-8 can activate executioner caspases such as caspase-3 and -7, which directly leads to apoptosis execution, or it can cleave the BH3-only protein BID to tBID providing a crosstalk to the intrinsic apoptotic pathway. Intracellular stressors, but also growth factor withdrawal and chemotherapy are triggers for the intrinsic apoptotic pathway. BH3-only proteins that are upregulated or activated by these stressors either inhibit anti-apoptotic BCL-2 family proteins or directly activate the pro-apoptotic effector proteins BAX and BAK. Pore formation by BAX and BAK in the outer mitochondrial membrane results in a loss of mitochondrial membrane potential and releases proteins residing in the intermitochondrial space. One of these is SMAC that reverses the inhibitory effect of IAPs on caspases, hence leading to caspase activation. Another one is Cyt c which forms a complex with APAF-1 and mediates the activation of caspase-9 in a complex termed apoptosome. Eventually, caspase-9 (and depending on the cellular context and trigger also caspase-8) activate further caspases which in turn accomplish apoptosis by cleaving their target proteins. Scheme modified from (84).

2.2.3 BCL-2 family proteins: regulators of apoptosis

2.2.3.1 Members, structure and subcellular localization

BCL-2 proteins are the gatekeepers of the intrinsic apoptotic pathway (95). The BCL-2 protein family is founded on BCL-2 that was first discovered in follicular B-cell lymphoma at the t(14;18) translocation breakpoint. Due to this translocation, BCL-2 is controlled by the enhancer and promoter of the immunoglobulin heavy chain and is thus overexpressed (96,97). In 1988 Vaux, Cory and Adams revealed that BCL-2, in contrast to other oncogenes, does not promote cellular proliferation, but instead acts as an inhibitor of cell death (98). Since then more and more BCL-2 relatives have been discovered and their affiliation to the BCL-2 family is grounded on their sequence homology regarding four distinct BH domains (84). It must be noted that the respective sequences are not clearly defined and partly shared by other proteins that do not have any impact on pore formation nor affinity to other BCL-2 relatives (99). Nevertheless, all BCL-2 family proteins harbor the amphipatic BH3 domain characterized by a 7-13 amino acid long sequence including an aspartate four residues C-terminal to a leucine (99,100). The BH3 domain is indispensable for the binding of other BCL-2 family members to build homo-or heterodimers as the aspartate interacts with a conserved arginine in the BH1 domain (101).

Based on the presence of distinct BH domains, BCL-2 family proteins can be classified into three different subgroups (Figure 2.3). The first group are the multi-domain anti-apoptotic BCL-2 proteins that comprise all four BH domains and consist of BCL-2, B-cell lymphoma extra-large (BCL-X_L), BCL-2 like 2 (BCL-w), Myeloid cell leukemia-1 (MCL-1), BCL-2-related protein A1 (BCL2A1) and BCL-2-like protein 10 (BCL-B). Secondly, BAX, BAK and BCL-2 related ovarian killer (BOK) belong to the multi-domain pro-apoptotic effector BCL-2 proteins lacking the BH4 domain. The last subgroup only harbors the BH3 domain and are thus referred to as (pro-apoptotic) BH3-only proteins. BCL-2 family members belonging to this subset include BCL-2 interacting killer (BIK), Harakiri (HRK), BCL-2-interacting mediator of cell death (BIM), BCL-2-associated agonist of cell death (BAD), BID, P53-upregulated modulator of apoptosis (PUMA), Phorbol-12-myristate-13-acetate-induced protein 1 (NOXA) and BCL-2-modifying factor (BMF). In addition to the BH domains, most BCL-2 family members contain a transmembrane domain (TM) which is necessary to attach to the membranes of cell organelles (84,102-105).

Mitochondria are the central platform for apoptosis mediation (87). Consequently, almost all of the BCL-2 family proteins can be localized at the mitochondria, either by anchoring in the membrane via their TM domain or by heterodimerization with another BCL-2 relative (106). Moreover, MCL-1 fulfills a crucial role in the mitochondrial matrix by supporting mitochondrial bioenergetics (107). Not only can BCL-2 proteins be found at the mitochondria, but they also have important functions in other compartments such as the endoplasmatic reticulum (ER), the nucleus and the cytosol (106). Anti-apoptotic (MCL-1, BCL-X_L and BCL-2), pro-apoptotic effectors (BAX, BAK, BOK) as well

as BH3-only proteins (BIK, BIM) are ER-residents and vital regulators of Ca^{2+} release from the ER (106). The biological relevance of BCL-2 family members in the nucleus is yet less investigated. However, Wu and colleagues revealed in 2017 that BCL-2, BCL-X_L and MCL-1 could promote their expression in a feedforward mechanism by binding to suppressor of fused homolog (SUFU) thus impeding its interaction with glioma-associated oncogene (GLI). Consequently, this leads to expression of GLI target genes (including BCL-2, BCL-X_L and MCL-1) (108). BCL-X_L is most commonly localized in the cytosol and shuttles BAX from the mitochondria to the cytosol to prevent it from pore formation. In addition, BCL-2 and MCL-1 have also been described to mediate this process termed “retrotranslocation”, albeit it is best investigated for BCL-X_L (109). BAK, which is mostly bound to the mitochondria, gets retrotranslocated as well, however to a lesser extent (110). In contrast to the other BCL-2 family proteins, BAX and BAK are additionally implicated in peroxisome/lysosome pathways as e.g. BAX was shown to affect lysosome permeability (106,111).

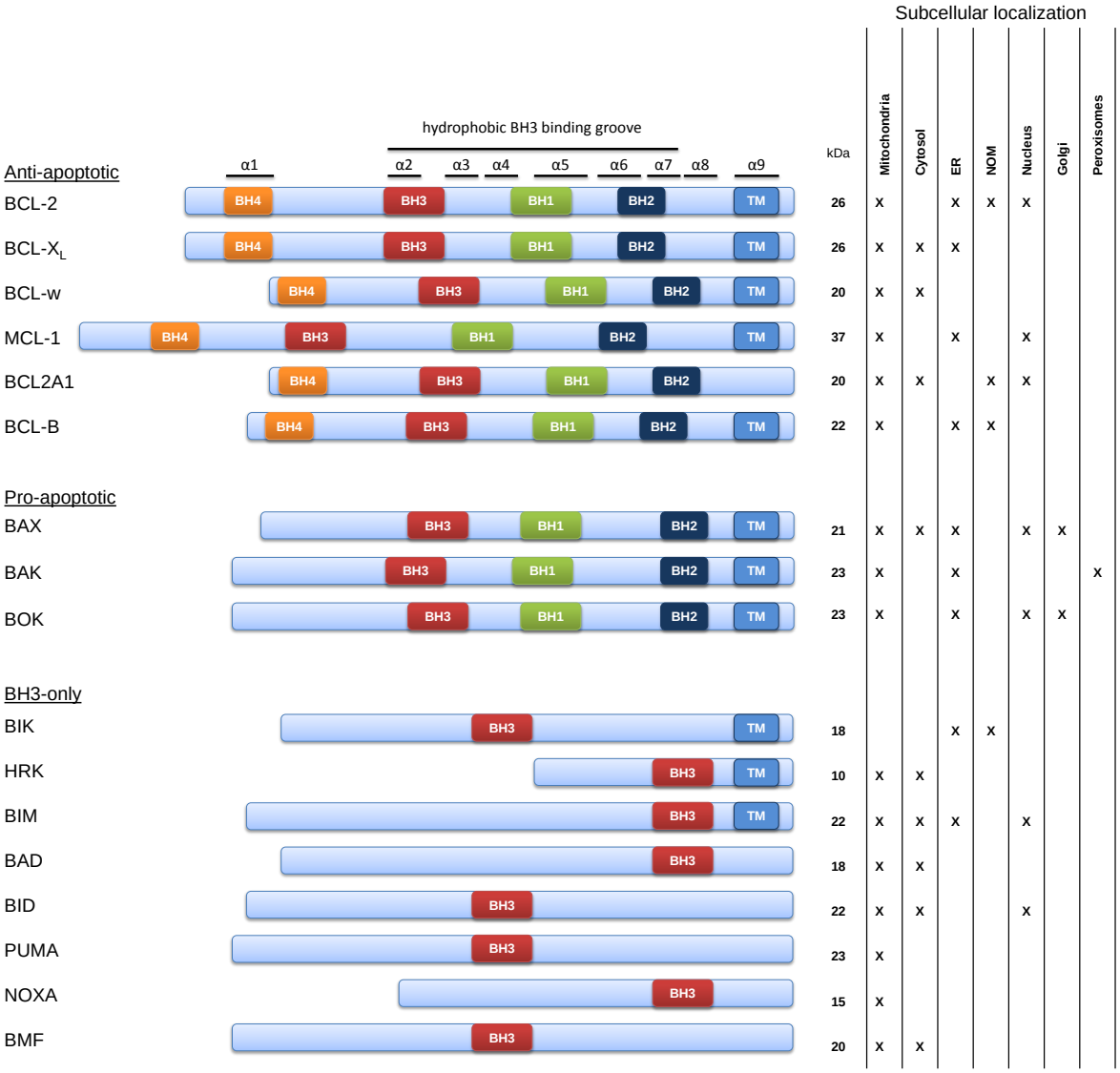

Figure 2.3: Members, structure and subcellular localization of the BCL-2 family proteins.

All BCL-2 family members share the BH3 domain. The pro-apoptotic effector proteins additionally harbor the BH1 and BH2 domain, but lack the BH4 domain which is exclusive for the anti-apoptotic BCL-2 family members. A TM domain to anchor in membranes can be found in the majority of the BCL-2 relatives. The hydrophobic binding group with which the anti-apoptotic BCL-2 proteins sequester the BH3 domain of their other members, stretches from the α2 to α7 helix. Location of helices within the protein structure are exemplary illustrated for BCL-2. BCL-2 family proteins are commonly located at the mitochondria, but also in the cytosol, the ER, the nucleus and the nuclear outer membrane (NOM). BAX, BAK and BOK are the only BCL-2 members that additionally exert functions at the Golgi and the peroxisomes. Image depicting BCL-2 family protein structures is modified from (73,84,112). Overview on the subcellular localization of BCL-2 family proteins is modified from (106).

2.2.3.2 Interaction pattern and BAX/BAK activation models

The interplay of the BCL-2 family proteins is complex (Figure 2.4A). In general, anti-apoptotic BCL-2 family members sequester BH3-only proteins as well as BAX and BAK, consequently impeding mitochondrial pore formation (85,113,114). BH3-only proteins can be divided into sensitizers and activators (115). The activator BH3-only proteins were shown to be able to activate BAX and BAK by directly binding to them in a way termed “hit and run” (116). This short interaction is sufficient to promote BAX/BAK integration into the mitochondrial membrane and the immediate detachment of the activator prevents a hindrance of the pore formation (117). PUMA, BIM and BID are activator BH3-only proteins (116,118-120). While some publications present data that NOXA exerts BAX/BAK activation as well, others could not confirm this finding (121-124). Hence, the activator function of NOXA remains to be more closely investigated and might be context- or cell line-dependent. In contrast to the activator BH3-only proteins, the sensitizers (BIK, BMF, HRK and BAD) are incapable to bind and activate BAX or BAK (115). They execute their pro-apoptotic function by sequestering the anti-apoptotic members, preventing their binding to BAX and BAK. Furthermore, sensitizer BH3-only proteins can also release activator BH3-only proteins by displacing them from anti-apoptotic BCL-2 family proteins, and thereby enable BAX/BAK activation (85,115). Of note, displacement within the BCL-2 family members is dependent on their cellular abundance and their respective affinities (85).

Importantly, the BCL-2 family binding pattern is highly selective. While BIM, PUMA and BID bind to all anti-apoptotic BCL-2 members, BAD is only sequestered by BCL-2, BCL-X_L and BCL-w (113,125,126). The sensitizer BH3-only proteins BIK and BMF are commonly bound by BCL-2, BCL-w, BCL-X_L and MCL-1 (125). HRK and NOXA are the most selective BH3-only proteins since they display high affinities only for BCL-X_L or MCL-1 and BCL-2A1, respectively (125,127). Finally, BAX can be bound and thus antagonized by all anti-apoptotic BCL-2 members, whereas BAK is not interacting with BCL-2 or BCL-w (128,129).

Regarding the regulatory mechanisms leading to the activation of BAX/BAK, several models have evolved during the last years (Figure 2.4B). According to the “direct activation” model, the activator BH3-only proteins induce a conformational alteration in the effector proteins BAX and BAK. In contrast, the sensitizers interrupt the interactions of anti-apoptotic members with activator BH3-only proteins, in turn enabling their action (115,124,130). The “indirect activation” model implies that the BH3-only proteins do not directly interact with BAX/BAK, but rather that BAX/BAK are constitutively active and sequestered by the anti-apoptotic BCL-2 proteins preventing them from pore formation. In order to liberate active BAX/BAK they have to be replaced by BH3-only proteins. This was for instance demonstrated by Willis and colleagues who showed that the interaction of BAK with BCL-X_L and MCL-1 can be impeded by BAD and NOXA. These proteins displace BAK from its binding to the anti-apoptotic proteins (128,131,132).

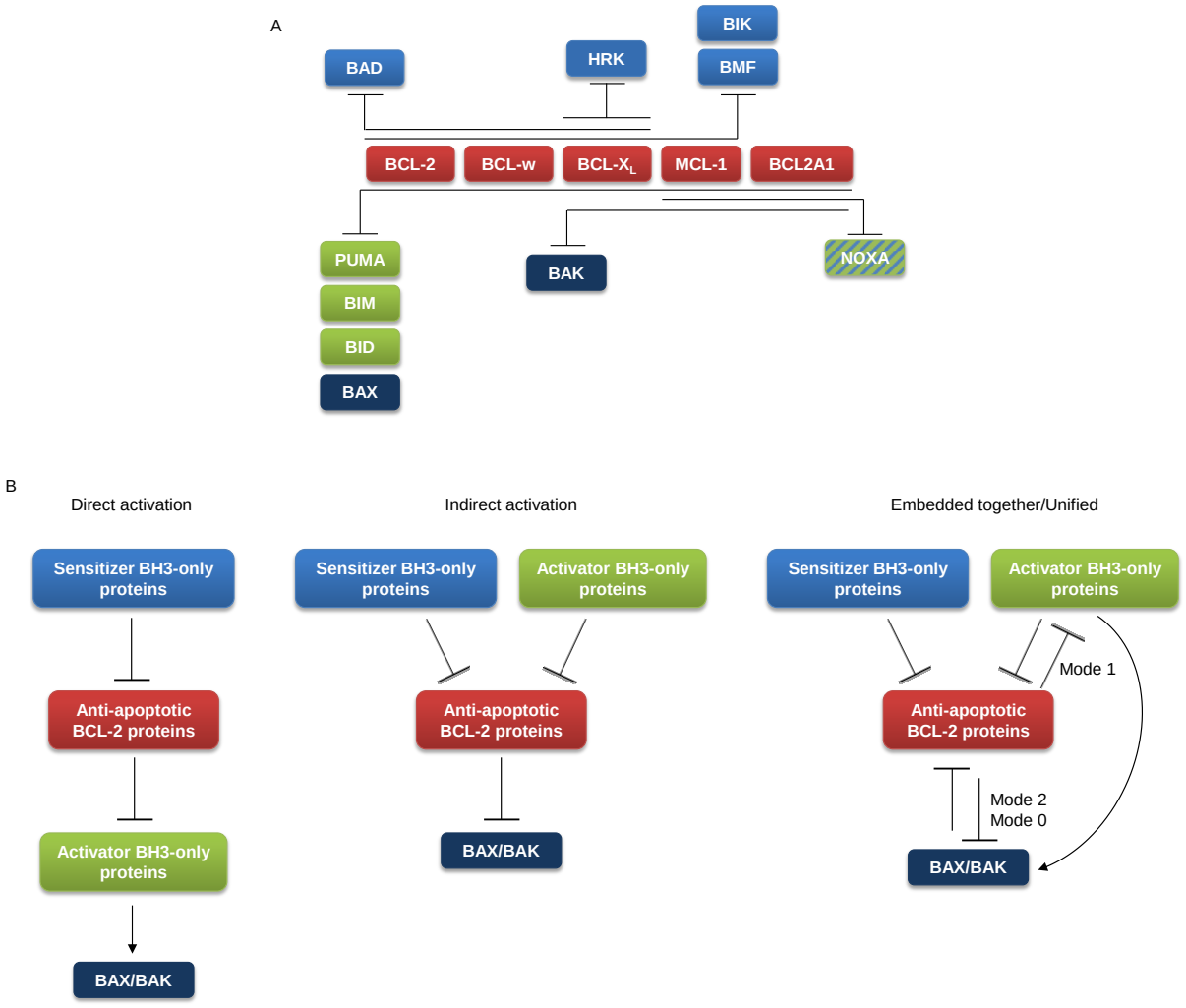

Figure 2.4: Models of selective interactions of the BCL-2 family proteins.

Color code: light blue: BH3-only activator proteins; green: BH3-only sensitizer proteins; red: anti-apoptotic BCL-2 family proteins, dark blue: pro-apoptotic effector proteins. (A): BCL-2 family proteins interact in a selective manner based on their respective affinities. The role of NOXA as an activator is debated. (B): Direct activation model: Sensitizer BH3-only proteins prevent their anti-apoptotic relatives from binding activator BH3-only proteins thus enabling the activator BH3-only proteins to directly facilitate activation of BAX/BAK. Indirect activation: Sensitizer and activator BH3-only proteins do not directly interact with the pro-apoptotic effector proteins, but only with the anti-apoptotic members. Thereby, they displace BAX/BAK, which are sequestered in their active conformation to the anti-apoptotic BCL-2 proteins. Embedded together/Unified model: The indirect and direct activation model act side by side to mediate BAX/BAK activation. Anti-apoptotic BCL-2 proteins fulfill a dual role by interacting with activator BH3-only proteins (Mode 1) and BAX/BAK (Mode 2). A special form of this sequestration is Mode 0 that refers to the retrotranslocation of BAX by BCL-X_L from the mitochondria to the cytosol. Schemes are modified from (95,133-135).

The “embedded together” model unites the statements made in the previous models and additionally highlights the necessity of the mitochondrial membrane as a platform of interaction (136,137). Hence, activator BH3-only proteins can directly facilitate BAX/BAK activation whereas sensitizers only interact with their anti-apoptotic relatives. These play a dual role by sequestering BAX/BAK as well as the activators. Both function prevent the activation and pore formation of the

effector proteins (114,137). BAX and BAK need to be in their active conformation to be bound by the anti-apoptotic BCL-2 proteins. This step is mediated by the BH3-only proteins, further supporting the complex interplay of the BCL-2 proteins described in the embedded together model (138). In 2011 Llambi *et al*., additionally introduced different modes of sequestration summarized as “unified model”. Mode 1 refers to the binding of the anti-apoptotic BCL-2 proteins to activator BH3-only proteins, while the interaction of anti-apoptotic members with BAX/BAK was termed Mode 2. Interestingly, Mode 2 sequestration was found to be more efficient than Mode 1 to inhibit apoptosis initiation (134). Mode 0 specifically relates to the retrotranslocation of BAX by BCL-X_L (139). Recently, evidence emerged that an allosteric activation and liberation of tBID by BAD is possible if both are bound together in a complex with BCL-X_L and that released tBID in turn activates BAX (140). The fact that BAX and BAK are also capable to achieve their active conformation in a manner independent of BH3-only proteins further complicates the regulatory mechanisms between them (141). Indeed, BAX and BAK have been reported to autoactivate each other (121). Moreover, cells still undergo BAX/BAK dependent apoptosis if they lack all BH3-only proteins (Octa-KO) and if the anti-apoptotic BCL-2 family proteins are simultaneously inhibited (142).

2.2.3.3 Activation of the pore-forming proteins BAX and BAK

The integration of BAX and BAK into the mitochondrial membrane follows a defined sequence of conformational changes (Figure 2.5) (105). The majority of BAK molecules anchors at the mitochondrial membrane. In contrast, BAX is mainly present in the cytosol due to its retrotranslocation by the anti-apoptotic BCL-2 members and its more polar C-terminal α9 TM domain compared to the one of BAK (109,143,144). However, upon apoptotic signaling, BAX translocates to the mitochondria where voltage-dependent anion-selective channel protein 2 (VDAC2) can function as a receptor for BAX and BAK (145,146). Interestingly, a non-canonical “rear pocket” formed by the α1 and α6 helices of BAX, but not BAK, was shown to provide a docking site for BH3-only proteins. Sequestration of BAX by BH3-only proteins at this rear pocket causes a release of the TM domain from its surface groove, thus facilitating the insertion of the TM domain into the mitochondrial membrane (147,148). Of note, this interaction is not mandatory for the activation of BAX since its spontaneous activation in the presence of a lipid membrane has also been reported (142). In a second step, activator BH3-only proteins bind to the hydrophobic groove of membrane-inserted BAX or BAK and induce the exposure of the N-terminus including the α1 domain (134,149). Subsequently, BAX and BAK protein structure alters from a globular to a membrane-spanning form by separation of the core (helices α2 - α5) from the highly flexible latch domain (helices α6 - α8; also called piercing domain) (138,150). This conformational change eventually liberates the activator BH3-only proteins from BAX and BAK (138). The transience of the “hit and run” interaction of BH3-only proteins and BAX/BAK is crucial for apoptosis as it has

been demonstrated that the structural alterations cannot be induced in BAK in case the BH3-only proteins stay bound (151).

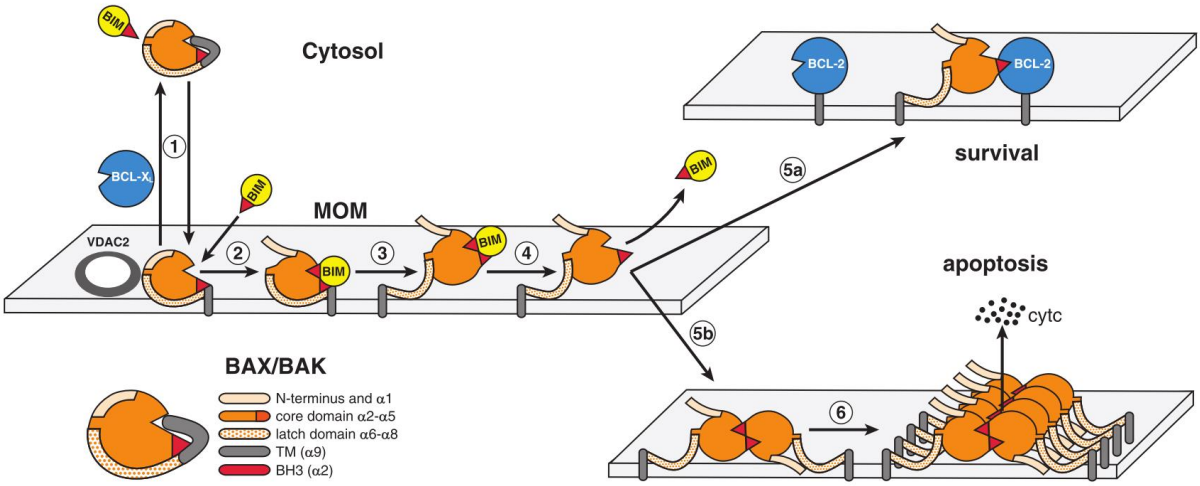

Figure 2.5: Model of the activation processes of BAX and BAK that lead to survival or apoptosis. Step1: BAX is retrotranslocated from the mitochondria to the cytosol by BCL-X_L. BAK is mainly bound to the mitochondrial membrane in association with VDAC2, which is also vital for BAX-mediated apoptosis. BH3-only proteins (exemplified by BIM) can bind a rear pocket in BAX helices α1 and α6, which releases the TM domain of BAX enabling its anchorage in the mitochondrial membrane. Step 2: BH3-only activator proteins bind the hydrophobic groove of BAX or BAK resulting in the exposure of the N-terminus including helix α1. Step 3: The globular fold of BAX or BAK stretches into core and latch domain. Step 4: This conformational change ejects the activator BH3-only protein and exposes the BH3 domain of BAX or BAK. Step 5a: In case anti-apoptotic BCL-2 family proteins are available and not inhibited by their relatives, they sequester activated BAX or BAK, which causes survival of the cell. Step 5b: If anti-apoptotic BCL-2 members are not present in abundance or inhibited, BAX or BAK form dimers by engaging the other´s BH3 domain. Step 6: This is followed by organization into higher order oligomers that accomplish membrane permeabilization and apoptosis. Image taken from (103).

A consequence of the departure of the BH3-only proteins is an exposure of the α2 helix harboring the BH3 domain, which can result in two possible scenarios (117,134). Firstly, the BH3 domain is accessible to anti-apoptotic BCL-2 members that, if they are not occupied themselves, might sequester and thereby block BAX/BAK pore formation (128,134). Secondly, BAX or BAK monomers build homodimers by engaging each other's BH3 domain (117,138,150). At this step, BAX/BAK can also autoactivate each other (121). Further, pore formation is enabled by the assembly of higher order oligomers of BAX and BAK (105,152). Many details about the pore association remain to be elucidated and are subject to intense research. For instance, it is not clear whether BAX/BAK heterodimers might exist and how many BAX or BAK molecules it takes to achieve mitochondrial permeabilization (117,153,154). Arch-like and ring-like structures as well as lines have been observed as pores form, however the exact composition of the pores is uncertain (154). Most likely is a toroidal lipidic pore whose interface comprises both lipids and proteins (155). Moreover, there exist several models explaining how the dimers might insert into the membrane,

e.g. like a hairpin, in plane or like a clamp (156). Additionally, BAX and BAK can also switch to their active conformation when they are exposed to heat or non-ionic detergents (149,157).

2.2.3.4 Levels of regulation

Mechanisms finely regulating the activation status of the individual BCL-2 family members range from a transcriptional level to posttranslational modifications (PTM) and the subcellular localization (84). The following section gives a brief insight into some of the most relevant ones. Since BH3-only proteins are stress sensors, their expression can frequently be induced by transcription factors (104). For instance, this is the case for PUMA and NOXA, both being transcriptionally upregulated by TP53 upon DNA damage, and BIM whose expression is induced by the class O forkhead box transcription factor-3A (FOXO3A) upon growth factor withdrawal (158-160). BCL-X_L, on the other hand, can be transcriptionally upregulated by growth factors via the janus kinase - signal transducer and activators of transcription (JAK-STAT) pathway (161). Furthermore, the subcellular localization of the BCL-2 members can negatively regulate their activation status as it is best exemplified for the BH3-only proteins BMF and BIM that are kept in an inactive state by binding to the myosin V motor complex and microtubule-associated dynein motor complex, respectively. Upon apoptotic signaling, they traffic to the mitochondria (104,162). The most commonly occurring PTM with regard to BCL-2 proteins is their phosphorylation with BCL-2, MCL-1, BAD, BIM and BAX being the ones most frequently affected (163). Phosphorylations can either be activating or inactivating. Whereas phosphorylation by Jun N-terminal kinase (JNK) increases the pro-apoptotic activity of BIM, its phosphorylation by extracellular signal-regulated kinase (ERK) targets it for proteasomal degradation (164). An anti-apoptotic member with a short half-life, and thus a particularly fast turnover, is MCL-1 as it is rapidly ubiquitinated and degraded upon pro-death signaling (165).

2.2.3.5 Roles of anti-apoptotic BCL-2 proteins in development and tissue homeostasis

Regulated execution of apoptosis is necessary for normal tissue homeostasis and especially in developing cells (72). The following section highlights some key roles of the most relevant anti-apoptotic BCL-2 family proteins in developing as well as in differentiated cells. Remarkably, BCL-2 proteins exert their function in a plethora of distinct cell types, above all in cells of the hematopoietic system (72) (Table 2.1). Few roles have been implied for BCL-w and BCL-2A1. The absence of BCL-w leads to male sterility, suggesting a function in spermatogenesis (166,167). Moreover, BCL-w was found to play a role in B cell survival and lymphomagenesis (168). BCL-2A1 was reported to be involved in neutrophil and B cell development (169). BCL-2 deficient mice are generally viable, however they die early due to polycystic kidney disease and massive apoptosis in B and T lymphocytes. Additionally, these mice present with grey hair since BCL-2 is crucial for melanocyte survival (170,171). Together with MCL-1 and BCL-X_L, BCL-2 promotes neuronal

development. Particularly, it is connected to the early phase of development and BCL-2 expression declines once the formation of the neural tube is completed (172,173). In 2018, a publication by Fogarty *et al.* explored the roles of MCL-1 and BCL-X_L in the developing nervous system and revealed that these two proteins can have compensatory roles. However, MCL-1 had an overall stronger contribution to the survival of neuronal progenitor cells, while the importance of BCL-X_L was increasing with the neuronal maturation status (174). MCL-1 is the member amongst the anti-apoptotic BCL-2 proteins with an impact on the greatest variety of cell types (72). Its knockout (KO) is embryonic lethal on day E3.5 and MCL-1 is a key player for survival of virtually all cell types of the hematopoietic system during all developmental stages including the hematopoietic stem cell (72,175). Interestingly, MCL-1 has additionally been demonstrated to maintain mature cardiomyocyte survival (176). Additionally, also the genetic ablation of BCL-X_L is embryonic lethal, albeit to a later time point (E13), resulting from massive apoptosis in the brain and in a range of lymphocyte/erythrocyte precursors (177). Further, MCL-1 and BCL-X_L act together to sustain hepatocyte survival (178,179) and loss of a single allele of either gene is sufficient to produce craniofacial defects (180). Recently, a publication showed that combined loss of MCL-1 and BCL-2 decreased the overall size of mice while leaving the individual tissue development unaffected (181). It is of utmost importance to keep the respective functions of the anti-apoptotic BCL-2 family proteins in mind when it comes to their pharmacological targeting. This could explicitly be seen from clinical studies with the BH3 mimetic ABT-263 that inhibits BCL-2, BCL-X_L and BCL-w. Thrombocytopenia, a side effect related to the role of BCL-X_L in the maintenance of platelet survival, was the most common adverse event (182-184). Thus, the physiological roles of the anti-apoptotic BCL-2 family members can be revealing about potential side effects that should be focused on in clinical and preclinical studies.

Table 2.1: Functions of anti-apoptotic BCL-2 family proteins in development and tissue maintenance.

(modified from (185))

	BCL-w	BCL2A1	BCL-2	BCL-X_L	MCL-1
Lymphocytes	X	X	X	X	X
Erythrocytes				X	X
Neutrophils		X			X
Platelets				X	
Cardiomyocytes					X
Neurons			X	X	X
Spermatocytes	X				
Melanocytes			X		
Kidney cells			X		
Hepatocytes				X	X

2.2.4 Caspases: executioners of apoptosis

Caspases are cysteine proteases that perform the task to dissect the cellular constituents in a coordinated manner during cell death. Both the intrinsic and the extrinsic apoptotic pathway culminate in caspase activation. Distinct caspases have been identified and depending on their cellular roles, they can be divided into inflammatory (e.g. caspase-1,-4,-5,-11), initiator (e.g. caspase-8,-9,-10) and executioner (effector) caspases (e.g. caspase-3,-6,-7). Caspases cleave their targets via a cysteine in their active site that cuts the respective protein after an aspartic acid residue. A range from a few up to several hundred target proteins have been described depending on the individual caspase and the cellular context (186-188).

A crucial caspase target is the inhibitor caspase-activated DNAse (ICAD) that is cleaved to CAD, which in turn facilitates DNA fragmentation (189). Moreover, PS is commonly located in the inner and outer cell membrane adhering to a certain ratio. Enzymes called flippases and scramblases control its distribution. The latter are cleaved by caspases causing an augmented exposure of PS that is recognized as an “eat-me” signal by macrophages (77). Furthermore, caspases mediate the inactivation of poly(ADP-ribose)-polymerase (PARP), a central player of the DNA repair machinery. Another prominent example of caspase targets are components of the cytoskeleton and also BCL-2 family proteins such as MCL-1 (190,191).

2.3 Therapeutic intervention of the intrinsic apoptotic pathway by BH3 mimetics

2.3.1 BCL-2 family proteins in cancer

As guardians of apoptosis, a hallmark of cancer, BCL-2 family proteins contribute strongly to malignant transformation (75,192). Cells that become cancerous have to cope with an increased amount of stressors originating from DNA damage, cell cycle checkpoint evasion, the unfolded protein response or oxidative stress. Intracellular stressors result in the activation or upregulation of pro-apoptotic BH3-only proteins, which is a potential fatal process for the cancer cell. Hence, the selection pressure is in favor of cells that compensate apoptotic signaling by an upregulation of anti-apoptotic family members, resulting in cell survival (75,103,125,192,193). The increasing number of complex formations between the BH3-only proteins and their anti-apoptotic relatives create a situation termed “primed for death” (194,195). This concept was especially coined by the group of Tony Letai and postulates that, compared to healthy cells, cancer cells are closer to the threshold towards apoptosis and thus are highly dependent on maintaining the inhibition of apoptosis initiation (193,195). Anti-apoptotic BCL-2 family proteins are overexpressed in many cancer types, especially in the ones being refractory to chemotherapy (196). The pro-survival protein BCL-X_L is particularly connected to chemoresistance (197). Notably, the expression of and the dependency on distinct anti-apoptotic BCL-2 members varies significantly among cancer entities. For instance, BCL-2 is amplified in diffuse large B-cell lymphoma (DLBCL) and small cell

lung cancer (SCLC) (198,199). Further, BCL-2 is overexpressed in breast cancer, ovarian cancer and chronic lymphocytic leukemia (CLL) and many more (102,200-202). BCL-X_L is most notably associated with solid tumors as it plays, for example, a role in the survival of colorectal cancer, neuronal tumors, subsets of breast cancer, bladder cancer and gastric cancer (102,203-205). In line with its physiological functions in the hematopoietic system, MCL-1 is frequently implied in multiple myeloma (MM), acute myeloid leukemia (AML), subtypes of lymphoma, but also solid tumors such as NB as well as lung and breast cancer (206-212).

Additionally, BCL-2 proteins were reported to play a role in soft tissue and bone sarcomas. For instance, the presence of BAX in RMS tissue samples has been connected with a prolonged median survival and its expression in RMS and other pediatric solid tumor cell lines was associated with higher resistance to doxorubicin and actinomycin D (213,214). Further, the PAX3/FOXO1 fusion gene, a common hallmark of ARMS, was demonstrated to transcriptionally induce BCL2L1 (coding for BCL-X_L) and NOXA expression (215,216). Excessive FGFR4 signaling and continuous STAT3 activation are further typical features of RMS (23). They have been demonstrated to mediate BIM degradation and induction of BCL-2 and BCL-2L1 genes, respectively (217,218). Moreover, enhanced hedgehog (hh) signaling, as present in RMS, can regulate expression levels of BCL-2, BCL-X_L and MCL-1 (108,219). Indeed, gene expression analysis reveals an upregulation of the majority of pro- and anti-apoptotic BCL-2 members, amongst them also MCL-1, BCL2L1, BCL2L11, PMAIP1 (coding for NOXA) and BAX (Table 2.2) (220). Consistently, MCL-1 has also been described by other publications to be frequently upregulated in RMS (196,221). Interestingly, BAK1 (coding for BAK) as well as BCL-2 were found to be underexpressed in RMS (220). Importantly, diminished BCL-2 levels suggest a more vital role of MCL-1 and BCL-X_L for RMS survival compared to BCL-2. The role of BCL-2 proteins in bone sarcomas, such as OS, is still debated since it was found that BCL2L1 expression did not correlate with patient survival in OS. Nevertheless, a selective BCL-X_L inhibitor sensitized OS cells to doxorubicin treatment (222,223). Concerning ES, its characteristic EWS-FLI1 fusion gene was reported to induce BCL-2 expression and interestingly inhibition of BCL-2 and BCL-X_L increases the susceptibility of ES cells to olaparib (224).

Since TP53 is mutated, non-functional or lost in ~90% of all cancers, transcriptional induction of NOXA and PUMA are often impaired (225). Moreover, epigenetic silencing or deletions of BH3-only proteins commonly develop during oncogenic transformation, additionally contributing to an overall surplus of anti-apoptotic BCL-2 family proteins (102). In fact, Soderquist and colleagues revealed that the majority of 78 tested cancer cell lines, representing a wide range of cancer entities, depend on at least one combination of the anti-apoptotic BCL-2 family proteins and some of them even on a single member (226). Besides their expression levels, it is the complex interplay of the BCL-2 relatives that define the cell's dependency on respective members. Co-dependencies frequently occur due to the partially redundant functions of anti-apoptotic BCL-2 proteins (85,226). For instance, BCL-X_L can compensate for the loss of MCL-1 to sequester BIM thereby rescuing MM

cells from cell death (212). Consistently, the MCL-1:BCL2L1 ratio was reported to be indicative of the response rate to pharmacological inhibition of MCL-1 (227). Consequently, this calls for treatment regimens tailored to the specific interaction patterns of the BCL-2 family proteins. By using synthetic BH3 peptides on digitonin-permeabilized cells, a method dubbed “BH3 profiling”, the “priming” status and susceptibility of cancer cells to a certain stimulus can be predicted (125). All in all, BCL-2 family proteins provide an Achilles heel for the targeting of cancer cells for apoptosis.

Table 2.2: BCL-2 family gene expression in RMS.

Gene expression analysis performed with “R2: Genomics Analysis and Visualization Platform” (samples (n=58, 33 fusion-positive and 25 fusion-negative RMS samples, Sun and Barr (228)) compared to normal healthy skeletal muscle samples (n=40, Assmann et al. (229) using MegaSampler). Significances were calculated using One Way ANOVA (220). ↑↑: strong overexpression ($p<10^{-11}$); ↑: overexpression ($p=0.05\text{-}10^{-11}$); ↓: underexpression ($p=0.05\text{-}10^{-11}$); ↓↓: strong underexpression ($p<10^{-11}$); →: no significant changes in expression.

Gene	Expression (RMS)
MCL-1	↑
BCL-2	↓↓
BCL2L1	↑↑
BCL-2A1	↑
BBC3	→
PMAIP1	↑↑
BCL2L11	↑↑
BMF	↑
BAD	→
BAX	↑↑
BAK1	↓
BOK	↑↑

2.3.2 BH3 mimetics

BH3 mimetics are small molecules that sequester and thereby inhibit their anti-apoptotic relatives. They do not directly engage BAX or BAK, but displace BH3-only proteins from their binding to the anti-apoptotic members and prevent novel interactions. Liberated BH3-only proteins can further inhibit anti-apoptotic BCL-2 members (in case they are sensitizers) or directly activate BAX/BAK (in case they are activators). Altogether, BH3 mimetics tip the balance between the BCL-2 members in favor at the pro-death signal (194,230,231). Due to their function as stress sensors, BH3-only proteins acted as a model to design drugs, which literally mimic the BH3 domain of these proteins (103,230). In detail, the hydrophobic amino acids of the BH3 mimetic molecule commonly target the hydrophobic pockets (P1-P4) of the anti-apoptotic BCL-2 family protein’s surface groove

(232). Several characteristics have been defined that need to be met to call an agent a BH3 mimetic. Firstly, the molecule has to imitate the BH3 domain of the BH3-only proteins in their function to bind the hydrophobic groove of their anti-apoptotic relatives. Secondly, they have to bind their target protein with high affinity. Thirdly, apoptosis initiated by a BH3 mimetic has to be executed in a BAX/BAK dependent manner. Fourthly, the expression levels of the target protein must correlate with the response of the cells to the respective BH3 mimetic (112). A number of agents that were designed with the aim to create a BH3 mimetic, but which do not fulfill these criteria are frequently referred to as “putative” BH3 mimetics (e.g. Obatoclax) (230,233).

Compared to other chemotherapeutic agents, BH3 mimetics present several advantages. First and foremost, their mechanism of action is well understood whereas for many chemotherapeutics it remains elusive as they have multiple cellular effects. As a consequence of their highly “primed” state, most cancer cells are specifically vulnerable to BH3 mimetic treatment and a wide range of cancer entities are predicted to display susceptibility. Moreover, in contrast to other treatments such as radiotherapy and DNA-damaging agents, BH3 mimetics are no mutagens, which might play a role in long-term patient survival. Finally, these agents directly access the apoptotic pathway instead of acting upstream, providing an explicitly targeted approach. In this context, BH3 mimetics act independently of the TP53 status of the cells, a favorable feature with regard to the high inactivation rate of TP53 in cancer (103,225,234).

In 2000, Wang *et al.,* were the first to attempt a small molecule (HA14-1) to inhibit BCL-2 (235). Since then, various agents have been discovered that target anti-apoptotic BCL-2 family proteins in a more or less selective manner (194). The BH3 mimetic ABT-737 is equipped to target BCL-2, BCL-X_L and BCL-w, but not MCL-1, in a BAD-like way (236). It triggered BAX/BAK dependent apoptosis as single agent or in combination with other agents (236,237). For clinical application, ABT-737 was refined to create the orally bioavailable compound ABT-263 (Navitoclax) that shares the target affinities with ABT-737 (238,239). ABT-263 showed potentially promising results in clinical studies, however, due to its targeting of BCL-X_L, thrombocytopenia was a major and limiting side effect (240). Importantly, alterations in dosing could markedly reduce thrombocytopenia in later studies (241). Unlike its predecessors, ABT-199 (Venetoclax) is a highly selective BCL-2-targeting BH3 mimetic (242) and founded the era of further selective BH3 mimetics for BCL-2, MCL-1 and BCL-X_L (194). The following three sections introduce the selective inhibitors utilized in this thesis.

2.3.2.1 The selective BCL-2 inhibitor ABT-199 (Venetoclax)

Using ABT-263 as a template, the orally bioavailable BCL-2 inhibitor ABT-199 was created by structure-based design. ABT-199 is highly selective for BCL-2 with a K_i < 0.01 nM and a 100-fold increased affinity for BCL-2 compared to BCL-X_L (242). ABT-199 sequesters BCL-2 by occupation of the hydrophobic pocket P2 with its 4-chlorophenyl residue and insertion into P4 via its azaindole residue. It binds in close proximity to the conserved Arg146 of the hydrophobic binding groove without directly interacting with it (Figure 2.6) (243). In contrast to ABT-263, ABT-199 does not interfere with platelet function and exerts promising anti-tumor effects in various BCL-2 dependent cancer entities, above all CLL. It potently induces intrinsic apoptosis and disrupts BCL-2:BIM interactions (242). Generally, ABT-199 seems to display especially marked effects in hematological cancers, however, also solid tumors such as breast cancer are susceptible to ABT-199 treatment (244,245). During recent years, a plethora of publications have explored the potential of ABT-199 as single agent or in combination with e.g. other BH3 mimetics, chemotherapeutics, histone acetylase (HDAC) inhibitors, CDK9 inhibitors, and many other drugs in numerous cancer entities such as Non-Hodgkin lymphoma (NHL), RMS, MM, various lymphomas and leukemias as well as other hematological cancers (242,246-253). ABT-199 was the first BH3 mimetic to be approved for cancer treatment and is the most advanced one in clinical trials (see section 2.3.3) (254).

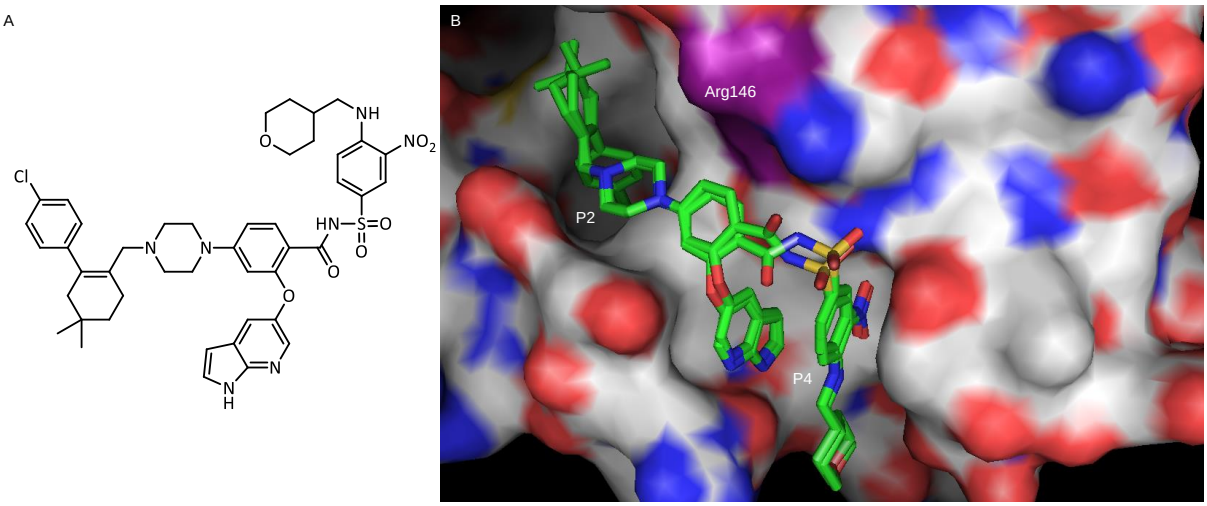

Figure 2.6: Chemical structure and binding of ABT-199 to BCL-2.

(A): Chemical structure of ABT-199 (242). (B): Crystal structure of ABT-199 binding to BCL-2 (PDB ID: 6O0K). BCL-2 is shown as surface model. The two possible conformations of ABT-199 inserting in the BH3 binding groove of BCL-2 are depicted. ABT-199 particularly interacts with the hydrophobic pockets P2 and P4 and binds in close proximity to the conserved Arg146 (purple) (243). Color code: BCL-2: grey - carbon, blue - nitrogen, red - oxygen. ABT-199: green - carbon, blue - nitrogen, red - oxygen, yellow - sulfur, cyan - chlorine. Illustration was created using PyMOL.

2.3.2.2 The selective MCL-1 inhibitors A-1210477 and S63845

Due to the relatively large, rigid BH3 binding groove of MCL-1, the development of selective inhibitors was lagging behind for a long time and progress was eagerly awaited (194,232). The selective MCL-1 inhibitor A-1210477 was designed in a structure-based manner and first published by Leverson *et al.* in 2015 (Figure 2.7A) (255). This inhibitor was described to induce cell death in MM, breast cancer and NSCLC in a BAX/BAK dependent manner and to exert its pro-apoptotic effect by disrupting BIM and/or NOXA from MCL-1 (207,255). Furthermore, it synergizes with Navitoclax to induce apoptosis in several cancer cell lines and sensitizes NHL to ABT-199 treatment (255,256).

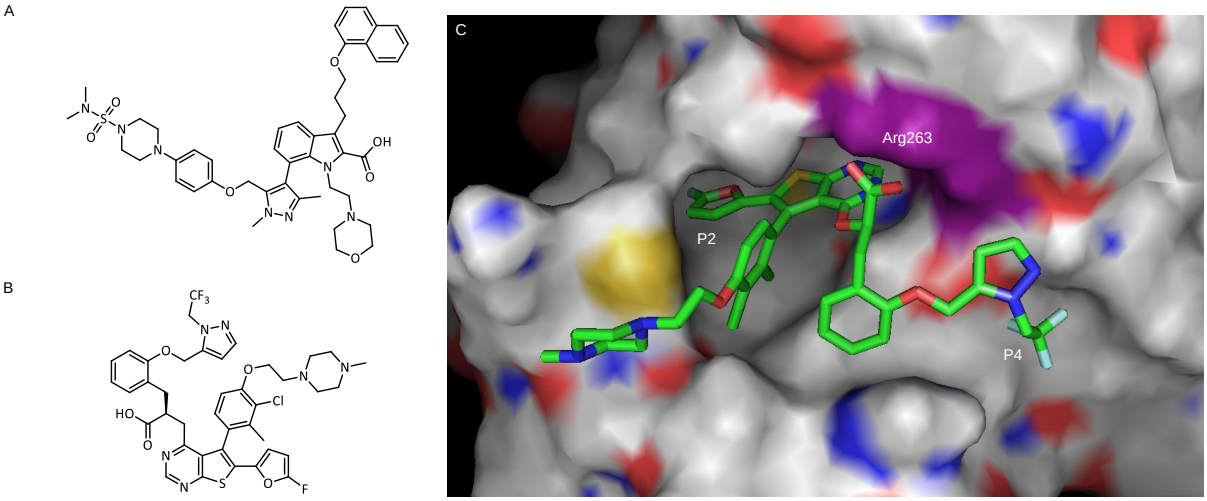

Figure 2.7: Chemical structure of A-1201477 and S63845 and binding of S63845 to MCL-1.
(A): Chemical structure of A-1201477 (255). (B): Chemical structure of S63845 (227). (C): Crystal structure of S63845 binding to MCL-1 (PDB ID: 5LOF). MCL-1 is shown as surface model. S63845 particularly interacts with the hydrophobic pockets P2 and P4 and the conserved Arg263 (purple) (227). Color code: MCL-1: grey - carbon, blue - nitrogen, red – oxygen, yellow - sulfur. S63845: green - carbon, blue - nitrogen, red - oxygen, yellow - sulfur, cyan - fluor. Illustration was created using PyMOL.

Using an NMR-based fragment screen followed by structure-guided drug discovery, Kotschy and colleagues designed the MCL-1 inhibitor S63845, which displays ~20-fold higher affinity to MCL-1 compared to A-1210477 (K_i S63845: <1.2 nM; A-1210477: 28 nM) (Figure 2.7B). A-1210477 was found to bind to serum proteins, whereas S63845 does not. Consequently, S63845 is 1000-fold more potent in killing H929 cells than A-1210477 (227). S63845 binds MCL-1 via a salt bridge between the carboxylic acid and the conserved Arg263, via the trifluoromethyl group in the hydrophobic pocket P4 and deep insertion of 2-fluorofuran into P2 (Figure 2.7C) (257). It mediates apoptosis in a BAX/BAK dependent manner by their displacement from MCL-1. Remarkably, S63845 achieves effects in all tested AML cell lines, almost all MM cell lines and the majority of lymphoma cells lines. Although it is significantly more effective in hematological cancers, S63845 additionally induces cell death in some solid cancer entities as a single agent or combined with

other chemotherapeutic agents. Interestingly, high BCL2L1 (coding for BCL-X_L) levels and loss of BAK were described to be potential causes for resistance. Despite the multifaceted functions of MCL-1 in tissue homeostasis and development, S63845 shows a tolerable *in vivo* treatment profile. Paradoxically, A-1210477 and S63845 increase MCL-1 levels by prolonging protein half-life, probably due to an interference with ubiquitination and proteasomal degradation of MCL-1 (227,255,258). Currently, S63845 demonstrates potent anti-tumor effects either alone or in combination with other BH3 mimetics (mainly ABT-199), chemotherapeutics, kinase inhibitors or bromodomain and extraterminal (BET) inhibitors in numerous cancer entities. Amongst them are: breast cancer, a subset of NSCLC, AML, T-ALL, Mantle cell lymphoma (MCL), pancreatic adenocarcinoma, MM, melanoma, lung squamous cell carcinoma and NB (258-269).

2.3.2.3 The selective BCL-X_L inhibitor A-1331852

The BH3 mimetic A-1331852 was first described by Leverson *et al*. in 2015 and is a highly potent inhibitor of BCL-X_L (K_i: <0.01 nM) (Figure 2.8). It was created using structure based design and can be orally administered. Furthermore, it is 10 - 50-fold more potent than its close relative A-1155463 (270). So far, no crystal structure of A-1331852 binding to BCL-X_L has been published. However, A-1331852 binds presumably to BCL-X_L in a similar way as A-1155463 by engaging the hydrophobic pockets P2 and P4 and building a salt bridge interaction with the conserved Arg139 of BCL-X_L. Notably, A-1331852 harbors a bulky adamantane ring, which inserts into the P4 hydrophobic pocket (232,271).

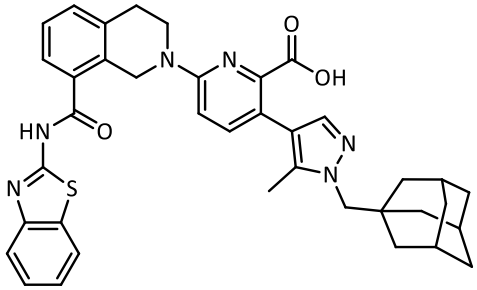

Figure 2.8: Chemical structure of A-1331852.

Obtained from (272).

A-1331852 acts in concert with docetaxel to inhibit tumor growth of NSCLC, breast and ovarian cancer xenografts. In Molt-4 cells, it was found to exert its effect by impairing the interaction between BCL-X_L and BIM (270). Furthermore, A-1331852 demonstrates efficacy both in chronic myelogenous leukemia (CML) in combination with imatinib, dasatinib and nilotinib and in lung squamous cell carcinoma when concomitantly applied with an FGFR inhibitor (269,273). In RMS, A-1331852 potently induces apoptosis together with etoposide or vincristine (274). Moreover, in several soft-tissue sarcoma cell lines, A-1331852 enhances cell death induction of dinaciclib and other conventional chemotherapeutics (275). A recent publication from our group utilizing

A-1331852 provides evidence that BCL-X_L could be a promising target in NB (267). Importantly, S63845 and A-1331852 act together to trigger cell death in pancreatic and colon cancer, NSCLC, melanoma and in squamous cell carcinoma of the head and neck (259,276,277). It has to be noted that, similar to ABT-263, A-1331852 shows senolytic activity, e.g. in cholangiocytes (278).

2.3.3 Application of BH3 mimetics as cancer treatment

The most clinically advanced BH3 mimetics are ABT-199 and ABT-263 (279). In clinical trials, ABT-199 demonstrates powerful effects, especially in relapsed CLL, with response rates of 80% and relatively minor side effects with neutropenia, nausea, diarrhea and upper respiratory tract infection being the most common ones. Its high potency even causes tumor lysis syndrome in some of the patients, which led to a dose escalation treatment schedule (280). Achieving a response rate of ~70%, ABT-199 shows promising effects in elderly AML patients when combined with hypomethylating agents and low-dose cytarabine (281,282). The Food and Drug Administration (FDA) granted ABT-199 the status of a major breakthrough therapy in certain types of relapsed and refractory (R/R) CLL and untreated AML in 2016. It received approval by the FDA and the European Medicines Agency (EMA) for CLL with a 17p chromosomal deletion or TP53 loss and previous unsuccessful therapy as well as for certain types of AML in the elderly (283,284). At present, ABT-199 is evaluated in more than 200 clinical trials as single agent or in combination therapies. Although it is mainly investigated for the treatment of hematological cancers, ABT-199 is getting more and more in the focus for the treatment of solid tumors (e.g. to treat solid tumors in pediatrics and young adults: NCT04029688) (279). However, preclinical data suggests that ABT-199 as a single agent is unlikely to be effective in solid cancers and highlights the requirement of combination therapies (285). Of note, other BCL-2 inhibitors such as S55746 have proceeded into clinical trials for CLL and NHL as well (NCT02920697). ABT-263 demonstrates especially promising effects in combination with rituximab for R/R CLL (286). Like ABT-199, it is now increasingly evaluated for the treatment of solid tumors, e.g. in combination with erlotinib and irinotecan in advanced solid tumors (287,288). Currently, there are no selective BCL-X_L inhibitors utilized in clinical trials (279). During recent years, there has been a boom in clinical trials investigating the effect of MCL-1 inhibitors as cancer regimens. So far, the four MCL-1 inhibitors S64315 (MIK665), AMG176, AZD6991 and ABBV-467 are evaluated in total in seven phase I and/or II clinical trials (NCT03797261, NCT02992483, NCT02979366, NCT0367295 NCT02675452, NCT04178902 and NCT03218683). Studies are conducted exclusively in hematological cancers (mainly MM, R/R lymphoma, DLBCL, AML, myeloplastic syndrome, NHL) and results are eagerly awaited. All of them, except ABBV-467, are investigated as combination therapies with ABT-199 in AML, NHL, DLBCL and other R/R hematological malignancies (NCT03797261, NCT0367295 and NCT03218683). Importantly, the MCL-1 inhibitor S63845 used in this thesis has not yet been evaluated in clinical studies (279).

3 Aim of Study

BH3 mimetics directly activate the apoptotic machinery by targeting anti-apoptotic BCL-2 family proteins. These agents demonstrate encouraging results in early clinical trials. Expression of BCL-2 family members is described to be modified in RMS (Table 2.2) and BCL-2 proteins are critical regulators in the pediatric sarcomas OS and ES (196,213,214,219,222-224). However, compared to other cancer entities, the functional relevance of BCL-2 family proteins in these tumors is not thoroughly investigated.

The overall aim of this study was to assess whether BCL-2 proteins represent promising therapeutic targets in pediatric solid tumors such as RMS, OS and ES. Previous work from our group provided first evidence that treatment with BH3 mimetics might be an efficient strategy to sensitize RMS cells to chemotherapeutics or HDAC inhibitors, respectively (246,274). In this dissertation, we aimed at providing a comprehensive evaluation of the potential of BH3 mimetics as a novel treatment option in pediatric solid tumors with a focus on RMS.

To begin with, we wanted to determine target expression in RMS, OS and ES and additionally investigate whether these cancer entities express the most relevant BCL-2 family members. Next, we were interested whether RMS, OS and ES are sensitive to selective BH3 mimetic treatment as single agents or combined regimens. Using Bliss synergy scoring, we wanted to explore if BH3 mimetics act together to mediate cell death in a synergistic manner. In this context, we sought to determine which BH3 mimetic combination might be most effective in pediatric cancer. Moreover, we intended to utilize available primary samples to confirm our findings in clinically relevant tissues.

In order to unravel the molecular mechanisms behind BH3 mimetic-stimulated cell death, we wanted to elucidate the involvement of the mitochondrial apoptotic pathway. Further, we intended to dissect the respective roles of BAX, BAK and the individual BH3-only proteins. We were particularly interested in alterations in the mutual sequestration patterns of BCL-2 family relatives that might occur upon BH3 mimetic treatment.

Finally, we wanted to provide insights into the translational relevance of BH3 mimetics in RMS. Therefore, we sought to investigate the response of RMS cells arranged as multicellular spheroids and in an *in vivo* embryonic chicken model to BH3 mimetics. Additionally, we wanted to explore if a future clinical application of BH3 mimetic treatment in patients is achievable without undesired toxicity on non-malignant cells by testing the effectiveness of a sequential BH3 mimetic treatment schedule.

4 Material and Methods

4.1 Material

4.1.1 Characteristics of cell lines

In this thesis, we conducted our investigations with commercially available established RMS, OS and ES cell lines (Tables 4.1-4.4). We intended to work with a balanced selection of cells concerning features such as ethnicity, sex, tumor location (primary site vs. metastases) and the underlying molecular background. Importantly, we included cell lines belonging to the embryonal and alveolar subtype of RMS, i.e. fusion-positive and fusion-negative cell lines. Moreover, chosen cell lines harbor mutations and genetic aberrations typical for the respective tumor entity. These are, for instance, overexpression of FGFR4, GLI and MYC as well as mutations in RAS and TP53 for RMS, the presence of EWSR1/FLI1 fusion protein for ES, underexpression of CDKN2A and mutations in TP53 for ES and OS (see Tables 4.1-4.4 for details). It should be noted that RD and TE381.T cells as well as RH30 and RMS13 cells are described to be derived from the same tumor sample, respectively (289,290). Currently, the subtype of the Kym-1 cell line has not been conclusively determined. In the literature, Kym-1 cells have mainly been described as embryonal, however, publications exist claiming them to be alveolar or suggesting to classify them as a malignant rhabdoid tumor instead of RMS (291-295). The fact that they originate from an infant and are negative for the PAX3/FOXO1 fusion gene rather indicates an embryonal subtype. Nevertheless, there is the possibility that they are PAX7/FOXO1 fusion-positive or fusion-negative ARMS, thus their subtype remains controversial. In addition to the established cell lines, we also utilized the primary-derived fusion-positive ARMS cell line CP1, which we cultivated using conventional cell culture and a primary malignant epithelioid mesothelioma that was directly investigated upon surgical resection.

Table 4.1: Characteristics of RMS cell lines.

Cell line	Sub-type	Fusion protein status	Translocation type	TP53 status	Aberrant gene expression (selection)	Origin of the primary tumor sample	Chemotherapy prior to cell line establishment
RH30	ARMS (290)	PAX3/FOXO1 (296)[a]	t(2;13)(p35;q14) (296)	mutated, but functional (297,298)	CDK4↑ (299-301) FGFR4↑ (302) GLI1↑ (302) IGF2R↑ (302) MYCN↑ (302)	16 - 17 years, Caucasian male, bone marrow metastasis (289,290,303)	untreated (290)
RMS13	ARMS (290)	PAX3/FOXO1 (304)[a]	t(2;13)(p35;q14) (304)	mutated, but functional (290,297, 298)	CDK4↑ (305) GLI1↑ (306)	16 - 17 years, Caucasian male, bone marrow metastasis (289,290,303)	untreated (290)
RH41	ARMS (290)	PAX3/FOXO1 (304)[a]	t(2;13)(p35;q14) (304)	deletion (307)	BAD↓ (302) FGFR4↑ (302)	7 years, female, lung metastasis (290)	treated (290)
Kym-1	contro-versial (291-295)	negative[a]	NA	WT (308)	BID↓ (302) CDK4↓ (302) FGFR1↑ (302) GLI1↑ (302) GLI2↑ (302) PMAIP1↓ (302)	9 month, Japanese, neck (309,310)	unknown
RD	ERMS (311)	negative (311)	NA	mutated (297,298)	FGFR1↑ (302) MYC↑ (312) NRAS mutated (20)	7 years, Caucasian female, pelvic mass (311)	treated (Cyclophos-phamide and radiation) (311)
TE381.T	ERMS (289)	ND	ND	ND	NRAS mutated (20)	RD passaged through fetal cat (289)	treated (Cyclophos-phamide and radiation) (311)

T174	ERMS (20)	ND	ND	ND	NRAS mutated (20)	44 years, male (313)	unknown
RH36	ERMS (290)	negative[a]	NA	WT (303)	HRAS mutated (20)	15 years, male, paratesticular relapse (303)	unknown
RH18	ERMS (290,314)	negative[a]	NA	WT (303)	CDK4↑ (302) FGFR4↑ (302) GLI1↑ (302) GLI2↑ (302) MDM2↑ (302,315)	2 years, perineal mass (316)	untreated (316)
TE441.T	ERMS (317)	negative[a]	NA	ND	BID↑ (302) BOK↑ (302) IGF2R↑ (302) PMAIP1↓ (302)	14 years, Black female, buttock (317)	untreated (317)

[a] tested for PAX3/FOXO1 by AG Beat Schäfer (Zurich) by qPCR (2018); NA: not applicable; ND: not determined; ↑: amplification, overexpression; ↓: underexpression

Table 4.2: Characteristics of OS cell lines.

Cell line	TP53 status	Aberrant gene expression (selection)	Origin of the primary tumor sample	Chemotherapy prior to cell line establishment
U2OS	WT (318,319)	CDKN2A↓ (318)	15 years, Caucasian female, tibia (318)	unknown
MG-63	mutated (319)	CDKN2A↓ (302) FGFR4↑ (302) PDGFRA↑ (302)	14 years, Caucasian male, bone (319)	unknown

NA: not applicable; ND: not determined; ↑: amplification, overexpression; ↓: underexpression

Table 4.3: Characteristics of ES cell lines.

Cell line	Fusion protein status	Translocation type	TP53 status	Aberrant gene expression (selection)	Origin of the primary tumor sample	Chemotherapy prior to cell line establishment
SK-ES-1	EWSR1/FLI1 (320)	t(11;22)(p24;q12) (318)	mutated (320-324)	BCL2L11↓ (302) CDKN2A↓ (318)	18 years, male, bone (318)	unknown
A4573	EWSR1/FLI1 (325)	t(11;22)(p24;q12) (325,326)	WT (327)	ND	17 years, female, clavicle (321)	unknown

ND: not determined; ↓: underexpression

Table 4.4: Characteristics of primary (-derived) cell lines.

Cell line	Cancer type	Fusion protein status	Translocation type	Aberrant gene expression (selection)	Origin of the primary tumor sample	Chemotherapy prior to cell line establishment
CP1	ARMS (246)[b]	PAX7/FOXO1 (246)[b]	t(1;13)(p36;q14)	ND	ND	ND
RY240806_4	malignant epithelioid meso-thelioma[b]	NA	NA	ND	pediatric, pelvis[b]	ND

[b] University Clinic Frankfurt am Main, Germany (Sibylle Wehner); NA: not applicable; ND: not determined

4.1.2 Origin of cell lines

All cell lines were authenticated by STR profiling at the Leibnitz Institute, German Collection of Microorganisms and Cell Cultures (Deutsche Sammlung von Mikroorganismen und Zellkulturen (DSMZ)).

4.1.2.1 Cancer cell lines

Table 4.5: Origin of cancer cell lines.

Cell line	Entity	Source
CP1	Primary-derived human ARMS	University Hospital Frankfurt am Main, Germany
RY240806_4	Primary malignant epithelioid mesothelioma	University Hospital Frankfurt am Main, Germany
RH30	Human ARMS	DSMZ
RH30-GFP	Human ARMS	AG Ullrich (University Hospital Frankfurt am Main, Germany)
RH41	Human ARMS	DSMZ
RMS13	Human ARMS	ATCC
Kym-1	Human RMS	JCRB
RD	Human ERMS	ATCC
RD-GFP	Human ERMS	AG Ullrich (University Hospital Frankfurt am Main, Germany)
RH18	Human ERMS	ATCC
RH36	Human ERMS	ATCC
T174	Human ERMS	unknown origin
TE381.T	Human ERMS	ATCC
TE441.T	Human ERMS	ATCC
A4573	Human ES	AG Roessig (WWU Münster, Germany)
SK-ES-1	Human ES	ATCC
MG63	Human OS	AG Nathrath (TUM München, Germany)
U2OS	Human OS	AG Nathrath (TUM München, Germany)

American Type Culture Collection (ATCC); Japanese Collection of Research Bioresources Cell Bank (JCRB)

4.1.2.2 Non-malignant cell lines

Table 4.6: Origin of non-malignant cell lines.

Cell line	Entity/Species	Source
HEK293T	2nd generation retrovirus producer cell line	ATCC
MRC5	Human fibroblasts	DSMZ
C2C12	Murine myoblasts	ATCC
Peripheral blood mononuclear cells (PBMCs)	Human	DRK Blutspendedienst Baden-Württemberg-Hessen gGmbH (Frankfurt am Main, Germany)

4.1.3 Cell culture reagents

Table 4.7: Cell culture reagents.

Reagent	Supplier
Dimethyl sulfoxide (DMSO)	Sigma Aldrich, Darmstadt, Germany
Doxycyclin hydrochloride	Sigma Aldrich, Darmstadt, Germany
Dulbecco's Modified Eagle Medium (DMEM) GlutaMAX™-I	Life Technologies, Darmstadt, Germany
Dulbecco's Phosphate-Buffered Saline (PBS)	Life Technologies, Darmstadt, Germany
Fetal Calf Serum (FCS)	Life Technologies, Darmstadt, Germany/ Biochrom, Berlin, Germany
4-(2-hydroxyehtyl)-1-piperazineethanesulfonic acid (HEPES)	Life Technologies, Darmstadt, Germany
Histopaque®-1077	Sigma Aldrich, Darmstadt, Germany
McCoy's 5A Medium GlutaMAX™-I	Life Technologies, Darmstadt, Germany
Opti-MEM® Transfection Medium	Life Technologies, Darmstadt, Germany
Penicillin/Streptomycin (10,000 U/ml)	Life Technologies, Darmstadt, Germany
Puromycin	Clontech Laboratories, Mountain View, CA, USA
Roswell Park Memorial Institute Medium (RPMI) 1640 GlutaMAX™-I	Life Technologies, Darmstadt, Germany
Sodium Pyruvate (100 mM)	Life Technologies, Darmstadt, Germany
Trypan Blue Solution, 0.4%	Life Technologies, Darmstadt, Germany
Trypsin/EDTA (0.05%), phenol red	Life Technologies, Darmstadt, Germany

4.1.4 Drugs and inhibitors

Table 4.8: Drugs and inhibitors.

Drug	Mode of Action	Supplier
A-1210477	MCL-1 inhibitor	Active Biochem, Bonn, Germany
A-1331852	BCL-X_L inhibitor	Selleck Chemicals, Houston, TX, USA
ABT-199 (Venetoclax)	BCL-2 inhibitor	Selleck Chemicals, Houston, TX, USA
S63845	MCL-1 inhibitor	Apexbio, Houston, TX, USA
zVAD.fmk	Pan-caspase inhibitor	Bachem, Heidelberg, Germany

4.1.5 Antibodies

4.1.5.1 Primary antibodies for Western blotting

Primary antibodies were diluted in 2% BSA in PBS.

Table 4.9: Primary antibodies for Western blotting.

Antibody	Species	Dilution	Supplier
anti-α-Tubulin	Mouse	1:10,000	Calbiochem, Darmstadt, Germany
anti-β-Actin	Mouse	1:10,000	Sigma Aldrich, Darmstadt, Germany
anti-BAK	Rabbit	1:1000	Merck Millipore, Darmstadt, Germany
anti-BAX	Rabbit	1:1000	Cell Signaling, Beverly, MA, USA
anti-BCL-2	Mouse	1:1000	Dako, Santa Clara, CA, USA
anti-BCL-X_L	Rabbit	1:1000	Cell Signaling, Beverly, MA, USA
anti-BIM	Rabbit	1:500	Cell Signaling, Beverly, MA, USA
anti-BMF	Rat	1:500	Enzo, Lörrach, Germany
anti-Caspase-3	Rabbit	1:1000	Cell Signaling, Beverly, MA, USA
anti-Caspase-8	Mouse	1:1000	Enzo, Lörrach, Germany
anti-Caspase-9	Rabbit	1:1000	Cell Signaling, Beverly, MA, USA
anti-GAPDH	Mouse	1:5000	HyTest, Turku, Finland
anti-MCL-1	Rabbit	1:1000	Enzo, Lörrach, Germany
anti-NOXA	Mouse	1:1000	Enzo, Lörrach, Germany
anti-PARP cleaved	Mouse	1:1000	Cell Signaling, Beverly, MA, USA
anti-PUMA	Rabbit	1:500	Cell Signaling, Beverly, MA, USA

4.1.5.2 Secondary antibodies for Western blotting

Secondary horse radish peroxidase (HRP)-conjugated antibodies were diluted in 5% milk in PBS-T. Secondary infrared (IR)Dye-conjugated antibodies were diluted in 2% BSA in PBS.

Table 4.10: Secondary antibodies for Western blotting.

Antibody	Species	Dilution	Supplier
HRP-conjugated anti-mouse IgG	Goat	1:5000	Abcam, Cambridge, UK
HRP-conjugated anti-rabbit IgG	Goat	1:10,000	Abcam, Cambridge, UK
HRP-conjugated anti-rat IgG	Goat	1:5000	Abcam, Cambridge, UK
IRDye800-conjugated anti-rabbit IgG	Donkey	1:10,000	LI-COR, Bad Homburg, Germany
IRDye680-conjugated anti-mouse IgG	Donkey	1:10,000	LI-COR, Bad Homburg, Germany

4.1.5.3 Primary antibodies for immunoprecipitation

Table 4.11: Primary antibodies for immunoprecipitation.

Antibody	Species	Supplier
anti-BAK clone AB-1	Mouse	Calbiochem, Darmstadt, Germany
anti-BAK	Rabbit	Abcam, Cambridge, UK
anti-BAX clone 6A7	Mouse	Sigma Aldrich, Darmstadt, Germany
anti-BAX	Rabbit	BD Biosciences, Heidelberg, Germany
anti-BCL-2	Hamster	BD Biosciences, Heidelberg, Germany
anti-BCL-X_L	Rabbit	Abcam, Cambridge, UK
anti-MCL-1	Rabbit	Enzo, Lörrach, Germany

4.1.5.4 Fluorescent dyes

Table 4.12: Fluorescent dyes.

Antibody	Working dilution	Supplier
Annexin V-FITC	0.1 µl/sample	University of Leicester/ In-house production
CellEvent™ Caspase-3/7 Activity Green Detection Kit	2 µM	Life Technologies, Darmstadt, Germany
Hoechst 33342	1 µg/ml	Sigma Aldrich, Darmstadt, Germany
Propidium iodide (PI)	1 µg/ml	Sigma-Aldrich, Darmstadt, Germany
Tetramethylrhodamine methylester (TMRM)	100 ng/ml	Sigma-Aldrich, Darmstadt, Germany

4.1.5.5 Primary antibodies for immunohistochemistry

Table 4.13: Secondary antibodies for immunohistochemistry.

Antibody	Working dilution	Species	Supplier
Anti-cleaved caspase-3 (Asp175)	1:300 in SignalStain antibody diluent	Rabbit	Cell Signaling, Danvers, MA, USA

4.1.6 Plasmids

Table 4.14: List of plasmids.

Vector backbone	Origin
pLentiCRISPRv2	Addgene #52961
pMD2.G	Addgene #12259
psPAX2	Addgene #12260

4.1.7 Guide RNAs (gRNA)

Table 4.15: List of gRNAs.

gRNA	Target	Sequence code
BAK #1	BAK	CACCGGTAGACGTGTAGGGCCAGA
BAK #2	BAK	CACCGCTCACCTGCTAGGTTGCAG
BAK #3	BAK	CACCGAAGACCCTTACCAGAAGCAG
Non-human target (NHT) #1	eGFP	GGAGCGCACCATCTTCTTCA
Non-human target (NHT) #2	eGFP	GGCCACAAGTTCAGCGTGTC
Non-human target (NHT) #3	eGFP	GGGCGAGGAGCTGTTCACCG

4.1.8 Small-interfering RNA (siRNA)

All siRNAs were purchased from Thermo Fisher Scientific as Silencer® Select siRNA and prepared to a stock solution of 20 µM.

Table 4.16: List of siRNAs.

siRNA	Target	Sequence code	siRNA concentration used in RD cells	siRNA concentration used in Kym-1 cells
siBAK#1	BAK	s1880	20 nM	50 nM
siBAK#2	BAK	s1881	20 nM	50 nM
siBAX#1	BAX	s1888	20 nM	50 nM
siBAX#2	BAX	s1890	20 nM	50 nM

siBCL-X#1	BCL-X_L	s1920	20 nM	50 nM
siBCL-X#2	BCL-X_L	s1921	20 nM	50 nM
siBIM#1	BIM	s195011	10 nM	50 nM
siBIM#2	BIM	s195012	10 nM	50 nM
siBIM#3	BIM	s223065	10 nM	50 nM
siBMF#1	BMF	s40385	10 nM	50 nM
siBMF#2	BMF	s40387	10 nM	50 nM
siCtrl	non-targeting control	4390843	10-40 nM	50-100 nM
siMCL-1#1	MCL-1	s8383	20 nM	50 nM
siMCL-1#2	MCL-1	s8385	20 nM	50 nM
siNOXA#1	NOXA	s10708	10 nM	50 nM
siNOXA#2	NOXA	s10709	10 nM	50 nM
siPUMA#1	PUMA	s25840	10 nM	50 nM
siPUMA#2	PUMA	s25842	10 nM	50 nM
siPUMA#3	PUMA	s25841	10 nM	50 nM

4.1.9 Primer sequences for qPCR

Table 4.17: List of Primer sequences.

Target	Primer sequence forward	Primer sequence reverse
28S	TTGAAAATCCGGGGGAGAG	ACATTGTTCCAACATGCCAG
BMF	GAGACTCTCTCCTGGAGTCACC	CTGGTTGGAACACATCATCCT
GAPDH	CAAGGTCATCCATGACAATTTG	GGGTCCAAGTTGTCCAGAATGC

4.1.10 Chemicals and compounds

Table 4.18: List of chemicals and compounds.

Chemical/Compound	Supplier
2-propanol	Carl Roth, Karlsruhe, Germany
Acetic acid	Carl Roth, Karlsruhe, Germany
Acrylamide mix, 30% (Rotiphorese)	Carl Roth, Karlsruhe, Germany
Albumin fraction V (BSA)	Carl Roth, Karlsruhe, Germany
Ammonia solution, 32%	Carl Roth, Karlsruhe, Germany
Ammonium persulfate (APS)	Carl Roth, Karlsruhe, Germany
β-Glycerophosphate	Sigma-Aldrich, Darmstadt, Germany
Bromophenolblue	Carl Roth, Karlsruhe, Germany
Calcium chloride ($CaCl_2$)	Carl Roth, Karlsruhe, Germany

Cholamidopropyldimethyl ammonio propane sulfonate (CHAPS)	Sigma-Aldrich, Darmstadt, Germany
Citric acid, anhydrous	Carl Roth, Karlsruhe, Germany
Dihydro threitol (DTT)	Millipore, Darmstadt, Germany
Dimethyl sulfoxide (DMSO)	Sigma-Aldrich, Darmstadt, Germany
Disodium phosphate (Na_2HPO_4)	Carl Roth, Karlsruhe, Germany
Eosin Y	Sigma-Aldrich, Darmstadt, Germany
Ethanol	Carl Roth, Karlsruhe, Germany
Ethylene diamine tetraacetic acid (EDTA)	Carl Roth, Karlsruhe, Germany
Formaldehyde	Carl Roth, Karlsruhe, Germany
Glycerol	Carl Roth, Karlsruhe, Germany
Glycine	Carl Roth, Karlsruhe, Germany
Hematoxylin solution	Carl Roth, Karlsruhe, Germany
Hexadimethrine bromide (polybrene)	Carl Roth, Karlsruhe, Germany
Hydrochlorid acid (HCl)	Carl Roth, Karlsruhe, Germany
Hydrogen peroxide (H_2O_2, 30%)	Carl Roth, Karlsruhe, Germany
Hydroxyethyl piperazinylethane sulfonic acid (HEPES)	Carl Roth, Karlsruhe, Germany
Magnesium chloride ($MgCl_2$)	Carl Roth, Karlsruhe, Germany
Methanol	Carl Roth, Karlsruhe, Germany
Milk powder	Carl Roth, Karlsruhe, Germany
Paraffin	Carl Roth, Karlsruhe, Germany
Paraformaldehyde	Carl Roth, Karlsruhe, Germany
Phenylmethylsulfonyl fluoride (PMSF)	Carl Roth, Karlsruhe, Germany
Potassium chloride (KCl)	Carl Roth, Karlsruhe, Germany
Potassium dihydrogen phosphate (KH_2PO_4)	Carl Roth, Karlsruhe, Germany
Sodium chloride (NaCl)	Carl Roth, Karlsruhe, Germany
Sodium dodecyl sulfate (SDS)	Carl Roth, Karlsruhe, Germany
Sodium fluoride	Sigma-Aldrich, Darmstadt, Germany
Sodium hydroxide (NaOH)	Carl Roth, Karlsruhe, Germany
Sodium orthovanadate	Sigma-Aldrich, Darmstadt, Germany
Tetramethylethylenediamine (TEMED)	Carl Roth, Karlsruhe, Germany
TrisBase	Carl Roth, Karlsruhe, Germany
TrisHCl	Carl Roth, Karlsruhe, Germany
Trisodium citrate dihydrate ($Na_3C_6H_5O_7$)	Carl Roth, Karlsruhe, Germany
Triton X-100	Carl Roth, Karlsruhe, Germany
Tween 20	Carl Roth, Karlsruhe, Germany
Xylol	Carl Roth, Karlsruhe, Germany

4.1.11 Buffers

Table 4.19: List of buffers.

Buffer	Ingredients
Annexin V binding buffer	10 mM HEPES pH 7.4, 150 mM NaCl, 5 mM KCl, 1 mM $MgCl_2$, 1.8 mM $CaCl_2$
Blocking buffer (5% milk powder in PBS-T)	5 g milk powder in 100 ml PBS-T
Blotting buffer, 1x	5.8 g/l TrisBase, 2.9 g/l Glycine, 0.04% SDS, 20% Methanol
CHAPS lysis buffer	10 mM HEPES, 150 mM NaCl, 1% CHAPS, pH 7.4
Citrate buffer	10 mM citric acid, 0.05% Tween 20, pH 6.0
Nicoletti buffer	0.05% Trisodium citrate dehydrate pH 7.4, 0.05% Triton X-100, 10% Glycerol, 50 mg/ml Propidium iodide
Peroxidase quenching solution	1 ml 30% H_2O_2 in 9 ml methanol
Phosphate-buffered saline (PBS), 10x	80 g/l NaCl, 2 g/l KCl, 2 g/l KH_2PO_4, 14.4 g/l Na_2HPO_4, pH 7.4
PBS-T	1x PBS, 0.1% Tween20
SDS Running buffer, 5x	15.1 g/l TrisBase, 94 g/l Glycin, 0.5% SDS
SDS Loading Dye, 6x	360 mM TrisBase pH 6.8, 30% Glycerol, 10% SDS, 93 mg/ml DTT, 0.12 mg/ml Bromophenol blue
Triethanolamine (TEA) buffer	0.2 M Triethanolamine in ddH_20, pH 8.2
Tris buffer	50 mM TrisBase in ddH_20, pH 7.5
Triton X-100 lysis buffer	30 mM TrisHCl, 150 mM NaCl, 10% Glycerol, 0.5 mM PMSF, 2 mM DTT, 1% Triton X-100, 1x cOmplete (Roche)

4.1.12 Reagents and kits

Table 4.20: List of reagents and kits.

Reagent/Kit	Supplier
10% normal goat serum, ready-to-use	Life Technologies, Darmstadt, Germany
CellTiter-Glo® Luminescent Cell Viability Assay	Promega, Mannheim, Germany
cOmplete Protease Inhibitor Cocktail (PIC), 25x	Roche Diagnostics, Mannheim, Germany
Dynabeads™ anti-mouse IgG	Life Technologies, Darmstadt, Germany
Dynabeads™ Protein G	Life Technologies, Darmstadt, Germany
Entellan, mounting medium	Merck, Darmstadt, Germany
FACS Clean/Rinse solution	BD Bioscience, Heidelberg, Germany
FACS Flow sheath fluid	BD Bioscience, Heidelberg, Germany
FACS Shutdown solution	BD Bioscience, Heidelberg, Germany

FuGENE® HD Transfection Reagent	Promega, Mannheim, Germany
Histostain-Plus IHC Kit, AEC, broad spectrum	Life Technologies, Darmstadt, Germany
Lipofectamine RNAiMAX	Life Technologies, Darmstadt, Germany
Matrigel, phenol-red free	BD Bioscience, Heidelberg, Germany
Neon® Transfection System 100 µl Kit	Thermo Fisher Scientific, Roskilde, Denmark
PageRuler™ Plus Prestained Protein Ladder	Thermo Fisher Scientific, Roskilde, Denmark
PEQ-Gold total RNA kit	PEQLAB, Erlangen, Germany
Pierce BCA Protein Assay	Thermo Fisher Scientific, Roskilde, Denmark
Pierce ECL Western Blotting Substrate	Thermo Fisher Scientific, Roskilde, Denmark
RevertAid First Strand cDNA Synthesis Kit	Thermo Fisher Scientific, Roskilde, Denmark
ROENTOROLL HC X-Ray Developer	TETENAL, Norderstedt, Germany
SignalStain antibody diluent	Cell Signaling, Danvers, MA, USA
SUPERFIX MRP X-Ray Fixer	TETENAL, Norderstedt, Germany
SYBR Green Master Mix	Thermo Fisher Scientific, Roskilde, Denmark

4.1.13 Consumables

Table 4.21: List of consumables.

Material	**Supplier**
Aluminum foil	Carl Roth, Karlsruhe, Germany
Cell culture dishes (6 cm, 10 cm or 14.5 cm)	Greiner Bio-One, Frickenhausen, Germany
Cell culture flasks (25 cm^2, 75 cm^2, 175 cm^2)	Greiner Bio-One, Frickenhausen, Germany
Cell culture plates (96-well (transparent and white), 24-well, 6-well)	Greiner Bio-One, Frickenhausen, Germany
Cell scraper	BD Bioscience, Heidelberg, Germany
Combitips (all sizes, (un)sterile)	Eppendorf, Hamburg, Germany
Centrifuge tubes (15 ml, 50 ml)	Greiner Bio-One, Frickenhausen, Germany
Corning® Costar® Ultra-low attachment 96-well plate (round bottom)	Sigma-Aldrich, Darmstadt, Germany
Cover glass (24x50 mm)	VWR, Deisenhofen, Germany
Cover slips (15 mm in diameter)	VWR, Deisenhofen, Germany
Cryogenic vials (1.8 ml)	Starlab, Hamburg, Germany

Disposal bags	Carl Roth, Karlsruhe, Germany
Filter tips (10 µl, 200 µl, 1000 µl)	Starlab, Hamburg, Germany
Filter paper	Carl Roth, Karlsruhe, Germany
Hybond ECL nitrocellulose membrane	GE Healthcare, Buckinghamshire, UK
Hyperfilm ECL	GE Healthcare, Buckinghamshire, UK
Leukosilk® tape	BSN Medical, Hamburg, Germany
MicroAMP™ optical reaction plate (96-well)	Thermo Fisher Scientific, Roskilde, Denmark
Microcentrifuge tubes (all sizes, (un)sterile)	Starlab, Hamburg, Germany
Nitrile gloves, sterile, powder-free	Starlab, Hamburg, Germany
Parafilm	VWR, Deisenhofen, Germany
Pasteur pipettes (15 cm, 30 cm)	Carl Roth, Karlsruhe, Germany
PCR tubes	Starlab, Hamburg, Germany
Pipette tips (all sizes, (un)sterile)	Starlab, Hamburg, Germany
Round-bottom tubes	BD Bioscience, Heidelberg, Germany
Scalpels	B. Braun, Melsungen, Germany
Slides, X-tra adhesive/positive charged	Leica Biosystems, Wetzlar, Germany
Sterile filters (0.22 µm, 0.45 µm)	Merck Millipore, Darmstadt, Germany
Sterile pipettes (2 ml, 5 ml, 10 ml, 25 ml)	Greiner Bio-One, Frickenhausen, Germany
Syringes (5 ml)	BD Bioscience, Heidelberg, Germany
Whatman paper	Thermo Fisher Scientific, Roskilde, Denmark

4.1.14 Equipment and instruments

Table 4.22: List of equipment and instruments.

Equipment/Instrument	**Supplier**
Airflow-Control	ARGE Labor, Wathlingen, Germany
ARE heating magnetic stirrer	VELP Scientifica, Usmate, Italy
Avanti J-26 XP ultracentrifuge	Beckman Coulter, Krefeld, Germany
Centrifuge MIKRO 200 R	Hettich, Baden-Baden, Germany
Centrifuge ROTIXA 50 RS	Hettich, Baden-Baden, Germany
Centrifuge ROTANTA 460 R	Hettich, Baden-Baden, Germany
CO_2 incubator	SANYO, Wehr, Germany
Dispenser	Eppendorf, Hamburg, Germany
Easypet® (3)	Eppendorf, Hamburg, Germany
Electronic analytical balance EW	Kern, Balingen, Germany
Electronic precision balance 770	Kern, Balingen, Germany
FACSCanto II	BD Bioscience, Heidelberg, Germany

Freezer (-20°C)	EWALD Innovationstechnik, Bad Nenndorf, Germany
Freezer (-80°C)	SANYO, Wehr, Germany
Fridge (+4°C)	EWALD Innovationstechnik, Bad Nenndorf, Germany
Food Steamer	Braun (P&G Germany), Schwalbach am Taunus, Germany
Gel chambers, glass plates and additional chamber material	Bio-Rad Laboratories, München, Germany
Heating block	Eppendorf, Hamburg, Germany
HeraSafe class II biological safety cabinet	Kendro, Langenselbold, Germany
Humidified staining chamber	Simport Scientific, Saint-Mathieu-de-Beloeil, Canada
ImageXpress Micro XLS system	Molecular Devices, Sunnyvale, CA, USA
Infinite M100 microplate reader	Tecan, Crailsheim, Germany
Inolab© pH7310 pH meter	WTW, Weilheim, Germany
Leica confocal laser scanning microscope	Leica Biosystems, Wetzlar, Germany
Magnetic rack	AMS Biotechnology Ltd, Abington, UK
Mastercycler® pro	Eppendorf, Hamburg, Germany
Microcentrifuge	Benning, Bocholt, Germany
Microscope CK X41, cell culture	Olympus, Hamburg, Germany
Microscope CK 41, histology	Olympus, Hamburg, Germany
Microscope IX71, fluorescence	Olympus, Hamburg, Germany
Mini-PROTEAN Tetra cell electrophoresis system	Bio-Rad Laboratories, München, Germany
Multipette® plus	Eppendorf, Hamburg, Germany
Nalgene® Mr Frosty freezing container	Sigma-Aldrich, Darmstadt, Germany
NanoDrop 1000 sprectrophotometer	PEQLAB, Erlangen, Germany
Neon Transfection System	Thermo Fisher Scientific, Roskilde, Denmark
Neubauer improved counting chamber	Carl Roth, Karlsruhe, Germany
Odyssey infrared imaging system	LI-COR, Bad Homburg, Germany
PerfectBlue™ Dual Gel Twin L electrophoresis system	PEQLAB, Erlangen, Germany
Pipettes Research plus (2.5 µl, 10 µl, 20 µl, 100 µl, 200 µl, 1000 µl)	Eppendorf, Hamburg, Germany
Power Pac™ HC high-current power supply	Bio-Rad Laboratories, München, Germany
QuantStudio 7 Flex Real-time PCR system	Applied Biosystems, Darmstadt, Germany
Rocking shaker	MS-L, Wiesloch, Germany

Roller mixer	Ratek, Victoria, Australia
SANYO incubator MIR-262	New Brunswick Scientific, Edison, NJ, USA
Spinning wheel	MS-L, Wiesloch, Germany
Sunrise microplate reader	Tecan, Crailsheim, Germany
Thermomixer comfort	Eppendorf, Hamburg, Germany
Trans-Blot® SD semi-dry transfer cell	Bio-Rad Laboratories, München, Germany
V-15 autoclave	SysTec, Bergheim-Glessen, Germany
Vacuum pump HLC	Ditabis, Pforzheim, Germany
Vortex mixer (ZX classic, wizard X)	VELP Scientifica, Usmate, Italy
Water bath SWB20	Medingen, Arnsdorf, Germany
X-Ray cassette type G	Rego X-Ray, Augsburg, Germany

4.1.15 Software

Table 4.23: List of software.

Software	Version	Company
Applied Biosystems Quantstudio™	1.3	Thermo Fisher Scientific, Roskilde, Denmark
EndNote	X7.4	Thomson Reuters, Toronto, Canada
FACSDiva™	6.1.3	BD Bioscience, Heidelberg, Germany
GraphPad Prism®	5.02	GraphPad Software, San Diego, CA, USA
Tecan i-control	1.10	Tecan, Crailsheim, Germany
ImageJ	1.52e	National Institute of Health, USA
Image Studio	3.1.4	LI-COR, Bad Homburg, Germany
Magellan™ Data Analysis Software	7.2	Tecan, Crailsheim, Germany
MetaXpress®	5.1.0.41	Molecular Devices, Sunnyvale, CA, USA
MS-Office	2013, 2016	Microsoft Deutschland GmbH
NanoDrop Software	3.8.1	PEQLAB, Erlangen, Germany
PyMOL	2.3.4	Schrödinger LLC, Germany
SynergyFinder	1.0	Institute for Molecular Medicine Finland (FIMM), Helsinki, Finland

4.1.16 Fertilized chicken eggs

Fertilized chicken eggs that were utilized in the chorioallantoic membrane (CAM) assay were supplied by LSL Rhein-Main Geflügelvermehrungsbetriebe GmbH & Co.KG, Dieburg, Germany.

4.2 Methods

4.2.1 Cell culture

All cell lines and primary cells were cultivated at 37 °C in a humidified atmosphere containing 5% CO_2. All cell lines were authenticated by STR profiling. Absence of mycoplasma contamination was confirmed by regular PCR testing.

4.2.1.1 Cultivation of cells

RH30, RMS13, Kym-1, RH41, A4573 cells, PBMCs and primary-derived CP1 cells were cultivated in RPMI 1640 GlutaMAX™-I supplemented with 10% fetal calf serum (FCS), 1% Penicillin/Streptomycin and 1 mM sodium pyruvate. Kym-1 cells were additionally supplemented with 1% HEPES. RD, TE381.T, RH36, TE441.T, RH18, T174, SK-ES-1, U2OS, MG-63, MRC5, C2C12 and HEK293T cells were cultured in DMEM GlutaMAX™-I supplemented with 10% fetal calf serum (FCS), 1% Penicillin/Streptomycin and 1 mM sodium pyruvate. RH18 cells were additionally supplemented with 20% FCS. Cells were passaged twice a week when they were 80 - 90% confluent. Therefore, medium was aspirated, cells were washed with pre-warmed PBS and were then detached by use of Trypsin/EDTA dissociation reagent for 5 min at 37°C and 5% CO_2 atmosphere. Subsequently, trypsination was inhibited by addition of culture medium and cells were split at a ratio of 1:3 to 1:12, depending on the cell line and confluency, into a new cell culture flask for further culturing. Cell culture was terminated when cells reached passage 30 - 35. The primary sample RY240806_4 was not cultivated as conventional cell culture but cells were seeded in RPMI 1640 GlutaMAX™-I supplemented with 10% fetal calf serum (FCS), 1% Penicillin/Streptomycin and 1 mM sodium pyruvate directly upon resection. Similarly, pellets for Western blotting were frozen directly upon resection. This was done to instantaneously investigate the effect of BH3 mimetics using as freshly isolated cells as possible.

4.2.1.2 Freezing and thawing of cells

For long-term storage, cells were centrifuged at 1800 rpm for 5 min at room temperature (RT). The cell pellet was resuspended in medium supplemented with 10% DMSO and aliquoted into cryogenic vials. Cryogenic vials were cooled down to -80°C in a Mr.Frosty™ containing isopropanol overnight and were stored at -80°C for long-term preservation. To defrost cryopreserved cells, a previously frozen cryogenic vial was heated to 37°C in a water bath and the cell suspension was added to 10 ml of pre-warmed culture medium. After centrifugation at 1800 rpm for 5 min at RT cells were resuspended in culture medium and cultivated in culture flasks as described above.

4.2.1.3 Isolation of PBMCs

PBMCs were isolated from buffy coats of healthy donors by separation by Histopaque®-1077. Therefore, whole blood from the buffy coat was carefully added on top of 15 ml of Histopaque®-1077 and the solution was centrifuged for 30 min at 1200 rpm at 20°C (centrifuge

acceleration=1; centrifuge break=1). The layer containing PBMCs was diluted in pre-warmed medium, centrifuged for 10 min at 200 rpm at 20°C and the pellet was resuspended in medium. PBMCs were immediately seeded and treated for experiments.

4.2.1.4 Plating of cells *in vitro*

To prevent overgrowth of cells during experiments, cells were seeded at an appropriate density. Generally, all cell lines were seeded at a density of 30,000 cells/cm^2 for 24 h of treatment, 20,000 cells/cm^2 for 48 h of treatment and 10,000 cells/cm^2 for 72 h of treatment. RH18 cells were seeded at a density of 50,000 cells/cm^2, TE441.T at a density of 60,000 cells/cm^2, C2C12 cells at a density of 1000 cells/cm^2 and CP1 cells at a density of 500 cells/cm^2 for 48 h of treatment. For immunoprecipitation experiments, cells were seeded at a density of 30,000 cells/cm^2. For protein and RNA analysis, cells were seeded at a density of 30,000 - 40,000 cells/cm^2 for 24 h until harvesting of cells and at 20,000 cells/cm^2 for later time points. For plating of cells, medium was aspirated and the remaining medium was removed by washing the cells with pre-warmed PBS. Subsequently, cells were detached using pre-warmed Trypsin/EDTA dissociation reagent for 5 min at 37°C and 5% CO_2-atmosphere. Fresh pre-warmed medium was added to the detached cells in order to block the trypsination and the number of viable cells per ml was counted by a Neubauer improved cell counting chamber. Dead cells were excluded by the use of Trypan Blue. Subsequently, an appropriate volume of the cell suspension was diluted in fresh medium to yield the desired cell density for seeding depending on the experimental design and time point of treatment. Cells were incubated for approximately 24 h before treatment was applied.

4.2.1.5 Generation of multicellular spheroids

For spheroid generation cells were counted as described in 4.2.1.4 and, depending on the experimental setting and cell line, 1000 - 10,000 cells/well were seeded in a round bottom ultra-low attachment 96-well plate. Cells were centrifuged for 10 min at 2020 rpm at 37°C (break=1). Spheroids were allowed to form for 3 days before treatment was applied. Cautious medium change was achieved by replacing half of the medium or adding fresh medium on top of the consumed medium every 3 - 4 days.

4.2.1.6 Treatment of cells *in vitro*

In order to treat cells with drugs and/or inhibitors, medium was aspirated and fresh pre-warmed medium containing the indicated drug and/or inhibitor concentration was applied to the respective cell culture plates or dishes for indicated time points. For pre-treatment of the cells or for treatment of spheroids, substances were added in definite higher concentrations to the medium. This ensured that the desired final concentration of the treatment was achieved.

4.2.2 Transfection techniques

In order to transiently knockdown proteins, cells were transfected with siRNA either by reverse RNAiMAX transfection (RD cells) or by electroporation (Kym-1 cells). As the transfection procedure increases cell death, RD cells were seeded at a density of 30,000 cells/cm^2 and Kym-1 cells were seeded at a density of 40,000 cells/cm^2.

4.2.2.1 Reverse RNAiMAX® transfection

For reverse transfection of cells, Opti-MEM® and Lipofectamine RNAiMAX® were utilized in amounts as indicated by the manufacturer. Lipofectamine RNAiMAX® or Silencer® Select siRNA at indicated concentrations (see 4.1.7) were prediluted in Opti-MEM®. The Lipofectamine RNAiMAX® mix and the Silencer® Select siRNA mix were merged by pipetting up and down thoroughly. After incubation for 10 - 15 min at RT the transfection mix was distributed in culture dishes or plates depending on the experimental design. Subsequently, cells suspended in culture medium were added at the appropriate density to the transfection mix. Medium change was conducted 6 h later in order to minimize toxic effects mediated by Lipofectamine RNAiMAX®. Knockdown efficiency was confirmed by Western Blotting or qRT-PCR (for BMF).

4.2.2.2 Electroporation

In order to transfect cells with siRNA by electroporation, an appropriate amount of cells to achieve the desired final cell density of 40,000 cells/cm^2 were washed with pre-warmed PBS. Next, cells were resuspended in Resuspension buffer R (from Neon® Transfection System 100 µl Kit) and for each individual sequence of Silencer® Select siRNA 100 µl of the cell suspension was added to the respective Silencer® Select siRNA at indicated concentrations (see 4.1.7). After the suspension was thoroughly mixed, electroporation was performed utilizing a Neon® transfection system with 1200 V, 20 ms and 2 pulses. Subsequently, cells were transferred into pre-warmed medium without Penicillin/Streptomycin and, depending on the experimental setting, further diluted to achieve the desired final cell density before they were seeded in culture dishes or plates. Knockdown efficiency was confirmed by Western Blotting or qRT-PCR (for BMF).

4.2.2.3 Transfection with FuGENE® HD Transfection Reagent

Transfections with FuGENE® HD Transfection Reagent were performed to produce virus supernatant and generate BAK KO cells utilizing Clustered Regularly Interspaced Short Palindromic Repeats (CRISPR) associated protein 9 (CAS9) (4.2.3.1).

4.2.3 Generation of genetically modified cell lines

4.2.3.1 CRISPR/CAS9

CRISPR/CAS9 was utilized to generate BAK KO cells. Therefore, virus was produced to enable lentiviral transduction of target cells. First, HEK293T cells were seeded in 6-well plates (4.2.1.4) in DMEM without Penicillin/Streptomycin. On the next day, cells were co-transfected with 1.1 µg of each pLentiCRISPRv2-BAKgRNA #1-3 or NHT#1-3 (4.1.6 and 4.1.7) as well as with 1 µg pMD2.G and 2.7 µg psPAX2 in a total volume of 200 µl Opti-MEM®. FuGENE® HD Transfection Reagent was added to the Opti-MEM®/plasmid mix in a ratio of 1:3. After 15 min incubation at RT the transfection mix was added dropwise to the HEK293T cells. On day 3 medium was discarded and fresh Penicillin/Streptomycin containing medium was added to the cells. Viral particle containing supernatant was collected on day 4 and 5, pooled and filtered through a 0.45 µm filter. Until further use virus supernatant was snap-frozen in liquid nitrogen and stored at -80°C.

The above described procedure was performed by Lisa Kowald and Meike Vogler.

For target cell transduction, RD and Kym-1 cells were seeded in 6-well plates at a density of 10,000 cells/cm^2. On the next day, 8 µg/ml polybrene followed by 500 µl virus-containing supernatant were added per well and the cells were incubated with the virus-containing supernatant for 72 h. Then transduction medium was discarded and replaced by fresh DMEM containing puromycin (RD cells: 1 µg/ml puromycin, Kym-1 cells: 10 µg/ml puromycin) serving as selection medium. Cells were selected using puromycin until all cells of the untreated control were dead. Single clones were seeded in conditioned media (10% sterile-filtered medium from a dense grown RD or Kym-1 cell culture, respectively, and 90% fresh medium) and were expanded. KO efficacy was determined by Western blotting and Sanger DNA sequencing conducted by LGC Genomics GmbH, Berlin.

4.2.4 Cell death and cell viability measurements

4.2.4.1 Determination of cell death using PI staining

Loss of cell membrane integrity is a characteristic feature of cell death and can be displayed by the uptake of propidium iodide (PI) which is a DNA intercalating dye unable to pass intact cell membranes. PI/Hoechst-33342 co-staining was used to assess cell membrane integrity and thereby to determine cell death. Therefore, cells were seeded in 96-well plates (4.2.1.4 and 4.2.1.5) and treated as indicated (4.2.1.6). In order to co-stain cells, PI and Hoechst-33342 were pre-diluted in PBS and administered to the cells at a final concentration of 1 µg/ml each for 5 - 10 min at 37°C in a 5% CO_2-atmosphere. ImageXpress® Micro XLS System (4x objective) was utilized to measure PI positive cells (using tetramethylrhodamine (TRITC) channel) and Hoechst-33342 positive cells (using 4′,6-Diamidin-2-phenylindol (DAPI) channel) according to the manufacturer‘s instructions. “Cell Scoring” application of MetaXpress® analysis software was used to quantify the frequency of

PI positive cells related to Hoechst-33342 positive cells. To determine cell death in spheroids, treatment was applied for 48 h on day 3 upon seeding. Then, PI and/or Hoechst-33342 were utilized at a final concentration of 2 µg/ml and an incubation time of 30 – 60 min. Imaging and analysis was performed as described in 4.2.5.

4.2.4.2 Determination of cell death using DNA fragmentation

In order to measure DNA fragmentation as a characteristic apoptosis marker, cells were seeded in 24-well plates (4.2.1.4) and treated as indicated (4.2.1.6). Cells were harvested at indicated time points upon treatment by transferring the supernatant containing detached cells into round-bottom tubes. Further, attached cells were incubated with Trypsin/EDTA dissociation solution for 5 min at 37°C in a 5% CO_2-atmosphere, rinsed with ice-cold PBS and added to the corresponding supernatant. After cells were centrifuged at 1800 rpm for 5 min at 4°C the supernatant was discarded and the pellet was washed with ice-cold PBS followed again by centrifugation at 1800 rpm for 5 min at 4°C. Next, the supernatant was decanted and the pellet was resuspended in 50 - 100 µl Nicoletti buffer containing Triton X to allow whole DNA staining by PI in cells with still intact cell membranes. Cells were incubated in Nicoletti buffer for 30 - 60 min at 4°C in the dark and then subjected to flow cytometry. Forward scatter (FSC)/ side scatter (SSC) pre-gating was utilized to exclude cell debris. The amount of nuclear DNA fragmented cells was quantified by analysis of the hypodiploid (SubG1) cell population in a histogram of the PE channel (328).

4.2.4.3 Determination of cell death using Annexin V/ PI co-staining

The exposure of PS on the cell membrane is a feature of early apoptosis and can be measured by the binding of fluorescein isothiocyanate (FITC)-conjugated Annexin V to PS in flow cytometry (329). To this end, cells were seeded in 24-well plates (4.2.1.4) and treated as indicated (4.2.1.6). Next, cells were harvested as described in 4.2.4.2 and each sample was resuspended in 50 - 100 µl of Annexin V/PI master mix (100 µl Annexin V binding buffer, 0.03 µl Annexin V-FITC, 5 µl 50 µg/ml PI). After 10 min incubation at RT, cells were analyzed by flow cytometry. FSC/SSC pre-gating was utilized to exclude cell debris. Early-apoptotic (Annexin V+/PI-) and late-apoptotic (Annexin V+/PI+) cell populations were summarized as Annexin V+ cells.

4.2.4.4 Determination of cell viability using CellTiter-Glo® (CTG)

To determine cell viability, we utilized a CellTiter-Glo® Luminescent Cell Viability Assay according to the manufacturer‘s instructions. The luciferase reaction in this assay is dependent on the cell‘s ATP level. Therefore, emerging luminescence is proportional to the cell‘s ATP levels and thereby to its viability. In detail, cells were seeded in white flat bottom 96-well plates (4.2.1.4 or 4.2.1.5) and treated as indicated (4.2.1.6). Then, 5 µl of CellTiter-Glo® Luminescent Cell Viability Assay solution was applied per well, samples were incubated for 10 min - 3 h at 37°C in a 5% CO_2-atmosphere and luminescence was measured by a microplate reader. In order to measure cell viability of

multicellular spheroids, CTG was performed as described above with the exceptions that ultra-low attachment 96-well plates were utilized and cells were incubated for 20 min on a rocking shaker at RT.

4.2.4.5 Determination of mitochondrial membrane potential (MMP)

Loss of MMP is an indicator of the mitochondrial apoptotic pathway and was assessed by TMRM staining. TMRM is a fluorescent dye accumulating in negatively charged mitochondria. Loss of MMP leads to leakage of TMRM from the mitochondria which can be determined by flow cytometry. Hence, cells were seeded in 24-well plates (4.2.1.4) and treated as indicated (4.2.1.6). 20 min before harvesting of cells, 50 nM TMRM dye was added to each well and incubated at 37°C in a 5% CO_2-atmosphere. Cells were harvested as described in 4.2.4.2 without last washing step. Instead, cells were directly resuspended in 50 - 100 µl PBS and analyzed by flow cytometry immediately. FSC/SSC pre-gating was utilized to exclude cell debris and loss of MMP was quantified by analysis of the PI intensity in a histogram of the PE channel. To ensure appropriate gating the mitochondrial uncoupling reagent FCCP (100 µM) was used as a positive control and an unstained sample was used as a negative control.

4.2.4.6 Determination of caspase activity using CellEvent™ Caspase-3/7 activity assay

For assessment of caspase-3/7 activity we performed a CellEvent™ Caspase-3/7 activity assay according to the manufacturer‘s instructions. CellEvent™ Caspase-3/7 Green Detection Reagent is a peptide harboring a DEVD (“Asp-Glu-Val-Asp”) domain which is conjugated to a DNA-binding dye. The DEVD domain inhibits the DNA binding as well as the fluorescent properties of the peptide until it is cleaved by caspase-3/7 resulting in a fluorescent signal. Cells were seeded in 96-well plates (4.2.1.4) and treated as indicated (4.2.1.6). CellEvent™ Caspase-3/7 Green Detection Reagent (2 µM) was added to the cells together with the treatment. At the time point of measurement, cells were stained with 1 µg/ml Hoechst-33342 and were incubated for 5 - 10 min at 37°C in a 5% CO_2-atmosphere. ImageXpress® Micro XLS System (4x objective) was utilized to measure Caspase-3/7 active cells (using FITC channel) and Hoechst-33342 positive cells (using DAPI channel) according to the manufacturer‘s instructions. “Cell Scoring” application of MetaXpress® analysis software was used to quantify the frequency of Caspase-3/7 active cells related to Hoechst-33342 positive cells.

4.2.5 Imaging and analysis of spheroids

ImageXpress® Micro XLS System (4x or 10x objective) was utilized to record 40 horizontal z-stacks per spheroid with 20 µm step size, respectively. To obtain representative images, z-stacks were merged to a best focus image. PI signal was measured using the TRITC channel, GFP signal utilizing the FITC channel and Hoechst-33342 using the DAPI channel according to the manufacturer‘s instructions. During measurement, spheroids were continuously exposed to a 5% CO_2-atmosphere and 37°C. Analysis was performed with the MetaXpress® analysis software.

Either the “Find Blob” application (analyzing the best focus images) or the “Find Spherical Object” application (analyzing the individual z-stacks) was used. In detail, the average spheroid diameter was determined by the “Find Spherical Object” application on GFP or Hoechst-33342 while the average intensities of the individual signals and the average spheroid are was assessed by the “Find Blob” application.

4.2.6 RNA analysis

4.2.6.1 RNA isolation

Isolation of RNA was performed by peqGold total RNA kit according to the manufacturer‘s instructions. In detail, cells were seeded in 10 cm dishes (4.2.1.4) and treated as indicated (4.2.1.6). At indicated time points medium was discarded and 350 µl RT lysis buffer was added to the cells. Next, cells were transferred to a DNA-removing column and 70% ethanol was added to the remaining solution (ratio 1:1). After subjecting the solution to an RNA-binding column and washing of the resulting RNA extract with provided buffers, purified RNA was eluted in nuclease-free water. RNA concentration and purity was determined by a NanoDrop 1000 spectrophotometer by absorbance analysis at 260 nm, 260/280 nm and 260/230 nm. RNA was stored at -20°C or -80°C for long-term storage.

4.2.6.2 cDNA synthesis

For transcription of RNA to cDNA 1 µg RNA was used as a template and the RevertAid H Minus First Strand cDNA Synthesis Kit with random primers was used according to the manufacturer‘s instructions. cDNA was diluted 1:10 in nuclease-free water.

4.2.6.3 Quantitative Real-Time PCR (qRT-PCR)

In order to assess relative mRNA levels, qRT-PCR was performed using QuantStudio 7 Flex Real-Time PCR System with the following program: initial heating to 95°C for 10 min, 40 cycles of 95°C for 15 sec followed by 60°C for 1 min, and finally cooling down to 4°C. For this purpose, 1 µl cDNA was applied to a MicroAMP^{TM} optical reaction 96-well plate and 20 µl of SYBR-Green PCR Master Mix (10 pmol/µl forward or reverse primer of the genes of interest (listed in 4.1.8.), nuclease-free water, SYBR-Green PCR Master Mix (final concentration 1x)) was added. Nuclease-free water was utilized as a negative control. Melting curves were inspected to ensure the specificity of the amplified product. Relative levels of RNA expression were calculated with the $\Delta\Delta C_t$ method and normalized using 28S RNA and GAPDH RNA as housekeeping genes.

4.2.7 Western Blot analysis

4.2.7.1 Protein extraction

For the extraction of proteins cells were seeded in 10 cm or 15 cm dishes (4.2.1.4) and treated as indicated (4.2.1.6). Subsequently, cells were harvested by scratching in ice-cold PBS using a cell

scraper. Dishes were rinsed once with ice-cold PBS and detached cells and their supernatant were collected in a 50 ml reaction tube. The cell suspension was centrifuged for 5 min at 1800 rpm at 4°C and the supernatant was decanted. After pellets were washed once with ice-cold PBS (5 min at 1800 rpm at 4°C), they were lysed in Triton X lysis buffer supplemented with phosphatase inhibitors (1 mM sodium orthovanadate, 1 mM β-glycerophosphate and 5 mM sodium fluoride). Volume of lysis buffer used was corresponding to the pellet size. Pellets lysed with Triton X were incubated for 25 min on ice and pellets lysed with CHAPS buffer were incubated for 30 – 60 min on ice. Afterwards, cell debris was removed by centrifugation for 25 min at 14,000 rpm at 4°C. Protein-containing supernatant was transferred into a new Eppendorf reaction tube and stored at -20°C or at -80°C for long-term storage.

4.2.7.2 Determination of protein concentration

Determination of protein concentration was performed using BCA Protein Assay Kit according to the manufacturer‘s instructions. In brief, the amount of protein per sample was assessed by measuring absorbance at 550 nm with a microplate reader. A protein standard (BSA in ddH_2O) was used for calculation of protein concentration.

4.2.7.3 Sodium dodecyl sulfate polyacrylamide gel electrophoresis (SDS-PAGE) and Western blotting

In order to separate proteins according to their size SDS-PAGE was performed. Therefore, stacking and resolving gels were cast consisting of the following ingredients: stacking gel (5%): 5% acrylamide, 125 mM TrisHCl (pH 6.8), 0.1% SDS, 0.1% APS, 0.1% TEMED; resolving gel (12% or 15%): 12% or 15% acrylamide, 250 mM TrisHCl (pH 8.8), 0.1% SDS, 0.1% APS, 0.04% TEMED. Whether a 12% or a 15% resolving gel was used was dependent on the molecular weight of the proteins of interest. For preparation of lysates for electrophoresis, 50 µg of protein were diluted in 1x loading dye. Samples were adjusted to an equal volume using ddH_2O. Then, samples were denatured for 5 min at 96°C on a shaker and loaded onto a polyacrylamide gel. Electrophoresis was carried out in 1x running buffer with 100 - 120 mV to collect proteins in the stacking gel and 120 - 160 mV to separate proteins in the resolving gel. A protein size ladder was utilized to monitor the separation process and electrophoresis was aborted when an appropriate state of separation was reached. Subsequently, proteins were transferred to a nitrocellulose membrane using a semi-dry blotting system. Whatman paper, gel and membrane were soaked in 1x blotting buffer and stacked in the following order: 2x Whatman paper, membrane, gel, 2x Whatman paper. Then, protein transfer was performed with a constant current of 1 mA per cm^2 of gel area for 70 – 105 min, depending on the molecular weight of the proteins of interest.

4.2.7.4 Protein detection

To avert unspecific binding of antibodies, the nitrocellulose membrane was washed in 5% milk/PBS-T for 1 h. Subsequently, the membrane was washed three times for 10 min with PBS-T before it was incubated with primary antibodies (4.1.5.1) overnight at 4°C under constant rotation. After the membrane was washed three times for 10 min with PBS-T, secondary antibodies conjugated to HRP or IRDye (4.1.5.2) were applied and incubated for at least 1 h at RT followed by another three washing steps for 10 min with PBS-T. Secondary antibodies were detected by ECL with Pierce™ ECL Western Blot Substrate and developing solutions (ratio 1:1) according to the manufacturer‘s protocol or by infrared detection according to the manufacturer‘s instructions. For detection with ECL, membranes were positioned into an X-ray developer cassette and X-ray films were placed on the membrane for a timeframe between a few seconds and 2 h in a darkroom. Films were developed with the appropriate solutions according to the manufacturer‘s instructions. For infrared detection IRDye-conjugated secondary antibodies were detected at 680 nm or 800 nm utilizing an Odyssey imaging system. In case another protein was to be detected which has a similar molecular weight as the previous one, the membrane was stripped. Therefore, the membrane was incubated with 0.4 M NaOH for 10 min at RT, washed three times for 10 min in PBS-T and blocked in 5% milk/PBS-T as described above before new primary antibodies were applied. If not indicated otherwise, a representative blot from at least two independent experiments is shown.

4.2.7.5 Quantification of Western blots

Quantifications of protein expression levels were performed by ImageJ software. Therefore, high resolution digital scans of the Western blot bands were analyzed according to the software‘s instructions. The area under the curve was utilized to determine the signal intensity of each band. Calculated protein expression levels were normalized to their individual loading control, respectively, and are displayed relative to one of the cell lines. For quantification at least three independent experiments were used.

4.2.8 Immunoprecipitation (IP)

4.2.8.1 BAK/BAX activation IP

BAX and BAK are undergoing a conformational change when they are activated (154). Hence, this structural alteration can be utilized to determine the activation status of BAX and BAK. Antibodies binding an epitope on helix α1 which is only exposed in activated BAX or BAK (149,330), respectively, can be employed to determine their activation status. Thus, we performed immunoprecipitations with antibodies recognizing activated BAX or BAK, respectively. Therefore, cells were seeded in 15 cm dishes (4.2.1.4), were treated as indicated (4.2.1.6) and then harvested and lysed in CHAPS buffer (4.2.7.1). 500 µg protein lysate was incubated with 10 µl Dynabeads™ anti-mouse IgG and 2 µl anti-BAX or anti-BAK antibody (4.1.5.3), respectively, in a total volume of 400 µl CHAPS buffer overnight at 4°C on a spinning wheel. On the next day, precipitates were

washed with CHAPS buffer for at least three times. Loading dye (2x) was added and samples were processed for Western blotting as described in 4.2.7.3. 50 µg protein lysate was used for the input. Interactions between activated BAX and BAK or activated BAK and BAX were detected by Western blotting.

4.2.8.2 MCL-1, BCL-X_L, BCL-2, BAK and BAX Co-IP

To investigate interactions between MCL-1 or BCL-X_L and pro-apoptotic BCL-2 family proteins Co-IPs were performed. To this end, cells were seeded in 15 cm dishes (4.2.1.4), were treated as indicated (4.2.1.6) and then harvested and lysed in Triton X buffer (MCL-1 or BCL-X_L Co-IPs) or CHAPS buffer (BAX or BAK Co-IPs) (4.2.7.1). 1000 - 1500 µg protein lysate was incubated with Dynabeads™ Protein G crosslinked to either 5 µl rabbit anti-MCL-1 antibody, 5 µl rabbit anti-BCL-X_L antibody, 5 µl hamster anti-BCL-2 antibody, 5 µl rabbit anti-BAK antibody or 10 µl rabbit anti-BAX antibody (see 4.1.5.3). For all washing steps a magnetic rack was used. To perform crosslinking, Dynabeads™ Protein G were washed with PBS + 0.05% Tween-20 three times and incubated with the respective antibody for 1 h at 4°C on a spinning wheel. Next, antibodies were crosslinked to Dynabeads™ Protein G utilizing 20 mM DMP freshly prepared in 0.2 M TEA buffer (pH 8.2). After incubation for 30 min at RT crosslinking reaction was quenched by 50 mM Tris buffer (pH 7.5) for 15 min at RT. Protein lysates were incubated with crosslinked antibodies in a total volume of 400 µl CHAPS or Triton X buffer overnight at 4°C on a spinning wheel. Precipitates were washed with Triton X buffer (MCL-1, BCL-X_L IP) or CHAPS buffer (BAK, BAX IP) at least five times on the next day. Loading dye (2x) was added and samples were processed for Western blotting as described in 4.2.7.3. For the input 50 µg protein lysate was used. Interactions of BCL-X_L or MCL-1 with BIM, NOXA, BAX and BAK were analyzed by Western blotting.

4.2.9 CAM assay

In order to test the *in vivo* efficacy of drugs, a CAM assay, being a well established *in vivo* tumor model, was performed. To this end, fertilized chicken eggs were incubated at 37.5°C for four days with the blunt end up. On day four eggs were turned upside down and a tiny part of the egg shell on the pointed end of the egg was removed by drilling a hole and cutting out a small piece of the egg shell. The remaining egg shell was stabilized using Leukosilk® tape. On day 8 upon fertilization $2x10^6$ Kym-1 cells suspended in 0.9% NaCl were mixed with matrigel in a ratio of 1:1. Cells were applied onto the CAM within a silicon ring. On the next day, tumor formation was checked macroscopically and tumors were treated with 0.25 µM A-1331852 and/or 0.3 µM S63845 for three consecutive days (day 9 - 11). DMSO treated tumors served as untreated controls. Subsequently, on day 12, tumors were resected from the CAM and were fixed in 4% paraformaldehyde for at least one day. Tumors were embedded in paraffin, cut into 3 µm sections and were further processed by immunohistochemistry (4.2.10).

4.2.10 Active caspase-3 and hematoxylin and eosin (HE) staining

Before staining, tumor sections were deparaffinized and rehydrated by incubation in xylol (2 x 10 min), 100% ethanol (2 x 10 min), 96% ethanol (2 x 10 min), 70% ethanol (2 x 10 min) and short-time in ddH_2O. In order to stain tumor sections for active caspase-3, slides were boiled for 10 min in citrate buffer using a food steamer. After slides were cooled down to RT they were washed with PBS-T (2 x 5 min) and put into a humidified staining chamber. Next, unspecific antibody binding was blocked by peroxidase quenching solution for 10 min and slides were again washed with PBS-T (2 x 5 min) followed by incubation with ready-to-use 10% goat serum for 30 min at RT. Anti-cleaved caspase-3 antibody was applied in SignalStain antibody diluent (1:300) either for 1 h or overnight at 4°C. Histostain-Plus IHC AEC broad-spectrum kit was utilized in order to detect cleaved caspase-3 positive cells according to the manufacturer's instructions. Further, tumor sections were counterstained with ready-to-use hematoxylin solution (10 min) and then washed with tap water (3 times). Next, slides were immersed in ammoniac water (500 µl ammonia solution in 250 ml tap water) for 10 sec, and washed once in tap water. Afterwards, tumor sections were incubated in 1% eosin solution (1 g eosin Y in 100 ml 70% ethanol, 1 drop acetic acid) for 10 min and dehydrated by washing in 2 x 70% ethanol, 2 x 96% ethanol, 2 x 100% ethanol, and 2 x xylol. Eventually, tumor slides were covered with Entellan mounting medium followed by a cover glass. Digital images of stained tumor sections were used for quantification of caspase-3 positive area per tumor area by Image J. In brief, tumor tissue area was marked and the color deconvolution function was utilized to create a diaminobenzidine (DAB) image. The area of stained cells in the DAB image was quantified.

4.2.11 Determination of Bliss synergy scores

Drug synergy was assessed by Bliss synergy scores using SynergyFinder (331). The Bliss independence model is a stochastic approach with the basic assumption that two individual drugs mediate their effects independent of each other. It is expressed by the following equation:

$$B\ (Bliss\ expectation) = (X + Y) - (X * Y)$$

with X and Y representing the fractional effects of the single compounds at the same dose (331,332). The Bliss score displays the difference between the predicted effect if two compounds act independently (Bliss expectation) and the measured combined effect at the same dose (Bliss excess) (332,333). Positive values (indicated by red color in the heat maps) imply synergism, 0 (indicated by white color in the heat maps) signifies additivity and negative values (indicated by green color in the heat maps) show antagonism.

4.2.12 Statistical analysis

In order to determine whether there is a significant statistical difference between two groups of data, a Student´s t-test (equal variance, two-sample, two-sided) was performed in Microsoft Excel. A one-way ANOVA followed by a Tukey´s multiple comparison post-hoc test was performed in GraphPad Prism® to compare more than two groups. Data are shown as mean + standard deviation of at least three independent experiments performed in triplicate if not indicated otherwise. Data of the CAM assay are shown as mean + SEM. Level of significance was indicated by p-values as followed: p-value ≤ 0.05 (significant, *), p-value ≤ 0.01 (very significant, **) and p-value ≤ 0.001 (highly significant, ***).

5 Results

Large parts of this work were published in the peer-reviewed journal Cancer Letters in 2020 with the title:

"Targeting BCL-2 proteins in pediatric cancer: Dual inhibition of BCL-X_L and MCL-1 leads to rapid induction of intrinsic apoptosis" (334).

5.1 Targeting anti-apoptotic BCL-2 family proteins in pediatric cancer

Parts of the experiments with OS and ES cells were performed by the M.Sc. student Barnabas Irmer during his research internship, which is indicated in the figure legends accordingly.

5.1.1 BCL-2 family proteins are expressed in a panel of RMS cell lines

BCL-2 family proteins are differentially expressed in RMS in comparison to normal skeletal muscle tissue (220). Significantly, MCL-1 was reported to be frequently upregulated in RMS (196,221) and the expression of BAX in primary tissue samples has been connected to longer median overall survival in RMS (213). Thus, we initially assessed the expression levels of the most relevant anti- and pro-apoptotic BCL-2 family proteins in ten different established RMS cell lines by Western blotting (Figure 5.1A). These cell lines included the ARMS as well as the ERMS subtype and are frequently used in RMS research (for characteristic features of these cell lines see Table 4.1 and Table 4.4). Moreover, to confirm the clinical relevance of our screen, we included a primary ARMS sample (CP1) (Figure 5.1B). Importantly, all investigated RMS cell lines expressed the anti-apoptotic proteins MCL-1, BCL-X_L and BCL-2, except Kym-1 cells, which lack BCL-2. Further, the pro-apoptotic BCL-2 family proteins BIM, NOXA, BAX and BAK were detected in all of the RMS cell lines apart from TE441.T and Kym-1 cells, which did not display NOXA expression. The primary ARMS cell line CP1 expressed all anti-and pro-apoptotic BCL-2 family proteins. To account for loading differences, we additionally quantified the protein levels by calculating the expression levels in relation to the loading control and a reference cell line (RH30) (Table 5.1). Due to limited material size of the primary ARMS sample CP1, we performed Western blotting experiments only twice here and therefore refrained from quantification. All in all, the quantification confirmed that a large part of the RMS cell lines express all pro-and anti-apoptotic BCL-2 family proteins, albeit to different extents.

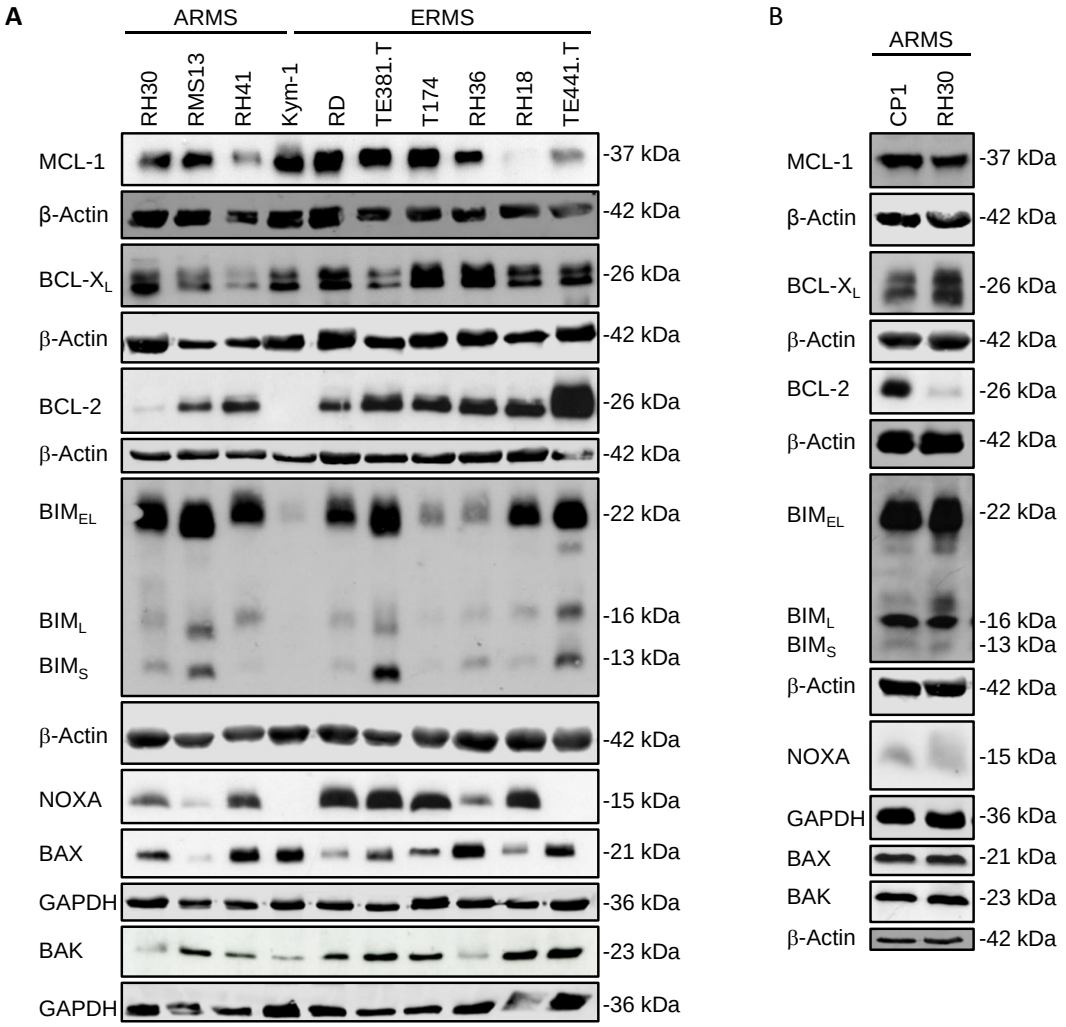

Figure 5.1: BCL-2 family proteins are expressed in a panel of RMS cell lines.

Basal expression levels of anti-and pro-apoptotic BCL-2 family proteins in established RMS cell lines (A) and the primary-derived cell line CP1 (B). Protein expression levels were analyzed by Western blotting with β-Actin or GAPDH serving as a loading control. Representative blots of at least two independent experiments are shown.

Table 5.1: Quantification of BCL-2 family protein expression levels in RMS cell lines.

Individual protein expression levels were normalized to the loading control and are shown relative to the reference cell line RH30. At least three independent experiments were utilized for quantification.

Cell Line	BCL-2	BCL-X_L	MCL-1	BAX	BAK	BIM	NOXA
RH30	1.00	1.00	1.00	1.00	1.00	1.00	1.00
RMS13	13.95	1.03	1.28	0.20	3.34	1.48	0.45
RH41	16.80	0.28	1.23	1.04	0.91	0.60	2.63
Kym-1	0.00	1.11	0.96	1.19	0.43	0.23	0.00
RD	12.47	1.03	0.99	0.26	0.55	0.53	3.61
TE381.T	18.43	0.97	1.56	0.44	1.28	1.49	3.91
T174	14.17	1.75	1.44	0.45	1.10	0.13	4.90
RH36	16.44	1.61	1.15	1.06	0.40	0.14	0.85
RH18	12.61	1.01	0.22	0.52	2.42	0.44	1.59
TE441.T	46.68	0.45	0.97	0.79	1.98	1.14	0.00

5.1.2 A panel of RMS cell lines is largely insensitive towards pharmacological inhibition of BCL-2, MCL-1 or BCL-X_L

Since we observed that RMS cell lines widely express anti-apoptotic BCL-2 family proteins, we aimed to investigate the overall efficacy of their individual pharmacological inhibition. To this end, we utilized BH3 mimetics selectively targeting MCL-1 (S63845, A-1210477), BCL-2 (ABT-199) or BCL-X_L (A-1331852) and screened a panel of ten RMS cell lines with regard to their cell viability. Cell viability was determined by CellTiterGlo® viability assay upon treatment with subtoxic increasing concentrations of BH3 mimetics (Figure 5.2). To quantify the effect, IC_{50} values were assessed.

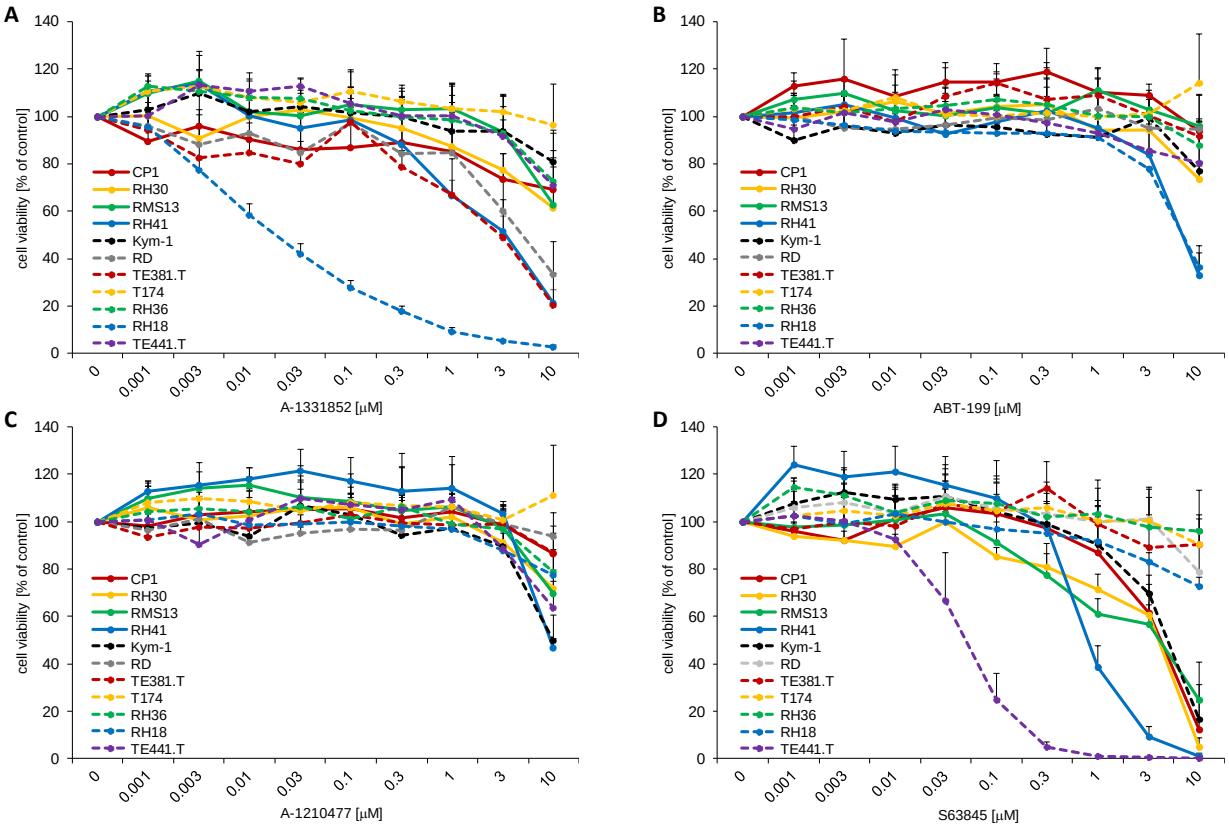

Figure 5.2: RMS cell lines are largely insensitive to single treatment with A-1331852, ABT-199, A-1210477 or S63845.

RMS cell lines were treated with indicated concentrations of A-1331852 (A), ABT-199 (B), A-1210477 (C) or S63845 (D) for 48 h. CellTiter-Glo® Luminescent Cell Viability Assay was used to determine ATP levels and thereby cell viability. Mean and SD of at least three independent experiments performed in triplicates are shown.

Notably, RMS cell lines demonstrated limited responsiveness to A-1331852 treatment since cell viability only markedly decreased at higher concentrations (Figure 5.2A) as evidenced by high IC_{50} values (>3 µM; RH41: 2.1 µM) (Table 5.2). RH18 cells constitute an exception showing distinct sensitivity to BCL-X_L inhibition (IC_{50}: 0.006 µM). Moreover, all RMS cell lines were resistant to BCL-2 blockade by ABT-199 (Figure 5.2B) and to MCL-1 inhibition by A-1201477 (Figure 5.2C) as

all IC_{50} values were above 3 µM (Table 5.2). Inhibition of MCL-1 by S63845, on the other hand, revealed a more pronounced, yet moderate, decrease of cell viability for some cell lines such as RMS13 (IC_{50}: 2.6 µM), RH41 (IC_{50}: 0.7 µM) and TE441.T (IC_{50}: 0.05 µM) (Figure 5.2D), while all other RMS cell lines displayed an IC_{50} value above 3 µM (Table 5.2). Due to the higher potency of the novel MCL-1 inhibitor S63845 compared to A-1214077, which is in line with a previous report (227), we thus focused on S63845 for further experiments.

Table 5.2: Effect of BH3 mimetics on the viability of RMS cell lines.

IC_{50} values were determined for the treatment with A-1331852, ABT-199, A-1210477 and S63845 based on data shown in Fig.5.3. Calculations were performed with at least three independent experiments performed in triplicates.

Cell Line	IC_{50} [µM] A-1331852	IC_{50} [µM] ABT-199	IC_{50} [µM] A-1210477	IC_{50} [µM] S63845
CP1	>3	>3	>3	>3
RH30	>3	>3	>3	>3
RMS13	>3	>3	>3	2.6
RH41	2.1	>3	>3	0.7
Kym-1	>3	>3	>3	>3
RD	>3	>3	>3	>3
TE381.T	>3	>3	>3	>3
T174	>3	>3	>3	>3
RH36	>3	>3	>3	>3
RH18	0.006	>3	>3	>3
TE441.T	>3	>3	>3	0.05

5.1.3 A-1331852/S63845 co-treatment induces highly synergistic cell death in a panel of RMS cell lines

As the majority of RMS cell lines were insensitive to single BH3 mimetic treatment, we hypothesized that BCL-2, MCL-1 and BCL-X_L might be able to compensate each other‘s loss. Hence, we tested whether combinatorial application of BH3 mimetics triggered cell death in the panel of previously tested RMS cell lines. Due to the fact that inhibition of MCL-1 and BCL-X_L seemed to be most promising, whereas none of the RMS cell lines displayed sensitivity to BCL-2 blockade (Figure 5.2), we chose to start with investigating the effect of A-1331852/S63845 co-treatment. To this end, we measured cell death by PI uptake to assess loss of cell membrane integrity, a typical feature of cell death (Figure 5.3).

Interestingly, combined inhibition of MCL-1 and BCL-X_L resulted in massive dose-dependent induction of cell death in all tested RMS cell lines. This effect could already be observed at nanomolar concentrations. Similar to our findings concerning cell viability (Figure 5.2), rising doses of S63845 or A-1331852 alone caused none or only minor increases in cell death. Notably, cell lines found to be particularly sensitive to A-1331852 (RH18) or S63845 (TE441.T) in the cell viability screen, consistently demonstrated higher rates of cell death upon single A-1331852 or S63845 treatment, respectively.

To determine whether the interaction of drugs is synergistic, we calculated Bliss synergy scores for all drug combinations and their corresponding effect on cell death from Figure 5.3 according to Ianevski *et al.* (331). Importantly, A-1331852/S63845 co-treatment proved to be highly synergistic in all RMS cell lines as evidenced by positive Bliss synergy scores (Table 5.3). Of note, A-1331852/S63845-mediated cell death was also synergistic in the single sensitive RH18 (Bliss score: 21.8) and TE441.T cells (Bliss score: 3).

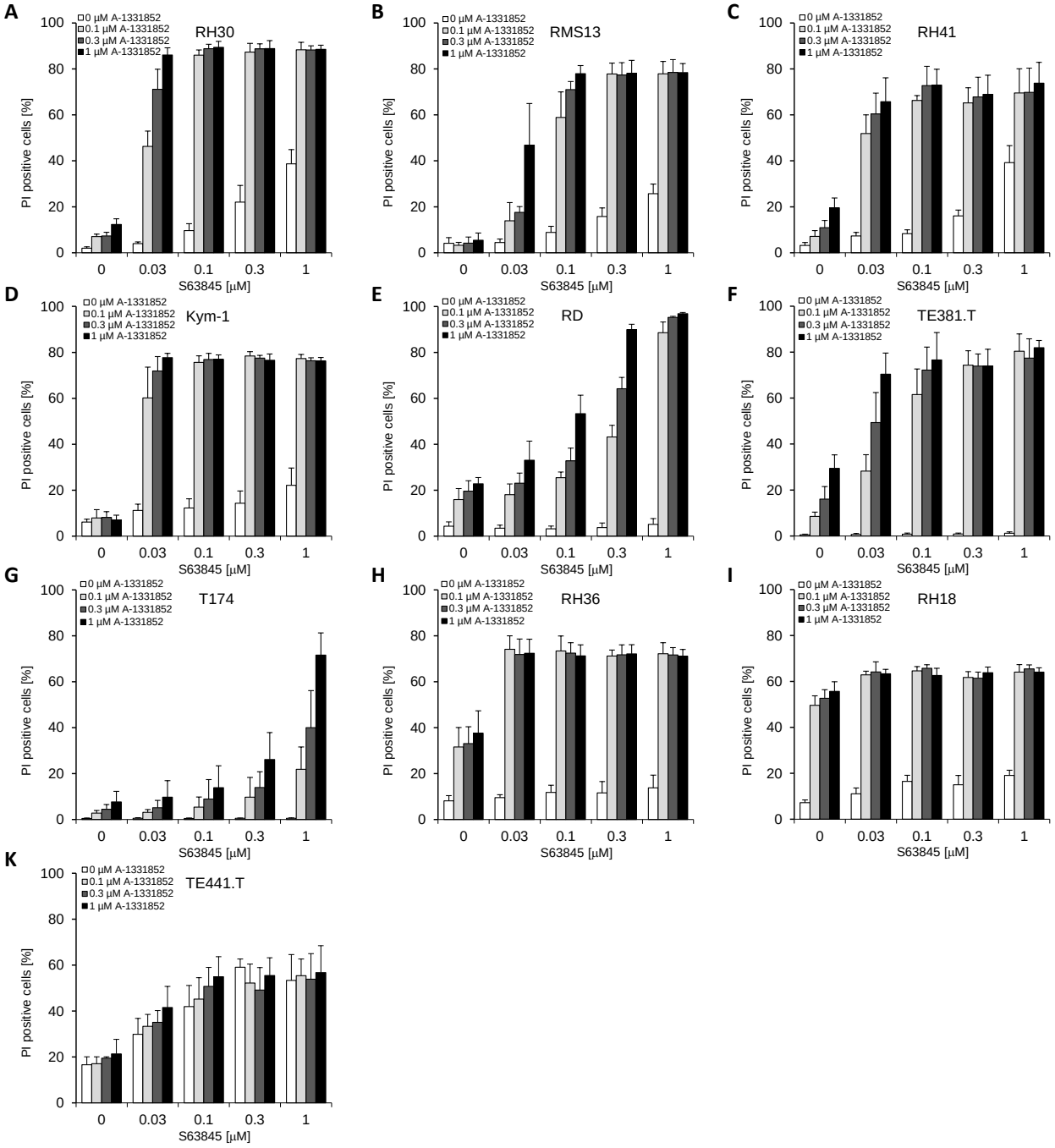

Figure 5.3: A-1331852/S63845 co-treatment synergistically induces cell death in RMS cell lines.

(A-K): RMS cell lines were treated with indicated concentrations of A-1331852 and/or S63845 for 48 h. Cell death was determined by fluorescence microscope analysis of PI uptake using Hoechst 33342/PI co-staining. Mean and SD of at least three independent experiments performed in triplicates are shown.

Table 5.3: Bliss synergy scores of combined A-1331852/S63845 treatment in RMS cell lines.

Calculations are based on data shown in Figure 5.3 and were conducted with at least three independent experiments performed in triplicates.

Cell Line	Bliss score A-1331852 + S63845
RH30	66.4
RMS13	50.3
RH41	49.2
Kym-1	61.0
RD	40.4
TE381.T	55.7
T174	10.9
RH36	51.8
RH18	21.8
TE441.T	3.0

Figure 5.4 depicts Bliss synergy score maps illustrating synergism (indicated in red color) at individual combinatorial doses as well as the average Bliss score. Interestingly, TE441.T was the only cell line for which we observed antagonistic drug interaction (indicated in green color) at some concentrations.

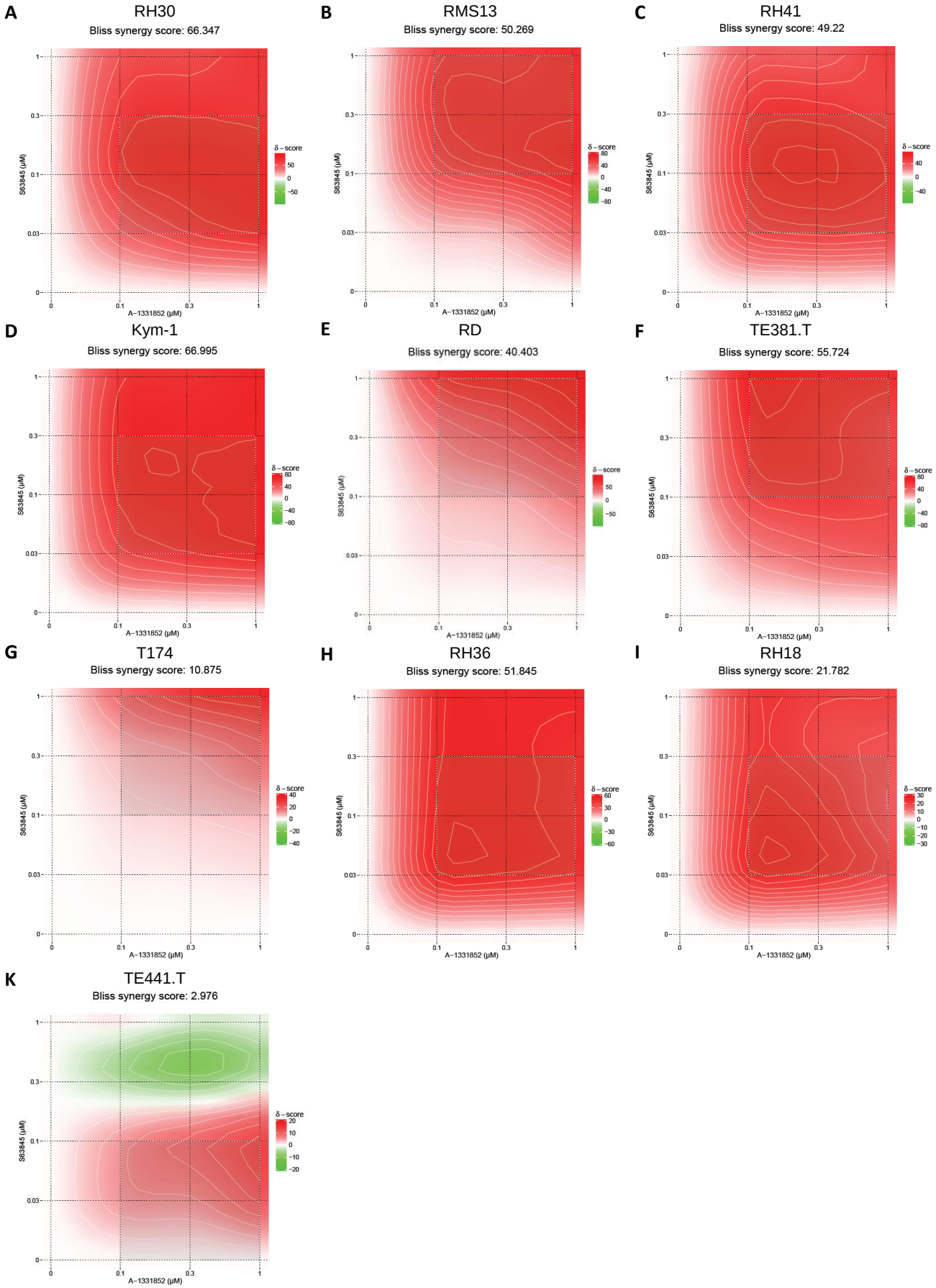

Figure legend on next page

Figure 5.4: Bliss synergy score maps of A-1331852/S63845 co-treatment-induced cell death in RMS cell lines.

(A-K): Bliss synergy scores are illustrated as heat maps at different concentrations of A-1331852/S63845 co-treatment in RMS cell lines. Red indicates “synergy”, white “additivity” and green “antagonism”. Average Bliss synergy score of the respective cell line is shown on top of the heat map. Calculations were based on results presented in Figure 5.3.

5.1.4 A-1331852/ABT-199 or S63845/ABT-199 co-treatments are less effective than co-treatment with A-1331852/S63845 in RMS cell lines

To explore whether dual blockade of BCL-2/MCL-1 or BCL-2/BCL-X_L exerts an equally strong induction of cell death as MCL-1/BCL-X_L co-inhibition, we selected three representative RMS cell lines for testing. RD and RH30 were chosen as they are frequently used ERMS and ARMS cell lines and Kym-1 cells due to their lack of BCL-2, thus serving as a control for the on-target specificity of ABT-199 (Figure 5.5). Intriguingly, increasing doses of ABT-199/A-1331852 and ABT-199/S63845 co-treatment resulted in mostly minor enhancement of cell death induction demonstrating that A-1331852/S63845 co-treatment was vastly superior in inducing cell death in all tested RMS cell lines. This notion was confirmed by calculation of Bliss synergy scores proving that synergism was higher for A-1331852/S63845 co-treatment compared to combinations with ABT-199 (RD: 40.4 vs. 10.3 and 3.9; RH30: 66.4 vs. 5.7 and 13.1; Kym-1: 61 vs. -0.7 and 3.9) (Table 5.3 and Table 5.4). Expectedly, co-application of ABT-199 with A-1331852 or S63845 in Kym-1 cells did not enhance cell death compared to treatment with either inhibitor alone. These results confirm the specificity of ABT-199 as a selective BCL-2 inhibitor as there are no cell death inducing off-target effects in the absence of BCL-2.

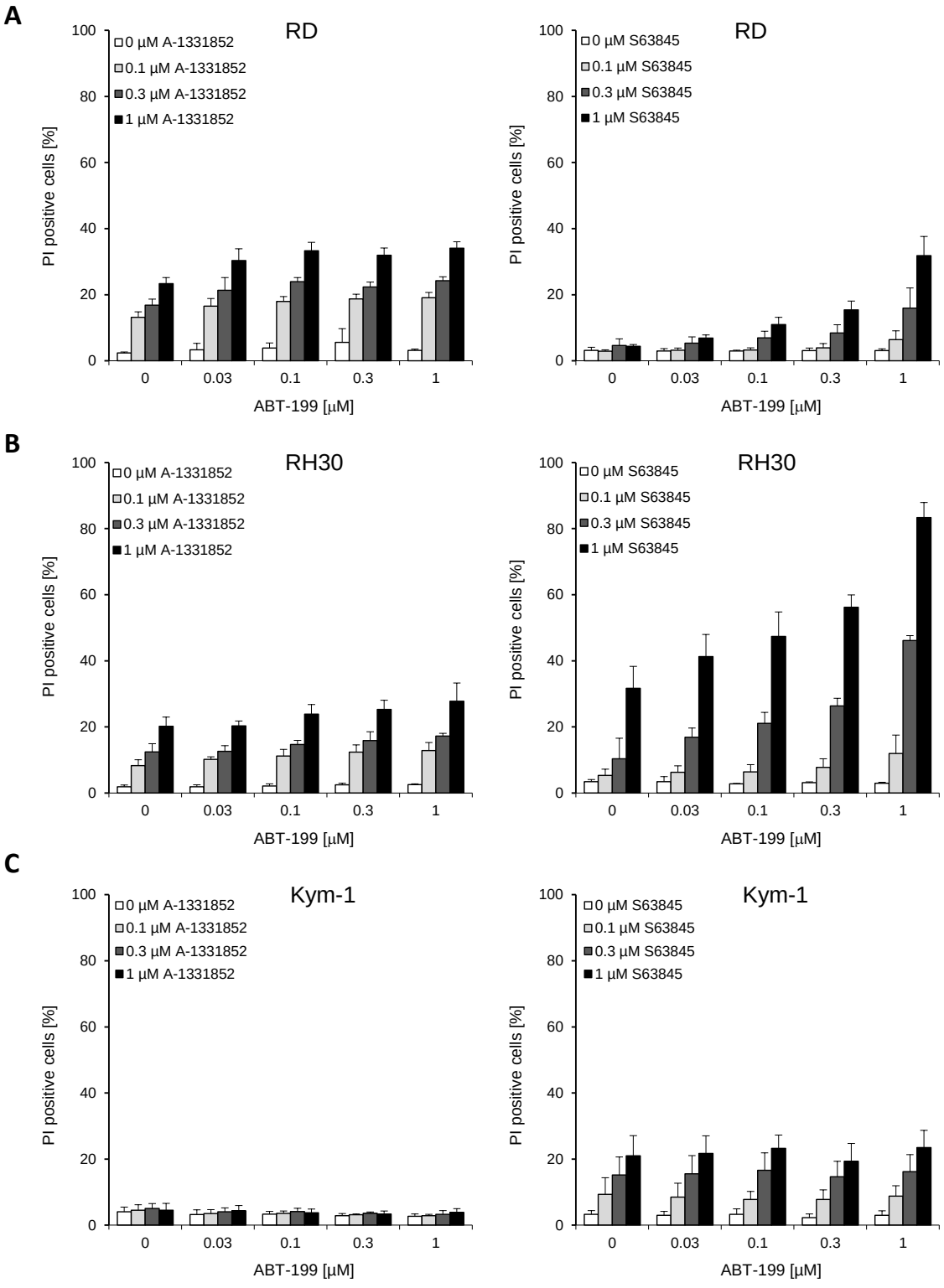

Figure 5.5: Effect of combination treatments with ABT-199 and A-1331852 or S63845 on RMS cell lines. RD (A), RH30 (B) and Kym-1 (C) cells were treated with indicated concentrations of ABT-199 in combination with increasing concentrations of A-1331852 or S63845 for 48 h. Cell death was determined by fluorescence microscope analysis of PI uptake using Hoechst 33342/PI co-staining. Mean and SD of at least three independent experiments performed in triplicates are shown.

Table 5.4: Bliss synergy scores of combination treatments with ABT-199 and A-1331852 or S63845 in RMS cell lines.

Calculations are based on data shown in Figure 5.5 and were conducted with at least three independent experiments performed in triplicates.

Cell Line	Bliss score ABT-199 + A-1331852	Bliss score ABT-199 + S63845
RD	10.3	3.9
RH30	5.7	13.1
Kym-1	-0.7	3.9

5.1.5 BCL-2 family proteins are expressed in a selection of OS and ES cell lines

BCL-2 family proteins might not only be relevant in RMS pathogenesis, but also in other pediatric cancers, such as OS and ES (223,224). Hence, we extended our study to frequently utilized OS and ES cell lines (for characteristic features of these cell lines see Table 4.2 and Table 4.3) and assessed the expression levels of anti- and pro-apoptotic BCL-2 family proteins (Figure 5.6).

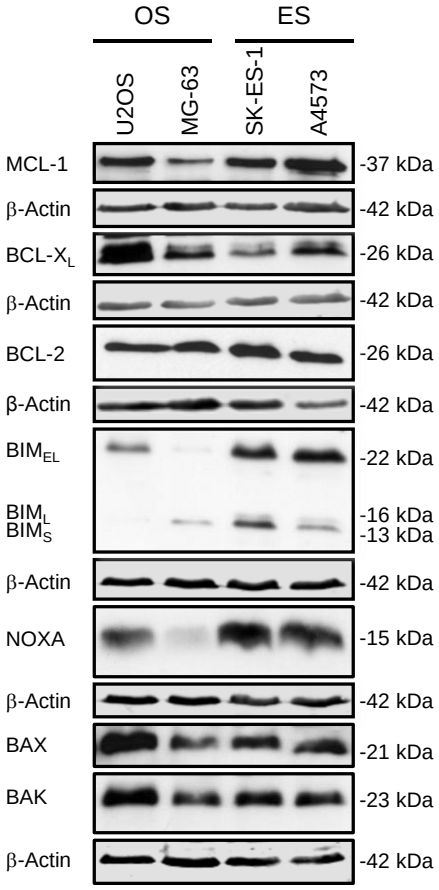

Figure 5.6: BCL-2 family proteins are expressed in a selection of OS and ES cell lines.

Basal expression levels of anti-and pro-apoptotic BCL-2 family proteins in established OS and ES cell lines. Protein expression levels were analyzed by Western blotting with β-Actin serving as a loading control. Representative blots of at least two independent experiments are shown. Experiments were partly performed by Barnabas Irmer.

Similar to RMS cell lines, we observed that all screened OS and ES cell lines expressed the analyzed anti- and pro-apoptotic BCL-2 family proteins to variable amounts as evidenced by Western blotting. Expression levels were further quantified by determining the protein expression levels in relation to the loading control and a reference cell line (U2OS) (Table 5.5). These experiments revealed that MG-63 cells consistently showed lower levels of all BCL-2 family protein members compared to U2OS and ES cells.

Table 5.5: Quantification of BCL-2 family protein expression levels in OS and ES cell lines.
Individual protein expression levels were normalized to the loading control and are shown relative to the reference cell line U2OS. At least three independent experiments were utilized for quantification.

Cell Line	BCL-2	BCL-X_L	MCL-1	BAX	BAK	BIM	NOXA
U2OS	1.00	1.00	1.00	1.00	1.00	1.00	1.00
MG-63	0.77	0.34	0.70	0.57	0.41	0.06	0.33
SK-ES-1	1.30	0.39	1.33	1.01	0.71	1.89	1.45
A4573	1.69	0.59	1.39	0.59	0.81	2.37	1.72

5.1.6 A selection of ES cell lines displays reduced cell viability upon pharmacological inhibition of MCL-1 or BCL-X_L while OS cell lines show no or limited responsiveness

In order to examine whether individual inhibition of BCL-2, MCL-1 or BCL-X_L might be effective in OS and ES cell lines, we monitored cell viability upon subtoxic rising doses of S63845, ABT-199 or A-1331852 (Figure 5.7).

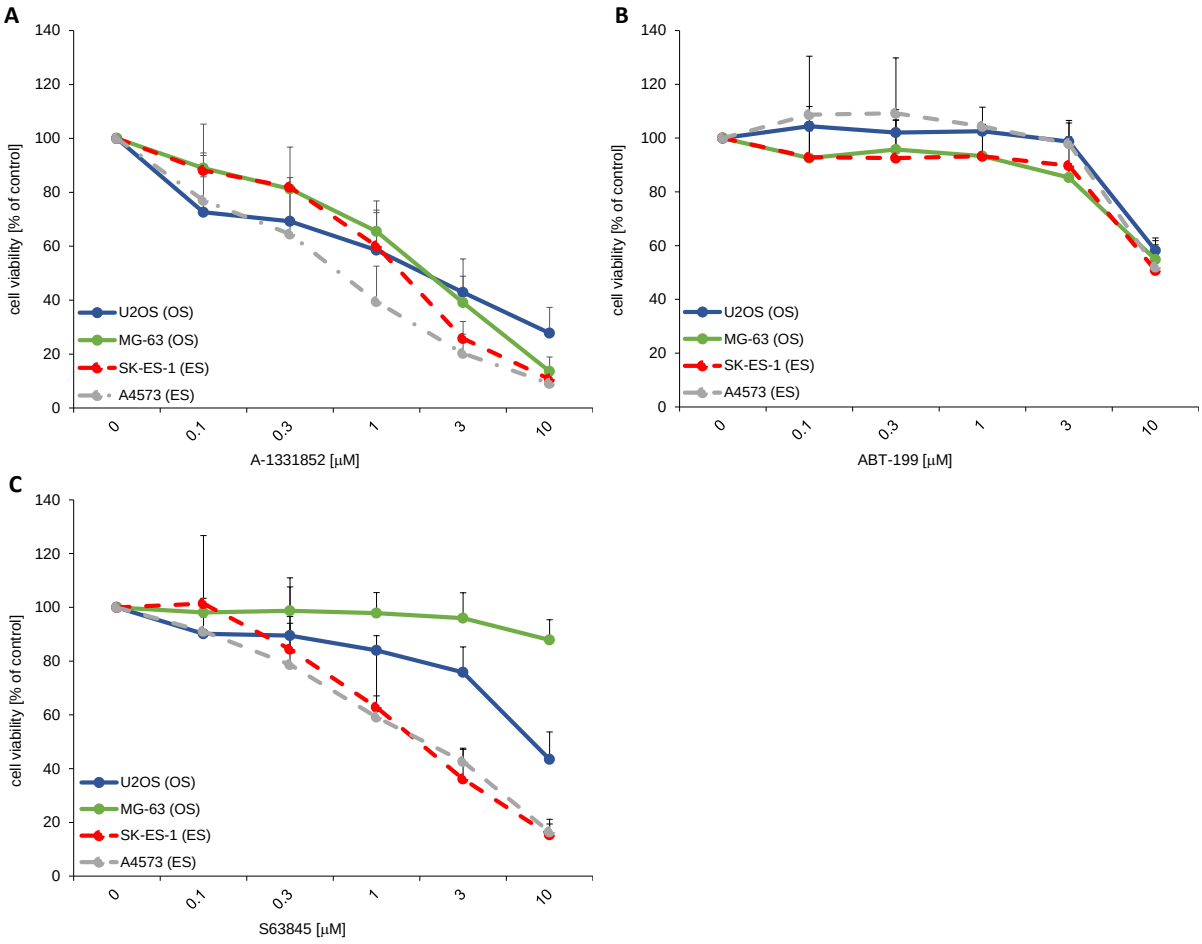

Figure 5.7: A selection of ES cell lines displays reduced cell viability treatment with A-1331852 or S63845 while OS cell lines show no or limited responsiveness.

OS and ES cell lines were treated with indicated concentrations of A-1331852 (A), ABT-199 (B), or S63845 (C) for 48 h. CellTiter-Glo® Luminescent Cell Viability Assay was used to determine ATP levels and thereby cell viability. Mean and SD of at least three independent experiments performed in triplicates are shown. Experiments were performed by Barnabas Irmer.

Remarkably, treatment with A-1331852 (Figure 5.7A) led to profound decrease of cell viability especially in ES cell lines as evidenced by low IC_{50} values (Table 5.6). Inhibition of BCL-2 by ABT-199, on the contrary, left cell viability largely unaffected (IC_{50} >3 µM) (Figure 5.7B). Further, only ES, but not OS cell lines demonstrated a marked decrease in cell viability upon S63845 treatment (IC_{50} (SK-ES-1): 1.3 µM; IC_{50} (A4573): 1.8 µM) (Figure 5.7C).

Table 5.6: Effect of BH3 mimetics on the viability of OS and ES cell lines.

IC_{50} values were determined for the treatment with A-1331852, ABT-199 and S63845 based on data shown in Figure 5.7. Calculations were performed with at least three independent experiments performed in triplicates.

Cell Line	IC_{50} [µM] A-1331852	IC_{50} [µM] ABT-199	IC_{50} [µM] S63845
U2OS	>3	>3	>3
MG-63	2.4	>3	>3
SK-ES-1	1.6	>3	1.3
A4573	0.8	>3	1.8

5.1.7 A-1331852/S63845 co-treatment triggers highly synergistic cell death in OS and ES cell lines

As A-1331852/S63845 co-treatment showed promising results in RMS, we checked whether this holds true also for OS and ES cell lines. Thus, we assessed cell death by PI uptake utilizing ImageXpress® Micro XLS System for OS cell lines upon A-1331852/S63845 co-treatment. Previous experiments from our group by Dr. Lilly Weiß showed an ineffective PI uptake of ES cell lines in the context of Hoechst 33342/PI co-staining using ImageXpress® Micro XLS System. Hence, we resorted to another classical hallmark of cell death and quantified the amount of DNA fragmentation in ES cell lines upon A-1331852/S63845 co-treatment. Indeed, inhibition of both MCL-1 and BCL-X_L exerted high efficacy in OS (Figure 5.8A+B) and ES cell lines (Figure 5.8C+D). Moreover, a dose-dependent moderate increase of cell death upon A-1331852 or S63845 single treatment in ES cell lines was observed, in line with the results of the cell viability screen (Figure 5.7).

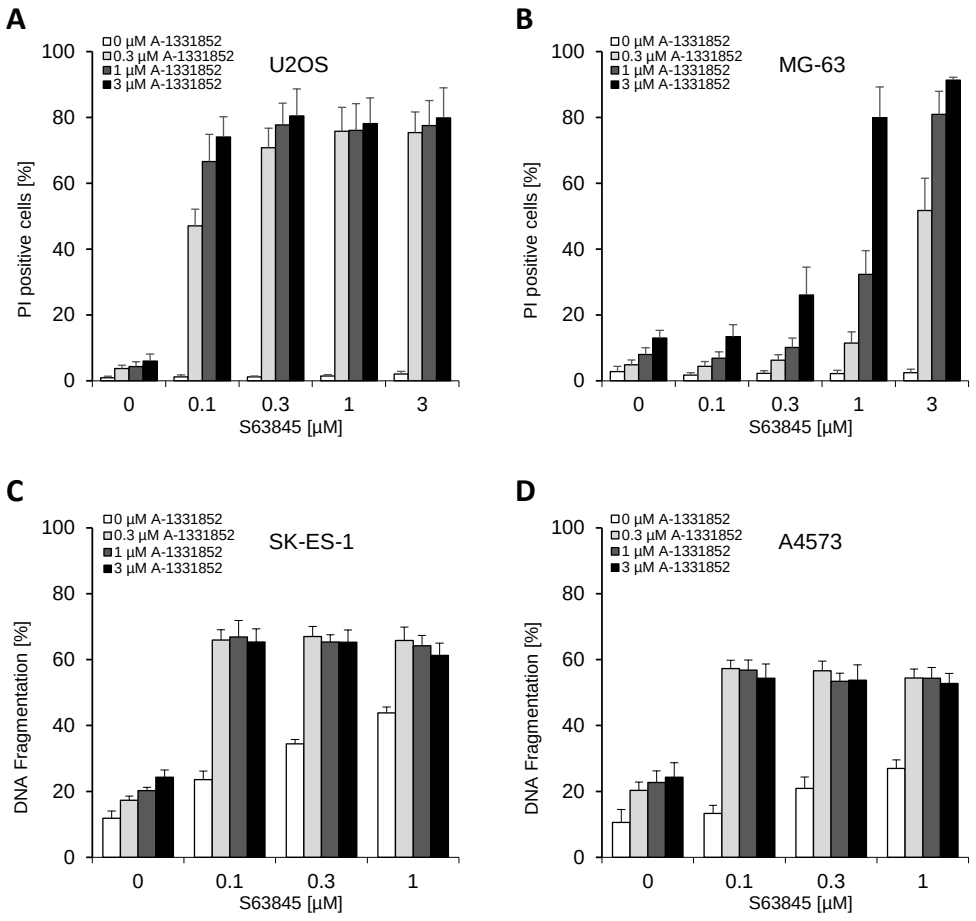

Figure 5.8: A-1331852/S63845 co-treatment synergistically induces cell death in OS and ES cell lines. OS (A+B) and ES (C+D) cell lines were treated with indicated concentrations of A-1331852 and/or S63845 for 48 h. Cell death was determined by fluorescence microscope analysis of PI uptake using Hoechst 33342/PI co-staining or analysis of DNA fragmentation of PI-stained nuclei. Mean and SD of at least three independent experiments performed in triplicates are shown. Experiments were partly performed by Barnabas Irmer.

Determination of Bliss synergy scores (Table 5.7) clearly proved a synergistic interaction of A-1331852 and S63845 underlining the high potency of this combination not only in RMS, but also in OS and ES cell lines.

Table 5.7: Bliss synergy scores of combination treatments with ABT-199 and A-1331852 or S63845 in OS and ES cell lines.

Calculations are based on data shown in Figure 5.8 and were conducted with at least three independent experiments performed in triplicates.

Cell Line	Bliss score A-1331852 + S63845
U2OS	70.8
MG-63	22.9
SK-ES-1	36.6
A4573	32.9

5.1.8 A-1331852/ABT-199 or S63845/ABT-199 co-treatments are less effective than co-treatment with A-1331852/S63845 in OS and ES cell lines

Next, we aimed at evaluating whether A-1331852/S63845 co-treatment is more effective than combinations of either inhibitor with ABT-199 in OS and ES cells. To this end, we performed a side-by-side comparison of the different combination treatments. Subsequent determination of cell death showed that dual inhibition of MCL-1/BCL-X_L was significantly more powerful in causing cell death than single or dual blockade of BCL-2/MCL-1 or BCL-2/BCL-X_L in all tested OS and ES cell lines (Figure 5.9). Furthermore, in the OS cell line MG-63 A-1331852/ABT-199 co-treatment led to significantly higher percentage of cell death than single ABT-199 application (Figure 5.9A). However, this effect could largely be attributed to cell death induction by A-1331852 alone. Similarly, A-1331852/ABT-199 co-treatment induced a significantly higher amount of cell death compared to single ABT-199 treatment and/or the untreated control in both ES cell lines which was mainly mediated by A-1331852 alone (Figure 5.9B). Additionally, in the ES cell line A4573 A-1331852/ABT-199 co-treatment was more efficient to induce cell death than dual treatment with S63845/ABT-199, which showed almost no enhancing impact on cell death.

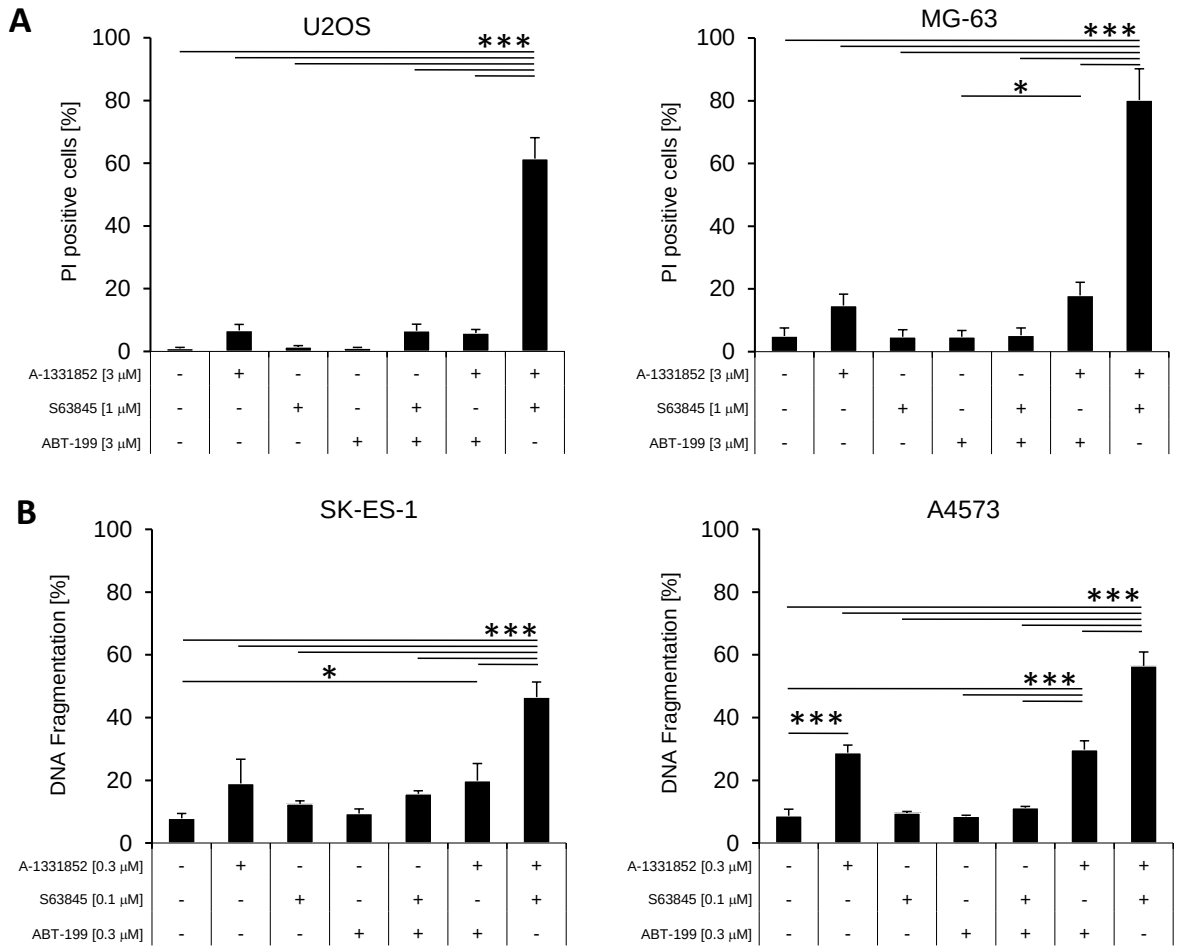

Figure 5.9: A-1331852/ABT-199 or S63845/ABT-199 co-treatments are less effective than co-treatment with A-1331852/S63845 in OS and ES cell lines.

(A+B): OS and ES cell lines were treated with indicated concentrations of ABT-199 and/or A-1331852 and/or S63845 for 48 h. Cell death was determined by fluorescence microscope analysis of PI uptake using Hoechst 33342/PI co-staining or analysis of DNA fragmentation of PI-stained nuclei. Mean and SD of at least three independent experiments performed in triplicates are shown. *P < 0.05, ***P < 0.001. Experiments were performed by Barnabas Irmer.

5.1.9 A-1331852/S63845 co-treatment causes synergistic cell death in a primary pediatric sample of a malignant epithelioid mesothelioma

Mesothelioma is described to be provoked by contact with asbestos and thus to be rare in children (335,336). Nevertheless, especially these particularly rare pediatric solid tumors require broad research to ensure future treatment options for such cases. On this account, we explored the potential of inhibiting anti-apoptotic BCL-2 family proteins in a primary sample of pediatric malignant epithelioid mesothelioma (RY240806_4). First, expression levels of anti- and pro-apoptotic BCL-2 family members in comparison to RMS cell lines were determined by Western blotting (Figure 5.10A). Importantly, the pediatric malignant epithelioid mesothelioma sample RY240806_4 expressed similar levels of MCL-1 and BCL-X_L as all tested RMS cell lines and BCL-2 levels comparable to RD cells. Concerning pro-apoptotic BCL-2 family proteins, RY240806_4 showed BIM expression in similar amounts as for RH30 cells, while NOXA was undetectable. Additionally, expression levels of BAX in RY240806_4 were lower compared to all tested RMS cell lines, whereas BAK levels were observed to be equal. We refrained from quantification of BCL-2 family protein expression levels for reasons of limited sample size. Thus, as Western blotting results revealed that the primary pediatric malignant epithelioid mesothelioma sample RY240806_4 was equipped with the expression of BCL-2 family proteins, we proceeded to elucidate whether it was sensitive to BH3 mimetic treatment. To this end, we assessed the impact of individual ABT-199, S63845 or A-1331852 treatment on the cell viability of RY240806_4 (Figure 5.10B). Clearly, individual treatment with increasing doses of BH3 mimetics had largely no effect on cell viability of RY240806_4 cells (IC_{50} >3 µM) (Table 5.8). Evaluating the response of RY240806_4 cells to co-inhibition of BH3 mimetics (Figure 5.10C), we noticed no increase of cell death upon ABT-199/A-1331852 application (Table 5.8). In contrast, combinations of S63845 with either A-1331852 or ABT-199 triggered minor induction of cell death, which was determined to be moderately synergistic (11.7 and 2.4). Importantly, similar to RMS, OS and ES cells, dual inhibition of MCL-1 and BCL-X_L tended to be the most powerful BH3 mimetic combination also for the primary pediatric malignant epithelioid mesothelioma sample investigated in the study at hand.

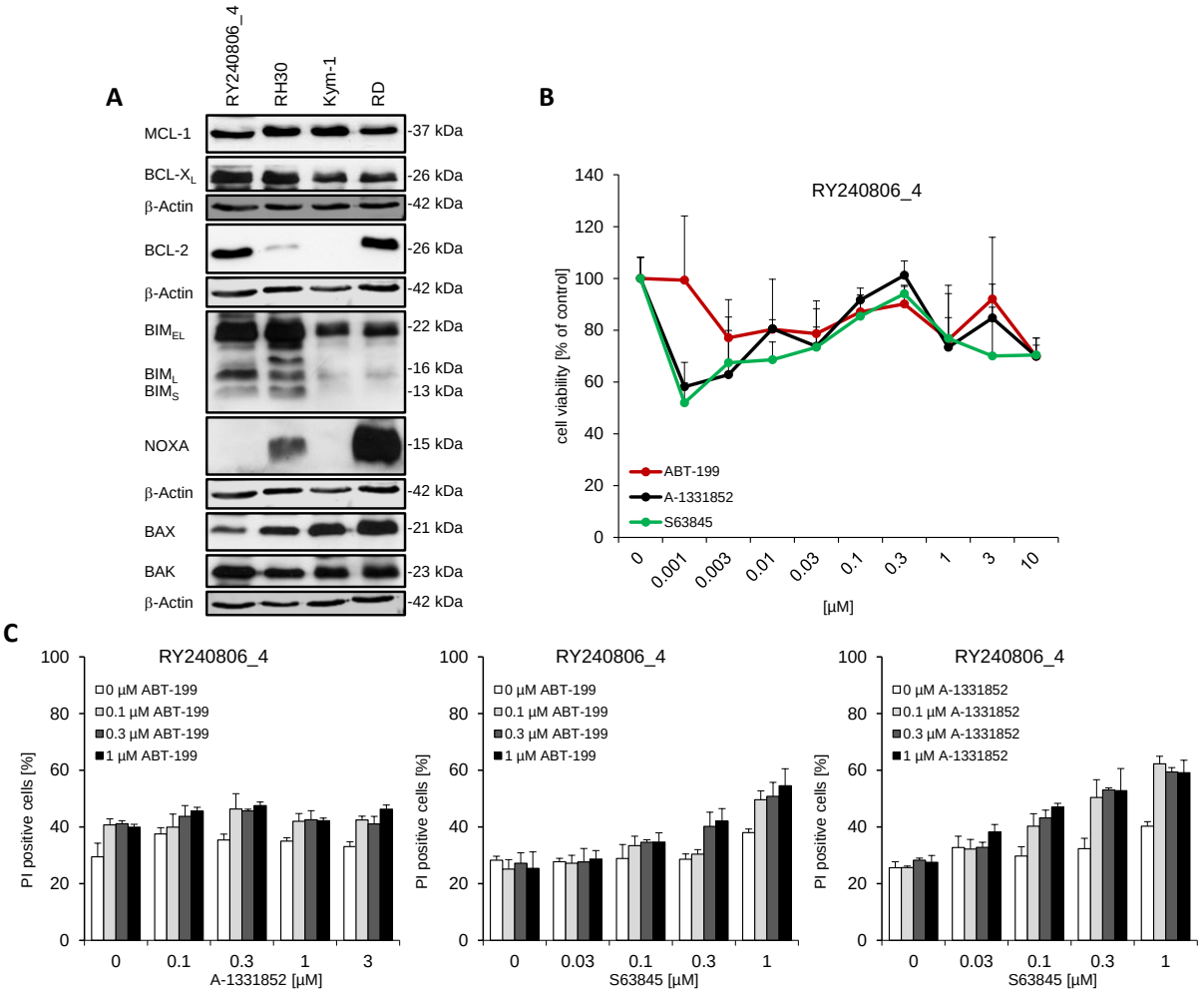

Figure 5.10: A-1331852/S63845 co-treatment causes synergistic cell death in a primary pediatric sample of a malignant epithelioid mesothelioma.

(A): Basal expression levels of anti- and pro-apoptotic BCL-2 family proteins in a primary pediatric sample of a malignant epithelioid mesothelioma (RY240806_4) compared to established RMS cell lines. Protein expression levels were analyzed by Western blotting with β-Actin serving as a loading control. Western blotting was performed once. (B): RY240806_4 cells were treated with indicated concentrations of A-1331852, ABT-199, or S63845 for 48 h. CellTiter-Glo® Luminescent Cell Viability Assay was used to determine ATP levels and thereby cell viability. (C): RY240806_4 cells were treated with indicated concentrations of ABT-199 and/or A-1331852 and/or S63845 for 48 h. Cell death was determined by fluorescence microscope analysis of PI uptake using Hoechst 33342/PI co-staining. Mean and SD of one experiment performed in triplicates are shown.

Table 5.8: Effect of BH3 mimetics on the viability of RY240806_4 cells and Bliss synergy scores of combined BH3 mimetic treatment in RY240806_4 cells.

IC_{50} values and Bliss synergy scores were determined for the treatment with A-1331852, ABT-199 and S63845 based on data presented in Figure 5.10. Calculations were conducted with one experiment performed in triplicates.

Cell Line	IC_{50} [µM] ABT-199	IC_{50} [µM] A-1331852	IC_{50} [µM] S63845	Bliss score ABT-199 + A-1331852	Bliss score ABT-199 + S63845	Bliss score S63845 + A-1331852
RY240806_4	>3	>3	>3	-5.7	2.4	11.7

In summary, this set of experiments demonstrated that i) BCL-2 family proteins were expressed in pediatric solid cancers such as (primary) RMS, OS, ES and a primary sample of malignant epithelioid mesothelioma, thus providing a promising drug target; ii) cell death induced by A-1331852/S63845 co-treatment was highly synergistic in the above mentioned entities and iii) A-1331852/S63845 co-treatment was vastly superior to combinations of ABT-199 with either inhibitor.

5.2 Exploring the cell death mechanism induced by A-1331852/S63845 co-treatment in RMS cells

With the goal to elucidate the molecular mechanism of cell death mediated by A-1331852/S63845 co-treatment, we focused on RMS and selected two RMS cell lines for further studies. These were the Kym-1 cell line, which lacks BCL-2, and RD cells, a well-established and frequently utilized RMS cell line, which expresses BCL-2 (Figure 5.1A).

5.2.1 Combination of genetic silencing and pharmacological inhibition of MCL-1 or BCL-X_L leads to cell death in RMS cells

In order to verify that A-1331852/S63845 co-treatment-induced cell death was specifically due to dual MCL-1 and BCL-X_L inhibition and thereby exclude off-target effects of the pharmacological inhibitors, we genetically silenced MCL-1 and/or BCL-X_L via two siRNA constructs, respectively (Figure 5.11). Efficient knockdown (KD) was confirmed by Western blotting.

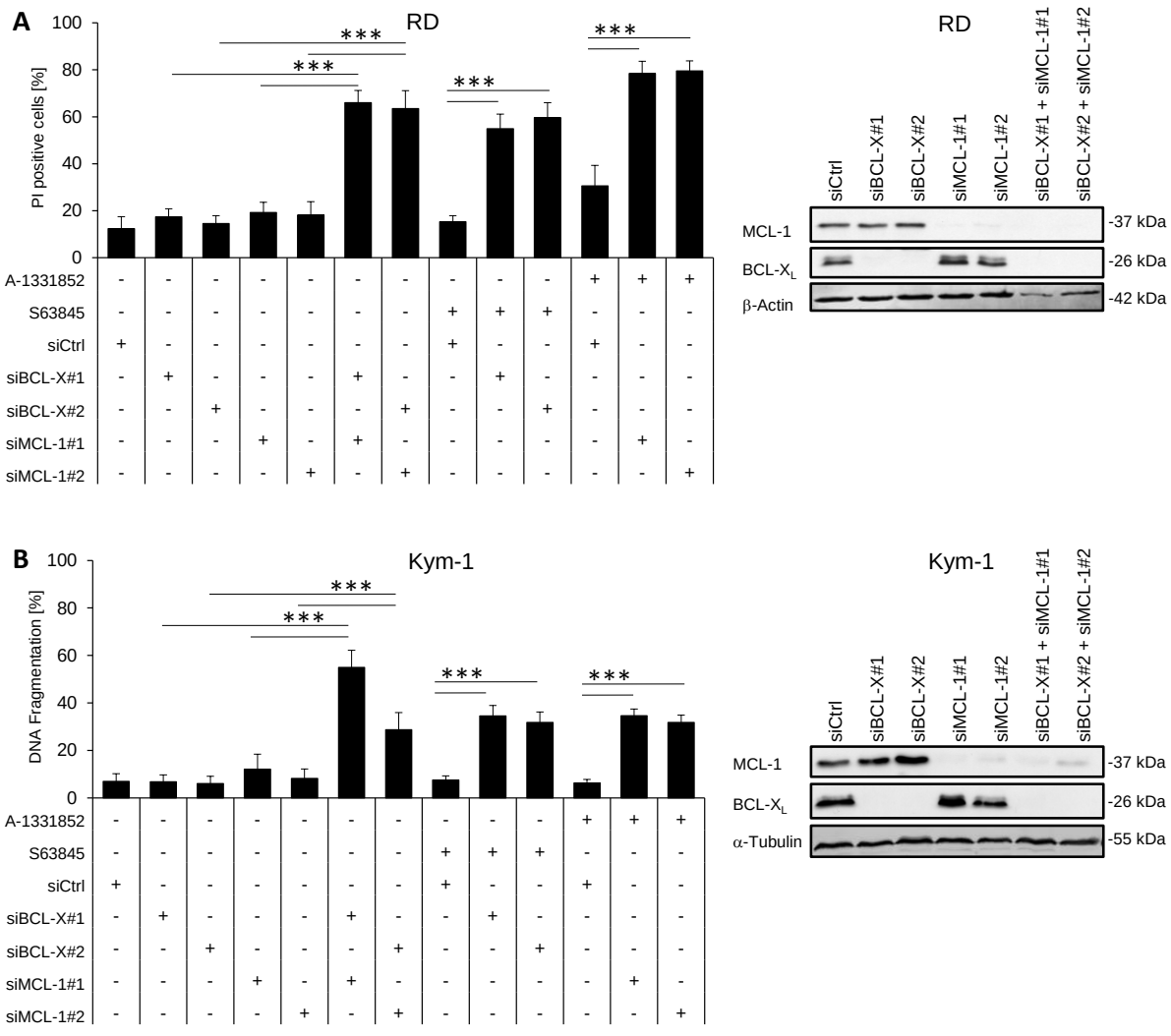

Figure legend on next page

Figure 5.11: Combination of genetic silencing and pharmacological inhibition of MCL-1 or BCL-X_L leads to cell death in RMS cells.

MCL-1 and/or BCL-X_L were transiently silenced in RD (A) and Kym-1 (B) cells by utilizing siRNA. Non-targeting siRNA was used as a control (siCtrl). Reduction of MCL-1 and/or BCL-X_L protein levels was determined by Western blotting 48 h (RD) or 72 h (Kym-1) upon transfection with β-Actin or α-Tubulin serving as a loading control. Representative blots of at least two independent experiments are shown. RD and Kym-1 cells were treated with 0.25 μM A-1331852 and 0.3 μM (RD) or 0.03 μM (Kym-1) S63845 where indicated and cell death was determined by fluorescence microscope analysis of PI uptake using Hoechst 33342/PI co-staining or analysis of DNA fragmentation of PI-stained nuclei 48 h (RD) or 72 h (Kym-1) after KD. Mean and SD of at least three independent experiments performed in triplicates are shown. ***P < 0.001.

Importantly, only transient silencing of MCL-1 and BCL-X_L caused a significant increase in cell death in RMS cell lines, while their individual KDs had no effect. Additionally, by combining pharmacological and genetic interference, we observed that only approaches targeting both MCL-1 and BCL-X_L significantly enhanced cell death, being fully in line with our previous findings. Consequently, we provide a proof of principle of the functional relevance of MCL-1 and BCL-X_L with regard to A-1331852/S63845-triggered cell death.

5.2.2 A-1331852 and S63845 act in concert to trigger rapid apoptosis in RMS cells

Next, we aimed to elucidate the type of cell death induced by A-1331852/S63845 co-treatment and to ascertain the kinetics with which it is accomplished. BH3 mimetics are reported to induce rapid intrinsic apoptosis (337). In order to assess whether this holds true also in the present work, exposure of phosphatidylserine, being a classical feature of apoptosis (77), was determined together with PI uptake by flow cytometry at 1, 2, 3, 6 and 24 h upon A-1331852/S63845 co-treatment (Figure 5.12).

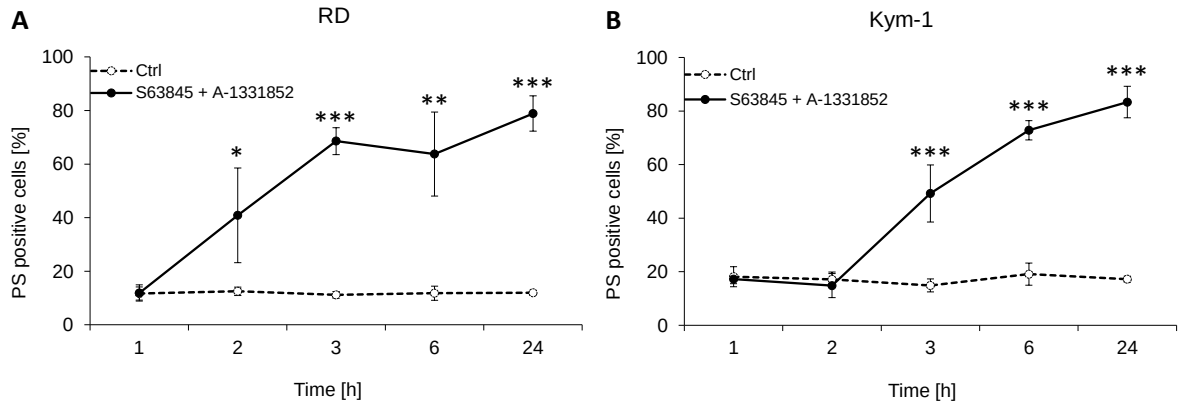

Figure 5.12: A-1331852 and S63845 act in concert to trigger rapid apoptosis in RMS cells.

RD (A) and Kym-1 (B) cells were treated with 0.25 μM A-1331852 and 0.3 μM (RD) or 0.03 μM (Kym-1) S63845. Cell death was assessed at indicated time points by determining PS exposure as an apoptotic marker using PI and Annexin/V-FITC co-staining. Mean and SD of at least three independent experiments performed in triplicates are shown. *P < 0.05, **P < 0.01, ***P < 0.001.

Remarkably, ~40% of RD cells exhibited apoptosis as soon as 2 h upon dual treatment with A-1331852 and S63845 (Figure 5.12A). The amount of apoptotic RD cells increased further from ~70% at 3 h to ~80% at 24 h. Apoptosis in Kym-1 cells started slightly later with ~50% of apoptotic cells at 3 h while no induction of apoptosis could be measured at 2 h upon treatment (Figure 5.12B). Moreover, apoptosis rate in Kym-1 cells rose further over time and peaked at 24 h with ~80% of apoptotic cells.

5.2.3 A-1331852/S63845 co-treatment-mediated apoptosis in RMS cells is dependent on swift caspase activation

Apoptosis is largely dependent on caspases, the executioners of apoptosis (187). To question whether caspase activation plays a role in A-1331852/S63845 co-treatment-mediated cell death, we conducted experiments using the broad range caspase inhibitor zVAD.fmk. Initially, cleavage and hence activation of caspases was assessed by Western blotting 1, 2 and 3 h upon A-1331852/S63845 co-treatment in RD and Kym-1 cells (Figure 5.13A).

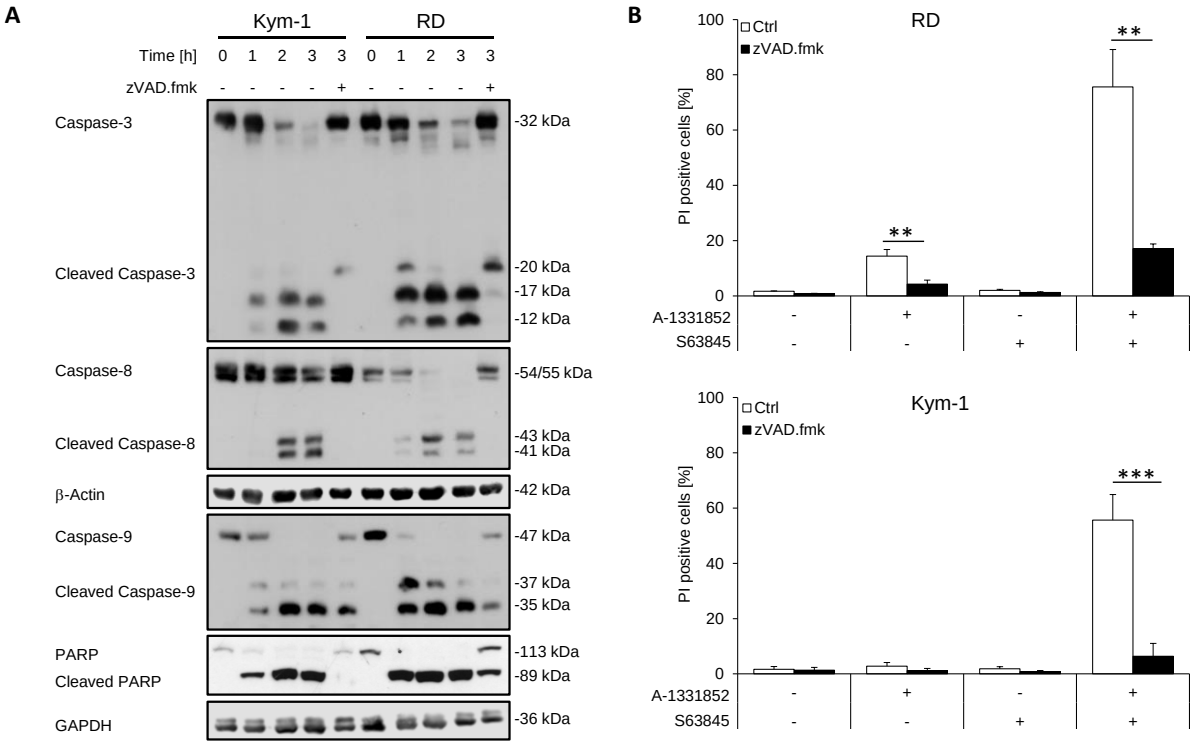

Figure 5.13: A-1331852/S63845 co-treatment-induced apoptosis in RMS cells is dependent on swift caspase activation.

(A+B): RD and Kym-1 cells were treated with 0.25 μM A-1331852 and 0.3 μM (RD) or 0.03 μM (Kym-1) S63845 either with or without 50 μM zVAD.fmk pre-treatment for 1 h where indicated. (A): Cells were analyzed for the cleavage of caspase-3, -8, -9 and PARP at indicated time points by Western blotting with β-Actin or GAPDH serving as a loading control. Representative blots of at least two independent experiments are shown. (B): Cell death was determined by fluorescence microscope analysis of PI uptake using Hoechst 33342/PI co-staining 48 h upon treatment. Mean and SD of at least three independent experiments performed in triplicates are shown. **P < 0.01, ***P < 0.001.

Intriguingly, cleavage of caspase-3, -8, -9 and PARP, being a prominent caspase target, were detected already 1 h upon treatment and increased over time. Of note, caspase-3 cleavage occurs in two subsequent steps. The first one splits the 32 kDa mature enzyme into 12 kDa and 20 kDa subunits. In the following, second step, the 20 kDa subunit is further cleaved into a 17 kDa and 3 kDa subunit (338). Importantly, A-1331852/S63845 co-treatment led to full cleavage of caspase-3 into 17 kDa and 12 kDa fragments. Pre-treatment with zVAD.fmk partially rescued A-1331852/S63845-stimulated cleavage of caspase-3 since only the 20 kDa fragment resulting from the first cleavage step of caspase-3 was detected. This points to a block in the last hydrolysis step which is in line with the described mechanism of action of zVAD.fmk (338). Similarly, also A-1331852/S63845-mediated cleavage of caspase-9 was partially rescued by the addition of zVAD.fmk as evidenced by the presence of both the uncleaved caspase-9 pro-form as well as the cleaved caspase-9 subunits at 35 kDa and 37 kDa. In contrast to caspase-3 and -9, cleavage of caspase-8 upon A-1331852/S63845 co-treatment was completely inhibited by zVAD.fmk indicating that caspase-8 is activated downstream of caspase-3 and -9. Consistently, zVAD.fmk significantly prevented cell death triggered by A-1331852/S63845 co-treatment as well as the low percentage of cell death induced by A-1331852 single treatment in RD cells (Figure 5.13B), thus confirming the functional relevance of caspase activation upon treatment with A-1331852/S63845.

5.2.4 A-1331852/S63845 co-treatment of RMS cells induces a caspase-dependent loss of MCL-1 while leaving other BCL-2 family proteins unaffected

In order to monitor the impact of caspase activation on BCL-2 family proteins, we assessed their expression levels upon A-1331852/S63845 co-treatment. Significantly, treatment did not alter the expression levels of the anti-apoptotic BCL-2 family proteins BCL-X_L and BCL-2, or the pro-apoptotic members BIM and NOXA. This was evidenced by protein detection at 1, 2 and 3 h upon treatment (Figure 5.14). Interestingly, loss of MCL-1, which started at 2 h upon A-1331852/S63845 co-treatment, was observed for both RMS cell lines. Rescue of MCL-1 protein levels by zVAD.fmk unveiled that this decrease was caspase-dependent.

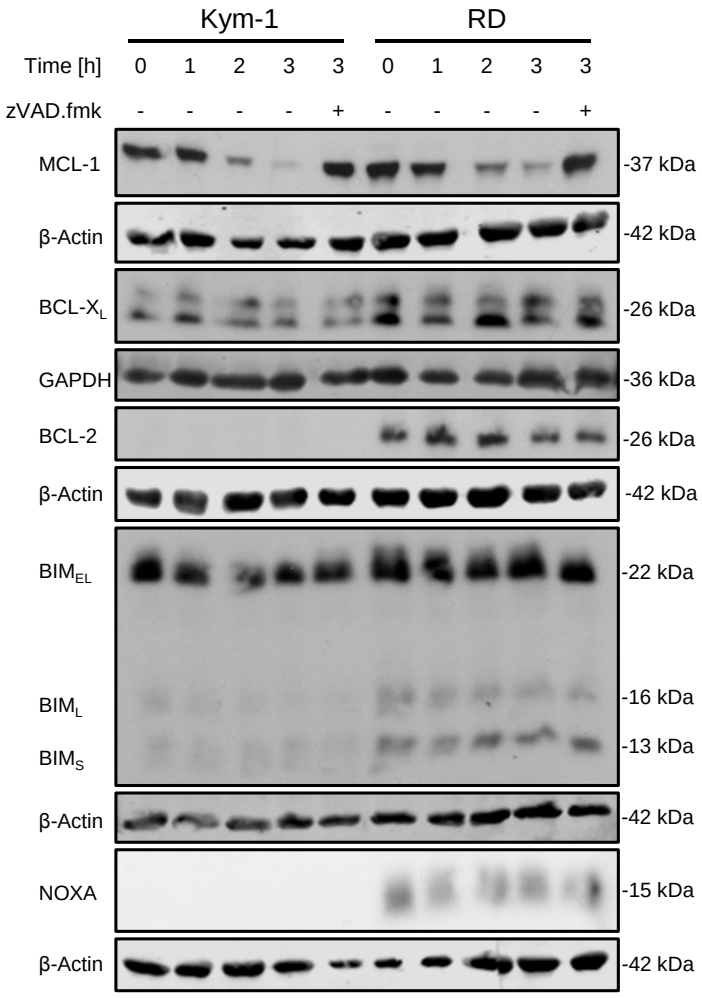

Figure 5.14: A-1331852/S63845 co-treatment of RMS cells induces a caspase-dependent loss of MCL-1 while leaving other BCL-2 family proteins unaffected.

RD and Kym-1 cells were treated with 0.25 μM A-1331852 and 0.3 μM (RD) or 0.03 μM (Kym-1) S63845 either with or without 50 μM zVAD.fmk pre-treatment for 1 h where indicated. Protein expression levels were analyzed at indicated time points by Western blotting with β-Actin serving as a loading control. Representative blots of at least two independent experiments are shown.

5.2.5 A-1331852 and S63845 act together to trigger rapid loss of MMP in RMS cells

Loss of MMP is a characteristic hallmark of the mitochondrial intrinsic apoptosis pathway (87). To elucidate whether concomitant inhibition of MCL-1 and BCL-X_L resulted in loss of MMP, we stained cells with the positively-charged fluorescent dye TMRM, which accumulates in active negatively-charged mitochondria and leaks out during loss of MMP. Analysis by flow cytometry at 1, 2, 3, 6 and 24 h upon A-1331852/S63845 co-treatment showed a marked and rapid loss of MMP in both RMS cell lines (Figure 5.15).

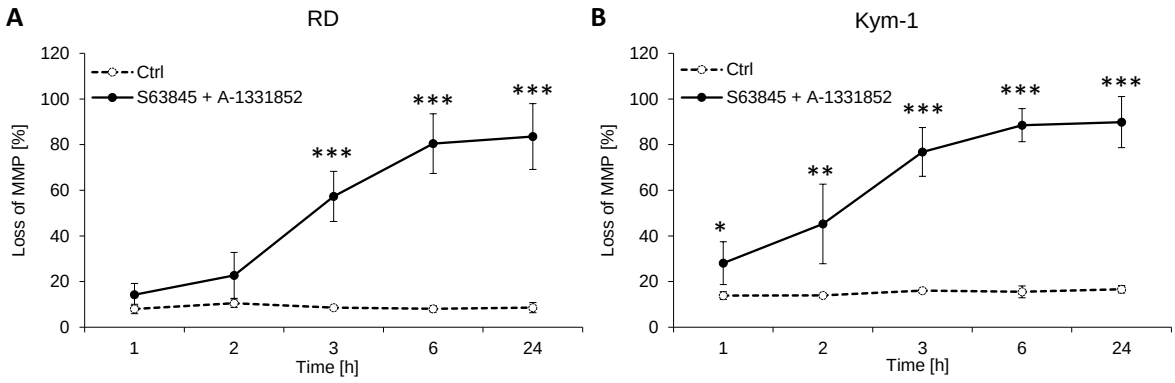

Figure 5.15: A-1331852 and S63845 act together to trigger rapid loss of MMP in RMS cells.

RD (A) and Kym-1 (B) cells were treated with 0.25 μM A-1331852 and 0.3 μM (RD) or 0.03 μM (Kym-1) S63845. Loss of MMP was assessed at indicated time points by TMRM staining and flow cytometry. Mean and SD of at least three independent experiments performed in triplicates are shown. *P < 0.05, **P < 0.01, ***P < 0.001.

After 3 h of A-1331852/S63845 co-treatment ~60% of RD cells showed loss of MMP. This percentage further increased over time and plateaued at ~80% after 6 h. (Figure 5.15A). In comparison to RD cells, Kym-1 cells followed a faster kinetic. A significant increase in loss of MMP was already measured 1 h after A-1331852/S63845 co-treatment (Figure 5.15B) rising in a time-dependent manner to its highest value of ~90% after 6 h.

Overall, this set of experiments showed that concomitant inhibition of BCL-X_L and MCL-1, either by a genetic or pharmacological approach, resulted in a marked induction of cell death. Furthermore, they shed light on the A-1331852/S63845-stimulated type of cell death mechanism, which i) was defined to be caspase-dependent apoptosis; ii) followed rapid kinetics; iii) led to caspase-dependent loss of MCL-1 and iv) engaged the mitochondrial apoptotic pathway.

5.3 The role of BAX and BAK in A-1331852/S63845-induced cell death in RMS cells

As A-1331852/S63845 co-treatment activated the mitochondrial apoptotic pathway, we further pursued to characterize the involved molecular players. BAX and BAK are key regulators of mitochondrial apoptosis (105) leading us to hypothesize that they might be involved in A-1331852/S63845-mediated apoptosis.

5.3.1 A-1331852/S63845 co-treatment causes BAX and BAK activation in RMS cells

The pro-apoptotic proteins BAX and BAK are crucial for pore formation in the mitochondrial membrane to facilitate intrinsic apoptosis (154). In order to do so, they undergo a conformational change, which can be determined by immunoprecipitation (149,330). To elucidate whether BAX and BAK were functionally relevant in A-1331852/S63845-induced apoptosis, we monitored their activation status upon treatment (Figure 5.16).

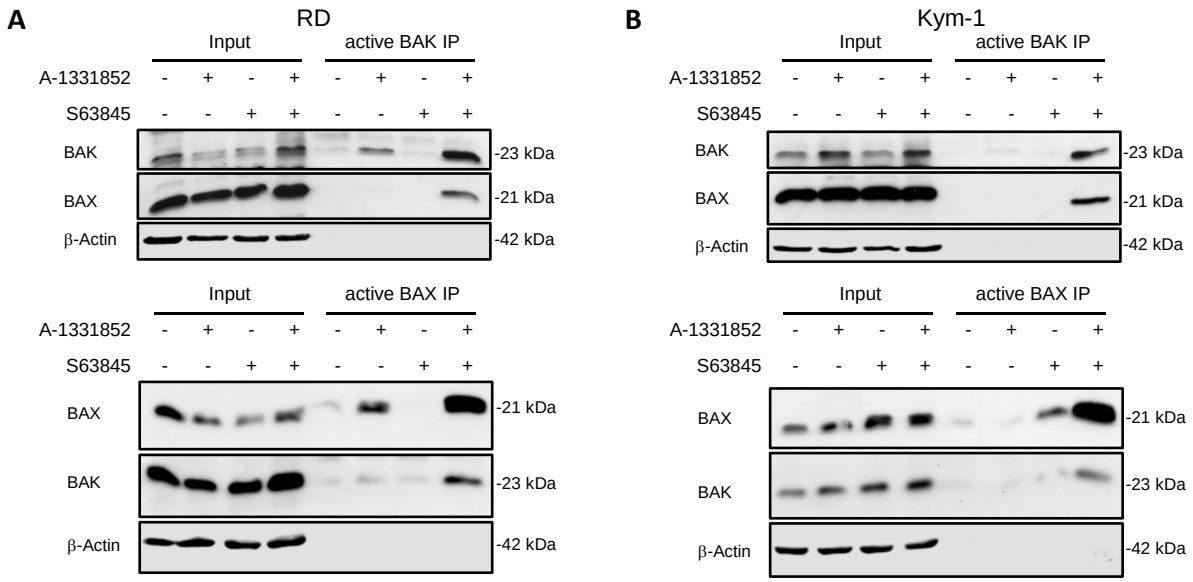

Figure 5.16: A-1331852/S63845 co-treatment causes an activation of BAX and BAK in RMS cells.
RD (A) and Kym-1 cells (B) were treated with 0.25 μM A-1331852 and/or 0.3 μM (RD) or 0.03 μM (Kym-1) S63845 for 3 h. Utilizing an active conformation-specific anti-BAK or anti-BAX antibody, activated BAK or BAX was immunoprecipitated. Presence of active BAX and BAK was analyzed by Western blotting together with total BAX and BAK expression levels and β-Actin. Representative blots of at least two independent experiments are shown.

Interestingly, we observed pronounced BAK and BAX activation upon A-1331852/S63845 co-treatment in both RMS cell lines. In addition, detection of co-immunoprecipitated BAX or BAK, being bound to the activated immunoprecipitated BAK or BAX, respectively, points to BAX/BAK complex formation upon treatment. Further, faint activation of BAK and BAX was noticed already upon A-1331852 single treatment in RD cells (Figure 5.16A). On the other hand, in Kym-1 cells,

BAX, but not BAK, was slightly activated by S63845 treatment alone (Figure 5.16B).

5.3.2 Individual or combined knockdown of BAX or BAK protects RMS cells from A-1331852/S63845-mediated cell death

To determine whether the presence of BAX and BAK was necessary for A-1331852/S63845-mediated apoptosis, BAX and/or BAK were genetically silenced in RD and Kym-1 cells via two siRNA constructs, respectively. KD efficiency was confirmed by Western blotting (Figure 5.17).

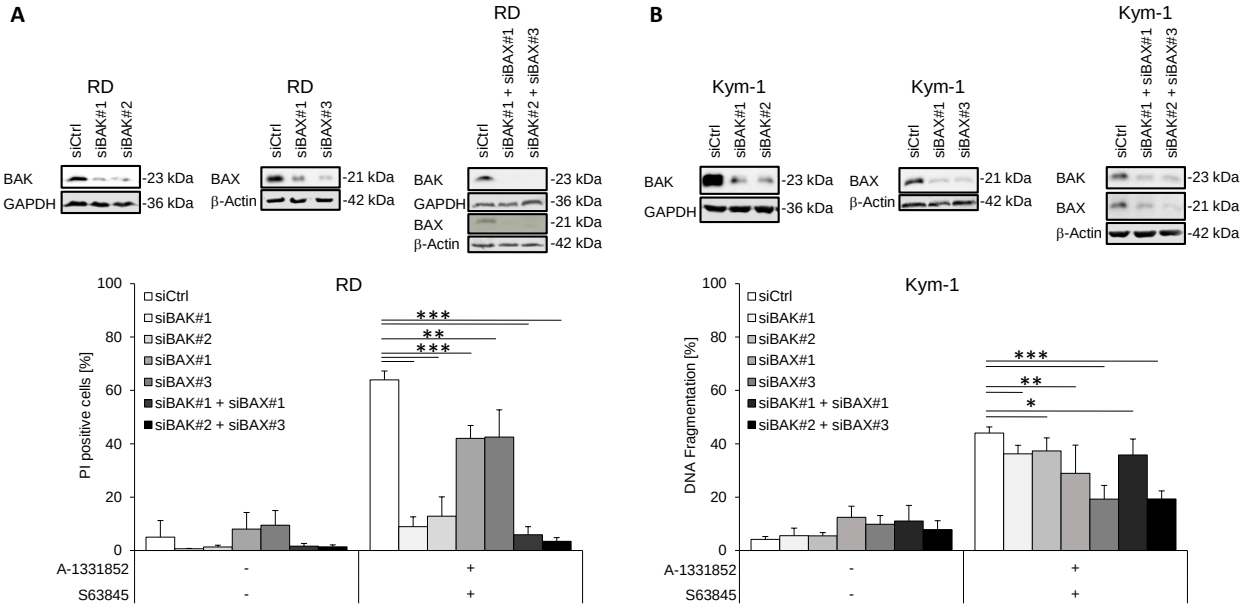

Figure 5.17: Individual or combined knockdown of BAX or BAK rescues RMS cells from A-1331852/S63845-mediated cell death.

BAX and/or BAK were transiently silenced in RD (A) and Kym-1 (B) cells by siRNA. Non-targeting siRNA was used as a control (siCtrl). Reduction of BAX and/or BAK protein levels was determined by Western blotting 48 h upon transfection with β-Actin or GAPDH serving as a loading control. Representative blots of at least two independent experiments are shown. RD and Kym-1 cells were treated with 0.25 μM A-1331852 and 0.3 μM (RD) or 0.03 μM (Kym-1) S63845 and cell death was determined by fluorescence microscope analysis of PI uptake using Hoechst 33342/PI co-staining (RD) or analysis of DNA fragmentation of PI-stained nuclei (Kym-1) 24 h upon treatment. Mean and SD of at least three independent experiments performed in triplicates are shown. *P < 0.05, **P < 0.01, ***P < 0.001.

Indeed, KD of BAK alone as well as BAK/BAX double KD completely rescued cell death triggered by A-1331852/S63845 co-treatment in RD cells (Figure 5.17A). In addition, single silencing of BAX led to a significant, albeit partial rescue of apoptosis in RD cells. Of note, reduction of BAK alone caused a significant, however minor decrease of cell death in Kym-1 cells (Figure 5.17B), while BAX single KD prevented A-1331852/S63845-induced apoptosis in this cell line more effectively. In line with this, the protective effect of BAK/BAX double KD in Kym-1 cells was mainly attributed to the effect of BAX KD alone.

5.3.3 BAX knockdown in BAK knockout RD cells, but not BAK knockout alone, rescues from A-1331852/S63845 co-treatment-induced cell death

Silencing of BAX and BAK by siRNA as performed in the previous section does not produce a complete lack of these proteins. Therefore, we aimed at a system in which these proteins were fully absent and possibly be able to provide a proof of principle concerning the previous results. To this end, we exploited the CRISPR/CAS9 system to generate RD and Kym-1 cells with genetic deletion of BAK (Figure 5.18).

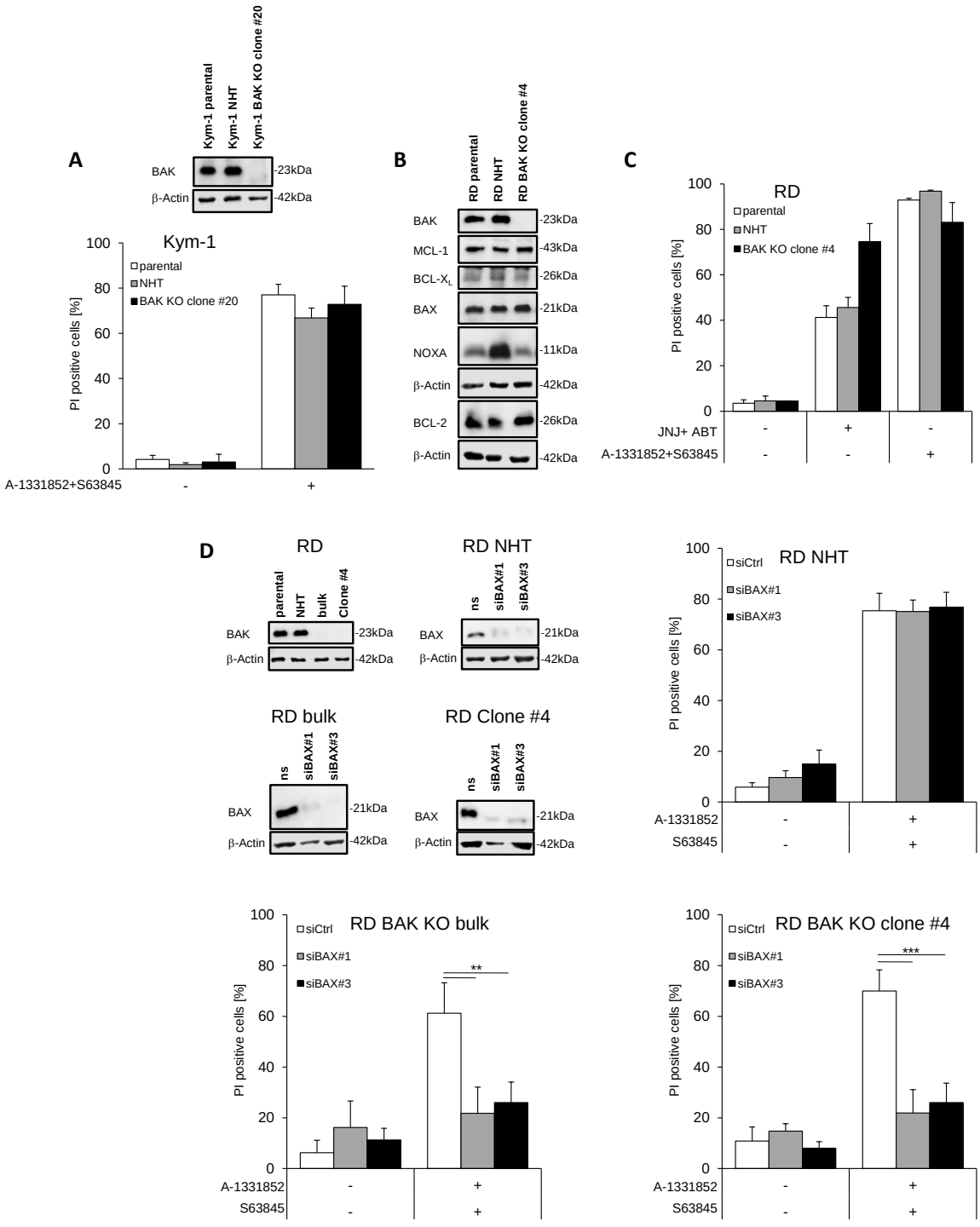

Figure legend on next page

Figure 5.18: BAX knockdown in BAK knockout RD cells, but not BAK knockout alone, rescues from A-1331852/S63845 co-treatment-induced cell death.

(A-C): Parental, BAK KO and BAK NHT Kym-1 cells (A) and parental, BAK KO clone #4 and BAK NHT RD cells (C) were treated with 0.25 μM A-1331852 and 0.3 μM (RD) or 0.03 μM (Kym-1) S63845. Treatment with 15 nM JNJ and 5 μM ABT-199 was utilized as a control for BAK dependent apoptosis in RD cells. Cell death was determined by fluorescence microscope analysis of PI uptake using Hoechst 33342/PI co-staining 24 h upon treatment. (A+B): Protein expression levels were analyzed by Western blotting with β-Actin serving as a loading control. Representative blots of at least two independent experiments are shown. (D): BAX was transiently silenced in RD NHT cells, RD BAK KO bulk cells and RD BAK KO clone #4 by utilizing siRNA. Non-targeting siRNA was used as a control (siCtrl). Reduction of BAX protein levels was determined by Western blotting 48 h upon transfection. Protein expression levels were analyzed by Western blotting with β-Actin serving as a loading control. Representative blots of at least two independent experiments are shown. Cells were treated and cell death was assessed as described in (A-C). Mean and SD of at least three independent experiments (two independent experiments in RD cells treated with JNJ+ABT) performed in triplicates are shown. **P < 0.01, ***P < 0.001.

After single cell clones were expanded, Western blotting analysis of BAK was performed to test the KO efficacy. Importantly, BAK was completely absent in the generated single cell clones (exemplarily clone #20 is shown for Kym-1 cells and clone #4 is shown for RD cells; other clones not shown), while BAK was still expressed in non-human target (NHT) control cells (Figure 5.18A+B). In addition, Sanger sequencing confirmed successful cutting of CAS9 at gRNA specific DNA sequences (data not shown). Unexpectedly, Kym-1 BAK KO clone #20 and RD BAK KO clone #4 were not significantly protected from A-1331852/S63845-induced cell death (Figure 5.18A+C). Of note, all other tested clones displayed the same inability to rescue cell death upon A-1331852/S63845 co-treatment (data not shown). Heinicke and Haydn *et al.* showed that BAK KD rescued JNJ/ABT-199-induced cell death from ~40% to ~15 - 20% (246), thereby providing a positive control for BAK-dependent cell death in RD cells. However, RD BAK KO clone #4 failed to rescue from JNJ/ABT-199-triggered cell death and even enhanced cell death (Figure 5.18C). To our best knowledge, there was no established, profound positive control for BAK-dependent cell death in Kym-1 cells determined in the literature.

After obtaining these surprising results, we hypothesized that KO of BAK could lead to alterations of BCL-2 family proteins that could compensate for the loss of BAK. However, Western blotting analysis performed in RD BAK clone #4 demonstrated neither increase nor decrease of BCL-2 family members (Figure 5.18B). Of note, the expression levels of NOXA were inconsistent in RD NHT cells throughout the replicates compared to parental RD cells. Nevertheless, there was no difference monitored in the NOXA expression levels of parental and RD BAK KO clone #4.

Since the observed findings could not be explained by changes in the investigated BCL-2 family expression levels, we questioned whether BAX might compensate for the loss of BAK in RD BAK KO cells. This might serve as an adaptation process evolving as a means to circumvent apoptosis initiation. To test this hypothesis, we silenced BAX by two siRNA constructs in RD BAK KO cells

(Figure 5.18D). Besides the RD BAK KO clone #4, we further included the RD BAK KO bulk culture in our study to account for alterations that might have developed throughout the single clone selection process. KD efficacy was confirmed by Western blotting and BAK KO was also present in the RD BAK KO bulk culture. In contrast to the data obtained in parental cells (Figure 5.17A), BAX KD almost completely prevented A-1331852/S63845-induced cell death in RD BAK KO clone #4 as well as in the RD BAK KO bulk culture. This suggests a differential function of BAX in RD BAK KO cells compared to parental RD cells. A partial rescue was also expected in RD NHT cells comparable to the one in parental RD cells presented in the previous figure (Figure 5.17A), this was, however, not observed.

Experiments with RD BAK KO cells led to unclear results regarding the reliability of the system when it comes to unaltered functional relevance of BCL-2 family proteins and their interaction patterns compared to parental RMS cells. For this reason, no BAX KO RMS cell lines were created.

5.3.4 Co-treatment with A-1331852/S63845 displaces BAK from MCL-1 and BCL-X_L in RMS cells

MCL-1 and BCL-X_L were reported to interact with BAK in order to prevent apoptosis (Mode 2 of sequestration) (128,134). Therefore, A-1331852/S63845 co-treatment might influence the interactions between BAK and MCL-1 and/or BCL-X_L thus leading to activation and complex formation of BAK and BAX resulting in apoptosis initiation. With the aim to investigate whether there was a change in the binding pattern of MCL-1/BCL-X_L with BAK, Co-IPs of BAK were performed (Figure 5.19).

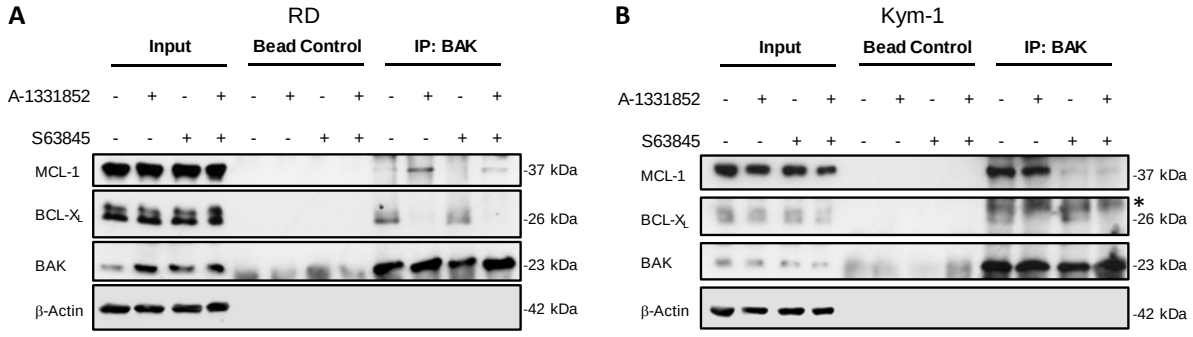

Figure 5.19: A-1331852/S63845 co-treatment displaces BAK from MCL-1 and BCL-X_L in RMS cells. RD (A) and Kym-1 cells (B) were pre-treated with zVAD.fmk for 1 h and afterwards treated with 0.25 μM A-1331852 and/or 0.3 μM (RD) or 0.03 μM (Kym-1) S63845 for 3 h. Subsequently, a BAK IP was performed and precipitates were analyzed for interactions with BCL-X_L and MCL-1. β-Actin served as a loading control. Representative blots of at least two independent experiments are shown. An asterisk indicates an unspecific band.

Strikingly, BAK was endogenously bound to BCL-X_L in RD cells, while it was strongly sequestered by MCL-1 in Kym-1 cells. Furthermore, in RD cells A-1331852 treatment alone disrupted the interaction between BAK and BCL-X_L and shifted BAK to MCL-1 (Figure 5.19A). Of note, additional treatment with S63845 markedly blocked this shift. Likewise, we detected a faint interaction between BAK and BCL-X_L in Kym-1 cells that was presumably disrupted by A-1331852 single treatment or A-1331852/S63845 co-treatment (Figure 5.19B). Moreover, we observed that S63845 single treatment and A-1331852/S63845 co-treatment displaced BAK from MCL-1 in Kym-1 cells.

5.3.5 BAX does not interact with MCL-1 or BCL-X_L in untreated or A-1331852/S63845 co-treated Kym-1 cells

Similar to BAK, also BAX is described to be bound to MCL-1 and BCL-X_L, which prevents it to exert its pro-apoptotic action (Mode 0 / Mode 2 of sequestration) (109,110,134). In order to check whether A-1331852/S63845 co-treatment had comparable effects on BAX as on BAK interactions (Figure 5.19), we analyzed the interaction pattern of BAX with MCL-1/BCL-X_L by conducting BAX Co-IPs. However, we did not detect any interactions of BAX with MCL-1 or BCL-X_L, neither in A-1331852/S63845-treated, nor in untreated Kym-1 cells (Figure 5.20). Additionally, in BCL-X_L and MCL-1 Co-IPs no interactions of MCL-1 or BCL-X_L with BAX were detected (data not shown), which confirms the observations in the vice versa BAX Co-IPs.

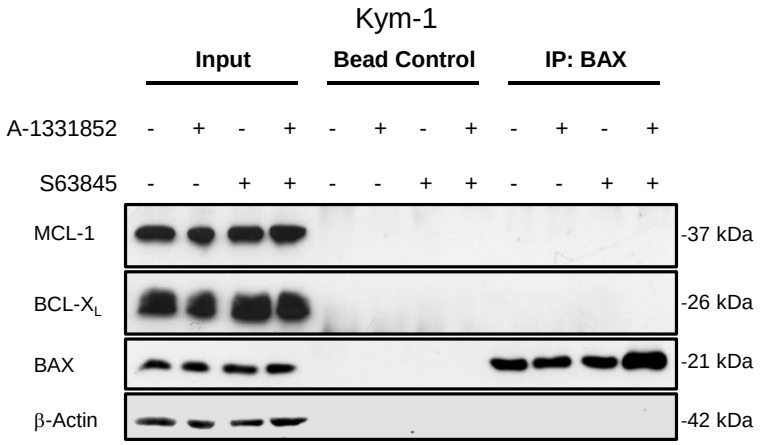

Figure 5.20: BAX does not interact with MCL-1 or BCL-X_L in untreated or A-1331852/S63845 co-treated Kym-1 cells.

Kym-1 cells were pre-treated with zVAD.fmk for 1 h and afterwards treated with 0.25 μM A-1331852 and 0.03 μM S63845 for 3 h. Subsequently, a BAX IP was performed and precipitates were analyzed for interactions with BCL-X_L and MCL-1. β-Actin served as a loading control. Representative blots of at least two independent experiments are shown.

With regard to the BAX Co-IP, we initially focused on the Kym-1 cell line for two reasons: Firstly, BAX protein levels were higher in Kym-1 cells compared to RD cells (Table 5.1). Secondly, KD experiments of BAX and BAK in Kym-1 cells demonstrated a higher relevance of BAX than BAK in this cell line (Figure 5.17). Since the BAX Co-IP required extensive optimization and BAX was found

to be less relevant in RD cells for A-1331852/S63845-mediated cell death (Figure 5.16 and Figure 5.17), we decided to not follow this up further.

In this subpart of the study, we demonstrated the importance and functional relevance of the pro-apoptotic BCL-2 family proteins BAX and BAK in executing apoptosis induced by A-1331852/S63845-co-treatment. In conclusion, i) BAX and/or BAK were (partially) necessary to mediate A-1331852/S63845-triggered apoptosis in a cell line-dependent manner; ii) A-1331852/S63845 co-treatment facilitated the activation and complex formation of BAX and BAK; iii) A-1331852 and/or S63845 released BAK from MCL-1 and BCL-X_L; iv) the results from our experiments lead us to hypothesize that in Kym-1 cells BAX is not endogenously bound to BCL-X_L or MCL-1 and thereby cannot be displaced by A-1331852/S63845 co-treatment.

5.4 The role of BH3-only proteins in A-1331852/S63845-caused cell death in RMS cells

Not only BAX and BAK, but also BH3-only proteins such as BIM, NOXA, PUMA and BMF are crucial performers in intrinsic apoptosis (121). Since it is known that BH3 mimetics are able to disrupt pro-apoptotic BH3-only proteins from their binding with MCL-1 and BCL-X_L (227,270), we speculated that this might also be the case for A-1331852/S63845-induced apoptosis.

5.4.1 The BH3-only proteins BIM and NOXA contribute to A-1331852/S63845-induced cell death in a cell line-dependent manner

To begin with, we aimed at determining whether the presence of BIM, NOXA, PUMA and BMF was critical for apoptosis caused by A-1331852/S63845-co-treatment. To this end, these proteins were transiently silenced utilizing two or three siRNA constructs in RD (Figure 5.21) and Kym-1 cells (Figure 5.22). Western blotting evidenced KD efficacy. Interestingly, BIM KD resulted in a slight, however statistically significant, prevention of A-1331852/S63845-mediated cell death in RD, but not in Kym-1 cells (Figure 5.21 and Figure 5.22A). Furthermore, KD of NOXA alone or combined NOXA/BIM KD markedly rescued A-1331852/S63845-induced cell death in RD cells from ~60% to ~25 - 40% (Figure 5.21B+C). Due to the lack of NOXA expression in Kym-1 cells (Figure 5.1), we refrained from conducting a NOXA KD in this cell line. Moreover, transient silencing of PUMA failed to protect both RD and Kym-1 cells from cell death mediated by concomitant A-1331852/S63845 treatment (Figure 5.21D and Figure 5.22B). Finally, we examined a potential role of BMF in this context. However, similar to PUMA, reduction of BMF by siRNA was incapable to decrease cell death induced by A-1331852/S63845 co-treatment (Figure 5.21E and Figure 5.22C). RMS cell lines display only minor expression of BMF, thus making it challenging to prove the reduction of BMF expression upon KD by Western blotting. Consequently, we performed qPCR and confirmed a tendency towards a decrease of BMF mRNA levels upon KD, which was statistically significant at least in Kym-1 cells (Figure 5.21E and Figure 5.22C).

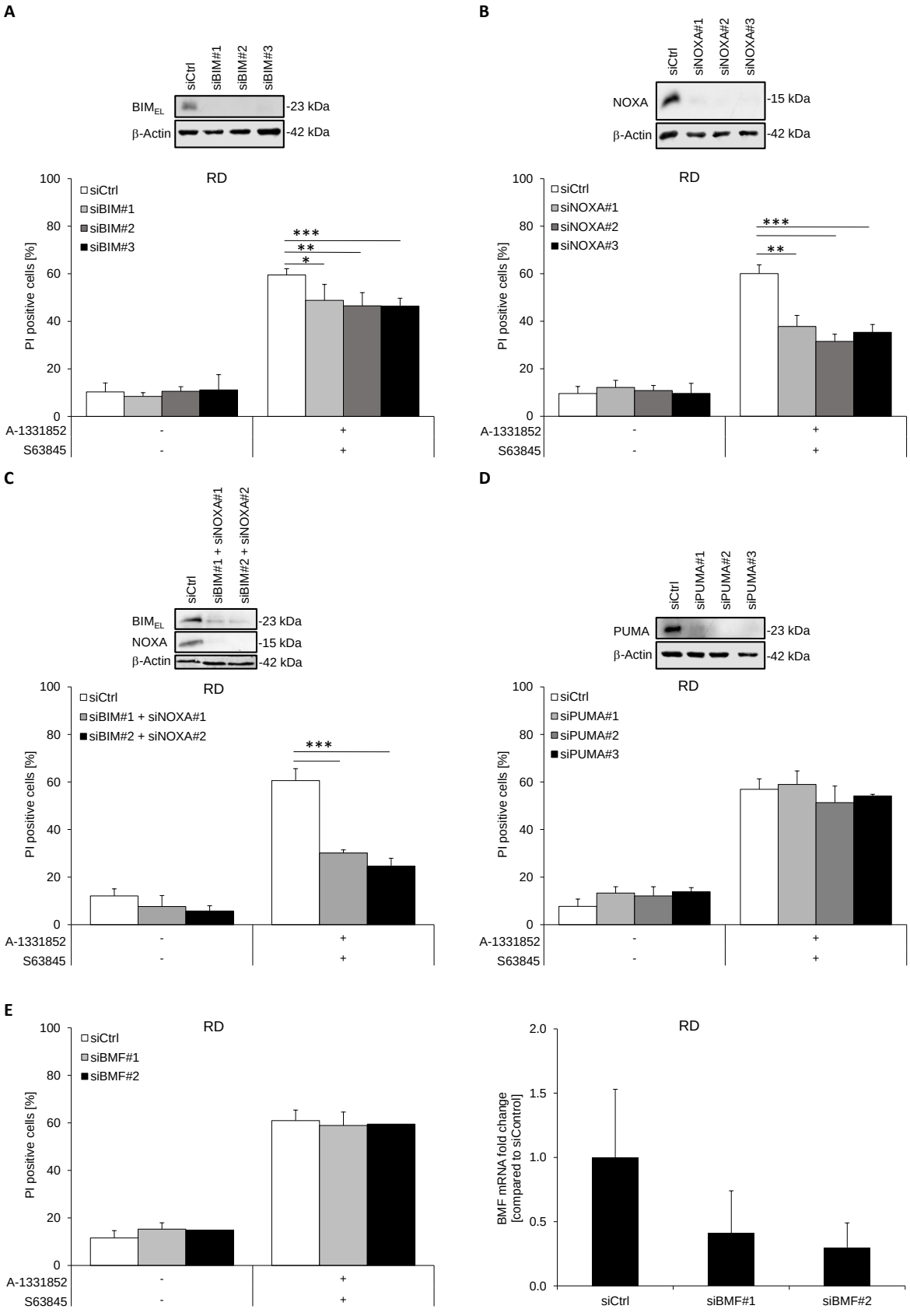

Figure legend on next page

Figure 5.21: The BH3-only proteins BIM and NOXA contribute to A-1331852/S63845-mediated cell death in RD cells.

BIM and/or NOXA (A-C), PUMA (D) or BMF (E) were transiently silenced in RD cells by siRNA. Non-targeting siRNA was used as a control (siCtrl). Reduction of respective protein levels was determined by Western blotting 48 h after transfection with β-Actin serving as a loading control. Representative blots of at least two independent experiments are shown. (A-D). Reduction of BMF mRNA levels was assessed 48 h after transfection by q-PCR (at least three independent experiments were performed) (E). RD cells were treated with 0.25 μM A-1331852 and 0.3 μM S63845 and cell death was determined by fluorescence microscope analysis of PI uptake using Hoechst 33342/PI co-staining 24 h upon treatment. Mean and SD of at least three independent experiments performed in triplicates are shown. *P < 0.05, **P < 0.01, ***P < 0.001.

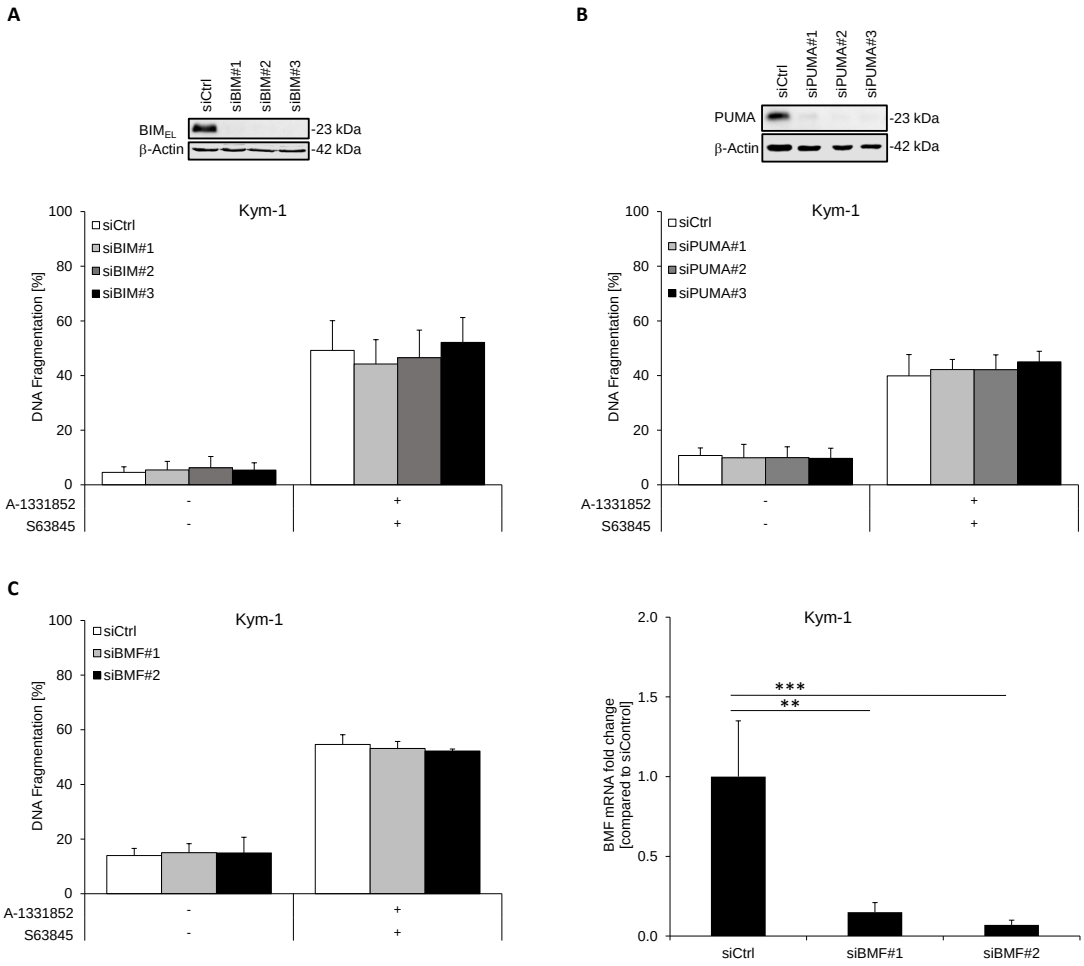

Figure 5.22: The BH3-only proteins BIM, PUMA and BMF do not contribute to A-1331852/S63845-mediated cell death in Kym-1 cells.

BIM (A), PUMA (B) or BMF (C) were transiently silenced in Kym-1 cells by siRNA. Non-targeting siRNA was used as a control (siCtrl). Reduction of respective protein levels was determined by Western blotting 48 h after transfection with β-Actin serving as a loading control. Representative blots of at least two independent experiments are shown (A+B). Reduction of BMF mRNA levels was assessed 48 h after transfection by q-PCR (at least three independent experiments were performed) (C). Kym-1 cells were treated with 0.25 μM A-1331852 and 0.03 μM S63845 and cell death was determined by analysis of DNA fragmentation of PI-stained nuclei 24 h upon treatment. Mean and SD of at least three independent experiments performed in triplicates are shown. **P < 0.01, ***P < 0.001.

5.4.2 A-1331852/S63845 co-treatment leads to a shift in the interaction pattern of BH3-only and anti-apoptotic BCL-2 family proteins in RD, but not in Kym-1 cells

As BIM and NOXA played a role in implementing A-1331852/S63845-induced cell death in RD cells, the question inevitably arose how BIM and NOXA performed their function. Therefore, we analyzed the interaction pattern of the anti-apoptotic BCL-2 family proteins MCL-1, BCL-X_L and BCL-2 with the BH3-only proteins NOXA and BIM by performing Co-IPs of MCL-1, BCL-X_L and BCL-2 (Figure 5.23).

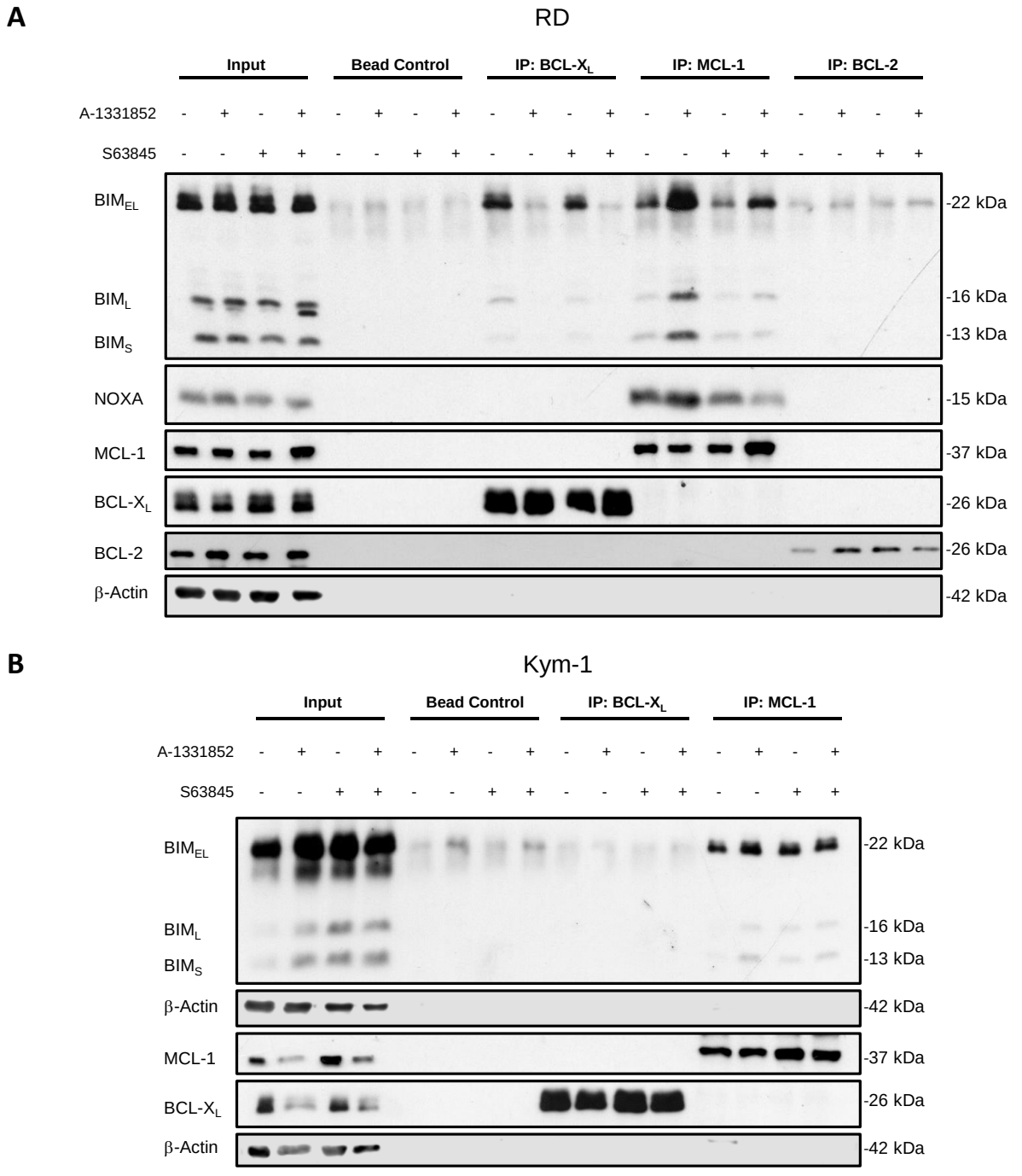

Figure legend on next page

Figure 5.23: A-1331852/S63845 co-treatment leads to a shift in the interaction pattern of BH3-only and anti-apoptotic BCL-2 family proteins in RD, but not in Kym-1 cells.

RD (A) and Kym-1 (B) cells were pre-treated with zVAD.fmk for 1 h and afterwards treated with 0.25 μM A-1331852 and 0.3 μM (RD) or 0.03 μM (Kym-1) S63845 for 3 h. Subsequently, MCL-1, BCL-X_L and BCL-2 IPs were performed and precipitates were analyzed for interactions with BIM and NOXA. β-Actin served as a loading control. Representative blots of at least two independent experiments are shown.

In RD cells, BIM was endogenously sequestered by BCL-X_L and MCL-1 (Figure 5.23A). Strikingly, A-1331852 single treatment shuttled BIM from BCL-X_L to MCL-1, a process that could partly be averted by concomitant treatment with S63845. Furthermore, endogenous binding of NOXA with MCL-1 in RD cells was disrupted by S63845 alone and A-1331852/S63845 co-treatment. Neither was BIM endogenously interacting with BCL-2, nor was it shuttled from MCL-1 or BCL-X_L to BCL-2 upon A-1331852/S63845 co-treatment.

Next, we investigated the binding pattern of BCL-2 family proteins in Kym-1 cells as well. Even though BIM was endogenously interacting with MCL-1, S63845 as single agent or in combination with A-1331852 did not provoke any alteration of this binding (Figure 5.23B), thus providing additional evidence that BIM is not involved in A-1331852/S63845-stimulated cell death in Kym-1 cells. In contrast to RD cells, BIM was not endogenously sequestered by BCL-X_L in this cell line. As Kym-1 cells did not express NOXA (Figure 5.1), we did not probe for any interactions with this protein.

In summary, this set of experiments highlighted the role of BIM and NOXA in A-1331852/S63845-induced cell death in RD cells and showed that i) the BH3-only proteins BIM and NOXA contributed to execute apoptosis triggered by A-1331852/S63845 co-treatment in RD, but not in Kym-1 cells; ii) the BH3-only proteins PUMA and BMF did not contribute to A-1331852/S63845-mediated apoptosis in RMS cells; iii) A-1331852/S63845 co-treatment influenced the interaction pattern of BIM and NOXA with BCL-X_L and MCL-1 in RD, but not in Kym-1 cells.

5.5 Investigating A-1331852/S63845 co-treatment with regard to future clinical applications in RMS cells

In the previous parts of the thesis, we explored the potency of A-1331852/S63845 co-treatment in pediatric solid tumor cells and shed light on its molecular mechanism in RMS. In order to pave the way for this highly effective combination treatment to the clinic, additional studies focusing on its application are indispensable. Therefore, we evaluated different treatment schedules as well as the effect of A-1331852/S63845-co-treatment on non-malignant cells, in a spheroid-based 3D approach and in an *in vivo* CAM model.

Experiments with RMS spheroids were performed in cooperation with the Ph.D. student Vinzenz Särchen (indicated in the Figure legends), who contributed equally to the establishment of spheroid cell culture.

5.5.1 Non-malignant cells are largely spared by A-1331852/S63845 co-treatment

It is of utmost importance that cancer treatment is selectively targeting cancer cells while sparing healthy cells. As A-1331852/S63845 co-treatment was found to be the most effective BH3 mimetic combination in all tested pediatric solid cancers, we proceeded to study its effect on non-malignant tissue. To this aim, we used A-1331852 and/or S63845 at concentrations relevant for further studies.

First, we checked whether the human fibroblast cell line MRC5 was susceptible to dual blockade of MCL-1 and BCL-X_L. Remarkably, A-1331852/S63845 co-treatment caused no or only a slight increase in cell death or activation of caspase-3 and -7 (Figure 5.24A+B). This faint rise was mainly mediated by A-1331852 alone. Since the MCL-1 inhibitor S63845 is administered intravenously (i.v.) (227), we extended our study to human peripheral blood mononuclear cells (PBMCs). After isolation of PBMCs from Buffy coats of three individual human healthy donors, their response towards A-1331852/S63845 co-treatment was monitored (Figure 5.24C). In line with MRC5 cells, PBMCs did not display a marked increase in cell death upon treatment.

In this context, Western blotting analysis was performed to assess the presence of BCL-2 family proteins in MRC5 cells and PBMCs in direct comparison to RMS cell lines. In general, MRC5 cells as well as all three individual PBMCs samples showed the expression of all BCL-2 family proteins (Figure 5.24D). Exceptionally, expression of NOXA was unclear in PBMCs as the detected signal for this protein was faint or absent. BCL-2 family proteins were expressed to slightly variable, however similar extents throughout PBMCs, MRC5 and RMS cells. Two outstanding differences were apparent: Firstly, MCL-1 expression levels were lower in PBMCs compared to MRC5 and RMS cells. Secondly, BIM expression was decreased in MRC5 cells in comparison to RMS cell lines.

To account for the fact that RMS cells, which were mainly used throughout this thesis, presumably originate from mesenchymal muscle progenitor cells (9), we explored the vulnerability of the murine myoblast cell line C2C12 towards A-1331852/S63845 co-treatment. Strikingly, A-1331852/S63845 co-treatment induced no or only a slight increase in cell death or activation of caspase-3 and -7 which was primarily attributed to A-1331852 treatment alone (Figure 5.24D). Since C2C12 cells are of murine origin and the antibodies used throughout the study were not suitable to detect murine proteins, BCL-2 family protein expression levels in C2C12 cells were not included in the Western blotting analysis.

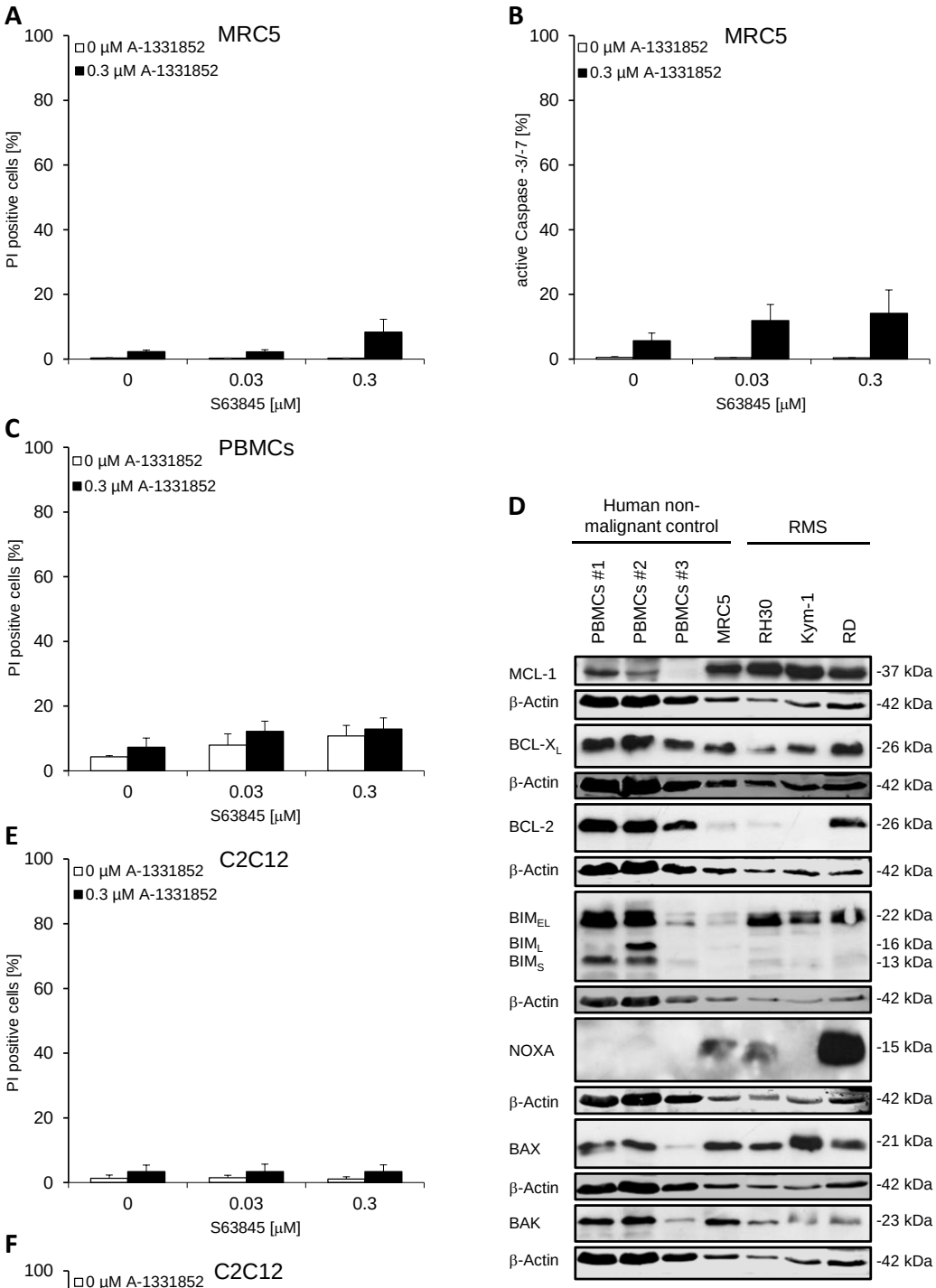

Figure legend on next page

Figure 5.24: Non-malignant cells are largely spared by A-1331852/S63845 co treatment.

MRC5 cells (A,B), human PBMCs isolated from three individual buffy coats of healthy donors (C) and C2C12 cells (E,F) were treated with indicated concentrations of A-1331852 and/or S63845 for 48 h. Cell death was determined by fluorescence microscope analysis of PI uptake using Hoechst 33342/PI co-staining (A,C,E). CellEvent™ Caspase 3/7 assay was utilized to assess caspase activity (B,F). Mean and SD of at least three independent experiments performed in triplicates are shown. (D): Basal expression levels of anti- and pro-apoptotic BCL-2 family proteins in RMS cell lines were compared to non-malignant cells. Protein expression levels were analyzed by Western blotting with β-Actin serving as a loading control. Representative blots of at least two independent experiments (MRC5 and RMS cell lines) or one experiment (PBMCs of three individual donors) are shown.

5.5.2 A treatment schedule including BH3 mimetic pre-treatment is feasible to induce cell death in RMS cells

Administering A-1331852 and S63845 at the same time might present a challenge to clinical studies concerning side effects in the patients since inhibition of MCL-1 and/or BCL-X_L provokes apoptosis in hepatocytes (178,179). However, cancer treatments exercised in the clinic frequently include repetitive treatment schedules with consecutive drug administration. In order to examine whether successive treatment of BH3 mimetics led to similar amounts of cell death as simultaneous application of the drugs, pre-treatment with either one of the BH3 mimetics was performed before the second drug was added 24 h later. Cell death was determined after another 24 h (Figure 5.25). Of note, BH3 mimetics pre-treatment significantly decreased the percentage of cell death compared to concomitant drug treatment in both RMS cell lines. Nevertheless, A-1331852 and S63845 pre-treatment still yielded ~45 - 50% and ~25 - 30% cell death, respectively. Interestingly, pre-treatment with A-1331852 resulted in a stronger effect than S63845 pre-treatment in both Kym-1 and RD cells.

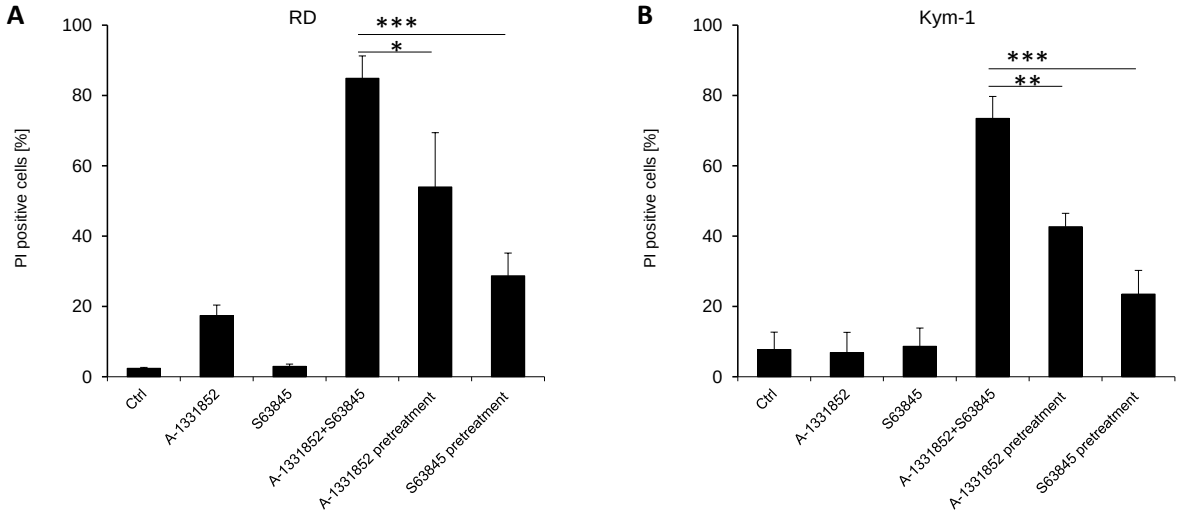

Figure legend on next page

Figure 5.25: A treatment schedule including BH3 mimetic pre-treatment is feasible to induce cell death in RMS cells.

RD (A) and Kym-1 (B) cells were treated with 0.25 μM A-1331852 and 0.3 μM (RD) or 0.03 μM (Kym-1) S63845 in a sequential manner: Cells were pre-treated with one of the agents and 24 h later the second BH3 mimetic was added. Cell death was determined by fluorescence microscope analysis of PI uptake using Hoechst 33342/PI co-staining 24 h upon treatment with the second agent. Mean and SD of at least three independent experiments performed in triplicates are shown. *P < 0.05, **P < 0.01, ***P < 0.001.

5.5.3 RMS spheroids are sensitive to A-1331852/S63845 co-treatment

Cells naturally grow in a three-dimensional (3D) environment. Therefore, two-dimensional (2D) conventional cell culture has only limited validity regarding the response of tumor cells to a certain treatment. 3D multicellular spheroids can enable a more realistic prediction of drug sensitivity (339-341). Hence, we sought to generate multicellular RMS spheroids with the aim to explore their vulnerability to A-1331852/S63845 co-treatment. To start with, we chose GFP-labelled RD and RH30 cells (RD-GFP and RH30-GFP) to facilitate fluorescence microscope imaging. In addition, we utilized Kym-1 cells that are not yet available with GFP expression. Depending on the cell line, spheroids were prepared with cell numbers ranging from 1000 – 10,000 and their growth was monitored for seven days upon seeding (Figures 5.26-5.28). Long-term culture of spheroids was possible 13 – 17 days after seeding (data not shown).

Importantly, all three cell lines were capable to build spheroids that increased in size over time in a cell number-dependent manner. Interestingly, the spheroid phenotype varied between the different RMS cell lines as RD-GFP cells formed particularly compact and round spheroids with a sharp border to its environment (Figure 5.26A). On the other hand, Kym-1 spheroids were characterized by a more loose assembly, but still displayed defined borders (Figure 5.27A). RH30-GFP spheroids displayed a denser phenotype than Kym-1 cells, however they were not as compact as RD-GFP spheroids and developed a dense boundary only at later stages (d7) (Figure 5.28A). Strikingly, RD-GFP cells showed an outstanding ability to generate especially tight aggregations within 24 h upon seeding while this was not apparent for RH30-GFP and Kym-1 spheroids to this extent. Moreover, depending on the day of acquisition and cell numbers seeded, RD-GFP spheroids had an average diameter of 600 – 800 μm (Figure 5.26B). Kym-1 and RH30-GFP cells built larger spheroids ranging from 1300 – 2200 μm and 700 – 1600 μm, respectively (Figure 5.27B and Figure 5.28B). This is in line with the degree of spheroid compaction reflecting that, compared to RH30-GFP and Kym-1, RD-GFP spheroids had the lowest average diameter while being seeded with the highest cell number.

For further experiments, we chose cell numbers of 5000 cells for RD-GFP spheroids and 2500 cells for RH30-GFP and Kym-1 spheroids. This ensured appropriate spheroid compaction and size (RD-GFP: ~600 μm, Kym-1: ~1600 μm and RH30-GFP: ~800 μm) at the time-point of treatment with BH3 mimetics (d3).

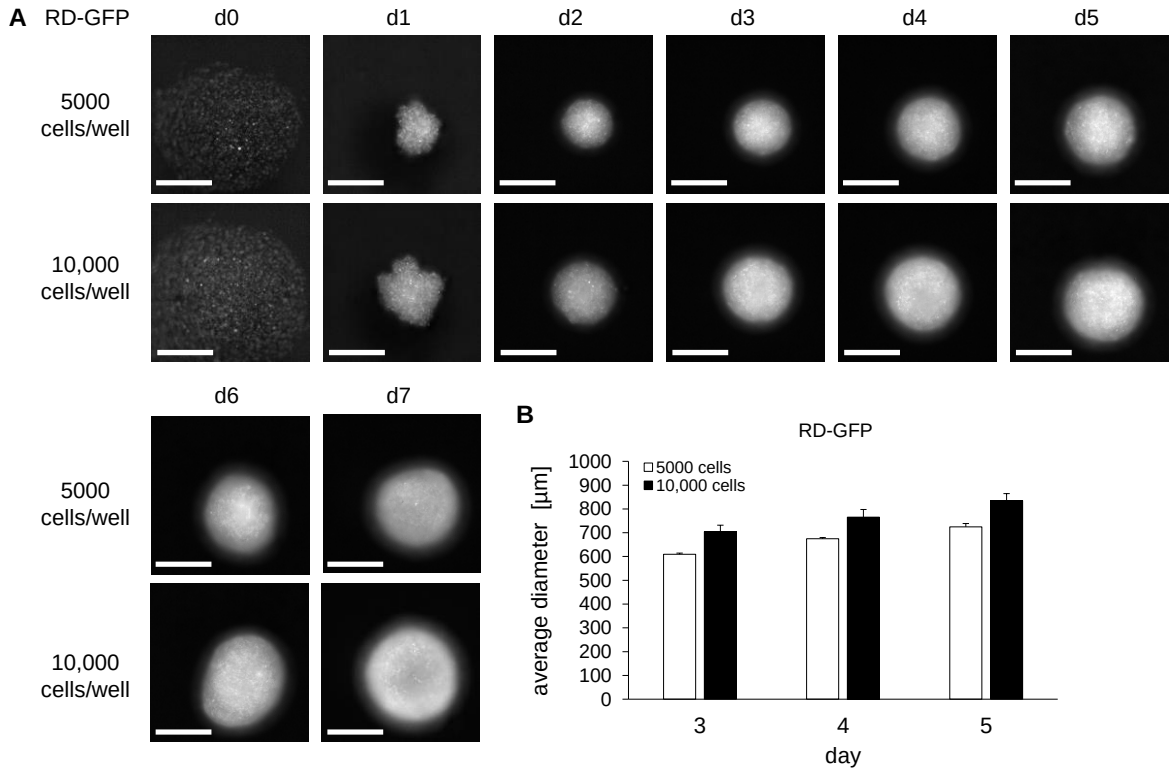

Figure 5.26: RD cells form spheroids in a cell number dependent size that grow over time.

(A): Spheroid growth was monitored using fluorescence microscopy on indicated days. GFP signal was assessed by 40 horizontal stacks through the spheroids with 20 µm step size. Representative best focus images are shown. Experiments were conducted one-two times in at least triplicates. Scale bar = 500 µm. (B): Quantification of the average spheroid diameter from data shown in (A) (n=7 spheroids) on day 3-5. Mean and SD are shown. Experiments were performed in cooperation with Vinzenz Särchen.

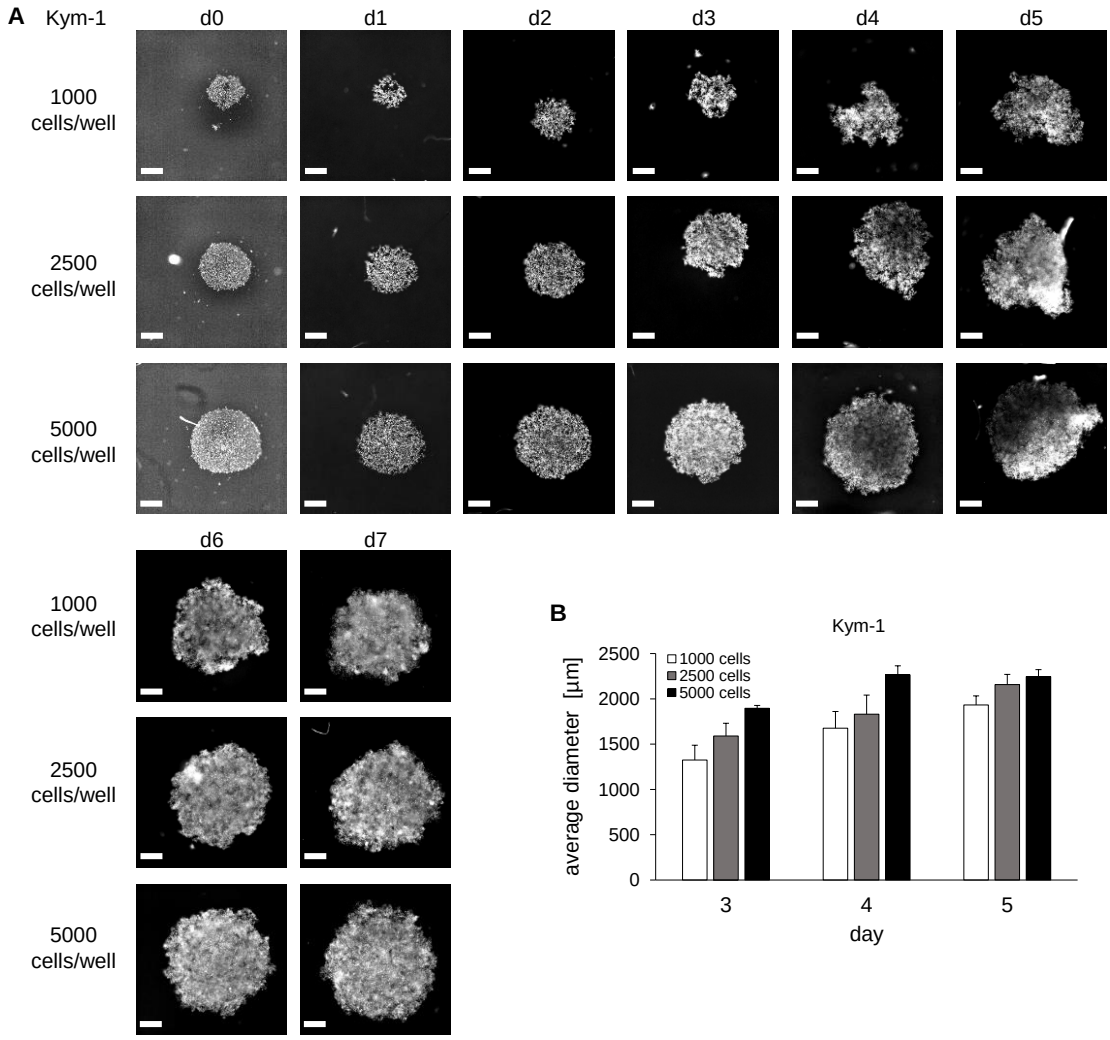

Figure 5.27: Kym-1 cells form spheroids in a cell number dependent size that grow over time.

(A): Spheroid growth was monitored using fluorescence microscopy on indicated days. Hoechst-33342 signal was assessed by 40 horizontal stacks through the spheroids with 20 µm step size. Representative best focus images are shown. Experiments were conducted one-two times in at least triplicates. Scale bar = 500 µm.

(B): Quantification of the average spheroid diameter from data shown in (A) (n=5-6 spheroids) on day 3-5. Mean and SD are shown.

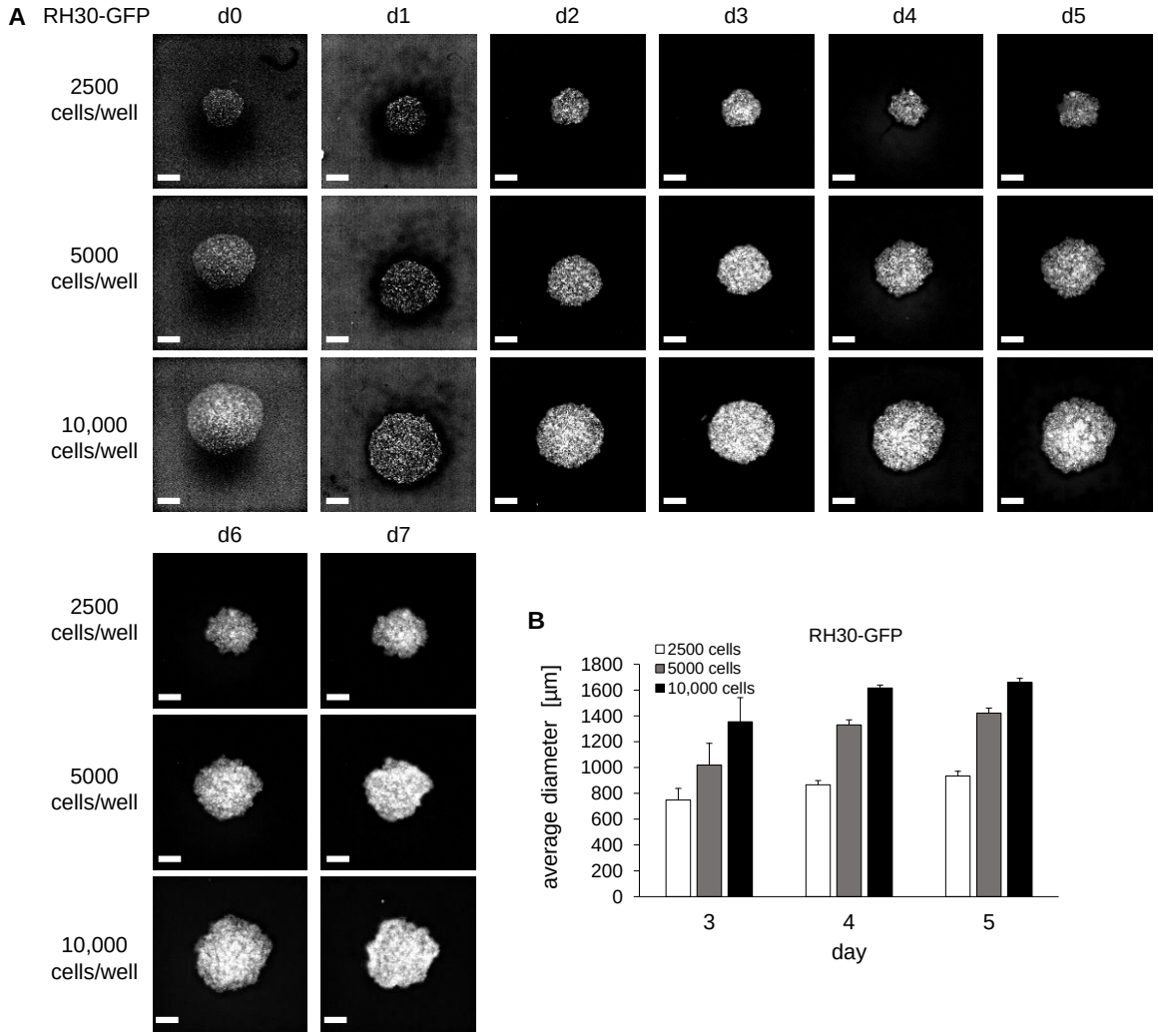

Figure 5.28: RH30 cells form spheroids in a cell number dependent size that grow over time.

(A): Spheroid growth was monitored using fluorescence microscopy on indicated days. GFP signal was assessed by 40 horizontal stacks through the spheroids with 20 µm step size. Representative best focus images are shown. Experiments were conducted one-three times in at least triplicates. Scale bar = 500 µm. (B): Quantification of the average spheroid diameter from data shown in (A) (n=4-7 spheroids) on day 3-5. Mean and SD are shown. Experiments were performed in cooperation with Vinzenz Särchen.

In order to evaluate whether RMS spheroids were similarly responsive to combined A-1331852/S63845 treatment as RMS cells in monolayer 2D cell culture, we exposed spheroid and conventional RD-GFP, Kym-1 and RH30-GFP cell cultures to increasing concentrations of A-1331852 and/or S63845. Determination of cell viability demonstrated a strong dose-dependent decrease in both spheroid and monolayer cell cultures already at nanomolar concentrations (Figure 5.29). Furthermore, assessment of Bliss synergy scores revealed a highly synergistic interaction of A-1331852 and S63845 to diminish cell viability in spheroid and monolayer cell cultures (Table 5.9). Interestingly, Bliss synergy scores were consistently lower for spheroids compared to monolayer cell cultures suggesting a decreased susceptibility of RMS spheroids to A-1331852/S63845 co-treatment in comparison to conventional cell cultivation.

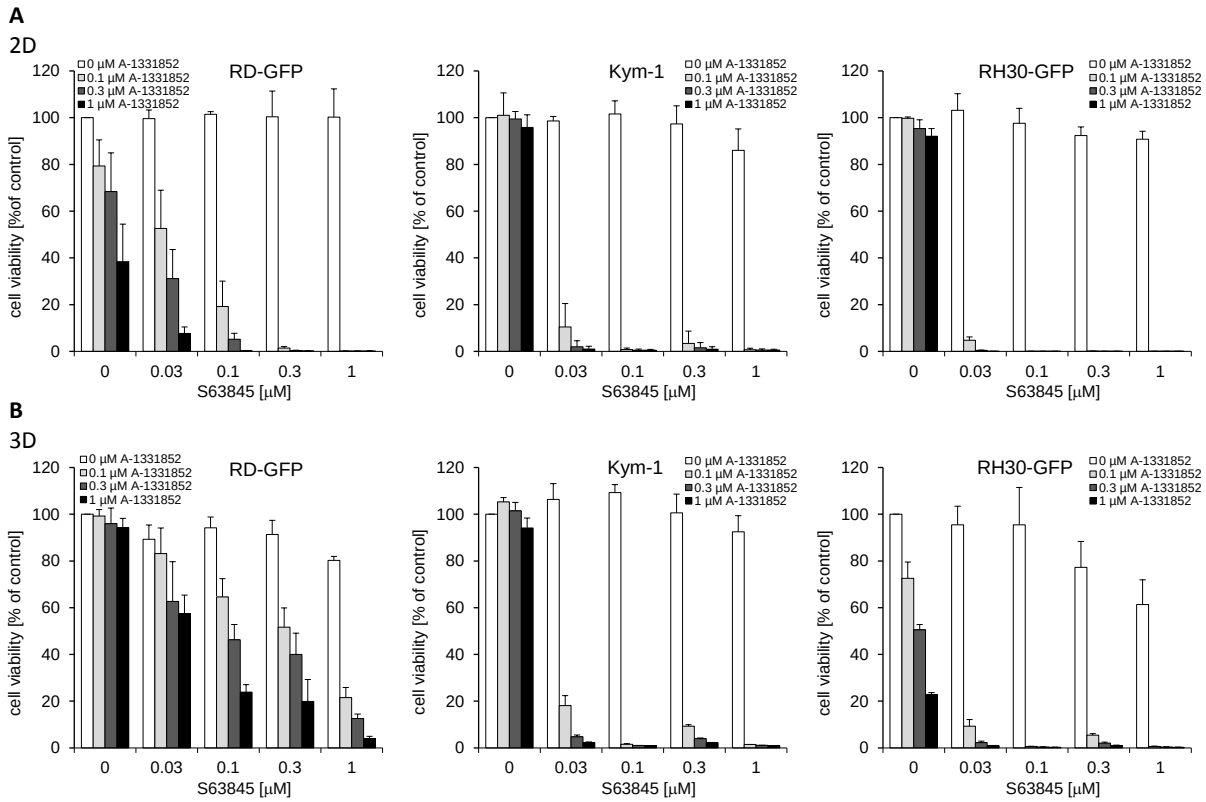

Figure 5.29: RMS spheroids display decreased cell viability upon A-1331852/S63845 co-treatment.
RMS cells (A: 2D) and RMS spheroids (B: 3D) were treated with indicated concentrations of A-1331852 and S63845 for 48 h. CellTiter-Glo® Luminescent Cell Viability Assay was used to determine ATP levels and thereby cell viability. Mean and SD of at least three independent experiments performed in triplicates are shown.

Table 5.9: Bliss synergy scores of combined A-1331852/S63845 treatment in RMS conventional (2D) vs. spheroid (3D) culture.

Cell Line	Bliss score 2D	Bliss score 3D
RD-GFP	66.3	48.6
Kym-1	93.6	86.8
RH30-GFP	89.5	54.7

Next, we wanted to investigate whether A-1331852/S63845 co-treatment induces cell death in RD-GFP and Kym-1 spheroids at concentrations used throughout the study. To this end, we administered the respective doses to RD-GFP and Kym-1 spheroids followed by measurement of cell death. PI staining was utilized to determine the amount of dead cells, Hoechst-33342 to stain all cells and GFP as a marker for alive cells, since dead cells lose the expression of GFP. Clearly, dual A-1331852/S63845 treatment triggered cell death in RD-GFP and Kym-1 spheroids as evidenced by a significant increase of the average PI/GFP or PI/Hoechst-33342 ratio upon co-treatment, but not upon single administration of the BH3 mimetics (Figure 5.30A+B and Figure 5.31A+B). Interestingly, RD-GFP spheroids displayed PI-positive cells mainly at its outer layer whereas the core remained viable (Figure 5.30A). In contrast, Kym-1 spheroids showed uniform PI-stained cells throughout its complete area (Figure 5.31A). This might be attributed to the

differential compaction and thereby diffusion barrier of RD-GFP and Kym-1 spheroids. Additionally, RD and Kym-1 spheroid size decreased markedly upon concomitant A-1331852/S63845 treatment (Figure 5.30C and Figure 5.31C).

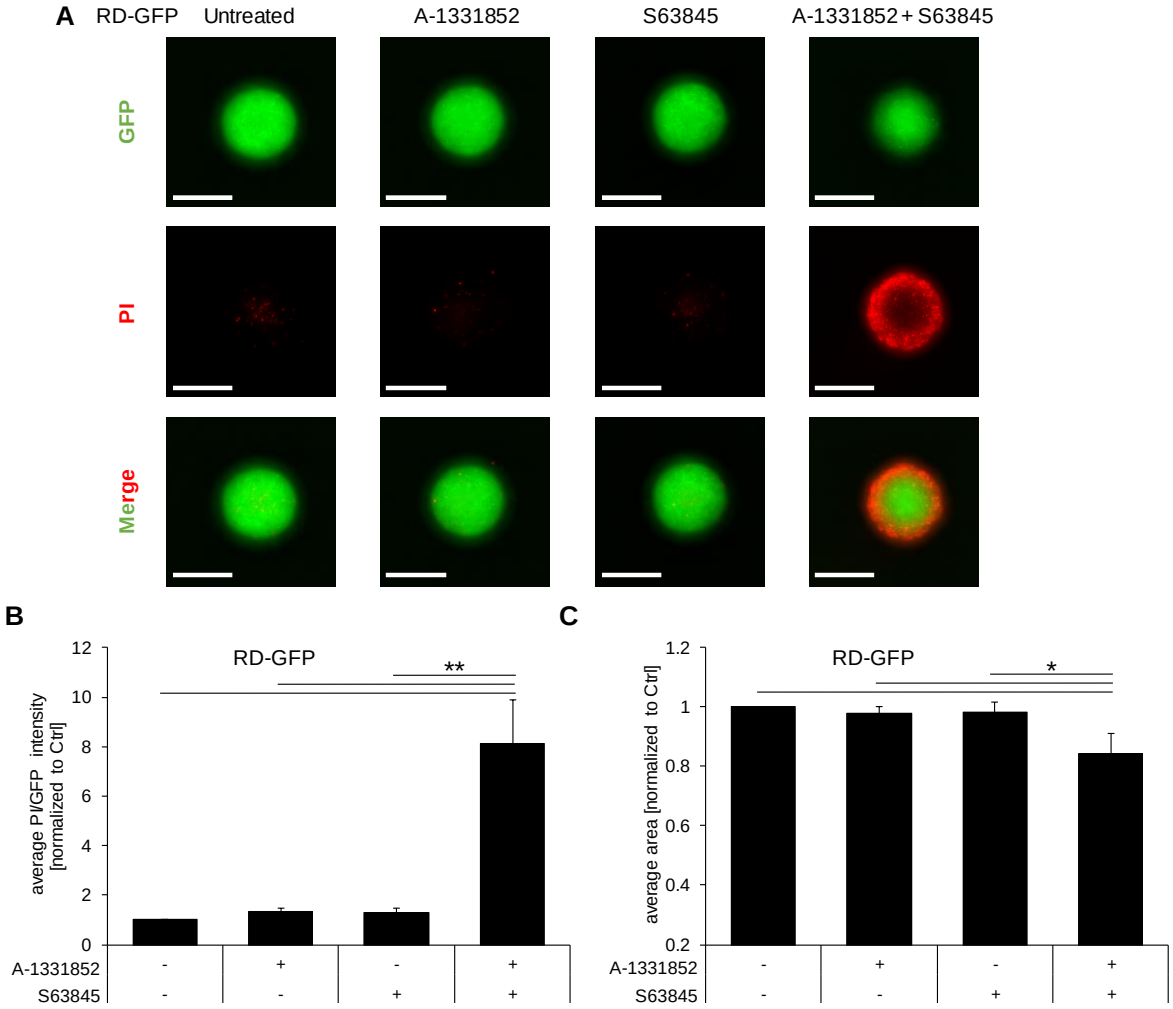

Figure 5.30: A-1331852/S63845 co-treatment induces cell death in RD spheroids.

RD spheroids were treated with 0.25 μM A-1331852 and 0.3 μM S63845 for 48 h followed by staining with PI, Hoechst-33342 and fluorescence microscope imaging. (A): GFP and PI signals were assessed by 40 horizontal stacks through the spheroids with 20 μm step size. Representative best focus images are shown. Scale bar = 500 μm. Quantification of the average PI/GFP intensity (B) and average area (utilizing Hoechst-33342 staining) (C) from data shown in (A). Mean and SD of at least three independent experiments performed in triplicates are shown. *P < 0.05, **P < 0.01.

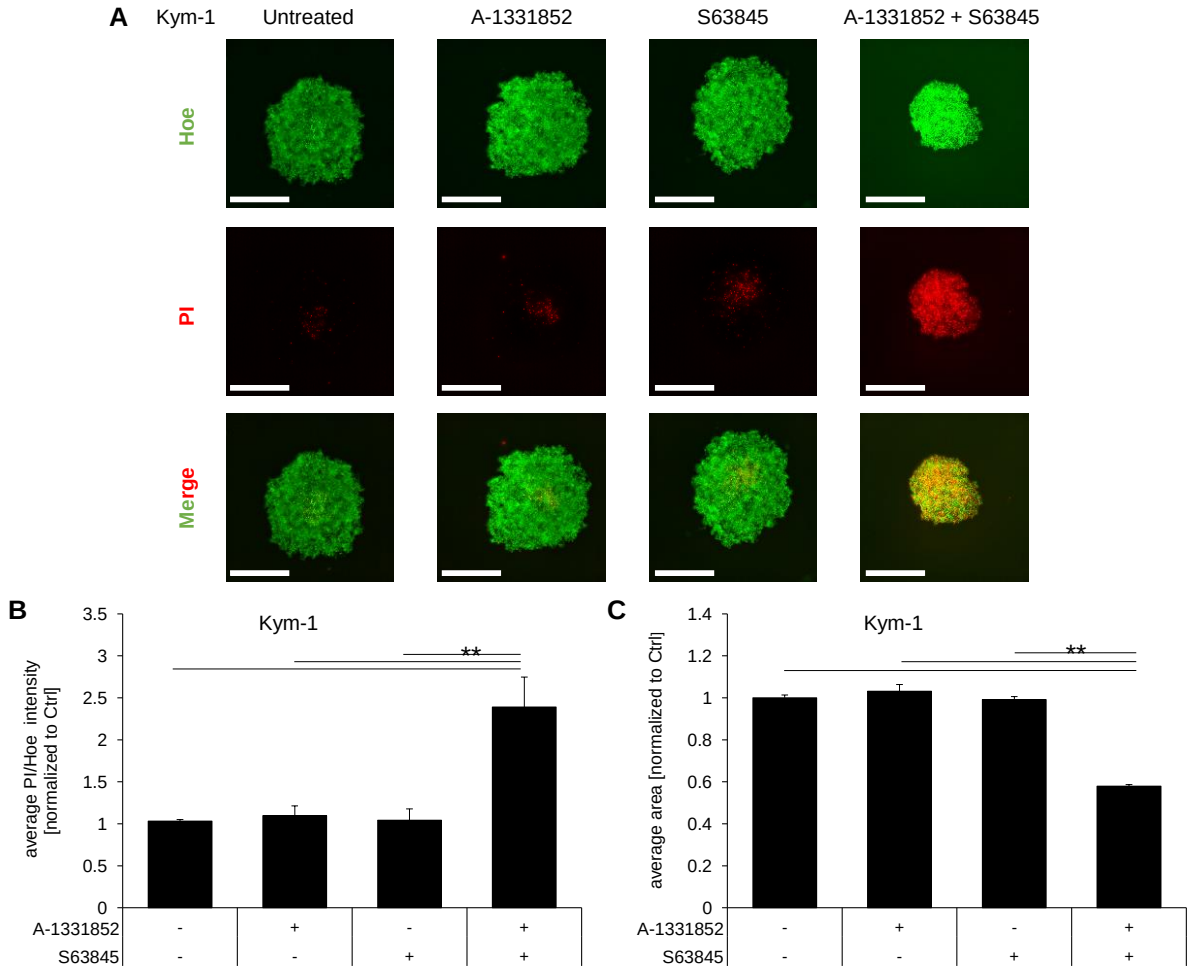

Figure 5.31: A 1331852/S63845 co-treatment induces cell death in Kym-1 spheroids.

Kym-1 spheroids were treated with 0.25 μM A-1331852 and 0.03 μM S63845 for 48 h followed by staining with PI, Hoechst-33342 and fluorescence microscope imaging. (A): Hoechst-33342 and PI signals were assessed by 40 horizontal stacks through the spheroids with 20 μm step size, respectively. Representative best focus images are shown. Scale bar = 500 μm. Quantification of the average PI/Hoe intensity (B) and average area (utilizing Hoechst-33342 staining) (C) from data shown in (A). Mean and SD of at least three independent experiments performed in triplicates are shown. **P < 0.01.

Furthermore, treatment with rising concentrations of A-1331852 and/or S63845 revealed that cell death in RMS spheroids increased in a dose-dependent way (Figure 5.32). Similar to observations made in conventional monolayer cell culture (Figure 5.3), RH30-GFP and Kym-1 cells were more sensitive than RD-GFP cells. We refrained from a calculation of Bliss synergy scores and the comparison between spheroid and conventional cell culture as performed for cell viability since assessment of Bliss synergy scores should be based on a defined readout range from 0 - 100 which is not present in the PI/GFP or PI/Hoechst-33342 ratio obtained here. Moreover, the analyses conducted to determine the amount of cell death differ between spheroid and conventional cell culture. Thus, the resulting Bliss synergy scores would not be comparable. Collectively, these experiments demonstrate that A-1331852/S63845 potently stimulates cell death also in RMS cells

cultured as multicellular spheroids and that the response to BH3 mimetics might differ between 2D and 3D culture.

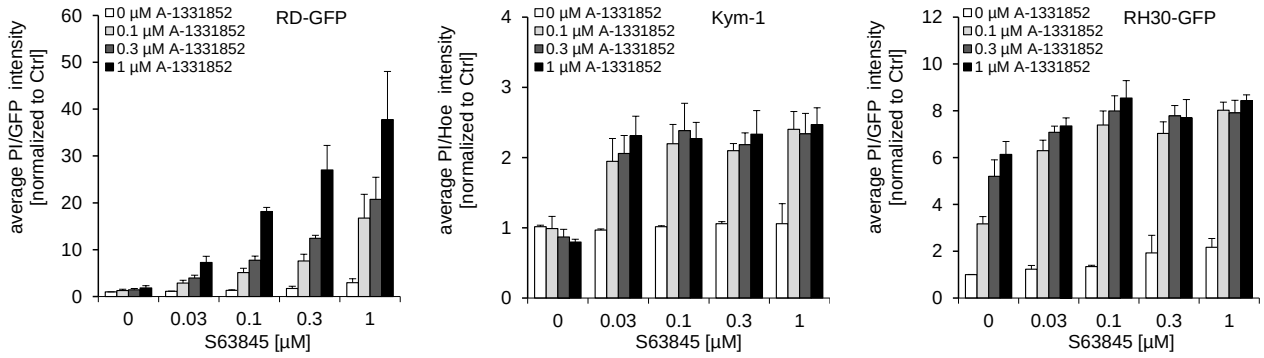

Figure 5.32: A-1331852/S63845-triggered cell death in RMS spheroids is dose-dependent.

RMS spheroids were treated with indicated concentrations of A-1331852 and/or S63845 for 48 h followed by staining with PI and/or Hoechst 33324. Cell death was determined by fluorescence microscope analysis of PI uptake using GFP/PI or Hoechst 33342/PI co-staining. Mean and SD of at least three independent experiments performed in triplicates are shown.

5.5.4 A-1331852/S63845 co-treatment significantly causes caspase-3 activation in a CAM model with Kym-1 cells

Concomitant inhibition of MCL-1 and BCL-X_L by A-1331852 and S63845 was reported to be challenging at “therapeutic doses” (269) as it resulted in acute liver toxicity in mice. For this reason, we exploited a less complex model, an *in vivo* embryonic chicken model (CAM assay), utilizing RMS cell lines. Figure 5.33A illustrates the CAM assay procedure and treatment schedule. Kym-1 cells were added on top of the CAM of chicken eggs 8 days upon fertilization. A-1331852 and/or S63845 were applied on the three following days (day 9 - 11). One day later (day 12), tumors were extracted and immunohistochemically evaluated for active caspase-3. Indeed, A-1331852/S63845 co-treatment led to a significant rise in active caspase-3-positive cells per tumor area in comparison to the DMSO control and A-1331852 treatment as single agent (Figure 5.33B+C). Additionally, A-1331852/S63845 co-treatment increased caspase-3 cleavage when compared to S63845 single treatment, albeit this tendency was not statistically significant. Instead, S63845 treatment alone already exhibited an enhanced cleavage of caspase-3 in comparison to the DMSO control.

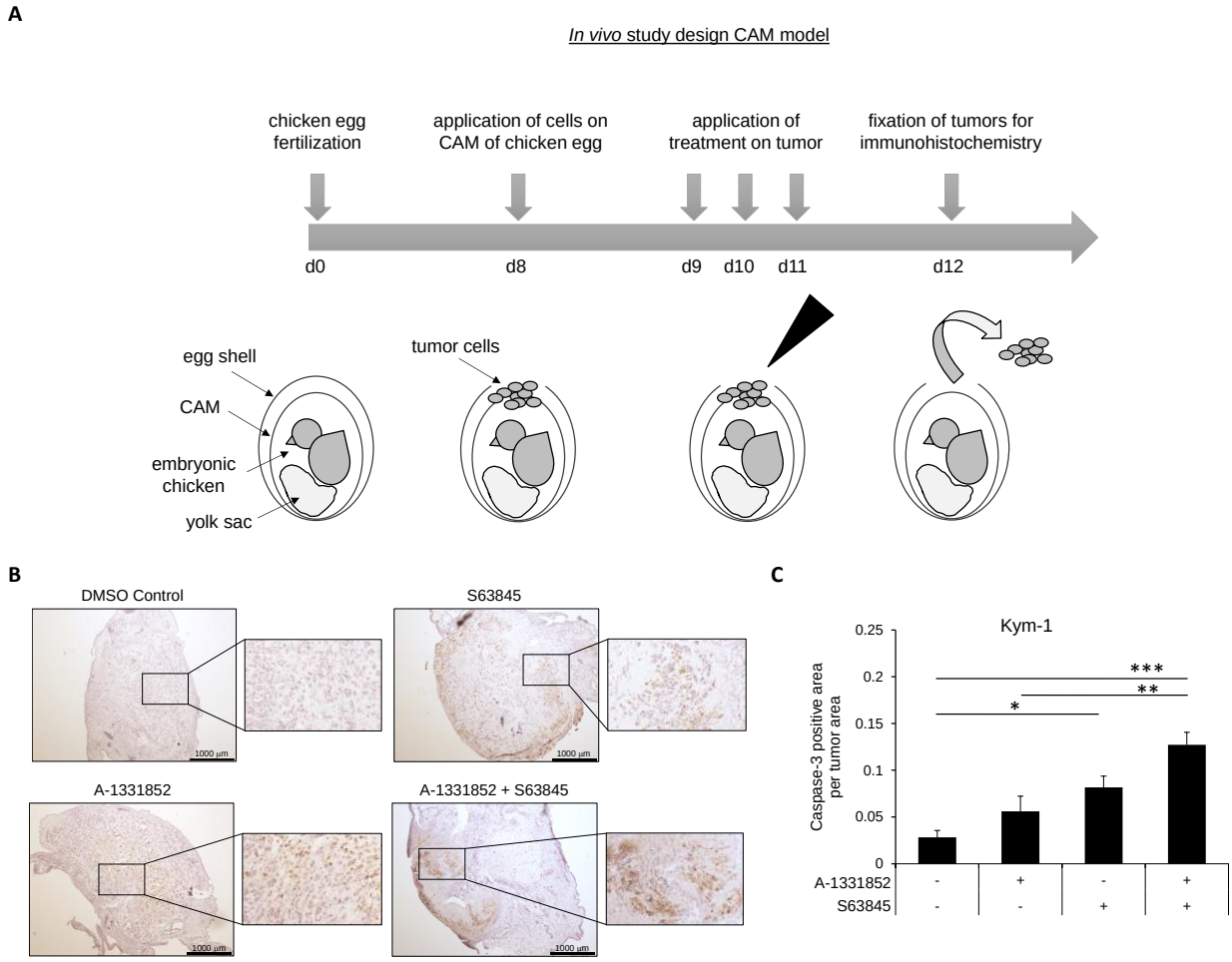

Figure 5.33: A-1331852/S63845 co-treatment significantly causes caspase-3 activation in a CAM model with Kym-1 cells.

(A): Scheme of *in vivo* study design of the CAM model: On day 8 upon fertilization of the chicken egg Kym-1 cells were implanted on the CAM. The grown tumor was treated with 0.25 µM A-1331852 and/or 0.3 µM S63845 for three consecutive days (day 9-11). Tumors were extracted from the CAM and fixed for immunohistochemistry in order to prepare sections on day 12. (B): Tumor sections were stained with an antibody specific for cleaved caspase-3. Representative images of the sections are shown. Scale bar = 1000 µm. (C): Quantification of caspase-3 positive area per tumor area of 18 - 23 tumors. Mean and SEM of at least three independent experiments performed in triplicates are shown. *P < 0.05, **P < 0.01, ***P < 0.001.

Overall, this set of experiments showed that A-1331852/S63845 co-treatment i) was highly powerful in pediatric solid cancer cells but spared non-malignant control cells, hence pointing to some tumor selectivity; ii) achieved a significant induction of cell death when applied as a sequential treatment, albeit to a lower extent than in its concomitant administration; iii) decreased cell viability and triggered cell death in a dose-dependent manner in RMS spheroids; iv) demonstrated efficacy in an *in vivo* embryonic chicken model of RMS. Hence, these findings highlight the huge potential of dual MCL-1/BCL-X_L inhibition as a future treatment option for pediatric solid tumors such as RMS.

6 Discussion

This dissertation explores the potential of anti-apoptotic BCL-2 family proteins as therapeutic targets in pediatric solid cancers. BH3 mimetics have shown encouraging achievements especially in hematological cancers and might provide an interesting option for solid cancer treatment as well (194). Here, we investigate the response of different pediatric solid cancer cell lines to selective BH3 mimetics. Moreover, we unveil the underlying molecular mechanisms behind the highly synergistic interaction of A-1338152 and S63845 co-treatment to induce cell death in RMS. Finally, we underline the translational relevance of this co-treatment suggesting its evaluation in further preclinical and clinical studies.

6.1 Pediatric solid cancers are susceptible to combined inhibition of anti-apoptotic BCL-2 family proteins

6.1.1 Expression of BCL-2 family proteins: Predictors of response?

In the first section of the study, we demonstrate that a panel of RMS, OS and ES cell lines expresses pro- and anti-apoptotic BCL-2 family members. Hence, these cancer cells are equipped with anti-apoptotic target proteins enabling successful BH3 mimetic treatment. The expression of pro-apoptotic members is of equal importance since it is a prerequisite to “prime” the cells for apoptosis (193). Though expression levels of BCL-2 family proteins vary between the tested cell lines, the majority of the pediatric solid cancer cells expresses all BCL-2 members that were investigated in this study. Moreover, we cannot identify BCL-2 family protein expression patterns typical for the ARMS or ERMS subtype of RMS. However, our sample size (especially concerning the ARMS subtype that only included three cell lines) is likely too small to draw a reliable conclusion. In the current thesis, we observe that the examined RMS cell lines are almost exclusively insensitive to BH3 mimetic single treatment and this is independent of the BCL-2 family expression status. The question whether BCL-2 family expression levels commonly correlate with the cell’s response to BH3 mimetics, thus serving as a predictive biomarker, has not yet been conclusively answered. On the one hand, there are reports stating that there is no correlation between MCL-1, BCL-X_L or BCL-2 protein expression and the susceptibility to BH3 mimetics as it is e.g. the case for lung squamous cell carcinoma (269). On the other hand, for instance, BCL-2 protein expression was connected to ABT-199 sensitivity in MM and SCLC cells, implicating cell type-dependent differences (342-344). Interestingly, MCL-1 and BCL-X_L mRNA ratios were frequently reported to be indicative of the cell’s vulnerability to BH3 mimetics in various cancer entities (207,210,227,345). In our screen, two cell lines, namely RH18 and TE441.T cells, are outstanding since they demonstrate a single sensitivity to BCL-X_L or MCL-1 inhibition, respectively. RH18 cells express lower levels of MCL-1 compared to other RMS cell lines, whereas their BCL-X_L levels are comparatively high. In contrast, the MCL-1 dependent TE441.T cells show comparably low expression of MCL-1, however, they express massive amounts of BCL-2. Since RH18 and TE441.T

cells are the only cell lines in our screen that display single sensitivity together with this distinct expression pattern, our observations cannot be generalized and it remains unclear whether it is the reason for their response. Several publications suggested that the differential interaction pattern and thus the “priming” status rather than the expression levels might be able to predict a cancer’s susceptibility to BH3 mimetics (125,212,346). Although RMS cells are largely insensitive to single agent BH3 mimetics, we find that they are “primed” for apoptosis since the anti-apoptotic proteins BCL-X_L and MCL-1 are occupied by their pro-apoptotic relatives. Consistently, we observe that in RD cells BIM and BAK sequester BCL-X_L while they interact with MCL-1 in Kym-1 cells, which might explain why RD cells are more responsive to BCL-X_L inhibition and Kym-1 cells more susceptible to blockade of MCL-1. Interestingly, especially ES cells demonstrate an increased sensitivity to single agent A-1331852 or S63845. However, further investigations are required to determine whether this can be explained by the “priming” status of these cells. Collectively, our results imply that the complex interplay between the BCL-2 family proteins determines the sensitivity to BCL-2 inhibitors irrespective of their expression levels.

6.1.2 A-1331852/S63845 co-treatment synergistically induces cell death in all investigated pediatric solid tumor cell lines

As the vast majority of investigated pediatric solid cancer cell lines are resistant to treatment with selective BH3 mimetics as single agents, we assessed the potential of BH3 mimetics in combinations. Anti-apoptotic BCL-2 family proteins were described to be able to compensate each other’s loss providing the underlying rationale to investigate combinatorial regimens (212). Indeed, dual administration of A-1331852 and S63845 strongly triggers dose-dependent cell death in all tested RMS, OS and ES cell lines. These agents act together in a highly synergistic manner and further potentiate cell death even in the single sensitive RMS cell lines RH18 and TE441.T. Moreover, in ES cell lines that display a certain response to A-1331852 or S63845 single treatment, their concomitant application additionally sensitizes these cells to cell death. Importantly, genetic silencing of MCL-1 and/or BCL-X_L combined with their pharmacological inhibition confirmed the on-target specificity of A-1331852 and S63845 in RMS. In addition, we do not observe ARMS- or ERMS-specific differences in the sensitivity to dual MCL-1 and BCL-X_L blockade. Overexpression of FGFR4, MYC and GLI as well as mutations in TP53 and RAS are typical features of RMS cell lines. This is also the case for CDKN2A underexpression and TP53 mutations in OS and ES cells (refer to Tables 4.1-4.4). Clearly, combined inhibition of MCL-1 and BCL-X_L is effective in both TP53 wildtype and mutant cancer cell lines, which was expected since BH3 mimetics act downstream of TP53 (103,234). Furthermore, a relation between the potency of A-1331852/S63845 co-treatment and the mutation or over/underexpression of a specific gene cannot distinctly be identified. All in all, this implicates that A-1331852/S63845 co-treatment provides an equally promising treatment option for RMS, OS and ES independent of their mutation status and histological subtypes.

6.1.3 MCL-1 and BCL-X_L, but not BCL-2, are key therapeutic targets in RMS, OS as well as ES

It was reported that in solid tumors MCL-1 and BCL-X_L play a more crucial role to sustain survival than BCL-2 (245,277,347). Consistently, in the current study A-1331852/S63845 co-treatment is superior in inducing cell death compared to combinations of either inhibitor with ABT-199. This was observed for all tested RMS, OS and ES cell lines. Since we do not investigate all RMS cell lines for their response to co-treatments with ABT-199, we cannot exclude the possibility that there are some in which BCL-2 might play a similar vital role as MCL-1 and BCL-X_L. Moreover, in Kym-1 cells that lack BCL-2 expression additional treatment with ABT-199 does not further potentiate cell death caused by A-1331852 or S63845. Hence, we provide a proof of principle for the specificity of ABT-199 to target BCL-2, but not MCL-1 or BCL-X_L. Additionally, these results are in line with our finding that in RD cells BCL-2 does not have an active part in endogenously sequestering or taking over pro-apoptotic BCL-2 proteins upon their displacement from MCL-1 or BCL-X_L by A-1331852 and/or S63845. Importantly, this finding highlights the potency of A-1331852/S63845 co-treatment also in cell lines with high BCL-2 expression. Of note, in previous studies with RD cells, BCL-2 was shown to markedly sequester BIM. However, these Co-IP experiments were performed with CHAPS lysis buffer and not, as utilized in this study, Triton X lysis buffer. This might have an impact on the conformation of BCL-2 proteins and hence on the binding pattern, thus providing an explanation for the different results (246,348,349).

6.1.4 Potential relevance of dual MCL-1 and BCL-X_L inhibition as cancer treatment

Given that apoptosis is a hallmark of cancer and BCL-2 proteins are implicated in a plethora of cancer entities, targeting of the pro-death proteins MCL-1 and BCL-X_L is a compelling treatment strategy (75,226). In previous publications from our group, we have already highlighted the relevance of BCL-2 proteins in RMS in the context of co-treatments with the HDAC inhibitor JNJ-26481585 or chemotherapeutics (246,274). In this dissertation, we demonstrate a crucial role for MCL-1 and BCL-X_L in the survival of RMS, OS and ES cells. Furthermore, another study by our group showed comparable results for NB (267,334). By investigating a primary sample of malignant epithelioid mesothelioma, we identify an additional cancer entity that seems to express most of the relevant BCL-2 family proteins in comparable levels as RMS and shows the tendency to mainly rely on both MCL-1 and BCL-X_L. In line with this, Varin *et al.* demonstrated that malignant pleural mesothelioma cells are susceptible to combined genetic silencing of MCL-1 and BCL-X_L (350) Unfortunately, our sample size is limited to one and can only provide a first hint for the sensitivity of malignant epithelioid mesothelioma to BH3 mimetic combinations. Further experiments are required to be able to draw a reasonable conclusion. Importantly, a large screen with ten diverse cancer entities revealed that a huge fraction is vulnerable to MCL-1 and BCL-X_L co-inhibition. This was most significantly the case in AML, pancreatic ductal adenocarcinoma, melanoma and breast cancer (226). In fact, the approach to co-target MCL-1 and BCL-X_L has already been investigated

in pancreatic cancer, colorectal carcinoma, melanoma, cervical cancer, squamous cell carcinoma of the head and neck (SCCHN), MCL and NSCLC – with encouraging results (259,263,269,276,277,337,347,351). Nevertheless, the current thesis is the first one to explore its effect in pediatric solid tumors. Concisely, concomitant MCL-1 and BCL-X_L inhibition has an enormous potential for the treatment of various cancers that is waiting to be further explored in the future.

6.2 Unraveling the mechanisms of A-1331852/S63845-induced cell death

6.2.1 A-1331852/S63845 co-treatment leads to rapid intrinsic apoptosis

In accordance with their mechanism of action to directly engage the apoptotic machinery, we determine A-1331852/S63845-mediated cell death to be intrinsic apoptosis (103,112). There are several typical hallmarks that we identify indicating this type of cell death. Firstly, a time-dependent increase of loss of MMP shows an involvement of the mitochondrial pathway. Secondly, cell death is completely caspase-dependent as evidenced by the use of the pan-caspase inhibitor zVAD.fmk. A-1331852/S63845 co-treatment causes vast cleavage of caspases-3 and -9 and, in a slightly time-delayed way, also massive cleavage of caspase-8. This leads us to speculate that caspase-8 is presumably activated in a feedback loop. Thirdly, as a consequence of caspase activation, cells expose PS in a time-dependent manner. Additionally, A-1331852/S63845-mediated decline of MCL-1 levels might further enhance apoptosis. MCL-1 loss is clearly caspase-dependent, which is consistent with a report that highlights MCL-1 as a caspase target (190). Apoptosis in our system is executed with a particularly rapid kinetic. This is characteristic for BH3 mimetics as Leverson *et al*. stated that true BH3 mimetics exert their action within 2 - 4 h after application (255). In Kym-1 cells, loss of MMP and caspase activation are detected already 1 - 2 h upon treatment, followed by a significant increase in PS exposure after 3 h. Similarly, caspases are activated 1 - 2 h upon treatment in RD cells, even though loss of MMP only significantly rises 2 - 3 h after BH3 mimetic administration in this cell line. This implicates that the minor, albeit not significant, onset of loss of MMP at 1 - 2 h in RD cells is sufficient to mediate caspase activation.

6.2.2 A-1331852/S63845 co-treatment tips the balance of pro- and anti-apoptotic BCL-2 members in favor for pro-death signaling

Regarding the molecular mechanism, we elucidate that BAX and/or BAK are critically required for A-1331852/S63845-mediated apoptosis. BAK/BAX KD rescues cell death in a cell type-dependent manner. While RD cells show a prominent dependence on BAK, in Kym-1 cells the presence of BAX is more relevant. We hypothesize that the expression levels of these proteins might be responsible for this finding as BAK is expressed at higher levels in RD cells in comparison to Kym-1 cells and vice versa BAX is expressed in greater amounts in Kym-1 cells than in RD cells. Therefore, the relative abundance of BAX and BAK might contribute to the observation that RD cells rely more on BAK and Kym-1 cells more on BAX. Since siRNA mediated KD only reduces

protein levels, but does not lead to its complete absence, we utilize CRISPR/CAS9 to generate BAK KO RD and Kym-1 cells to further evaluate the role of BAK in A-1331852/S63845-induced apoptosis. Unexpectedly, KO of BAK does not rescue RD or Kym-1 cells from cell death. Given that concomitant KD of BAX achieves a profound decrease in cell death while there are no overt alterations in BCL-2 family protein levels, we speculate that BAX might compensate for the role of BAK. Interestingly, also other members of our lab found indications that the process of knocking out a BCL-2 family protein, especially in connection with single clone selection over a longer period of time, might have an impact on the expression levels or functional relevance of other BCL-2 family proteins (unpublished data). This is in line with findings showing that BAX and BAK have redundant roles in tissue development and were described to compensate for the other's absence (352-354). Consequently, this might explain why the BAK KO experiments do not confirm our previous findings obtained by performing BAX/BAK KD experiments. However, the exact underlying molecular processes require additional investigations.

Analyzing BCL-2 family interactions, we show that BAK and BIM are endogenously bound to BCL-X_L in RD cells. Treatment with A-1331852 impairs these interactions and shifts BAK and BIM to MCL-1. Even single administration of A-1331852 causes slight BAX/BAK activation and minor cell death in RD cells suggesting that treatment exhausts the capacity of MCL-1 to sequester anti-apoptotic members. Additional application of S63845 displaces NOXA from MCL-1 and results in marked BAX/BAK activation and in massive cell death. On the contrary, BAK mainly interacts with MCL-1, and only to a lesser extent with BCL-X_L, in untreated Kym-1 cells. Liberation of BAK from MCL-1 by S63845 leads to faint activation of BAX. This is consistent with the major role of BAX in A-1331852/S63845-caused apoptosis in Kym-1 cells as evidenced in BAX/BAK KD experiments. Nevertheless, concomitant inhibition of MCL-1 and BCL-X_L is necessary to efficiently kill this cell line, possibly by an additional release of BAK from BCL-X_L. Although MCL-1 sequesters BIM in Kym-1 cells, S63845 treatment does not interfere with this interaction. This is in line with the finding that KD of BIM does not rescue Kym-1 cells from cell death. KD of BIM and/or NOXA in RD cells implicates that their involvement in A-1331852/S63845-triggered apoptosis is only partial. Furthermore, PUMA and BMF are not involved in mediating cell death in neither RD nor Kym-1 cells. Therefore, the contribution of BH3-only proteins to A-1331852/S63845-induced apoptosis, for instance by direct activation of BAX and BAK, seems to be relevant to only marginal extents.

Importantly, these findings lead us to propose a key role for BAX and BAK in A-1331852/S63845-stimulated apoptosis. In accordance, O'Neill and colleagues discovered that cells deficient for the eight BH3-only proteins BID, HRK, PUMA, BIM, NOXA, BIK, BMF and BAD (OctaKO) exert BAX/BAK dependent apoptosis when BCL-X_L and MCL-1 are transiently silenced. BAX and BAK could even spontaneously associate with the mitochondrial membrane leading to their oligomerization in cells that lack all relevant BCL-2 members (142). Follow-up work from the same group presented additional evidence that BH3-only proteins rather mediate their pro-death effect by impeding BCL-X_L and MCL-1 than by directly activating BAX and BAK (132). Interestingly,

A-1331852/S63845 co-treatment was shown to elicit cell death in OctaKO cells (259). This points to a prevalent role of the indirect instead of the direct activation model in A-1331852/S63845-induced cell death, which is in line with the findings in our study. Strikingly, recent work by Bogner *et al.* suggested that the BH3-only sensitizer BAD activates BID in an allosteric way when both interact with BCL-X_L. Subsequently, BID can function as a direct activator of BAX (140). As we did not investigate the role of BID or BAD upon BH3 mimetic treatment in our study, it remains elusive whether BAX might be additionally activated by an allosteric mechanism.

Compellingly, treatment with A-1331852 and S63845 liberates BAK in RMS cells and causes the formation of BAX/BAK heterocomplexes. For this reason, we hypothesize that released BAK subsequently activates BAX and additional BAK molecules. Autoactivation of BAK and BAX has been reported as a BH3 independent mechanism acting as a feed-forward amplification loop to result in mitochondrial apoptosis. Of note, BAX/BAK autoactivation occurred upon downregulation of anti-apoptotic proteins, especially MCL-1 and BCL-X_L, which strengthens the hypothesis of a similar mechanism for A-1331852/S63845-triggered apoptosis (121,141). In this context, our data highlights a predominant role for BAK since, unlike BAX, it endogenously interacts with MCL-1 and BCL-X_L. This is consistent with a recent publication indicating that BAK more potently performs autoactivation than BAX (355). Moreover, we do not detect any interactions between BAX and MCL-1 or BCL-X_L in RMS cells. Additionally, vice versa in BCL-X_L and MCL-1 Co-IPs, BAX is not sequestered by these proteins confirming the observations made in the BAX Co-IP (data not shown). Naturally, a lack of interactions assessed by only one type of assay does not unequivocally proof that an interaction is indeed not present. However, the results from our experiments lead us to propose that, at least in Kym-1 cells, BAX is not endogenously bound to BCL-X_L or MCL-1 and thereby cannot be displaced by A-1331852/S63845 co-treatment. Collectively, we intriguingly demonstrate how the interplay between MCL-1 or BCL-X_L with their pro-apoptotic relatives, respectively, fine-tunes A-1331852/S63845-induced apoptosis in a cell type-specific manner. Figure 6.1 illustrates the molecular mechanism behind A-1331852/S63845-mediated cell death that we propose on the basis of our findings.

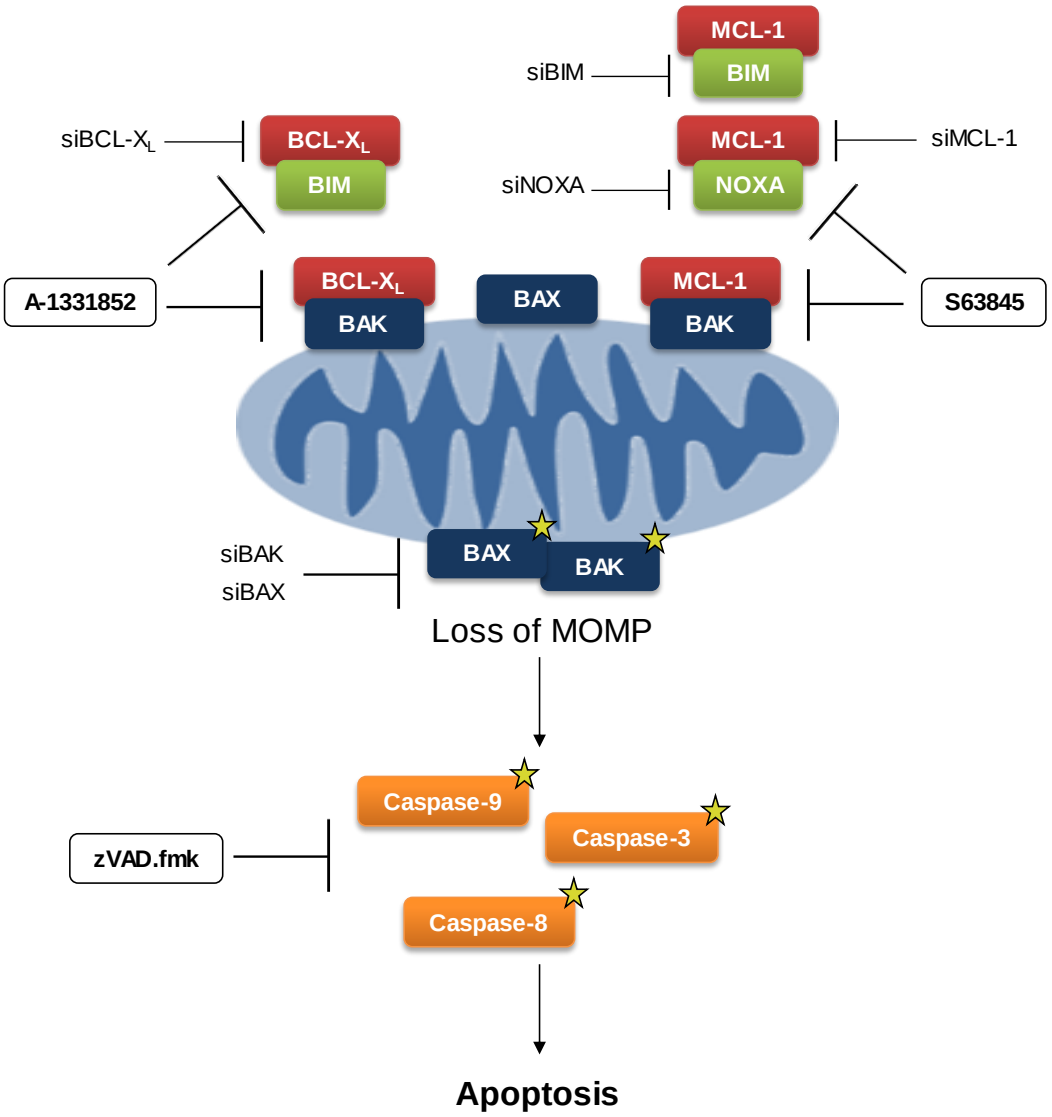

Figure 6.1: Proposed mechanism of A-1331852/S63845-mediated apoptosis

A-1331852 and S63845 act in concert to trigger intrinsic apoptosis in a cell line-dependent manner: A-1331852 displaces BAK and BIM from BCL-X_L and S63845 impedes interactions between MCL-1 and BAK, NOXA or BIM. Thereupon, released BAK presumably initiates an autoactivation of BAX/BAK leading to the formation of BAX/BAK heterocomplexes. Pore formation facilitates MOMP and downstream activation of caspase-3, -8 and -9 that can be prevented by the pan-caspase inhibitor zVAD.fmk. Concomitant genetic silencing of MCL-1 and BCL-X_L confirms on-target specificity of the pharmacological inhibitors. A-1331852/S63845-induced apoptosis can be partially rescued by KD of BIM, NOXA, BAX and/or BAK depending on the cell line.

6.3 Is concomitant MCL-1 and BCL-X_L inhibition feasible for clinical applications?

6.3.1 Low vulnerability of non-malignant cells might provide a therapeutic window for A-1331852/S63845 co-treatment *in vivo*

So far, we could demonstrate that MCL-1 and BCL-X_L constitute attractive targets for the treatment of pediatric solid cancers. Nevertheless, these proteins have vital roles not only in cancer cells, but also in healthy tissue development and homeostasis (72). Hence, this raises concerns about the sensitivity of non-malignant cells to dual inhibition of MCL-1 and BCL-X_L. Fortunately, A-1331852/S63845 co-treatment acts in a highly synergistic way implicating that relatively low doses of each drug can be utilized to achieve effective killing of cancer cells. Remarkably, the concentrations used throughout the study in RD and Kym-1 cells do not induce profound cell death nor marked caspase activation in human fibroblasts, human PBMCs and murine myoblasts. These cells express BCL-2 family proteins in similar levels as RMS cells. However, we observe a tendency for decreased MCL-1 expression in PBMCs compared to RMS cells and cannot exclude the possibility that this contributes to A-1331852/S63845 co-treatment resistance. On the other hand, the predictive value of the detected BCL-2 family expression levels is debatable especially in the view of our previous finding that sensitivity to BH3 mimetics is independent of BCL-2 family expression levels. Furthermore, a limitation to our study in murine myoblasts refers to the finding that S63845 targets human MCL-1 with a 6-fold higher affinity in comparison to murine MCL-1 (356). Therefore, it is likely that myoblasts of human origin display a higher susceptibility to A-1331852/S63845 co-treatment. Still, our findings underline that additional research might unveil a therapeutic window in which RMS cells are vulnerable while non-malignant cells are spared.

6.3.2 A-1331852/S63845 co-treatment shows encouraging results for future pre-clinical evaluations

In order to appropriately analyze the drug response of cancer cells, i*n vitro* models should mimic the *in vivo* environment as best as possible. Multicellular spheroids bridge the gap between conventional cell culture and animal models (341,357). Monolayer culture differs considerably from 3D culture. Gene expression comparable to solid tumors, cellular heterogeneity and extracellular matrix (ECM) decomposition are amongst the characteristics of a spheroid. Moreover, various gradients concerning for instance nutrients, pH and oxygen promote the formation of different layers. Proliferating cells are commonly associated with the spheroid outer layer, whereas cells acquire a senescent phenotype in the middle layer. Acidification and the lack of oxygen leads to a necrotic core (339,357,358). We utilized spheroids with a size between 600 - 1600 μm at the time-point of treatment. Of note, the development of a layered structure within these spheroids is

not investigated in the current work. Nevertheless, the reported diffusion limit for oxygen and nutrients is 150 – 200 μm and spheroids ranging from 150 – 300 μm were described to display layers as mentioned above (359-361). Therefore, we assume that the spheroids used throughout the study meet the requirements to form layers, at least with regards to their size. Sarcoma spheroids including RMS and ES have been published earlier, however, not in connection with BH3 mimetics (362-364). Significantly, A-1331852/S63845 co-treatment triggers cell death and decreases cell viability of RMS spheroids in a dose-dependent manner. Moreover, treatment reduces spheroid size at concentrations used in our previous experiments, emphasizing its potency also in a more complex *in vitro* system. Comparison of cell viability in 2D and 3D culture reveals a diminished response of 3D culture upon dual A-1331852/S63845 treatment. In addition, A-1331852/S63845 co-treatment induces cell death only in the outer layer of RD spheroids, which is likely due to their tight cellular aggregation and lack of drug penetration into the spheroid. This evidently illustrates a common challenge of drug application, namely to reach the core of a tumor. Consequently, this might explain the elevated resistance of 3D compared to conventional culture. Further experiments are necessary to assess whether this holds also true concerning cell death. The response of spheroids to BH3 mimetics has been investigated before and intriguingly A-1331852/S63845 co-treatment demonstrated clear effects in cervical cancer, melanoma and SCCHN (276,277,347). Overall, these results strengthen the potential of A-1331852/S63845 co-treatment as a cancer regimen. Yet, RMS spheroids require intense further characterization to determine their actual resemblance to solid tumors.

Administration of A-1331852 and/or S63845 on the CAM of fertilized chicken eggs enables first insights into their *in vivo* effects. A-1331852/S63845 co-application potently demonstrates anti-tumor activity in the CAM assay emphasizing the translational relevance of this treatment. Unlike predicted by the *in vitro* experiments, also single agent BH3 mimetic treatment induces substantial caspase-3 cleavage giving a first hint that response can differ *in vitro* and *in vivo*. Dual inhibition of MCL-1 and BCL-X_L in mice appears to be challenging as mice co-treated with A-1331852/S63845 were described to suffer from acute liver toxicity (269). This observation can be explained by the finding that loss of one allele of either MCL-1 or BCL-X_L results in hepatocyte apoptosis (179). Moreover, loss of MCL-1 in the liver causes hepatotoxicity (178). Since a CAM assay comprises a less complex system compared to mouse experiments, we consider it as an ideal pre-step. Albeit this assay provides certain advantages such as easy handling and the rapid generation of results, it comes with a number of limitations. Firstly, in the CAM assay drugs are applied directly onto the grown tumor. In contrast, BH3 mimetics are administered orally or injected i.v. in mice (227,269). Thus, concerning its complexity, the CAM model is inferior to mouse xenograft models and cannot adequately mimic drug application. Secondly, non-malignant cells are less exposed to A-1331852/S63845 co-treatment, which aggravates the evaluation of its effect in healthy tissue. Thirdly, long-term effects of the treatment cannot be assessed since the experimental procedure of the CAM assay is restricted to a few days. Due to the above named

reasons, it is indispensable to address the effect of A-1331852/S63845 co-treatment in additional pre-clinical models. A zebrafish xenograft model has already confirmed the anti-tumor capacity of A-1331852/S63845 co-treatment in SCCHN (276). Mouse experiments are the necessary next step to evaluate the potency and caveats of concomitant MCL-1 and BCL-X_L repression for the treatment of cancer. These experiments could elucidate possible side effects that will presumably limit A-1331852/S63845 co-application in clinic. An addiction to MCL-1 and BCL-X_L exists in a row of healthy cell types (see Table 2.1). Besides hepatic failure, as discussed above, major effects on cardiomyocytes as well as on the hematopoietic and neuronal system are predicted upon treatment with BH3 mimetics selectively targeting MCL-1 and BCL-X_L (72,174,176,185). Strikingly, S63845 was well tolerated in mice at concentrations effectively diminishing lymphoma tumor growth. S63845 exhibited largely no toxic effects on the heart, kidney, thymus, liver and spleen. Importantly, no histopathological alterations were detected in skeletal muscle, which is crucial in the context of RMS treatment. The only hematological cellular subset slightly affected by S63845 administration were immature B cells in the bone marrow (227). Caenepeel and colleagues discovered that the MCL-1 inhibitor AMG176 demonstrates similar effects on B cells and additionally on neutrophils and monocytes (345). This implicates that these findings might commonly arise for the class of MCL-1 selective BH3 mimetics independent of the respective inhibitor. Potential side effects of A-1331852 have not been as comprehensively studied yet. However, the initial evaluation of A-1331852 in various solid cancers showed neither apparent toxicities nor massive weight loss (270). Further, a recent publication investigating A-1331852 in liver cancer suggested that treatment does not damage non-tumorous tissue (365). On the other hand, efforts to combine A-1331852 with the cyclin-dependent kinase inhibitor dinaciclib in soft tissue sarcomas failed due to liver toxicities (275). Additionally, due to the crucial role of BCL-X_L in platelet survival, thrombocytopenia is anticipated under A-1331852 treatment (182-184). Therefore, advanced *in vivo* studies are required to ascertain that future BH3 mimetic administration is safe in humans. Interestingly, recent work by Khan and colleagues demonstrated that the use of a BCL-X_L proteolysis-targeting chimera (PROTAC) might be a promising strategy to eliminate BCL-X_L without causing thrombocytopenia (366). Overall, BH3 mimetics present with less severe side effects as initially anticipated by KO studies. A likely explanation is that pharmacological inhibitions are transient and might not cause as detrimental effects as a KO. Moreover, complete loss of an anti-apoptotic BCL-2 protein presumably impairs non-apoptotic functions more strongly compared to inhibition by BH3 mimetics that is not enduring (194,227). This calls for a careful evaluation of adjusted doses to exploit the therapeutic potential of these drugs for cancer treatment.

Additionally, treatment schedules might be helpful to identify a therapeutic window. In this context, we show that *in vitro* sequential BH3 mimetic treatment is still effective, albeit to lesser extents. Apparently, A-1331852 pre-treatment is more potent than pre-treatment with S63845 in both RMS cell lines. For RD cells, this is in line with their higher sensitivity to A-1331852 compared to S63845. However, in Kym-1 cells, MCL-1 seems to have a greater relevance than BCL-X_L and a higher

vulnerability to S63845 pre-treatment would have been expected for this cell line. These findings might be explained by a superior capability of A-1331852 to induce a “primed” state in RMS cells. To answer the questions whether this is indeed the case and what the underlying molecular backgrounds are, further experiments have to be conducted. In summary, A-1331852/S63845 co-treatment demonstrates efficacy in an RMS spheroid-based approach as well as *in vivo* in an embryonic chicken model of RMS. Our data provides promising implications that concomitant repression of MCL-1 and BCL-X_L might indeed be feasible for advanced preclinical and clinical studies. These are urgently needed to establish this potent co-treatment in clinical practice.

7 Outlook

In the thesis at hand, we explore the potential of selective BH3 mimetics targeting MCL-1 and BCL-X_L in pediatric solid cancer cells and elucidate the molecular mechanism leading to cell death in RMS. Nonetheless, various open questions remain.

Therapeutically, it is of utmost importance to investigate the tolerability, safety and efficacy of A-1331852/S63845 co-treatment in subcutaneous mouse xenograft models of solid tumors such as RMS. The outcome will decisively contribute to the further strategy pursued to enable its application in cancer patients. To account for the fact that S63845 exhibits a 6-fold higher affinity for human than for murine MCL-1, Brennan and colleagues generated a mouse strain harboring humanized MCL-1 (huMCL-1). Accordingly, these mice display a higher sensitivity to S63845 compared to wildtype mice (356). Preferentially, huMCL-1 mice should be utilized to conduct xenograft experiments evaluating A-1331852/S63845 co-treatment. The more accurate prediction might support the search for realistic dosing. However, these experiments are beyond the scope of this dissertation.

Multicellular spheroids are a compelling model system to gain further insights into the effect of BH3 mimetics in a 3D cellular system. RMS spheroids require extensive characterization, not least to unveil the limitations of this model. In detail, stainings with the autofluorescent dye doxorubicin in short defined intervals could help to illustrate the process of drug penetration. Secondly, the presence of the proliferative, senescent and hypoxic spheroidal layers should be determined by stainings with Ki67, β-galactosidase and HIF-1α, respectively. Additionally, the decomposition of the ECM could be assessed by collagen stainings. Besides, Backes and colleagues elegantly demonstrated the successful use of a vector termed pCasper3-GR in spheroids in an NK cell co-culture. This vector harbors a DEVD domain, a caspase-3/-7 cleavage target, and switches from a mainly RFP to a GFP signal upon cellular caspase activation. Thus, this enables a real-time cell death monitoring without the addition of external dyes (367). The fact that pCasper3-GR expression can be introduced in each cell is advantageous since it circumvents the challenge for external dyes to diffuse to the spheroid core. For all these goals, confocal microscopy might prove helpful to receive precise high-resolution imaging. Moreover, we have generated preliminary data based on Western blotting showing that RMS spheroids express BCL-2 family proteins. These expression levels seem to be widely comparable between the different spheroids suggesting a high reproducibility – a favorable feature concerning drug screenings. Nevertheless, our Western blotting experiments require further optimization with regards to effective protein lysis. Generally, RD cells might be the cell line of choice for further investigations since they impressively form very condensed spheroids compared to the other RMS cell lines. Finally, establishing a co-culture with RMS and human skeletal muscle cells would be beneficial to mimic an environment resembling *in vivo* conditions.

Outlook

In this work, we screened a range of established RMS, OS and ES cell lines for their response to BH3 mimetics. These cancer entities are infrequent and primary samples accordingly rare. As we investigated only one primary-derived ARMS sample and one primary pediatric malignant epithelioid mesothelioma, drawing a comprehensive conclusion concerning the effect of A-1331852/S63845 in primary samples is difficult. Therefore, further examinations of primary pediatric samples are critically required.

Furthermore, it would be interesting to understand potential resistance mechanisms that might lead to failure of A-1331852/S63845 co-treatment in patients. To address this question, a pooled genome-wide CRISPR/CAS lentiviral library could be exploited to identify proteins or whole pathways responsible for the development of resistance. Such a screen has been employed in the breast cancer cell line SK-BR-3 and identified BAK as a major resistance factor to S63845 treatment (258). Since BAK proved to play an essential role in A-1331852/S63845-induced cell death as well, similar results are to be expected in RMS cells.

We observe hints that RD BAK KO cells generated by CRISPR/CAS develop a compensatory mechanism by relying on BAX to avoid cell death. It would be interesting to analyze via Co-IPs whether this might be due to an altered interaction pattern between the different BCL-2 family members. A long single clone selection process after the KO might have led to the mentioned compensation. In order to avoid this, the use of doxycycline-inducible BAK and BAX KO cells represents a reasonable alternative. Moreover, the finding that BAX does not interact with its anti-apoptotic BCL-2 relatives in Kym-1 cells should be experimentally confirmed using another assay such as a label transfer protein interaction assay. These experiments could help to further dissect and confirm the involvement of BAX and BAK in A-1331852/S63845-triggered cell death.

Eventually, the single addiction of RH18 and TE441.T cells on BCL-X_L and MCL-1, respectively, could be further investigated. Importantly, their dependency should be genetically verified by siRNA or CRISPR/CAS9. Co-IPs might unravel an explanation for the cell's high susceptibility to single agent A-1331852 or S63845. Finding and including additional cell lines that display a similar single sensitivity would be valuable to understand the underlying molecular mechanisms.

Despite the mentioned limitations and pending questions, the current thesis underpins the potential of the selective BH3 mimetics A-1331852 and S63845 as a concomitant treatment, especially in, but not limited to, RMS. Moreover, we acquire detailed insight into the underlying molecular background. Collectively, this work provides a profound basis to qualify A-1331852/S63845 co-treatment for further preclinical and clinical evaluations.

8 Summary (Deutsche Zusammenfassung)

Obwohl nur etwa 1% aller Krebserkrankungen Kinder betreffen, ist Krebs eine der häufigsten Todesursachen während der Kindheit. Leukämien (~25%), Lymphome (~16%) und Tumore des Zentralnervensystems (~17%) machen den Großteil der in Kindern auftretenden Tumorentitäten aus. Die verbleibenden ~42% der pädiatrischen Krebserkrankungen sind solide Tumore, die in Organen, Knochen oder Muskeln lokalisiert sind. Aufgrund optimierter Behandlungsmöglichkeiten, stieg die 5-Jahres Überlebensrate für krebserkrankte Kinder von 63% (1975 - 1979) auf 84% (2008 - 2014) an. Allerdings schwankt dieser Wert in Abhängigkeit von Art und Metastasierungsgrad des Tumors, sowie des Alters des Kindes.

Das Rhabdomyosarkom (RMS) ist der häufigste maligne Weichgewebstumor in Kindern und Jugendlichen. Er entsteht vermutlich aus mesenchymalen Vorläuferzellen des Skelettmuskels, die nicht vollständig ausdifferenziert sind. RMS kann in verschiedensten Bereichen des Körpers Tumore und Metastasen bilden, am häufigsten sind jedoch die Extremitäten, der Urogenitaltrakt und die Hals/Nacken-Region betroffen. Die meisten RMS Fälle lassen sich dem embryonalen (ERMS) oder alveolären (ARMS) Subtyp dieses Tumors zuordnen. ERMS und ARMS unterscheiden sich nicht nur histologisch, sondern auch genetisch voneinander. Der ARMS Subtyp zeichnet sich im Großteil der Fälle durch eine chromosomale Translokation zwischen Chromosom 2 und 3 bzw. zwischen Chromosom 1 und 3 aus, welche zur Bildung des Fusionsproteins PAX3/FOXO1 bzw. PAX7/FOXO1 führt. Zu den charakteristischen genetischen Merkmalen des ERMS Subtyps gehört eine Deletion auf Chromosom 11, sowie Mutationen von TP53, RAS und MYC Amplifikationen. Im Allgemeinen hat ERMS eine bessere Prognose als ARMS, welches häufiger metastasiert. Die Behandlung von RMS ist multimodal und umfasst Bestrahlung, Chemotherapie und chirurgische Eingriffe. Der Goldstandard in der Chemotherapie stellt seit Jahren die sogenannte VAC Therapie dar, die aus Vincristin, Actinomycin-D und Cyclophosphamid besteht.

Beim Osteosarkom (OS) und Ewing Sarkom (ES) handelt es sich um die beiden häufigsten malignen Knochenkrebserkrankungen in Kindern und Jugendlichen. Das OS ist eine genetisch komplexe Erkrankung, die durch eine hohe genomische Instabilität charakterisiert ist. Dazu gehört beispielsweise eine hohe Anzahl an Variationen der Kopienzahl von genomischen Abschnitten. Die Ausbildung von Fusionsproteinen, vor allem die des EWSR1/FLI1 Fusionsproteins, zählt zu den typischen molekularen Merkmalen des ES. Ähnlich wie beim RMS werden OS und ES mit einer multimodalen Therapie behandelt.

Obwohl die Überlebenschancen für Kinder mit RMS, ES und OS in den letzten Jahren gestiegen sind, bleibt die Prognose für Patienten, die Metastasen ausbilden oder einen Rückfall erleiden, weiterhin schlecht. Nach wie vor besteht daher ein hoher Bedarf an verbesserten

Behandlungsmöglichkeiten dieser Tumore. Diese sollten eine hohe Ansprechrate erzielen und gleichzeitig Nebenwirkungen minimieren.

Die Apoptose, der bisher am besten untersuchte Zelltodmechanismus, ist in Krebszellen häufig inhibiert. Extrinsische und intrinsische Apoptose, die beiden Signalwege, welche zum apoptotischen Zelltod führen können, werden durch verschiedene Faktoren reguliert. Externe Stimuli, vermittelt durch Liganden von Zelltodrezeptoren, aktivieren den extrinischen Apoptose Signalweg, während Stressoren innerhalb der Zelle, wie zum Beispiel DNA Brüche, den intrinsischen Signalweg stimulieren. Bei Letzterem spielt das Mitochondrium eine entscheidende Rolle, da die Permeabilisierung der äußeren Mitochondrienmembran schlussendlich eine Aktivierung von Caspasen auslöst. Caspasen sind Cysteinproteasen, welche eine Vielzahl von zellulären Proteinen spalten und somit deren geordneten Abbau im Rahmen der Apoptose sichern.

BCL-2 Proteine sind die zentralen Akteure, welche die Initiierung der Apoptose regulieren. Sie lassen sich in die Untergruppen der anti-apoptotischen Proteine (z.B. MCL-1, BCL-X_L, BCL-2), der pro-apoptotischen Effektorproteine (z.B. BAX, BAK) und der pro-apoptotischen BH3-only Proteine (z.B. BIM, NOXA) unterteilen. Diese Subgruppen interagieren untereinander in komplexer Weise und mit unterschiedlichen Affinitäten. Die Expression der einzelnen Proteine und die Art ihrer Interaktionen bilden eine Balance, die je nach Stimulus, die Apoptose begünstigt oder hemmt. In den letzten Jahren haben sich verschiedene Modelle bezüglich der Interaktionen und gegenseitigen Aktivierungen der BCL-2 Proteine herausgebildet, bei denen allerdings in jedem Fall die Aktivierung von BAX und BAK am Ende steht. BAX und BAK Homodimere bilden Poren in der äußeren Membran des Mitochondriums, was zu dessen Permeabilisierung führt. BCL-2 Proteine können auf transkriptioneller sowie (post)translationaler Ebene durch eine Reihe von Modifikationen reguliert werden. Aufgrund ihrer fundamentalen Relevanz für die Apoptoseinduktion spielen sie eine wichtige Rolle in der Entstehung und Homöostase verschiedenster Zelltypen.

Anti-apoptotische BCL-2 Proteine sind für eine Vielzahl von Krebszellen von essentieller Bedeutung. Krebszellen unterschiedlichster Tumorentitäten weisen eine Abhängigkeit von MCL-1, BCL-X_L, BCL-2 oder Kombinationen dieser Proteine auf. Es wurde gezeigt, dass BCL-2 Proteine auch im RMS, OS und ES wichtige Regulatoren zur Apoptoseinduktion darstellen. Stressoren, die im Rahmen einer malignen Transformation in der Zelle auftreten, begünstigen eine Aktivierung und/oder Hochregulation von pro-apoptotischen sowie anti-apoptotischen BCL-2 Proteinen. Im Folgenden bilden sich vermehrt Komplexe zwischen pro-und anti-apoptotischen Proteinen. In diesem Zustand ist die Zelle „primed for apoptosis“, da ein apoptotischer Stimulus rasch die gebundenen pro-apoptotischen Proteine freisetzen und somit den Zelltod einleiten kann. Daher sind Krebszellen besonders anfällig für Substanzen, welche solch einen Effekt vermitteln. Die unterschiedlichen Interaktionsmuster innerhalb der BCL-2 Proteine können maßgeblich dafür entscheidend sein, ob eine Zelle auf einen bestimmten apoptotischen Stimulus anspricht oder nicht.

Summary (Deutsche Zusammenfassung)

BH3 mimetics sind kleine Moleküle, die gezielt anti-apoptotische BCL-2 Proteine binden und sie somit inhibieren. Die Bindung erfolgt an einer hydrophoben Grube auf dem anti-apoptotischen BCL-2 Protein, welche normalerweise der Sequestration der BH3 Domäne pro-apoptotischer BCL-2 Proteine dient. Auf diese Weise imitieren BH3 mimetics pro-apoptotische BCL-2 Proteine in ihrer Apoptose-vermittelnden Funktion. BH3 mimetics bieten einige Vorteile gegenüber herkömmlichen Chemotherapeutika. Beispielsweise ist ihr Wirkmechanismus genau bekannt und sie haben keinen mutagenen Effekt auf den Patienten. Durch kontinuierliche Forschung konnten während der letzten Jahre immer selektivere BH3 mimetics entwickelt werden, welche mit hoher Affinität an ein bestimmtes BCL-2 Protein binden. Die Substanzen A-1331852, S63845 und ABT-199 inhibieren jeweils BCL-X_L, MCL-1 und BCL-2. In Studien mit unterschiedlichen hämatologischen sowie soliden Krebsentitäten demonstrierten die oben genannten BH3 mimetics bereits vielversprechende Ergebnisse. Mit der Zulassung von ABT-199 zur Behandlung von bestimmten Subgruppen der CLL und AML, hielten BH3 mimetics Einzug in die klinische Praxis. Aktuell wird der Effekt von einigen BH3 mimetics als Einzel- oder Kombinationstherapie in klinischen Studien weiter untersucht.

Ziel dieser Arbeit war eine umfassende Evaluation der anti-apoptotischen BCL-2 Proteine MCL-1, BCL-2 und BCL-X_L als therapeutischen Angriffspunkt in der Behandlung von pädiatrischen soliden Tumoren wie beispielsweise RMS, OS und ES. Es sollte bestimmt werden, ob eine Einzel- oder Kombinationstherapie mit BH3 mimetics am effizientesten Zelltod in diesen Entitäten auslöst. Außerdem war die Entschlüsselung des dem Zelltod zu Grunde liegenden molekularen Mechanismus im RMS ein wichtiger Bestandteil der Arbeit. Abschließend sollte mithilfe von Studien an nicht-malignen Zellen und der Evaluation einer sequenziell erfolgenden Behandlung die Eignung einer BH3 mimetics Kombinationstherapie für weitere (prä)klinische Studien erfolgen. Außerdem sollte anhand eines multizellulären Spheroidmodells und eines *in vivo* Versuchs am embryonalen Huhn die translationale Relevanz der Kombinationstherapie bestimmt werden.

Zunächst untersuchten wir die basale Expression der BCL-2 Proteine in einer Reihe von RMS Zelllinien, sowie einer primären Zelllinie, welche aus einem ARMS Patienten stammt. Wir stellten fest, dass fast die gesamten getesteten RMS Zelllinien alle relevanten BCL-2 Proteine in unterschiedlichen Mengen exprimierten. Ausnahmen bildeten die Kym-1 Zellen, welche keine Expression von BCL-2 und NOXA zeigten, und die TE441.T Zellen, die ebenfalls kein NOXA exprimierten. Da RMS Zellen somit die nötigen Zielproteine exprimierten, adressierten wir die Frage, ob eine pharmakologische Inhibition mit selektiven BH3 mimetics die Viabilität der RMS Zellen senken kann. Der Großteil der RMS Zelllinien war resistent gegenüber der Behandlung mit diesen Agenzien. Allerdings zeigten die RH18 Zellen eine ausgeprägte Sensitivität gegenüber dem BCL-X_L-Inhibitor A-1331852 und der MCL-1-Inhibitor S63845 demonstrierte eine deutliche Abnahme der Zellviabilität in den TE441.T Zellen. Insgesamt schien die Sensitivität der RMS Zelllinien unabhängig von deren Expression der BCL-2 Proteinfamilie zu sein.

Da die Inhibierung von MCL-1 und BCL-X_L am vielversprechendsten war, untersuchten wir, ob eine Kombinationstherapie mit A-1331852 und S63845 Zelltod in RMS Zelllinien auslösen kann. Interessanterweise führte die kombinierte Blockade von MCL-1 und BCL-X_L zu einer massiven dosis-abhängigen Induktion des Zelltods in allen RMS Zelllinien. Die Berechnung der Bliss Synergy Scores demonstrierte, dass die Interaktion zwischen den beiden BH3 mimetics, mit der der Zelltod hervorgerufen wurde, höchst synergistisch war. Des Weiteren stellten wir fest, dass die ABT-199/A-1331852 und ABT-199/S63845 Kombinationstherapien weniger effizient waren als eine Behandlung mit A-1331852/S63845. Dies konnten wir ebenfalls durch die Bestimmung der Bliss Synergy Scores bestätigen.

Ähnliche Ergebnisse erzielten wir in Experimenten mit OS und ES Zelllinien. Hierbei zeigte sich, dass diese alle getesteten BCL-2 Proteine exprimierten. Außerdem bewirkte eine Einzelbehandlung mit A-1331852 oder S63845 eine Reduktion der ES Zellviabilität, während OS Zellen nur wenig oder keine erhöhte Sensitivität gegenüber diesen Substanzen aufwiesen. Vergleichbar mit den Effekten im RMS, führte eine A-1331852/S63845 Kombinationstherapie auch in OS und ES zu einer synergistischen Zelltodinduktion. Gleichermaßen war die Effizienz der ABT-199/A-1331852 und ABT-199/S63845 Kombinationstherapien Zelltod auszulösen geringer als die einer A-1331852/S63845 Behandlung. Beides konnten wir mit der Berechnung der Bliss Synergy Scores belegen. Ferner demonstrierten wir, dass die A-1331852/S63845 Kombinationstherapie ebenfalls in einer klinischen Probe eines pädiatrischen malignen epitheloiden Mesotheliom Wirkung zeigte. Auch frühere Studien beschrieben bereits eine besondere Bedeutung für MCL-1 und BCL-X_L in verschiedenen Tumorentitäten als Faktoren, die maßgeblich an deren Überleben beteiligt sind. Eine gemeinsame Inhibition von MCL-1 und BCL-X_L könnte daher ein großes Potential für die Behandlung von pädiatrischen soliden Tumoren bieten.

Um Rückschlüsse über die Art des Zelltodes und den zugrunde liegenden molekularen Mechanismus ziehen zu können, widmeten wir uns im nächsten Teil der Arbeit dem Wirkmechanismus der A-1331852/S63845 Kombinationstherapie in den RMS Zelllinien RD und Kym-1. Zuerst beschäftigten wir uns mit der Frage, ob die vorherige pharmakologische Inhibition von MCL-1 und BCL-X_L spezifisch war oder ob möglicherweise sogenannte „off-target“ Effekte zur beobachteten Zelltodinduktion geführt hatten. Hierfür induzierten wir eine transiente Reduktion der MCL-1- und/oder BCL-X_L-Level mittels siRNA („Knockdown“). Wie erwartet starben die RMS Zellen nur in denjenigen experimentellen Ansätzen, in denen MCL-1 und BCL-X_L beide durch pharmakologische und/oder genetische Inhibition blockiert waren. Somit konnten wir verifizieren, dass der Zelltod-induzierende Effekt der kombinierten A-1331852/S63845 Behandlung tatsächlich auf der Inhibition von MCL-1 und BCL-X_L beruhte.

Als nächstes bestimmten wir die Kinetik mit der der A-1331852/S63845-vermittelte Zelltod ablief. RMS Zellen zeigten schon nach 1 - 2 h eine geringe Präsentation von Phosphatidylserin auf ihrer äußeren Membran, ein Marker für Apoptose, und die Zellen starben innerhalb von 3 – 6 h. Des Weiteren detektierten wir die Spaltung und somit Aktivierung der Caspasen-3, -8 und -9 bereits

1 - 2 h nach Behandlung mit A-1331852/S63845. Eine Vorbehandlung mit dem pan-Caspase Inhibitor zVAD.fmk verhinderte größtenteils eine Caspasenaktivierung sowie den Zelltod. Darüber hinaus löste die A-1331852/S63845 Kombinationstherapie einen Caspasen-abhängigen Verlust von MCL-1 aus, der vermutlich das durch die Behandlung ausgelöste pro-apoptotische Signal weiter verstärkte. Um festzustellen, ob das Mitochondrium eine wesentliche Rolle im A-1331852/S63845-induzierten Zelltod spielt, analysierten wir das Potential der äußeren mitochondrialen Membran, welches durch eine intakte Mitochondrienmembran aufrecht erhalten wird. In der Tat wurde bereits 1 – 3 h nach kombinierter A-1331852/S63845 Behandlung ein ausgeprägter Abfall des Potentials detektiert. Zusammenfassend konnte der Zelltod als Caspasen-abhängige, mitochondriale intrinsische Apoptose identifiziert werden.

Die Tatsache, dass BCL-2 Proteine wichtige Regulatoren der Apoptose an den Mitochondrien darstellen, warf die Frage auf, inwieweit und auf welche Weise sie im A-1331852/S63845-vermittelten Zelltod involviert sein könnten. Daher analysierten wir, ob die pro-apoptotischen Effektorproteine BAX und BAK unter der A-1331852/S63845 Behandlung aktiviert werden, was tatsächlich der Fall war. Außerdem wurde eine Interaktion zwischen BAX- und BAK-Komplexen detektiert. Überdies untersuchten wir die Bedeutung von BAX und BAK im Kontext des A-1331852/S63845-stimulierten Zelltods. Hierfür bedienten wir uns der Reduktion der BAX und/oder BAK Expression mittels eines Knockdowns. Interessanterweise zeigte sich, dass in den RD Zellen vor allem BAK eine wichtige Rolle spielte, während ein BAX Knockdown den Zelltod nur partiell verhinderte. Die Kym-1 Zellen demonstrierten dagegen eine stärkere Abhängigkeit von BAX als von BAK. Da ein Knockdown nur eine Verminderung aber keinen vollständigen Verlust eines Proteins bewirkt, generierten wir RMS Zelllinien, die BAK nicht exprimieren („Knockout“). Allerdings konnten die Experimente mit den RD BAK Knockout Zellen unsere Ergebnisse aus den Knockdown Versuchen nicht bestätigen, da die BAK Deletion den A-1331852/S63845-induzierten Zelltod nicht hemmte. Wir beobachteten weiter, dass erst ein zusätzlicher BAX Knockdown Zelltod in den BAK Knockout RD Zellen induzierte. Das lässt vermuten, dass die BAK Knockout Zellen aufgrund des permanenten Verlusts von BAK eine verstärkte Abhängigkeit von BAX ausgebildet haben könnten. Um diese Hypothese zu testen sind jedoch weitere Untersuchungen notwendig. Weiterhin zeigten wir in Koimmunpräzipitationsexperimenten, dass in RMS Zellen BAK basal an BCL-X_L oder MCL-1 gebunden ist. Durch die A-1331852/S63845 Kombinationsbehandlung werden diese Interaktionen inhibiert, was im Folgenden zu einer Freisetzung von BAK führte. Die Durchführung von BAX Koimmunpräzipitationen zeigte in der hier untersuchten Kym-1 Zelllinie keine Interaktion von BAX mit MCL-1 oder BCL-X_L. Insgesamt haben BAX und BAK eine tragende Rolle im Mechanismus des A-1331852/S63845-induzierten Zelltods.

Ferner untersuchten wir, ob einzelne Mitglieder der pro-apoptotischen BH3-only Proteine, wie beispielsweise BIM und NOXA, von Bedeutung für den A-1331852/S63845-stimulierten Zelltod sein könnten. In den RD Zellen resultierte der Knockdown von BIM und/oder NOXA in einer partiellen Blockade des Zelltods. Diese Ergebnisse passten zu der Beobachtung, dass die

A-1331852/S63845 Kombinationstherapie die jeweilige Bindung dieser beiden Proteine an BCL-X_L und MCL-1 löste. In den Kym-1 Zellen führte die BH3 mimetic Behandlung nicht zu einer Beeinträchtigung der basal vorhandenen BIM:MCL-1 Bindung. Ebenso hatte auch der Knockdown von BIM keinen Effekt auf den A-1331852/S63845-induzierten Zelltod. Die BH3-only Proteine BMF und PUMA waren in beiden Zelllinien nicht in den A-1331852/S63845-vermittelten Zelltod involviert. Zusammenfassend kann daher festgehalten werden, dass die BH3-only Proteine keine oder nur eine untergeordnete Rolle in der Vermittlung des Zelltods durch A-1331852/S63845 spielen.

Abschließend stellte sich die Frage, ob die hier untersuchte A-1331852/S63845 Kombinationstherapie klinisch relevant sein könnte. Deshalb führten wir Experimente mit nicht-malignen humanen Fibroblasten und mononukleären Zellen des peripheren Blutes, sowie murinen Myoblasten durch. Bemerkenswerterweise löste die Behandlung mit A-1331852/S63845 in Konzentrationen, welche in Krebszellen den Zelltod bewirkte, weder eine nennenswerte Caspasenaktivierung, noch Zelltod aus. Diese Ergebnisse legen nahe, dass es ein therapeutisches Fenster geben könnte, in dessen Rahmen eine Behandlung mit diesen Agenzien möglich ist. Zudem konnten wir demonstrieren, dass auch eine sequenziell erfolgende A-1331852/S63845 Behandlung signifikant Zelltod auslöste, obgleich der Effekt im Vergleich zur gleichzeitigen Behandlung schwächer war. Mithilfe eines multizellulären Spheroidmodells erforschten wir, ob und in welchem Ausmaß die A-1331852/S63845 Kombinationsbehandlung auch Zelltod in einer dreidimensionalen Zellkultur hervorrief. In der Tat führte die Behandlung mit den BH3 mimetics dosis-abhängig zur Reduktion der Zellviabilität sowie zu massivem Zelltod in drei verschiedenen RMS Zelllinien. Interessanterweise zeigte die Berechnung von Bliss Synergy Scores basierend auf Zellviabilitätsexperimenten, dass Zellen im Spheroidverband im Vergleich zu Zellen in konventioneller Zellkultur resistenter gegenüber der A-1331852/S63845 Kombinationsbehandlung waren. Schließlich konnte der Effekt einer gemeinsamen MCL-1- und BCL-X_L-Inhibition mittels eines *in vivo* Versuchs am embryonalen Huhn belegt werden. Diese Ergebnisse unterstreichen die translationale Relevanz dieser Arbeit.

Insgesamt konnten wir das große Potenzial einer A-1331852/S63845 Kombinationsbehandlung in pädiatrischen soliden Tumoren aufzeigen und die zugrunde liegenden molekularen Mechanismen im RMS entschlüsseln. Die Untersuchungen der vorliegenden Arbeit leisten einen wertvollen Beitrag im Hinblick auf eine weitere präklinische und klinische Evaluation von BH3 mimetics in pädiatrischen soliden Tumoren.

9 References

1. Howlader N. NAM, Krapcho M., Miller D., Brest A., Yu M., Ruhl J., Tatalovich Z., Mariotto A-, Lewis D.R., Chen H.S., Feuer E.J., Cronin K.A. (eds). SEER Cancer Statistics Review, 1975-2016. National Cancer Institute Bethesda, MD **2019**
2. Steliarova-Foucher E, Colombet M, Ries LAG, Moreno F, Dolya A, Bray F*, et al.* International incidence of childhood cancer, 2001-10: a population-based registry study. Lancet Oncol **2017**;18:719-31
3. Ries LS, MA; Gurney, JG; Linet, M; Tamra, T; Young, JL; Bunin, GR (eds). Cancer Incidence and Survival among Children and Adolescents: United StatesSEER Program 1975-1995, National Cancer Institute, SEER Program. NIH. Bethesda; 1999.
4. Gupta S, Howard SC, Hunger SP, Antillon FG, Metzger ML, Israels T*, et al.* Treating Childhood Cancer in Low- and Middle-Income Countries. In: Gelband H, Jha P, Sankaranarayanan R, Horton S, editors. Cancer: Disease Control Priorities, Third Edition (Volume 3). Washington (DC)2015.
5. Howard SC, Zaidi A, Cao X, Weil O, Bey P, Patte C*, et al.* The My Child Matters programme: effect of public-private partnerships on paediatric cancer care in low-income and middle-income countries. Lancet Oncol **2018**;19:e252-e66
6. Landier W, Bhatia S. Cancer survivorship: a pediatric perspective. Oncologist **2008**;13:1181-92
7. Maeda M. Late effects of childhood cancer: life-threatening issues. J Nippon Med Sch **2008**;75:320-4
8. Ferrari A, Dileo P, Casanova M, Bertulli R, Meazza C, Gandola L*, et al.* Rhabdomyosarcoma in adults. A retrospective analysis of 171 patients treated at a single institution. Cancer **2003**;98:571-80
9. Saab R, Spunt SL, Skapek SX. Myogenesis and rhabdomyosarcoma the Jekyll and Hyde of skeletal muscle. Curr Top Dev Biol **2011**;94:197-234
10. Tonin PN, Scrable H, Shimada H, Cavenee WK. Muscle-specific gene expression in rhabdomyosarcomas and stages of human fetal skeletal muscle development. Cancer Res **1991**;51:5100-6
11. Raney RB, Maurer HM, Anderson JR, Andrassy RJ, Donaldson SS, Qualman SJ*, et al.* The Intergroup Rhabdomyosarcoma Study Group (IRSG): Major Lessons From the IRS-I Through IRS-IV Studies as Background for the Current IRS-V Treatment Protocols. Sarcoma **2001**;5:9-15
12. Yang P, Grufferman S, Khoury MJ, Schwartz AG, Kowalski J, Ruymann FB*, et al.* Association of childhood rhabdomyosarcoma with neurofibromatosis type I and birth defects. Genet Epidemiol **1995**;12:467-74
13. Diller L, Sexsmith E, Gottlieb A, Li FP, Malkin D. Germline p53 mutations are frequently detected in young children with rhabdomyosarcoma. J Clin Invest **1995**;95:1606-11
14. Stout A. Rhabdomyosarcoma of the skeletal muscles. Annals of surgery **1946**;123:447-72
15. Dziuba I, Kurzawa P, Dopierala M, Larque AB, Januszkiewicz-Lewandowska D. Rhabdomyosarcoma in children - current pathologic and molecular classification. Pol J Pathol **2018**;69:20-32
16. Patton RB, Horn RC, Jr. Rhabdomyosarcoma: clinical and pathological features and comparison with human fetal and embryonal skeletal muscle. Surgery **1962**;52:572-84
17. Enterline HT, Horn RC, Jr. Alveolar rhabdomyosarcoma; a distinctive tumor type. Am J Clin Pathol **1958**;29:356-66
18. Visser M, Sijmons C, Bras J, Arceci RJ, Godfried M, Valentijn LJ*, et al.* Allelotype of pediatric rhabdomyosarcoma. Oncogene **1997**;15:1309-14
19. Minniti CP, Luan D, O'Grady C, Rosenfeld RG, Oh Y, Helman LJ. Insulin-like growth factor II overexpression in myoblasts induces phenotypic changes typical of the malignant phenotype. Cell Growth Differ **1995**;6:263-9
20. Dolgikh N, Hugle M, Vogler M, Fulda S. NRAS-Mutated Rhabdomyosarcoma Cells Are Vulnerable to Mitochondrial Apoptosis Induced by Coinhibition of MEK and PI3Kalpha. Cancer Res **2018**;78:2000-13
21. Shern JF, Chen L, Chmielecki J, Wei JS, Patidar R, Rosenberg M*, et al.* Comprehensive genomic analysis of rhabdomyosarcoma reveals a landscape of alterations affecting a

common genetic axis in fusion-positive and fusion-negative tumors. Cancer Discov **2014**;4:216-31
22. Hachitanda Y, Toyoshima S, Akazawa K, Tsuneyoshi M. N-myc gene amplification in rhabdomyosarcoma detected by fluorescence in situ hybridization: its correlation with histologic features. Mod Pathol **1998**;11:1222-7
23. De Giovanni C, Landuzzi L, Nicoletti G, Lollini PL, Nanni P. Molecular and cellular biology of rhabdomyosarcoma. Future Oncol **2009**;5:1449-75
24. Turc-Carel C, Lizard-Nacol S, Justrabo E, Favrot M, Philip T, Tabone E. Consistent chromosomal translocation in alveolar rhabdomyosarcoma. Cancer Genet Cytogenet **1986**;19:361-2
25. Shapiro DN, Sublett JE, Li B, Downing JR, Naeve CW. Fusion of PAX3 to a member of the forkhead family of transcription factors in human alveolar rhabdomyosarcoma. Cancer Res **1993**;53:5108-12
26. Barr FG. The role of chimeric paired box transcription factors in the pathogenesis of pediatric rhabdomysarcoma. Cancer Res **1999**;59:1711s-5s
27. Nguyen TH, Barr FG. Therapeutic Approaches Targeting PAX3-FOXO1 and Its Regulatory and Transcriptional Pathways in Rhabdomyosarcoma. Molecules **2018**;23
28. Barr FG, Qualman SJ, Macris MH, Melnyk N, Lawlor ER, Strzelecki DM*, et al.* Genetic heterogeneity in the alveolar rhabdomyosarcoma subset without typical gene fusions. Cancer Res **2002**;62:4704-10
29. Williamson D, Missiaglia E, de Reynies A, Pierron G, Thuille B, Palenzuela G*, et al.* Fusion gene-negative alveolar rhabdomyosarcoma is clinically and molecularly indistinguishable from embryonal rhabdomyosarcoma. J Clin Oncol **2010**;28:2151-8
30. Sorensen PH, Lynch JC, Qualman SJ, Tirabosco R, Lim JF, Maurer HM*, et al.* PAX3-FKHR and PAX7-FKHR gene fusions are prognostic indicators in alveolar rhabdomyosarcoma: a report from the children's oncology group. J Clin Oncol **2002**;20:2672-9
31. Chen L, Shern JF, Wei JS, Yohe ME, Song YK, Hurd L*, et al.* Clonality and evolutionary history of rhabdomyosarcoma. PLoS Genet **2015**;11:e1005075
32. Malempati S, Hawkins DS. Rhabdomyosarcoma: review of the Children's Oncology Group (COG) Soft-Tissue Sarcoma Committee experience and rationale for current COG studies. Pediatr Blood Cancer **2012**;59:5-10
33. Ognjanovic S, Linabery AM, Charbonneau B, Ross JA. Trends in childhood rhabdomyosarcoma incidence and survival in the United States, 1975-2005. Cancer **2009**;115:4218-26
34. Breneman JC, Lyden E, Pappo AS, Link MP, Anderson JR, Parham DM*, et al.* Prognostic factors and clinical outcomes in children and adolescents with metastatic rhabdomyosarcoma--a report from the Intergroup Rhabdomyosarcoma Study IV. J Clin Oncol **2003**;21:78-84
35. Pappo AS, Anderson JR, Crist WM, Wharam MD, Breitfeld PP, Hawkins D*, et al.* Survival after relapse in children and adolescents with rhabdomyosarcoma: A report from the Intergroup Rhabdomyosarcoma Study Group. J Clin Oncol **1999**;17:3487-93
36. Cotterill SJ, Wright CM, Pearce MS, Craft AW, Group UMBTW. Stature of young people with malignant bone tumors. Pediatr Blood Cancer **2004**;42:59-63
37. Zhu L, McManus MM, Hughes DP. Understanding the Biology of Bone Sarcoma from Early Initiating Events through Late Events in Metastasis and Disease Progression. Front Oncol **2013**;3:230
38. Chen X, Bahrami A, Pappo A, Easton J, Dalton J, Hedlund E*, et al.* Recurrent somatic structural variations contribute to tumorigenesis in pediatric osteosarcoma. Cell Rep **2014**;7:104-12
39. Stephens PJ, Greenman CD, Fu B, Yang F, Bignell GR, Mudie LJ*, et al.* Massive genomic rearrangement acquired in a single catastrophic event during cancer development. Cell **2011**;144:27-40
40. Yu D, Zhang S, Feng A, Xu D, Zhu Q, Mao Y*, et al.* Methotrexate, doxorubicin, and cisplatinum regimen is still the preferred option for osteosarcoma chemotherapy: A meta-analysis and clinical observation. Medicine (Baltimore) **2019**;98:e15582
41. Carrle D, Bielack S. Osteosarcoma lung metastases detection and principles of multimodal therapy. Cancer Treat Res **2009**;152:165-84

42. Geller DS, Gorlick R. Osteosarcoma: a review of diagnosis, management, and treatment strategies. Clin Adv Hematol Oncol **2010**;8:705-18
43. Leary SE, Wozniak AW, Billups CA, Wu J, McPherson V, Neel MD*, et al.* Survival of pediatric patients after relapsed osteosarcoma: the St. Jude Children's Research Hospital experience. Cancer **2013**;119:2645-53
44. Ewing J. Classics in oncology. Diffuse endothelioma of bone. James Ewing. Proceedings of the New York Pathological Society, 1921. CA Cancer J Clin **1972**;22:95-8
45. Iwamoto Y. Diagnosis and treatment of Ewing's sarcoma. Jpn J Clin Oncol **2007**;37:79-89
46. Grunewald TGP, Cidre-Aranaz F, Surdez D, Tomazou EM, de Alava E, Kovar H*, et al.* Ewing sarcoma. Nat Rev Dis Primers **2018**;4:5
47. Pradhan A, Grimer RJ, Spooner D, Peake D, Carter SR, Tillman RM*, et al.* Oncological outcomes of patients with Ewing's sarcoma: is there a difference between skeletal and extra-skeletal Ewing's sarcoma? J Bone Joint Surg Br **2011**;93:531-6
48. Delattre O, Zucman J, Plougastel B, Desmaze C, Melot T, Peter M*, et al.* Gene fusion with an ETS DNA-binding domain caused by chromosome translocation in human tumours. Nature **1992**;359:162-5
49. Le Deley MC, Delattre O, Schaefer KL, Burchill SA, Koehler G, Hogendoorn PC*, et al.* Impact of EWS-ETS fusion type on disease progression in Ewing's sarcoma/peripheral primitive neuroectodermal tumor: prospective results from the cooperative Euro-E.W.I.N.G. 99 trial. J Clin Oncol **2010**;28:1982-8
50. Sorensen PH, Lessnick SL, Lopez-Terrada D, Liu XF, Triche TJ, Denny CT. A second Ewing's sarcoma translocation, t(21;22), fuses the EWS gene to another ETS-family transcription factor, ERG. Nat Genet **1994**;6:146-51
51. Guillon N, Tirode F, Boeva V, Zynovyev A, Barillot E, Delattre O. The oncogenic EWS-FLI1 protein binds in vivo GGAA microsatellite sequences with potential transcriptional activation function. PLoS One **2009**;4:e4932
52. de Alava EL, S.L; Sorensen, P.H. WHO Classification of Tumors of Soft Tissue and Bone. Fletcher CMB, J.A.; Hogendoorn, P.C.W.; Mertens, F., editor. Lyon: IARC; 2013.
53. Juergens C, Weston C, Lewis I, Whelan J, Paulussen M, Oberlin O*, et al.* Safety assessment of intensive induction with vincristine, ifosfamide, doxorubicin, and etoposide (VIDE) in the treatment of Ewing tumors in the EURO-E.W.I.N.G. 99 clinical trial. Pediatr Blood Cancer **2006**;47:22-9
54. Smith MA, Seibel NL, Altekruse SF, Ries LA, Melbert DL, O'Leary M*, et al.* Outcomes for children and adolescents with cancer: challenges for the twenty-first century. J Clin Oncol **2010**;28:2625-34
55. Cotterill SJ, Ahrens S, Paulussen M, Jurgens HF, Voute PA, Gadner H*, et al.* Prognostic factors in Ewing's tumor of bone: analysis of 975 patients from the European Intergroup Cooperative Ewing's Sarcoma Study Group. J Clin Oncol **2000**;18:3108-14
56. Khanna N, Pandey A, Bajpai J. Metastatic Ewing's Sarcoma: Revisiting the "Evidence on the Fence". Indian J Med Paediatr Oncol **2017**;38:173-81
57. Van Mater D, Wagner L. Management of recurrent Ewing sarcoma: challenges and approaches. Onco Targets Ther **2019**;12:2279-88
58. Riggi N, Stamenkovic I. The Biology of Ewing sarcoma. Cancer Lett **2007**;254:1-10
59. Bernstein M, Kovar H, Paulussen M, Randall RL, Schuck A, Teot LA*, et al.* Ewing's sarcoma family of tumors: current management. Oncologist **2006**;11:503-19
60. Kavalar R, Pohar Marinsek Z, Jereb B, Cagran B, Golouh R. Prognostic value of immunohistochemistry in the Ewing's sarcoma family of tumors. Med Sci Monit **2009**;15:CR442-52
61. Pishas KI, Lessnick SL. Recent advances in targeted therapy for Ewing sarcoma. F1000Res **2016**;5
62. May WA, Grigoryan RS, Keshelava N, Cabral DJ, Christensen LL, Jenabi J*, et al.* Characterization and drug resistance patterns of Ewing's sarcoma family tumor cell lines. PLoS One **2013**;8:e80060
63. Lockdhin RAW, C.M. Programmed cell death-II. Endocrine potentiation of the breakdown of the intersegmental muscles of silkmoths. Journal of Insect Physiology **1964**:634-9
64. Tait SW, Ichim G, Green DR. Die another way--non-apoptotic mechanisms of cell death. J Cell Sci **2014**;127:2135-44
65. Green DR, Llambi F. Cell Death Signaling. Cold Spring Harb Perspect Biol **2015**;7

66. Tang D, Kang R, Berghe TV, Vandenabeele P, Kroemer G. The molecular machinery of regulated cell death. Cell Res **2019**;29:347-64
67. Vogt C. Untersuchungen über die Entwicklungsgeschichte der Geburtshelferkröte (Alytes obstetricans). Schweiz: Jent & Gassmann; 1842.
68. Kerr JF, Wyllie AH, Currie AR. Apoptosis: a basic biological phenomenon with wide-ranging implications in tissue kinetics. Br J Cancer **1972**;26:239-57
69. Degterev A, Yuan J. Expansion and evolution of cell death programmes. Nat Rev Mol Cell Biol **2008**;9:378-90
70. Duprez L, Wirawan E, Vanden Berghe T, Vandenabeele P. Major cell death pathways at a glance. Microbes Infect **2009**;11:1050-62
71. Fuchs Y, Steller H. Live to die another way: modes of programmed cell death and the signals emanating from dying cells. Nat Rev Mol Cell Biol **2015**;16:329-44
72. Opferman JT, Kothari A. Anti-apoptotic BCL-2 family members in development. Cell Death Differ **2017**
73. Taylor RC, Cullen SP, Martin SJ. Apoptosis: controlled demolition at the cellular level. Nat Rev Mol Cell Biol **2008**;9:231-41
74. Rastogi RP, Sinha R, Sinha RP. Apoptosis: Molecular Mechanism and Pathogenicity. EXCLI J **2009**;8:155-81
75. Hanahan D, Weinberg RA. The hallmarks of cancer. Cell **2000**;100:57-70
76. Elmore S. Apoptosis: a review of programmed cell death. Toxicol Pathol **2007**;35:495-516
77. Segawa K, Nagata S. An Apoptotic 'Eat Me' Signal: Phosphatidylserine Exposure. Trends Cell Biol **2015**;25:639-50
78. Zargarian S, Shlomovitz I, Erlich Z, Hourizadeh A, Ofir-Birin Y, Croker BA*, et al.* Phosphatidylserine externalization, "necroptotic bodies" release, and phagocytosis during necroptosis. PLoS Biol **2017**;15:e2002711
79. Nagata S. Apoptosis and Clearance of Apoptotic Cells. Annu Rev Immunol **2018**
80. Fulda S, Debatin KM. Extrinsic versus intrinsic apoptosis pathways in anticancer chemotherapy. Oncogene **2006**;25:4798-811
81. Park YH, Jeong MS, Jang SB. Death domain complex of the TNFR-1, TRADD, and RIP1 proteins for death-inducing signaling. Biochem Biophys Res Commun **2014**;443:1155-61
82. Ashkenazi A, Dixit VM. Death receptors: signaling and modulation. Science **1998**;281:1305-8
83. Kischkel FC, Hellbardt S, Behrmann I, Germer M, Pawlita M, Krammer PH*, et al.* Cytotoxicity-dependent APO-1 (Fas/CD95)-associated proteins form a death-inducing signaling complex (DISC) with the receptor. EMBO J **1995**;14:5579-88
84. Youle RJ, Strasser A. The BCL-2 protein family: opposing activities that mediate cell death. Nat Rev Mol Cell Biol **2008**;9:47-59
85. Kale J, Osterlund EJ, Andrews DW. BCL-2 family proteins: changing partners in the dance towards death. Cell Death Differ **2017**
86. Westphal D, Kluck RM, Dewson G. Building blocks of the apoptotic pore: how Bax and Bak are activated and oligomerize during apoptosis. Cell Death Differ **2014**;21:196-205
87. Kalkavan H, Green DR. MOMP, cell suicide as a BCL-2 family business. Cell Death Differ **2017**
88. Tait SW, Parsons MJ, Llambi F, Bouchier-Hayes L, Connell S, Munoz-Pinedo C*, et al.* Resistance to caspase-independent cell death requires persistence of intact mitochondria. Dev Cell **2010**;18:802-13
89. Ichim G, Lopez J, Ahmed SU, Muthalagu N, Giampazolias E, Delgado ME*, et al.* Limited mitochondrial permeabilization causes DNA damage and genomic instability in the absence of cell death. Mol Cell **2015**;57:860-72
90. Salvesen GS, Duckett CS. IAP proteins: blocking the road to death's door. Nat Rev Mol Cell Biol **2002**;3:401-10
91. Deveraux QL, Takahashi R, Salvesen GS, Reed JC. X-linked IAP is a direct inhibitor of cell-death proteases. Nature **1997**;388:300-4
92. Cain K, Bratton SB, Langlais C, Walker G, Brown DG, Sun XM*, et al.* Apaf-1 oligomerizes into biologically active approximately 700-kDa and inactive approximately 1.4-MDa apoptosome complexes. J Biol Chem **2000**;275:6067-70

93. Slee EA, Harte MT, Kluck RM, Wolf BB, Casiano CA, Newmeyer DD*, et al.* Ordering the cytochrome c-initiated caspase cascade: hierarchical activation of caspases-2, -3, -6, -7, -8, and -10 in a caspase-9-dependent manner. J Cell Biol **1999**;144:281-92
94. McArthur K, Whitehead LW, Heddleston JM, Li L, Padman BS, Oorschot V*, et al.* BAK/BAX macropores facilitate mitochondrial herniation and mtDNA efflux during apoptosis. Science **2018**;359
95. Birkinshaw RW, Czabotar PE. The BCL-2 family of proteins and mitochondrial outer membrane permeabilisation. Semin Cell Dev Biol **2017**
96. Cleary ML, Smith SD, Sklar J. Cloning and structural analysis of cDNAs for bcl-2 and a hybrid bcl-2/immunoglobulin transcript resulting from the t(14;18) translocation. Cell **1986**;47:19-28
97. Tsujimoto Y, Cossman J, Jaffe E, Croce CM. Involvement of the bcl-2 gene in human follicular lymphoma. Science **1985**;228:1440-3
98. Vaux DL, Cory S, Adams JM. Bcl-2 gene promotes haemopoietic cell survival and cooperates with c-myc to immortalize pre-B cells. Nature **1988**;335:440-2
99. Aouacheria A, Combet C, Tompa P, Hardwick JM. Redefining the BH3 Death Domain as a 'Short Linear Motif'. Trends Biochem Sci **2015**;40:736-48
100. Kvansakul M, Hinds MG. The structural biology of BH3-only proteins. Methods Enzymol **2014**;544:49-74
101. Hinds MG, Day CL. Regulation of apoptosis: uncovering the binding determinants. Curr Opin Struct Biol **2005**;15:690-9
102. Delbridge AR, Grabow S, Strasser A, Vaux DL. Thirty years of BCL-2: translating cell death discoveries into novel cancer therapies. Nat Rev Cancer **2016**;16:99-109
103. Adams JM, Cory S. The BCL-2 arbiters of apoptosis and their growing role as cancer targets. Cell Death Differ **2017**
104. Happo L, Strasser A, Cory S. BH3-only proteins in apoptosis at a glance. J Cell Sci **2012**;125:1081-7
105. Moldoveanu T, Czabotar PE. BAX, BAK, and BOK: A Coming of Age for the BCL-2 Family Effector Proteins. Cold Spring Harb Perspect Biol **2019**
106. Popgeorgiev N, Jabbour L, Gillet G. Subcellular Localization and Dynamics of the Bcl-2 Family of Proteins. Front Cell Dev Biol **2018**;6:13
107. Perciavalle RM, Stewart DP, Koss B, Lynch J, Milasta S, Bathina M*, et al.* Anti-apoptotic MCL-1 localizes to the mitochondrial matrix and couples mitochondrial fusion to respiration. Nat Cell Biol **2012**;14:575-83
108. Wu X, Zhang LS, Toombs J, Kuo YC, Piazza JT, Tuladhar R*, et al.* Extra-mitochondrial prosurvival BCL-2 proteins regulate gene transcription by inhibiting the SUFU tumour suppressor. Nat Cell Biol **2017**;19:1226-36
109. Edlich F, Banerjee S, Suzuki M, Cleland MM, Arnoult D, Wang C*, et al.* Bcl-x(L) retrotranslocates Bax from the mitochondria into the cytosol. Cell **2011**;145:104-16
110. Todt F, Cakir Z, Reichenbach F, Emschermann F, Lauterwasser J, Kaiser A*, et al.* Differential retrotranslocation of mitochondrial Bax and Bak. EMBO J **2015**;34:67-80
111. Feldstein AE, Werneburg NW, Li Z, Bronk SF, Gores GJ. Bax inhibition protects against free fatty acid-induced lysosomal permeabilization. Am J Physiol Gastrointest Liver Physiol **2006**;290:G1339-46
112. Lessene G, Czabotar PE, Colman PM. BCL-2 family antagonists for cancer therapy. Nat Rev Drug Discov **2008**;7:989-1000
113. Chen L, Willis SN, Wei A, Smith BJ, Fletcher JI, Hinds MG*, et al.* Differential targeting of prosurvival Bcl-2 proteins by their BH3-only ligands allows complementary apoptotic function. Mol Cell **2005**;17:393-403
114. Billen LP, Kokoski CL, Lovell JF, Leber B, Andrews DW. Bcl-XL inhibits membrane permeabilization by competing with Bax. PLoS Biol **2008**;6:e147
115. Letai A, Bassik MC, Walensky LD, Sorcinelli MD, Weiler S, Korsmeyer SJ. Distinct BH3 domains either sensitize or activate mitochondrial apoptosis, serving as prototype cancer therapeutics. Cancer Cell **2002**;2:183-92
116. Wei MC, Lindsten T, Mootha VK, Weiler S, Gross A, Ashiya M*, et al.* tBID, a membrane-targeted death ligand, oligomerizes BAK to release cytochrome c. Genes Dev **2000**;14:2060-71

117. Dewson G, Ma S, Frederick P, Hockings C, Tan I, Kratina T*, et al.* Bax dimerizes via a symmetric BH3:groove interface during apoptosis. Cell Death Differ **2012**;19:661-70
118. Cartron PF, Gallenne T, Bougras G, Gautier F, Manero F, Vusio P*, et al.* The first alpha helix of Bax plays a necessary role in its ligand-induced activation by the BH3-only proteins Bid and PUMA. Mol Cell **2004**;16:807-18
119. Kim H, Rafiuddin-Shah M, Tu HC, Jeffers JR, Zambetti GP, Hsieh JJ*, et al.* Hierarchical regulation of mitochondrion-dependent apoptosis by BCL-2 subfamilies. Nat Cell Biol **2006**;8:1348-58
120. Kim H, Tu HC, Ren D, Takeuchi O, Jeffers JR, Zambetti GP*, et al.* Stepwise activation of BAX and BAK by tBID, BIM, and PUMA initiates mitochondrial apoptosis. Mol Cell **2009**;36:487-99
121. Chen HC, Kanai M, Inoue-Yamauchi A, Tu HC, Huang Y, Ren D*, et al.* An interconnected hierarchical model of cell death regulation by the BCL-2 family. Nat Cell Biol **2015**;17:1270-81
122. Dai H, Smith A, Meng XW, Schneider PA, Pang YP, Kaufmann SH. Transient binding of an activator BH3 domain to the Bak BH3-binding groove initiates Bak oligomerization. J Cell Biol **2011**;194:39-48
123. Du H, Wolf J, Schafer B, Moldoveanu T, Chipuk JE, Kuwana T. BH3 domains other than Bim and Bid can directly activate Bax/Bak. J Biol Chem **2011**;286:491-501
124. Kuwana T, Bouchier-Hayes L, Chipuk JE, Bonzon C, Sullivan BA, Green DR*, et al.* BH3 domains of BH3-only proteins differentially regulate Bax-mediated mitochondrial membrane permeabilization both directly and indirectly. Mol Cell **2005**;17:525-35
125. Certo M, Del Gaizo Moore V, Nishino M, Wei G, Korsmeyer S, Armstrong SA*, et al.* Mitochondria primed by death signals determine cellular addiction to antiapoptotic BCL-2 family members. Cancer Cell **2006**;9:351-65
126. Czabotar PE, Lessene G, Strasser A, Adams JM. Control of apoptosis by the BCL-2 protein family: implications for physiology and therapy. Nat Rev Mol Cell Biol **2014**;15:49-63
127. Deng J, Carlson N, Takeyama K, Dal Cin P, Shipp M, Letai A. BH3 profiling identifies three distinct classes of apoptotic blocks to predict response to ABT-737 and conventional chemotherapeutic agents. Cancer Cell **2007**;12:171-85
128. Willis SN, Chen L, Dewson G, Wei A, Naik E, Fletcher JI*, et al.* Proapoptotic Bak is sequestered by Mcl-1 and Bcl-xL, but not Bcl-2, until displaced by BH3-only proteins. Genes Dev **2005**;19:1294-305
129. Ku B, Liang C, Jung JU, Oh BH. Evidence that inhibition of BAX activation by BCL-2 involves its tight and preferential interaction with the BH3 domain of BAX. Cell Res **2011**;21:627-41
130. Kuwana T, Mackey MR, Perkins G, Ellisman MH, Latterich M, Schneiter R*, et al.* Bid, Bax, and lipids cooperate to form supramolecular openings in the outer mitochondrial membrane. Cell **2002**;111:331-42
131. Willis SN, Fletcher JI, Kaufmann T, van Delft MF, Chen L, Czabotar PE*, et al.* Apoptosis initiated when BH3 ligands engage multiple Bcl-2 homologs, not Bax or Bak. Science **2007**;315:856-9
132. Huang K, O'Neill KL, Li J, Zhou W, Han N, Pang X*, et al.* BH3-only proteins target BCL-xL/MCL-1, not BAX/BAK, to initiate apoptosis. Cell Res **2019**
133. Shamas-Din A, Kale J, Leber B, Andrews DW. Mechanisms of action of Bcl-2 family proteins. Cold Spring Harb Perspect Biol **2013**;5:a008714
134. Llambi F, Moldoveanu T, Tait SW, Bouchier-Hayes L, Temirov J, McCormick LL*, et al.* A unified model of mammalian BCL-2 protein family interactions at the mitochondria. Mol Cell **2011**;44:517-31
135. Vogler M, Walter HS, Dyer MJS. Targeting anti-apoptotic BCL2 family proteins in haematological malignancies - from pathogenesis to treatment. Br J Haematol **2017**;178:364-79
136. Lovell JF, Billen LP, Bindner S, Shamas-Din A, Fradin C, Leber B*, et al.* Membrane binding by tBid initiates an ordered series of events culminating in membrane permeabilization by Bax. Cell **2008**;135:1074-84
137. Leber B, Lin J, Andrews DW. Embedded together: the life and death consequences of interaction of the Bcl-2 family with membranes. Apoptosis **2007**;12:897-911

138. Czabotar PE, Westphal D, Dewson G, Ma S, Hockings C, Fairlie WD*, et al.* Bax crystal structures reveal how BH3 domains activate Bax and nucleate its oligomerization to induce apoptosis. Cell **2013**;152:519-31
139. Bleicken S, Hantusch A, Das KK, Frickey T, Garcia-Saez AJ. Quantitative interactome of a membrane Bcl-2 network identifies a hierarchy of complexes for apoptosis regulation. Nat Commun **2017**;8:73
140. Bogner C, Kale J, Pogmore J, Chi X, Shamas-Din A, Fradin C*, et al.* Allosteric Regulation of BH3 Proteins in Bcl-xL Complexes Enables Switch-like Activation of Bax. Mol Cell **2020**;77:901-12 e9
141. Jeng PS, Inoue-Yamauchi A, Hsieh JJ, Cheng EH. BH3-Dependent and Independent Activation of BAX and BAK in Mitochondrial Apoptosis. Curr Opin Physiol **2018**;3:71-81
142. O'Neill KL, Huang K, Zhang J, Chen Y, Luo X. Inactivation of prosurvival Bcl-2 proteins activates Bax/Bak through the outer mitochondrial membrane. Genes Dev **2016**;30:973-88
143. Suzuki M, Youle RJ, Tjandra N. Structure of Bax: coregulation of dimer formation and intracellular localization. Cell **2000**;103:645-54
144. Wolter KG, Hsu YT, Smith CL, Nechushtan A, Xi XG, Youle RJ. Movement of Bax from the cytosol to mitochondria during apoptosis. J Cell Biol **1997**;139:1281-92
145. Chin HS, Li MX, Tan IKL, Ninnis RL, Reljic B, Scicluna K*, et al.* VDAC2 enables BAX to mediate apoptosis and limit tumor development. Nat Commun **2018**;9:4976
146. Ma SB, Nguyen TN, Tan I, Ninnis R, Iyer S, Stroud DA*, et al.* Bax targets mitochondria by distinct mechanisms before or during apoptotic cell death: a requirement for VDAC2 or Bak for efficient Bax apoptotic function. Cell Death Differ **2014**;21:1925-35
147. Leshchiner ES, Braun CR, Bird GH, Walensky LD. Direct activation of full-length proapoptotic BAK. Proc Natl Acad Sci U S A **2013**;110:E986-95
148. Gavathiotis E, Reyna DE, Davis ML, Bird GH, Walensky LD. BH3-triggered structural reorganization drives the activation of proapoptotic BAX. Mol Cell **2010**;40:481-92
149. Hsu YT, Youle RJ. Bax in murine thymus is a soluble monomeric protein that displays differential detergent-induced conformations. J Biol Chem **1998**;273:10777-83
150. Brouwer JM, Westphal D, Dewson G, Robin AY, Uren RT, Bartolo R*, et al.* Bak core and latch domains separate during activation, and freed core domains form symmetric homodimers. Mol Cell **2014**;55:938-46
151. Moldoveanu T, Grace CR, Llambi F, Nourse A, Fitzgerald P, Gehring K*, et al.* BID-induced structural changes in BAK promote apoptosis. Nat Struct Mol Biol **2013**;20:589-97
152. Dewson G, Kratina T, Czabotar P, Day CL, Adams JM, Kluck RM. Bak activation for apoptosis involves oligomerization of dimers via their alpha6 helices. Mol Cell **2009**;36:696-703
153. Mikhailov V, Mikhailova M, Degenhardt K, Venkatachalam MA, White E, Saikumar P. Association of Bax and Bak homo-oligomers in mitochondria. Bax requirement for Bak reorganization and cytochrome c release. J Biol Chem **2003**;278:5367-76
154. Cosentino K, Garcia-Saez AJ. Bax and Bak Pores: Are We Closing the Circle? Trends Cell Biol **2017**;27:266-75
155. Bleicken S, Landeta O, Landajuela A, Basanez G, Garcia-Saez AJ. Proapoptotic Bax and Bak proteins form stable protein-permeable pores of tunable size. J Biol Chem **2013**;288:33241-52
156. Bleicken S, Assafa TE, Stegmueller C, Wittig A, Garcia-Saez AJ, Bordignon E. Topology of active, membrane-embedded Bax in the context of a toroidal pore. Cell Death Differ **2018**;25:1717-31
157. Subburaj Y, Cosentino K, Axmann M, Pedrueza-Villalmanzo E, Hermann E, Bleicken S*, et al.* Bax monomers form dimer units in the membrane that further self-assemble into multiple oligomeric species. Nat Commun **2015**;6:8042
158. Oda E, Ohki R, Murasawa H, Nemoto J, Shibue T, Yamashita T*, et al.* Noxa, a BH3-only member of the Bcl-2 family and candidate mediator of p53-induced apoptosis. Science **2000**;288:1053-8
159. Nakano K, Vousden KH. PUMA, a novel proapoptotic gene, is induced by p53. Mol Cell **2001**;7:683-94

160. Dijkers PF, Medema RH, Lammers JW, Koenderman L, Coffer PJ. Expression of the pro-apoptotic Bcl-2 family member Bim is regulated by the forkhead transcription factor FKHR-L1. Curr Biol **2000**;10:1201-4
161. Grad JM, Zeng XR, Boise LH. Regulation of Bcl-xL: a little bit of this and a little bit of STAT. Curr Opin Oncol **2000**;12:543-9
162. Puthalakath H, Villunger A, O'Reilly LA, Beaumont JG, Coultas L, Cheney RE*, et al.* Bmf: a proapoptotic BH3-only protein regulated by interaction with the myosin V actin motor complex, activated by anoikis. Science **2001**;293:1829-32
163. Kutuk O, Letai A. Regulation of Bcl-2 family proteins by posttranslational modifications. Curr Mol Med **2008**;8:102-18
164. Ley R, Ewings KE, Hadfield K, Cook SJ. Regulatory phosphorylation of Bim: sorting out the ERK from the JNK. Cell Death Differ **2005**;12:1008-14
165. Mojsa B, Lassot I, Desagher S. Mcl-1 ubiquitination: unique regulation of an essential survival protein. Cells **2014**;3:418-37
166. Print CG, Loveland KL, Gibson L, Meehan T, Stylianou A, Wreford N*, et al.* Apoptosis regulator bcl-w is essential for spermatogenesis but appears otherwise redundant. Proc Natl Acad Sci U S A **1998**;95:12424-31
167. Ross AJ, Waymire KG, Moss JE, Parlow AF, Skinner MK, Russell LD*, et al.* Testicular degeneration in Bclw-deficient mice. Nat Genet **1998**;18:251-6
168. Adams CM, Kim AS, Mitra R, Choi JK, Gong JZ, Eischen CM. BCL-W has a fundamental role in B cell survival and lymphomagenesis. J Clin Invest **2017**;127:635-50
169. Ottina E, Grespi F, Tischner D, Soratroi C, Geley S, Ploner A*, et al.* Targeting antiapoptotic A1/Bfl-1 by in vivo RNAi reveals multiple roles in leukocyte development in mice. Blood **2012**;119:6032-42
170. Veis DJ, Sorenson CM, Shutter JR, Korsmeyer SJ. Bcl-2-deficient mice demonstrate fulminant lymphoid apoptosis, polycystic kidneys, and hypopigmented hair. Cell **1993**;75:229-40
171. Kamada S, Shimono A, Shinto Y, Tsujimura T, Takahashi T, Noda T*, et al.* bcl-2 deficiency in mice leads to pleiotropic abnormalities: accelerated lymphoid cell death in thymus and spleen, polycystic kidney, hair hypopigmentation, and distorted small intestine. Cancer Res **1995**;55:354-9
172. Abe-Dohmae S, Harada N, Yamada K, Tanaka R. Bcl-2 gene is highly expressed during neurogenesis in the central nervous system. Biochem Biophys Res Commun **1993**;191:915-21
173. Merry DE, Veis DJ, Hickey WF, Korsmeyer SJ. bcl-2 protein expression is widespread in the developing nervous system and retained in the adult PNS. Development **1994**;120:301-11
174. Fogarty LC, Flemmer RT, Geizer BA, Licursi M, Karunanithy A, Opferman JT*, et al.* Mcl-1 and Bcl-xL are essential for survival of the developing nervous system. Cell Death Differ **2018**
175. Rinkenberger JL, Horning S, Klocke B, Roth K, Korsmeyer SJ. Mcl-1 deficiency results in peri-implantation embryonic lethality. Genes Dev **2000**;14:23-7
176. Wang X, Bathina M, Lynch J, Koss B, Calabrese C, Frase S*, et al.* Deletion of MCL-1 causes lethal cardiac failure and mitochondrial dysfunction. Genes Dev **2013**;27:1351-64
177. Motoyama N, Wang F, Roth KA, Sawa H, Nakayama K, Nakayama K*, et al.* Massive cell death of immature hematopoietic cells and neurons in Bcl-x-deficient mice. Science **1995**;267:1506-10
178. Vick B, Weber A, Urbanik T, Maass T, Teufel A, Krammer PH*, et al.* Knockout of myeloid cell leukemia-1 induces liver damage and increases apoptosis susceptibility of murine hepatocytes. Hepatology **2009**;49:627-36
179. Hikita H, Takehara T, Shimizu S, Kodama T, Li W, Miyagi T*, et al.* Mcl-1 and Bcl-xL cooperatively maintain integrity of hepatocytes in developing and adult murine liver. Hepatology **2009**;50:1217-26
180. Grabow S, Kueh AJ, Ke F, Vanyai HK, Sheikh BN, Dengler MA*, et al.* Subtle Changes in the Levels of BCL-2 Proteins Cause Severe Craniofacial Abnormalities. Cell Rep **2018**;24:3285-95 e4

181. Ke F, Lancaster GI, Grabow S, Murphy AJ, Strasser A. Combined reduction in the expression of MCL-1 and BCL-2 reduces organismal size in mice. Cell Death Dis **2020**;11:185
182. Mason KD, Carpinelli MR, Fletcher JI, Collinge JE, Hilton AA, Ellis S*, et al.* Programmed anuclear cell death delimits platelet life span. Cell **2007**;128:1173-86
183. Rudin CM, Hann CL, Garon EB, Ribeiro de Oliveira M, Bonomi PD, Camidge DR*, et al.* Phase II study of single-agent navitoclax (ABT-263) and biomarker correlates in patients with relapsed small cell lung cancer. Clin Cancer Res **2012**;18:3163-9
184. Gandhi L, Camidge DR, Ribeiro de Oliveira M, Bonomi P, Gandara D, Khaira D*, et al.* Phase I study of Navitoclax (ABT-263), a novel Bcl-2 family inhibitor, in patients with small-cell lung cancer and other solid tumors. J Clin Oncol **2011**;29:909-16
185. Opferman JT. Attacking cancer's Achilles heel: antagonism of anti-apoptotic BCL-2 family members. FEBS J **2016**;283:2661-75
186. Julien O, Wells JA. Caspases and their substrates. Cell Death Differ **2017**;24:1380-9
187. Li J, Yuan J. Caspases in apoptosis and beyond. Oncogene **2008**;27:6194-206
188. Timmer JC, Salvesen GS. Caspase substrates. Cell Death Differ **2007**;14:66-72
189. Enari M, Sakahira H, Yokoyama H, Okawa K, Iwamatsu A, Nagata S. A caspase-activated DNase that degrades DNA during apoptosis, and its inhibitor ICAD. Nature **1998**;391:43-50
190. Herrant M, Jacquel A, Marchetti S, Belhacene N, Colosetti P, Luciano F*, et al.* Cleavage of Mcl-1 by caspases impaired its ability to counteract Bim-induced apoptosis. Oncogene **2004**;23:7863-73
191. Fischer U, Janicke RU, Schulze-Osthoff K. Many cuts to ruin: a comprehensive update of caspase substrates. Cell Death Differ **2003**;10:76-100
192. Hanahan D, Weinberg RA. Hallmarks of cancer: the next generation. Cell **2011**;144:646-74
193. Montero J, Letai A. Why do BCL-2 inhibitors work and where should we use them in the clinic? Cell Death Differ **2017**
194. Merino D, Kelly GL, Lessene G, Wei AH, Roberts AW, Strasser A. BH3-Mimetic Drugs: Blazing the Trail for New Cancer Medicines. Cancer Cell **2018**;34:879-91
195. Letai AG. Diagnosing and exploiting cancer's addiction to blocks in apoptosis. Nat Rev Cancer **2008**;8:121-32
196. Beroukhim R, Mermel CH, Porter D, Wei G, Raychaudhuri S, Donovan J*, et al.* The landscape of somatic copy-number alteration across human cancers. Nature **2010**;463:899-905
197. Amundson SA, Myers TG, Scudiero D, Kitada S, Reed JC, Fornace AJ, Jr. An informatics approach identifying markers of chemosensitivity in human cancer cell lines. Cancer Res **2000**;60:6101-10
198. Monni O, Joensuu H, Franssila K, Klefstrom J, Alitalo K, Knuutila S. BCL2 overexpression associated with chromosomal amplification in diffuse large B-cell lymphoma. Blood **1997**;90:1168-74
199. Olejniczak ET, Van Sant C, Anderson MG, Wang G, Tahir SK, Sauter G*, et al.* Integrative genomic analysis of small-cell lung carcinoma reveals correlates of sensitivity to bcl-2 antagonists and uncovers novel chromosomal gains. Mol Cancer Res **2007**;5:331-9
200. Kuwashima Y, Uehara T, Kishi K, Shiromizu K, Matsuzawa M, Takayama S. Immunohistochemical characterization of undifferentiated carcinomas of the ovary. J Cancer Res Clin Oncol **1994**;120:672-7
201. Dawson SJ, Makretsov N, Blows FM, Driver KE, Provenzano E, Le Quesne J*, et al.* BCL2 in breast cancer: a favourable prognostic marker across molecular subtypes and independent of adjuvant therapy received. Br J Cancer **2010**;103:668-75
202. Cimmino A, Calin GA, Fabbri M, Iorio MV, Ferracin M, Shimizu M*, et al.* miR-15 and miR-16 induce apoptosis by targeting BCL2. Proc Natl Acad Sci U S A **2005**;102:13944-9
203. Krajewski S, Krajewska M, Ehrmann J, Sikorska M, Lach B, Chatten J*, et al.* Immunohistochemical analysis of Bcl-2, Bcl-X, Mcl-1, and Bax in tumors of central and peripheral nervous system origin. Am J Pathol **1997**;150:805-14
204. Kirsh EJ, Baunoch DA, Stadler WM. Expression of bcl-2 and bcl-X in bladder cancer. J Urol **1998**;159:1348-53

205. Kondo S, Shinomura Y, Kanayama S, Higashimoto Y, Miyagawa JI, Minami T*, et al.* Over-expression of bcl-xL gene in human gastric adenomas and carcinomas. Int J Cancer **1996**;68:727-30
206. Goodwin CM, Rossanese OW, Olejniczak ET, Fesik SW. Myeloid cell leukemia-1 is an important apoptotic survival factor in triple-negative breast cancer. Cell Death Differ **2015**;22:2098-106
207. Xiao Y, Nimmer P, Sheppard GS, Bruncko M, Hessler P, Lu X*, et al.* MCL-1 Is a Key Determinant of Breast Cancer Cell Survival: Validation of MCL-1 Dependency Utilizing a Highly Selective Small Molecule Inhibitor. Molecular Cancer Therapeutics **2015**;14:1837-47
208. Nalluri S, Peirce SK, Tanos R, Abdella HA, Karmali D, Hogarty MD*, et al.* EGFR signaling defines Mcl(-)1 survival dependency in neuroblastoma. Cancer Biol Ther **2015**;16:276-86
209. Glaser SP, Lee EF, Trounson E, Bouillet P, Wei A, Fairlie WD*, et al.* Anti-apoptotic Mcl-1 is essential for the development and sustained growth of acute myeloid leukemia. Genes Dev **2012**;26:120-5
210. Zhang H, Guttikonda S, Roberts L, Uziel T, Semizarov D, Elmore SW*, et al.* Mcl-1 is critical for survival in a subgroup of non-small-cell lung cancer cell lines. Oncogene **2011**;30:1963-8
211. Grabow S, Delbridge AR, Valente LJ, Strasser A. MCL-1 but not BCL-XL is critical for the development and sustained expansion of thymic lymphoma in p53-deficient mice. Blood **2014**;124:3939-46
212. Morales AA, Kurtoglu M, Matulis SM, Liu J, Siefker D, Gutman DM*, et al.* Distribution of Bim determines Mcl-1 dependence or codependence with Bcl-xL/Bcl-2 in Mcl-1-expressing myeloma cells. Blood **2011**;118:1329-39
213. Armistead PM, Salganick J, Roh JS, Steinert DM, Patel S, Munsell M*, et al.* Expression of receptor tyrosine kinases and apoptotic molecules in rhabdomyosarcoma: correlation with overall survival in 105 patients. Cancer **2007**;110:2293-303
214. McPake CR, Tillman DM, Poquette CA, George EO, Houghton JA, Harris LC. Bax is an important determinant of chemosensitivity in pediatric tumor cell lines independent of Bcl-2 expression and p53 status. Oncol Res **1998**;10:235-44
215. Marshall AD, Picchione F, Geltink RIK, Grosveld GC. PAX3-FOXO1 Induces Up-Regulation of Noxa Sensitizing Alveolar Rhabdomyosarcoma Cells to Apoptosis. Neoplasia **2013**;15:738-IN15
216. Margue CM, Bernasconi M, Barr FG, Schafer BW. Transcriptional modulation of the anti-apoptotic protein BCL-XL by the paired box transcription factors PAX3 and PAX3/FKHR. Oncogene **2000**;19:2921-9
217. Wei CC, Ball S, Lin L, Liu A, Fuchs JR, Li PK*, et al.* Two small molecule compounds, LLL12 and FLLL32, exhibit potent inhibitory activity on STAT3 in human rhabdomyosarcoma cells. Int J Oncol **2011**;38:279-85
218. Wachtel M, Rakic J, Okoniewski M, Bode P, Niggli F, Schafer BW. FGFR4 signaling couples to Bim and not Bmf to discriminate subsets of alveolar rhabdomyosarcoma cells. Int J Cancer **2014**;135:1543-52
219. Fulda S. Cell death pathways as therapeutic targets in rhabdomyosarcoma. Sarcoma **2012**;2012:326210
220. R2: Genomics Analysis and Visualization Platform (http://r2.amc.nl). **2019**
221. Pazzaglia L, Chiechi A, Conti A, Gamberi G, Magagnoli G, Novello C*, et al.* Genetic and molecular alterations in rhabdomyosarcoma: mRNA overexpression of MCL1 and MAP2K4 genes. Histol Histopathol **2009**;24:61-7
222. Wang ZX, Yang JS, Pan X, Wang JR, Li J, Yin YM*, et al.* Functional and biological analysis of Bcl-xL expression in human osteosarcoma. Bone **2010**;47:445-54
223. Baranski Z, de Jong Y, Ilkova T, Peterse EF, Cleton-Jansen AM, van de Water B*, et al.* Pharmacological inhibition of Bcl-xL sensitizes osteosarcoma to doxorubicin. Oncotarget **2015**;6:36113-25
224. Heisey DAR, Lochmann TL, Floros KV, Coon CM, Powell KM, Jacob S*, et al.* The Ewing family of tumors rely on BCL-2 and BCL-XL to escape PARP inhibitor toxicity. Clin Cancer Res **2018**

225. Villunger A, Michalak EM, Coultas L, Mullauer F, Bock G, Ausserlechner MJ*, et al.* p53- and drug-induced apoptotic responses mediated by BH3-only proteins puma and noxa. Science **2003**;302:1036-8
226. Soderquist RS, Crawford L, Liu E, Lu M, Agarwal A, Anderson GR*, et al.* Systematic mapping of BCL-2 gene dependencies in cancer reveals molecular determinants of BH3 mimetic sensitivity. Nat Commun **2018**;9:3513
227. Kotschy A, Szlavik Z, Murray J, Davidson J, Maragno AL, Le Toumelin-Braizat G*, et al.* The MCL1 inhibitor S63845 is tolerable and effective in diverse cancer models. Nature **2016**;538:477-82
228. Sun W, Chatterjee B, Wang Y, Stevenson HS, Edelman DC, Meltzer PS*, et al.* Distinct methylation profiles characterize fusion-positive and fusion-negative rhabdomyosarcoma. Mod Pathol **2015**;28:1214-24
229. Lanza IR, Short DK, Short KR, Raghavakaimal S, Basu R, Joyner MJ*, et al.* Endurance exercise as a countermeasure for aging. Diabetes **2008**;57:2933-42
230. Billard C. BH3 mimetics: status of the field and new developments. Mol Cancer Ther **2013**;12:1691-700
231. Opydo-Chanek M, Gonzalo O, Marzo I. Multifaceted anticancer activity of BH3 mimetics: Current evidence and future prospects. Biochem Pharmacol **2017**;136:12-23
232. Denis C, Sopkova-de Oliveira Santos J, Bureau R, Voisin-Chiret AS. Hot-Spots of Mcl-1 Protein. J Med Chem **2020**;63:928-43
233. Vogler M, Weber K, Dinsdale D, Schmitz I, Schulze-Osthoff K, Dyer MJ*, et al.* Different forms of cell death induced by putative BCL2 inhibitors. Cell Death Differ **2009**;16:1030-9
234. Anderson MA, Deng J, Seymour JF, Tam C, Kim SY, Fein J*, et al.* The BCL2 selective inhibitor venetoclax induces rapid onset apoptosis of CLL cells in patients via a TP53-independent mechanism. Blood **2016**;127:3215-24
235. Wang JL, Liu D, Zhang ZJ, Shan S, Han X, Srinivasula SM*, et al.* Structure-based discovery of an organic compound that binds Bcl-2 protein and induces apoptosis of tumor cells. Proc Natl Acad Sci U S A **2000**;97:7124-9
236. Oltersdorf T, Elmore SW, Shoemaker AR, Armstrong RC, Augeri DJ, Belli BA*, et al.* An inhibitor of Bcl-2 family proteins induces regression of solid tumours. Nature **2005**;435:677-81
237. van Delft MF, Wei AH, Mason KD, Vandenberg CJ, Chen L, Czabotar PE*, et al.* The BH3 mimetic ABT-737 targets selective Bcl-2 proteins and efficiently induces apoptosis via Bak/Bax if Mcl-1 is neutralized. Cancer Cell **2006**;10:389-99
238. Del Gaizo Moore V, Schlis KD, Sallan SE, Armstrong SA, Letai A. BCL-2 dependence and ABT-737 sensitivity in acute lymphoblastic leukemia. Blood **2008**;111:2300-9
239. Tse C, Shoemaker AR, Adickes J, Anderson MG, Chen J, Jin S*, et al.* ABT-263: a potent and orally bioavailable Bcl-2 family inhibitor. Cancer Res **2008**;68:3421-8
240. Roberts AW, Seymour JF, Brown JR, Wierda WG, Kipps TJ, Khaw SL*, et al.* Substantial susceptibility of chronic lymphocytic leukemia to BCL2 inhibition: results of a phase I study of navitoclax in patients with relapsed or refractory disease. J Clin Oncol **2012**;30:488-96
241. Wilson WH, O'Connor OA, Czuczman MS, LaCasce AS, Gerecitano JF, Leonard JP*, et al.* Navitoclax, a targeted high-affinity inhibitor of BCL-2, in lymphoid malignancies: a phase 1 dose-escalation study of safety, pharmacokinetics, pharmacodynamics, and antitumour activity. Lancet Oncol **2010**;11:1149-59
242. Souers AJ, Leverson JD, Boghaert ER, Ackler SL, Catron ND, Chen J*, et al.* ABT-199, a potent and selective BCL-2 inhibitor, achieves antitumor activity while sparing platelets. Nat Med **2013**;19:202-8
243. Birkinshaw RW, Gong JN, Luo CS, Lio D, White CA, Anderson MA*, et al.* Structures of BCL-2 in complex with venetoclax reveal the molecular basis of resistance mutations. Nat Commun **2019**;10:2385
244. Vaillant F, Merino D, Lee L, Breslin K, Pal B, Ritchie ME*, et al.* Targeting BCL-2 with the BH3 mimetic ABT-199 in estrogen receptor-positive breast cancer. Cancer Cell **2013**;24:120-9
245. Vogler M. Targeting BCL2-Proteins for the Treatment of Solid Tumours. Adv Med **2014**;2014:943648

246. Heinicke U, Haydn T, Kehr S, Vogler M, Fulda S. BCL-2 selective inhibitor ABT-199 primes rhabdomyosarcoma cells to histone deacetylase inhibitor-induced apoptosis. Oncogene **2018**;37:5325-39
247. Phillips DC, Jin S, Gregory GP, Zhang Q, Xue J, Zhao X*, et al.* A novel CDK9 inhibitor increases the efficacy of venetoclax (ABT-199) in multiple models of hematologic malignancies. Leukemia **2019**
248. Pan R, Hogdal LJ, Benito JM, Bucci D, Han L, Borthakur G*, et al.* Selective BCL-2 inhibition by ABT-199 causes on-target cell death in acute myeloid leukemia. Cancer Discov **2014**;4:362-75
249. Vandenberg CJ, Cory S. ABT-199, a new Bcl-2-specific BH3 mimetic, has in vivo efficacy against aggressive Myc-driven mouse lymphomas without provoking thrombocytopenia. Blood **2013**;121:2285-8
250. Peirs S, Matthijssens F, Goossens S, Van de Walle I, Ruggero K, de Bock CE*, et al.* ABT-199 mediated inhibition of BCL-2 as a novel therapeutic strategy in T-cell acute lymphoblastic leukemia. Blood **2014**;124:3738-47
251. Zhou L, Zhang Y, Sampath D, Leverson J, Dai Y, Kmieciak M*, et al.* Flavopiridol enhances ABT-199 sensitivity in unfavourable-risk multiple myeloma cells in vitro and in vivo. Br J Cancer **2018**;118:388-97
252. Niu X, Zhao J, Ma J, Xie C, Edwards H, Wang G*, et al.* Binding of Released Bim to Mcl-1 is a Mechanism of Intrinsic Resistance to ABT-199 which can be Overcome by Combination with Daunorubicin or Cytarabine in AML Cells. Clin Cancer Res **2016**;22:4440-51
253. Li Z, He S, Look AT. The MCL1-specific inhibitor S63845 acts synergistically with venetoclax/ABT-199 to induce apoptosis in T-cell acute lymphoblastic leukemia cells. Leukemia **2019**;33:262-6
254. Leverson JD, Sampath D, Souers AJ, Rosenberg SH, Fairbrother WJ, Amiot M*, et al.* Found in Translation: How Preclinical Research Is Guiding the Clinical Development of the BCL2-Selective Inhibitor Venetoclax. Cancer Discov **2017**
255. Leverson JD, Zhang H, Chen J, Tahir SK, Phillips DC, Xue J*, et al.* Potent and selective small-molecule MCL-1 inhibitors demonstrate on-target cancer cell killing activity as single agents and in combination with ABT-263 (navitoclax). Cell Death Dis **2015**;6:e1590
256. Phillips DC, Xiao Y, Lam LT, Litvinovich E, Roberts-Rapp L, Souers AJ*, et al.* Loss in MCL-1 function sensitizes non-Hodgkin's lymphoma cell lines to the BCL-2-selective inhibitor venetoclax (ABT-199). Blood Cancer J **2016**;6:e403
257. Fletcher S. MCL-1 inhibitors - where are we now (2019)? Expert Opin Ther Pat **2019**
258. Merino D, Whittle JR, Vaillant F, Serrano A, Gong JN, Giner G*, et al.* Synergistic action of the MCL-1 inhibitor S63845 with current therapies in preclinical models of triple-negative and HER2-amplified breast cancer. Sci Transl Med **2017**;9
259. Greaves G, Milani M, Butterworth M, Carter RJ, Byrne DP, Eyers PA*, et al.* BH3-only proteins are dispensable for apoptosis induced by pharmacological inhibition of both MCL-1 and BCL-XL. Cell Death Differ **2018**
260. Yasuda Y, Ozasa H, Kim YH, Yamazoe M, Ajimizu H, Yamamoto Funazo T*, et al.* MCL1 inhibition is effective against a subset of small-cell lung cancer with high MCL1 and low BCL-XL expression. Cell Death Dis **2020**;11:177
261. Moujalled DM, Pomilio G, Ghiurau C, Ivey A, Salmon J, Rijal S*, et al.* Combining BH3-Mimetics to target both BCL-2 and MCL1 has potent activity in pre-clinical models of acute myeloid leukemia. Leukemia **2018**
262. Li Z, He S, Look AT. The MCL1-specific inhibitor S63845 acts synergistically with venetoclax/ABT-199 to induce apoptosis in T-cell acute lymphoblastic leukemia cells. Leukemia **2018**
263. Dengler MA, Teh CE, Thijssen R, Gangoda L, Lan P, Herold MJ*, et al.* Potent efficacy of MCL-1 inhibitor-based therapies in preclinical models of mantle cell lymphoma. Oncogene **2019**
264. Castillo L, Young AIJ, Mawson A, Schafranek P, Steinmann AM, Nessem D*, et al.* MCL-1 antagonism enhances the anti-invasive effects of dasatinib in pancreatic adenocarcinoma. Oncogene **2020**;39:1821-9
265. Algarin EM, Diaz-Tejedor A, Mogollon P, Hernandez-Garcia S, Corchete LA, San-Segundo L*, et al.* Preclinical evaluation of the simultaneous inhibition of MCL-1 and BCL-

2 with the combination of S63845 and venetoclax in multiple myeloma. Haematologica **2020**;105:e116-e20
266. Tseng HY, Dreyer J, Al Emran A, Gunatilake D, Pirozyan M, Cullinane C*, et al.* Co-targeting BET proteins and MCL1 induces synergistic cell death in melanoma. Int J Cancer **2020**
267. Bierbrauer A, Jacob M, Vogler M, Fulda S. A direct comparison of selective BH3-mimetics reveals BCL-XL, BCL-2 and MCL-1 as promising therapeutic targets in neuroblastoma. Br J Cancer **2020**
268. Ewald L, Dittmann J, Vogler M, Fulda S. Side-by-side comparison of BH3-mimetics identifies MCL-1 as a key therapeutic target in AML. Cell Death Dis **2019**;10:917
269. Weeden CE, Ah-Cann C, Holik AZ, Pasquet J, Garnier JM, Merino D*, et al.* Dual inhibition of BCL-XL and MCL-1 is required to induce tumour regression in lung squamous cell carcinomas sensitive to FGFR inhibition. Oncogene **2018**
270. Leverson JD, Phillips DC, Mitten MJ, Boghaert ER, Diaz D, Tahir SK*, et al.* Exploiting selective BCL-2 family inhibitors to dissect cell survival dependencies and define improved strategies for cancer therapy. Sci Transl Med **2015**;7:279ra40
271. Hennessy EJ. Selective inhibitors of Bcl-2 and Bcl-xL: Balancing antitumor activity with on-target toxicity. Bioorg Med Chem Lett **2016**;26:2105-14
272. Tao ZF, Hasvold L, Wang L, Wang X, Petros AM, Park CH*, et al.* Discovery of a Potent and Selective BCL-XL Inhibitor with in Vivo Activity. ACS Med Chem Lett **2014**;5:1088-93
273. Lucas CM, Milani M, Butterworth M, Carmell N, Scott LJ, Clark RE*, et al.* High CIP2A levels correlate with an antiapoptotic phenotype that can be overcome by targeting BCL-XL in chronic myeloid leukemia. Leukemia **2016**;30:1273-81
274. Faqar-Uz-Zaman SF, Heinicke U, Meister MT, Vogler M, Fulda S. BCL-xL-selective BH3 mimetic sensitizes rhabdomyosarcoma cells to chemotherapeutics by activation of the mitochondrial pathway of apoptosis. Cancer Lett **2018**;412:131-42
275. Rello-Varona S, Fuentes-Guirado M, Lopez-Alemany R, Contreras-Perez A, Mulet-Margalef N, Garcia-Monclus S*, et al.* Bcl-xL inhibition enhances Dinaciclib-induced cell death in soft-tissue sarcomas. Sci Rep **2019**;9:3816
276. Carter RJ, Milani M, Butterworth M, Alotibi A, Harper N, Yedida G*, et al.* Exploring the potential of BH3 mimetic therapy in squamous cell carcinoma of the head and neck. Cell Death Dis **2019**;10:912
277. Lee EF, Harris TJ, Tran S, Evangelista M, Arulananda S, John T*, et al.* BCL-XL and MCL-1 are the key BCL-2 family proteins in melanoma cell survival. Cell Death Dis **2019**;10:342
278. Moncsek A, Al-Suraih MS, Trussoni CE, O'Hara SP, Splinter PL, Zuber C*, et al.* Targeting senescent cholangiocytes and activated fibroblasts with B-cell lymphoma-extra large inhibitors ameliorates fibrosis in multidrug resistance 2 gene knockout (Mdr2(-/-)) mice. Hepatology **2018**;67:247-59
279. U.S. National Library of Medicine, ClinicalTrials.gov (https://clinicaltrials.gov/).
280. Roberts AW, Davids MS, Pagel JM, Kahl BS, Puvvada SD, Gerecitano JF*, et al.* Targeting BCL2 with Venetoclax in Relapsed Chronic Lymphocytic Leukemia. N Engl J Med **2016**;374:311-22
281. DiNardo CD, Rausch CR, Benton C, Kadia T, Jain N, Pemmaraju N*, et al.* Clinical experience with the BCL2-inhibitor venetoclax in combination therapy for relapsed and refractory acute myeloid leukemia and related myeloid malignancies. Am J Hematol **2018**;93:401-7
282. DiNardo CD, Pratz KW, Letai A, Jonas BA, Wei AH, Thirman M*, et al.* Safety and preliminary efficacy of venetoclax with decitabine or azacitidine in elderly patients with previously untreated acute myeloid leukaemia: a non-randomised, open-label, phase 1b study. Lancet Oncol **2018**;19:216-28
283. U.S. Food and Drug Administration (FDA) (https://www.fda.gov/).
284. European Medicines Agency (EMA) (https://www.ema.europa.eu/en).
285. Cragg MS, Harris C, Strasser A, Scott CL. Unleashing the power of inhibitors of oncogenic kinases through BH3 mimetics. Nat Rev Cancer **2009**;9:321-6
286. Roberts AW, Advani RH, Kahl BS, Persky D, Sweetenham JW, Carney DA*, et al.* Phase 1 study of the safety, pharmacokinetics, and antitumour activity of the BCL2 inhibitor

navitoclax in combination with rituximab in patients with relapsed or refractory CD20+ lymphoid malignancies. Br J Haematol **2015**;170:669-78
287. Tolcher AW, LoRusso P, Arzt J, Busman TA, Lian G, Rudersdorf NS*, et al.* Safety, efficacy, and pharmacokinetics of navitoclax (ABT-263) in combination with irinotecan: results of an open-label, phase 1 study. Cancer Chemother Pharmacol **2015**;76:1041-9
288. Tolcher AW, LoRusso P, Arzt J, Busman TA, Lian G, Rudersdorf NS*, et al.* Safety, efficacy, and pharmacokinetics of navitoclax (ABT-263) in combination with erlotinib in patients with advanced solid tumors. Cancer Chemother Pharmacol **2015**;76:1025-32
289. American Type Culture Collection (ATCC), https://lgcstandards-atcc.org, 2020.
290. Hinson AR, Jones R, Crose LE, Belyea BC, Barr FG, Linardic CM. Human rhabdomyosarcoma cell lines for rhabdomyosarcoma research: utility and pitfalls. Front Oncol **2013**;3:183
291. Uno K, Takita J, Yokomori K, Tanaka Y, Ohta S, Shimada H*, et al.* Aberrations of the hSNF5/INI1 gene are restricted to malignant rhabdoid tumors or atypical teratoid/rhabdoid tumors in pediatric solid tumors. Genes Chromosomes Cancer **2002**;34:33-41
292. Dobson CC, Naing T, Beug ST, Faye MD, Chabot J, St-Jean M*, et al.* Oncolytic virus synergizes with Smac mimetic compounds to induce rhabdomyosarcoma cell death in a syngeneic murine model. Oncotarget **2017**;8:3495-508
293. Maurer HM, Ruymann FB, Pochedly C. Rhabdomyosarcoma and Related Tumors in Children and Adolescents. CRC Press, Inc.; 1991.
294. Hirotsu M, Setoguchi T, Matsunoshita Y, Sasaki H, Nagao H, Gao H*, et al.* Tumour formation by single fibroblast growth factor receptor 3-positive rhabdomyosarcoma-initiating cells. Br J Cancer **2009**;101:2030-7
295. Nakahata K, Uehara S, Nishikawa S, Kawatsu M, Zenitani M, Oue T*, et al.* Aldehyde Dehydrogenase 1 (ALDH1) Is a Potential Marker for Cancer Stem Cells in Embryonal Rhabdomyosarcoma. PLoS One **2015**;10:e0125454
296. Douglass EC, Valentine M, Etcubanas E, Parham D, Webber BL, Houghton PJ*, et al.* A specific chromosomal abnormality in rhabdomyosarcoma. Cytogenet Cell Genet **1987**;45:148-55
297. Felix CA, Kappel CC, Mitsudomi T, Nau MM, Tsokos M, Crouch GD*, et al.* Frequency and diversity of p53 mutations in childhood rhabdomyosarcoma. Cancer Res **1992**;52:2243-7
298. Miyachi M, Kakazu N, Yagyu S, Katsumi Y, Tsubai-Shimizu S, Kikuchi K*, et al.* Restoration of p53 pathway by nutlin-3 induces cell cycle arrest and apoptosis in human rhabdomyosarcoma cells. Clin Cancer Res **2009**;15:4077-84
299. Khatib ZA, Matsushime H, Valentine M, Shapiro DN, Sherr CJ, Look AT. Coamplification of the CDK4 gene with MDM2 and GLI in human sarcomas. Cancer Res **1993**;53:5535-41
300. Weber-Hall S, Anderson J, McManus A, Abe S, Nojima T, Pinkerton R*, et al.* Gains, losses, and amplification of genomic material in rhabdomyosarcoma analyzed by comparative genomic hybridization. Cancer Res **1996**;56:3220-4
301. Berner JM, Forus A, Elkahloun A, Meltzer PS, Fodstad O, Myklebost O. Separate amplified regions encompassing CDK4 and MDM2 in human sarcomas. Genes Chromosomes Cancer **1996**;17:254-9
302. Tate JG, Bamford S, Jubb HC, Sondka Z, Beare DM, Bindal N*, et al.* COSMIC: the Catalogue Of Somatic Mutations In Cancer (cancer.sanger.ac.uk). Nucleic Acids Res **2019**;47:D941-D7
303. Houghton PJ, Morton CL, Tucker C, Payne D, Favours E, Cole C*, et al.* The pediatric preclinical testing program: description of models and early testing results. Pediatr Blood Cancer **2007**;49:928-40
304. Missiaglia E, Shepherd CJ, Patel S, Thway K, Pierron G, Pritchard-Jones K*, et al.* MicroRNA-206 expression levels correlate with clinical behaviour of rhabdomyosarcomas. Br J Cancer **2010**;102:1769-77
305. Khan J, Simon R, Bittner M, Chen Y, Leighton SB, Pohida T*, et al.* Gene expression profiling of alveolar rhabdomyosarcoma with cDNA microarrays. Cancer Res **1998**;58:5009-13
306. Roberts WM, Douglass EC, Peiper SC, Houghton PJ, Look AT. Amplification of the gli gene in childhood sarcomas. Cancer Res **1989**;49:5407-13

307. Taylor AC, Shu L, Danks MK, Poquette CA, Shetty S, Thayer MJ*, et al.* P53 mutation and MDM2 amplification frequency in pediatric rhabdomyosarcoma tumors and cell lines. Med Pediatr Oncol **2000**;35:96-103
308. Muret J, Hasmim M, Stasik I, Jalil A, Mallavialle A, Nanbakhsh A*, et al.* Attenuation of soft-tissue sarcomas resistance to the cytotoxic action of TNF-alpha by restoring p53 function. PLoS One **2012**;7:e38808
309. Sekiguchi M, Shiroko Y, Suzuki T, Imada M, Miyahara M, Fujii G. Characterization of a human rhabdomyosarcoma cell strain in tissue culture. Biomed Pharmacother **1985**;39:372-80
310. Japanese Collection of Research Bioresources Cell Bank (JCRB), https://cellbank.nibiohn.go.jp/english/, 2020.
311. McAllister RM, Melnyk J, Finkelstein JZ, Adams EC, Jr., Gardner MB. Cultivation in vitro of cells derived from a human rhabdomyosarcoma. Cancer **1969**;24:520-6
312. Missiaglia E, Selfe J, Hamdi M, Williamson D, Schaaf G, Fang C*, et al.* Genomic imbalances in rhabdomyosarcoma cell lines affect expression of genes frequently altered in primary tumors: an approach to identify candidate genes involved in tumor development. Genes Chromosomes Cancer **2009**;48:455-67
313. Artimo P, Jonnalagedda M, Arnold K, Baratin D, Csardi G, de Castro E*, et al.* ExPASy: SIB bioinformatics resource portal (http://www.expasy.org). Nucleic Acids Res **2012**;40:W597-603
314. Linardic CM, Naini S, Herndon JE, 2nd, Kesserwan C, Qualman SJ, Counter CM. The PAX3-FKHR fusion gene of rhabdomyosarcoma cooperates with loss of p16INK4A to promote bypass of cellular senescence. Cancer Res **2007**;67:6691-9
315. Fiddler TA, Smith L, Tapscott SJ, Thayer MJ. Amplification of MDM2 inhibits MyoD-mediated myogenesis. Mol Cell Biol **1996**;16:5048-57
316. Houghton JA, Houghton PJ, Webber BL. Growth and characterization of childhood rhabdomyosarcomas as xenografts. J Natl Cancer Inst **1982**;68:437-43
317. McAllister RM, Nelson-Rees WA, Peer M, Laug WE, Isaacs H, Jr., Gilden RV*, et al.* Childhood sarcomas and lymphomas. Characterization of new cell lines and search for type-C virus. Cancer **1975**;36:1804-14
318. Ottaviano L, Schaefer KL, Gajewski M, Huckenbeck W, Baldus S, Rogel U*, et al.* Molecular characterization of commonly used cell lines for bone tumor research: a trans-European EuroBoNet effort. Genes Chromosomes Cancer **2010**;49:40-51
319. Hu X, Yu AX, Qi BW, Fu T, Wu G, Zhou M*, et al.* The expression and significance of IDH1 and p53 in osteosarcoma. J Exp Clin Cancer Res **2010**;29:43
320. Odri GA, Dumoucel S, Picarda G, Battaglia S, Lamoureux F, Corradini N*, et al.* Zoledronic acid as a new adjuvant therapeutic strategy for Ewing's sarcoma patients. Cancer Res **2010**;70:7610-9
321. Navarro S, Gonzalez-Devesa M, Ferrandez-Izquierdo A, Triche TJ, Llombart-Bosch A. Scanning electron microscopic evidence for neural differentiation in Ewing's sarcoma cell lines. Virchows Arch A Pathol Anat Histopathol **1990**;416:383-91
322. Westwood G, Dibling BC, Cuthbert-Heavens D, Burchill SA. Basic fibroblast growth factor (bFGF)-induced cell death is mediated through a caspase-dependent and p53-independent cell death receptor pathway. Oncogene **2002**;21:809-24
323. Kovar H, Auinger A, Jug G, Aryee D, Zoubek A, Salzer-Kuntschik M*, et al.* Narrow spectrum of infrequent p53 mutations and absence of MDM2 amplification in Ewing tumours. Oncogene **1993**;8:2683-90
324. Sonnemann J, Palani CD, Wittig S, Becker S, Eichhorn F, Voigt A*, et al.* Anticancer effects of the p53 activator nutlin-3 in Ewing's sarcoma cells. Eur J Cancer **2011**;47:1432-41
325. Huang HJ, Angelo LS, Rodon J, Sun M, Kuenkele KP, Parsons HA*, et al.* R1507, an anti-insulin-like growth factor-1 receptor (IGF-1R) antibody, and EWS/FLI-1 siRNA in Ewing's sarcoma: convergence at the IGF/IGFR/Akt axis. PLoS One **2011**;6:e26060
326. Whang-Peng J, Triche TJ, Knutsen T, Miser J, Kao-Shan S, Tsai S*, et al.* Cytogenetic characterization of selected small round cell tumors of childhood. Cancer Genet Cytogenet **1986**;21:185-208

327. Batra S, Reynolds CP, Maurer BJ. Fenretinide cytotoxicity for Ewing's sarcoma and primitive neuroectodermal tumor cell lines is decreased by hypoxia and synergistically enhanced by ceramide modulators. Cancer Res **2004**;64:5415-24
328. Nicoletti I, Migliorati G, Pagliacci MC, Grignani F, Riccardi C. A rapid and simple method for measuring thymocyte apoptosis by propidium iodide staining and flow cytometry. J Immunol Methods **1991**;139:271-9
329. Vermes I, Haanen C, Steffens-Nakken H, Reutelingsperger C. A novel assay for apoptosis. Flow cytometric detection of phosphatidylserine expression on early apoptotic cells using fluorescein labelled Annexin V. J Immunol Methods **1995**;184:39-51
330. Mandic A, Viktorsson K, Molin M, Akusjarvi G, Eguchi H, Hayashi SI*, et al.* Cisplatin induces the proapoptotic conformation of Bak in a deltaMEKK1-dependent manner. Mol Cell Biol **2001**;21:3684-91
331. Ianevski A, He L, Aittokallio T, Tang J. SynergyFinder: a web application for analyzing drug combination dose-response matrix data. Bioinformatics **2017**;33:2413-5
332. Borisy AA, Elliott PJ, Hurst NW, Lee MS, Lehar J, Price ER*, et al.* Systematic discovery of multicomponent therapeutics. Proc Natl Acad Sci U S A **2003**;100:7977-82
333. Wong M, Tan N, Zha J, Peale FV, Yue P, Fairbrother WJ*, et al.* Navitoclax (ABT-263) reduces Bcl-x(L)-mediated chemoresistance in ovarian cancer models. Mol Cancer Ther **2012**;11:1026-35
334. Kehr S, Haydn T, Bierbrauer A, Irmer B, Vogler M, Fulda S. Targeting BCL-2 proteins in pediatric cancer: Dual inhibition of BCL-XL and MCL-1 leads to rapid induction of intrinsic apoptosis. Cancer Lett **2020**
335. Mott FE. Mesothelioma: a review. Ochsner J **2012**;12:70-9
336. Fraire AE, Cooper S, Greenberg SD, Buffler P, Langston C. Mesothelioma of childhood. Cancer **1988**;62:838-47
337. Milani M, Byrne DP, Greaves G, Butterworth M, Cohen GM, Eyers PA*, et al.* DRP-1 is required for BH3 mimetic-mediated mitochondrial fragmentation and apoptosis. Cell Death Dis **2017**;8:e2552
338. Han ZH, E.A.; Bremner, T.A.; Wyche, J.H. A Sequential Two-Step Mechanism for the Production of the Mature p17:p12 Form of Caspase-3 in Vitro. The Journal of Biological Chemistry **1997**;272, No 20:13432–6
339. Costa EC, Moreira AF, de Melo-Diogo D, Gaspar VM, Carvalho MP, Correia IJ. 3D tumor spheroids: an overview on the tools and techniques used for their analysis. Biotechnol Adv **2016**;34:1427-41
340. Chatzinikolaidou M. Cell spheroids: the new frontiers in in vitro models for cancer drug validation. Drug Discov Today **2016**;21:1553-60
341. Hirschhaeuser F, Menne H, Dittfeld C, West J, Mueller-Klieser W, Kunz-Schughart LA. Multicellular tumor spheroids: an underestimated tool is catching up again. J Biotechnol **2010**;148:3-15
342. Lochmann TL, Floros KV, Naseri M, Powell KM, Cook W, March RJ*, et al.* Venetoclax is effective in small cell lung cancers with high BCL-2 expression. Clin Cancer Res **2017**
343. Inoue-Yamauchi A, Jeng PS, Kim K, Chen HC, Han S, Ganesan YT*, et al.* Targeting the differential addiction to anti-apoptotic BCL-2 family for cancer therapy. Nat Commun **2017**;8:16078
344. Punnoose EA, Leverson JD, Peale F, Boghaert ER, Belmont LD, Tan N*, et al.* Expression Profile of BCL-2, BCL-XL, and MCL-1 Predicts Pharmacological Response to the BCL-2 Selective Antagonist Venetoclax in Multiple Myeloma Models. Mol Cancer Ther **2016**;15:1132-44
345. Caenepeel S, Brown SP, Belmontes B, Moody G, Keegan KS, Chui D*, et al.* AMG 176, a Selective MCL1 Inhibitor, is Effective in Hematological Cancer Models Alone and in Combination with Established Therapies. Cancer Discov **2018**
346. Nangia V, Siddiqui FM, Caenepeel S, Timonina D, Bilton SJ, Phan N*, et al.* Exploiting MCL-1 dependency with combination MEK + MCL-1 inhibitors leads to induction of apoptosis and tumor regression in KRAS mutant non-small cell lung cancer. Cancer Discov **2018**
347. Abdul Rahman SF, Muniandy K, Soo YK, Tiew EYH, Tan KX, Bates TE*, et al.* Co-inhibition of BCL-XL and MCL-1 with selective BCL-2 family inhibitors enhances cytotoxicity of cervical cancer cell lines. Biochem Biophys Rep **2020**;22:100756

348. Boedicker C, Hussong M, Grimm C, Dolgikh N, Meister MT, Enssle JC*, et al.* Co-inhibition of BET proteins and PI3Kalpha triggers mitochondrial apoptosis in rhabdomyosarcoma cells. Oncogene **2020**
349. Meister MT, Boedicker C, Linder B, Kogel D, Klingebiel T, Fulda S. Concomitant targeting of Hedgehog signaling and MCL-1 synergistically induces cell death in Hedgehog-driven cancer cells. Cancer Lett **2019**;465:1-11
350. Varin E, Denoyelle C, Brotin E, Meryet-Figuiere M, Giffard F, Abeilard E*, et al.* Downregulation of Bcl-xL and Mcl-1 is sufficient to induce cell death in mesothelioma cells highly refractory to conventional chemotherapy. Carcinogenesis **2010**;31:984-93
351. Takahashi H, Chen MC, Pham H, Matsuo Y, Ishiguro H, Reber HA*, et al.* Simultaneous knock-down of Bcl-xL and Mcl-1 induces apoptosis through Bax activation in pancreatic cancer cells. Biochim Biophys Acta **2013**;1833:2980-7
352. Lindsten T, Ross AJ, King A, Zong WX, Rathmell JC, Shiels HA*, et al.* The combined functions of proapoptotic Bcl-2 family members bak and bax are essential for normal development of multiple tissues. Mol Cell **2000**;6:1389-99
353. Jang HS, Padanilam BJ. Simultaneous deletion of Bax and Bak is required to prevent apoptosis and interstitial fibrosis in obstructive nephropathy. Am J Physiol Renal Physiol **2015**;309:F540-50
354. Hemmati PG, Guner D, Gillissen B, Wendt J, von Haefen C, Chinnadurai G*, et al.* Bak functionally complements for loss of Bax during p14ARF-induced mitochondrial apoptosis in human cancer cells. Oncogene **2006**;25:6582-94
355. Iyer S, Uren RT, Dengler MA, Shi MX, Uno E, Adams JM*, et al.* Robust autoactivation for apoptosis by BAK but not BAX highlights BAK as an important therapeutic target. Cell Death Dis **2020**;11:268
356. Brennan MS, Chang C, Tai L, Lessene G, Strasser A, Dewson G*, et al.* Humanized Mcl-1 mice enable accurate pre-clinical evaluation of MCL-1 inhibitors destined for clinical use. Blood **2018**
357. Lin RZ, Chang HY. Recent advances in three-dimensional multicellular spheroid culture for biomedical research. Biotechnol J **2008**;3:1172-84
358. Friedrich J, Ebner R, Kunz-Schughart LA. Experimental anti-tumor therapy in 3-D: spheroids--old hat or new challenge? Int J Radiat Biol **2007**;83:849-71
359. Brophy CM, Luebke-Wheeler JL, Amiot BP, Khan H, Remmel RP, Rinaldo P*, et al.* Rat hepatocyte spheroids formed by rocked technique maintain differentiated hepatocyte gene expression and function. Hepatology **2009**;49:578-86
360. Thoma CR, Zimmermann M, Agarkova I, Kelm JM, Krek W. 3D cell culture systems modeling tumor growth determinants in cancer target discovery. Adv Drug Deliv Rev **2014**;69-70:29-41
361. Khaitan D, Chandna S, Arya MB, Dwarakanath BS. Establishment and characterization of multicellular spheroids from a human glioma cell line; Implications for tumor therapy. J Transl Med **2006**;4:12
362. Lawlor ER, Scheel C, Irving J, Sorensen PH. Anchorage-independent multi-cellular spheroids as an in vitro model of growth signaling in Ewing tumors. Oncogene **2002**;21:307-18
363. Karbach U, Gerharz CD, Groebe K, Gabbert HE, Mueller-Klieser W. Rhabdomyosarcoma spheroids with central proliferation and differentiation. Cancer Res **1992**;52:474-7
364. Voissiere A, Jouberton E, Maubert E, Degoul F, Peyrode C, Chezal JM*, et al.* Development and characterization of a human three-dimensional chondrosarcoma culture for in vitro drug testing. PLoS One **2017**;12:e0181340
365. Cucarull B, Tutusaus A, Subias M, Stefanovic M, Hernaez-Alsina T, Boix L*, et al.* Regorafenib Alteration of the BCL-xL/MCL-1 Ratio Provides a Therapeutic Opportunity for BH3-Mimetics in Hepatocellular Carcinoma Models. Cancers (Basel) **2020**;12
366. Khan S, Zhang X, Lv D, Zhang Q, He Y, Zhang P*, et al.* A selective BCL-XL PROTAC degrader achieves safe and potent antitumor activity. Nat Med **2019**;25:1938-47
367. Backes CS, Friedmann KS, Mang S, Knorck A, Hoth M, Kummerow C. Natural killer cells induce distinct modes of cancer cell death: Discrimination, quantification, and modulation of apoptosis, necrosis, and mixed forms. J Biol Chem **2018**;293:16348-63

10 Acknowledgements

Withdrawn from public version.

11 Eidesstattliche Erklärung

Ich, Sarah Kehr, erkläre hiermit an Eides Statt, dass ich die vorgelegte Dissertation

„Investigating the inhibition of anti-apoptotic BCL-2 family proteins in pediatric cancer cells“

selbstständig angefertigt und mich anderer Hilfsmittel als der in ihr angegebenen nicht bedient habe, insbesondere, dass alle Entlehnungen aus anderen Schriften mit Angabe der entsprechenden Schrift gekennzeichnet sind. Alle Beiträge von Kollegen werden in der Arbeit explizit erwähnt und sind im Folgenden nochmals aufgeführt:

- Figure 5.6: BCL-2 family proteins are expressed in a selection of OS and ES cell lines.; Barnabas Irmer (Masterstudent): teilweise Durchführung der Experimente, teilweise Auswertung und Zusammenstellung der Ergebnisse; eigener Beitrag: teilweise Durchführung der Experimente, teilweise Auswertung und Zusammenstellung der Ergebnisse, Konzeption und Supervision der Experimente
- Figure 5.7: A selection of ES cell lines displays reduced cell viability treatment with A-1331852 or S63845 while OS cell lines show no or limited responsiveness.; Barnabas Irmer (Masterstudent): Durchführung der Experimente, teilweise Auswertung und Zusammenstellung der Ergebnisse; eigener Beitrag: teilweise Auswertung und Zusammenstellung der Ergebnisse, Konzeption und Supervision der Experimente
- Figure 5.8: A-1331852/S63845 co-treatment synergistically induces cell death in OS and ES cell lines.; Barnabas Irmer (Masterstudent): teilweise Durchführung der Experimente, teilweise Auswertung und Zusammenstellung der Ergebnisse; eigener Beitrag: teilweise Durchführung der Experimente, teilweise Auswertung und Zusammenstellung der Ergebnisse, Konzeption und Supervision der Experimente
- Figure 5.9: A-1331852/ABT-199 or S63845/ABT-199 co-treatments are less effective than co-treatment with A-1331852/S63845 in OS and ES cell lines.; Barnabas Irmer (Masterstudent): Durchführung der Experimente, teilweise Auswertung und Zusammenstellung der Ergebnisse; eigener Beitrag: teilweise Auswertung und Zusammenstellung der Ergebnisse, Konzeption und Supervision der Experimente

Die Etablierung des RMS Spheroidmodells erfolgte zu gleichen Teilen in Kooperation mit Vinzenz Särchen (Doktorand). Dies beinhaltete im Detail:

- Etablierung der RMS Spheroidzellkultur
- Etablierung der Aufnahmen am Mikroskop
- Konzeption der Experimente zur Etablierung

Außerdem wirkte Vinzenz Särchen im Folgenden mit:

- Figure 5.26: RD cells form spheroids in a cell number dependent size that grow over time. und Figure 5.28: RH30 cells form spheroids in a cell number dependent size that grow over time.; Vinzenz Särchen (Doktorand): teilweise Durchführung der Experimente, teilweise Konzeption der Experimente; eigener Beitrag: teilweise Durchführung der Experimente, Auswertung und Zusammenstellung der Ergebnisse, teilweise Konzeption der Experimente
- Mitarbeit bei der Etablierung der Analysen zur Auswertung der Ergebnisse

Ich versichere, die Grundsätze der guten wissenschaftlichen Praxis beachtet und nicht die Hilfe einer kommerziellen Promotionsvermittlung in Anspruch genommen zu haben.

Frankfurt am Main, den 13.07.2020

12 Curriculum Vitae

Withdrawn from public version.